MECHANISM AND SIGNIFICANCE OF ADIPOSE INFLAMMATORY RECRUITMENT

Fahrettin Haczeyni

A thesis submitted for the degree of Doctor of Philosophy of

The Australian National University

December 2015

The Australian National University

Medical School

Canberra, Australia

Statement of Originality

The candidate hereby declares that this work, described in this thesis, has been carried out by the author in the Liver Research Laboratory within the Australian National University at The Canberra Hospital, Australia, during the period of September 2011 and April 2015 under the supervision of Professor Geoffrey C. Farrell. This thesis is original, has not been previously submitted in identical or similar form to obtain any other degree, and specifically acknowledges the contribution of collaborators where needed.

Canberra, 16th of December 2015

Fahrettin Haczeyni

ACKNOWLEDGEMENT

First and foremost, I am deeply indebted to Professor Geoffrey C. Farrell for his excellent supervision during my PhD degree. His extraordinary knowledge, wisdom and energy, bitter-sweet motivating methods, and big heart allowed me to reach my true potential and finish my PhD that was, perhaps, the most challenging task I have ever undertaken in my life. There are not enough words to express my gratitude and respect. I would also like to thank Professor Narcissus C.-H. Teoh. Her upbeat, constructive personality and scientific knowledge meant a lot to me during this journey.

I would like to acknowledge Professor Christopher J. Nolan who was always willing to share his medical knowledge; his door was always open whenever I needed. In addition, I am thankful to Professor Matthew M. Yeh and Dr W. Geoffrey Haigh for their kind support by liver histology and lipidomic analyses. I would also like to thank Dr Kim Bell-Anderson and Dr Anselm Enders for their valuable contribution to my PhD project.

It was a pleasure to work with Vanessa Barn, Dr Evi Arfianti, Teddi Dwyer-Engerer, Dr Auvro Mridha, and Dr Sharon Pok; great members of The Liver Group! I would like to thank Dr Mehmet Yabas for his support and lasting friendship. I would also like to acknowledge the most determined person I have met in my life, Dr Sophia Ang, for the countless nights and weekends of work where we motivated each other. I also want to thank Wendy Riley, HDR coordinator, for always being nice and helpful. Moreover, I would like to acknowledge my dear friend Bee Souvannaphong as well as Ayumi Hosaka and Dr Hannah Clarke from the research office for being a wonderful support team.

Completing a PhD is not only a scientific but also an emotional journey. It is my pleasure to acknowledge my lifetime friends Murat Dogru and Mahir Gunebakan for their indispensable company. Sebnem Kesaf has been a true friend and a good “listener” as well. I am most grateful to Erdal Uzunoglu, Barbaros Celikcevik and Hediye Guven for their tremendous support. You have believed in me since I was a young undergraduate student and look, I am a doctor now!

I would like to thank my greatest pal Daniel Wesolowski, cutest couple ever Ahsen and Sevket Alanya, good old friend Patrick Toohey, my foodie friend Trin Gong, Ali Ozturk, Kaan Cetinkaya, and Dr Mathieu Haddad. I would not be able to keep my sanity if I did not have your great friendship and support. My Australian, Turkish and international friends; it was my decision to move to the other side of the world and you have never left me feeling alone. You have been a family to me. I would like to express my sincere gratitude.

I have spent the last 10 years of my life waiting for this moment. Special acknowledgements go to secret heroes who always believed in me.

Lastly, I want to thank the most special person in my life, my mother Nilgun Gulesir. We shared many happy and sad days together and I have always felt her prayers by my side. This PhD thesis is my gift to her.

TEŞEKKÜRLER

Öncelikle ve tüm içtenliğimle, doktoram sürecindeki mükkemmel hocalığı için Profesör Geoffrey C. Farrell'a teşekkür ediyorum. Müthiş bilgi birikimi, acı tatlı motivasyonu ve kocaman kalbi ile gerçek potansiyelime ulaşmamı sağladı ve hayatımın belki de bu en zorlu sürecini sayesinde başarı ile bitiriyorum. Ona olan minnettarlığımı ve saygımı tarif etmem imkansız. Ayrıca Profesör Narcissus C.-H. Teoh'a da çok teşekkür etmek istiyorum. Kendisinin güven veren yol göstericiliği, kilit noktaları çok iyi görmesi ve yapıcılığı benim için ayrı bir anlam ifade etmektedir.

Doktoram süresince bilimsel desteğini ve diyabet konusundaki bilgilerini benden esirgemeyen ve kapısını benim için her zaman açık tutan Profesör Christopher J. Nolan'a teşekkür ediyorum. Profesör Matthew M. Yeh ve Dr. W. Geoffrey Haigh karaciğer histolojisi ve lipidomic analizleri ile tezime önemli katkı sağladılar. Bu süreçte doktorama bilgisel açıdan önemli katkıları olan Dr. Kim-Bell Anderson ve Dr. Anselm Enders'e de teşekkürlerimi sunmak isterim.

Vanessa Barn, Dr. Evi Arfianti, Teddi Dwyer-Engerer, Dr. Auvro Mridha ve Dr. Sharon Pok ile beraber calışmak benim için bir keyifti; biz burada, karaciğer grubunda büyük bir aileyiz! Avustralya'ya ilk adım attığım gün beni havalimanından alan, sonrasında da sohbetinden her zaman müthiş keyif aldığım Dr. Mehmet Yabaş'a, hastanede gece gündüz çalıştığımız zamanlar birbirimizi hep motive ettigimiz (her sey bilim için!) azimli insan Dr. Sophia Ang'e, ne zaman başım sıkışsa yardımıma koşan, güler yüzlü insan Wendy Riley'e, araştırma ofisinden canım dostum Bee Souvannaphong'e, Ayumi Hosaka'ya ve Dr. Hannah Clarke'a da destekleri için teşekkür ediyorum.

Kadim dostlarım Murat Doğru ve Mahir Günebakan'a buradan değerli arkadaşlıkları için teşekkür ediyorum. Şebnem Kesaf'ın da yeri ayrı. Üniversite yıllarımdan beri bana inanan ve bir şekilde bana bu yolda destek olan değerli abim Erdal Uzunoğlu'na, müdürüm Barbaros Çelikçevik'e ve Hedi'm Hediye Güven'e de teşekkürlerimi iletiyorum. Bakın doktor oldum ☺.

Doktora sadece bilimsel değil, aynı zamanda duygusal bir süreç. Bu süreçte yanımda olan, arkadaşlığının her dakikası ayrı keyifli Daniel Wesolosvski'ye, dünyanın en tatlı insanlarından Ahsen ve Şevket Alanya çiftine, good-old friend Pat Toohey'e, rakı sofralarının keyifli yareni Ali Öztürk'e, gurme arkadaşım Trin Gong'a, yine çok değerli dostlarım Kaan Çetinkaya, ve Dr. Mathieu Haddad'a da teşekkürlerimi iletiyorum. Dünya'nın dört bir tarafında, hayatımda olduğu için her gün şükrettiğim tüm arkadaşlarıma teşekkürlerimi iletiyorum. Hayat sizinle daha güzel !

Son 10 yılımı bugünü hayal ederek geçirdim! Bana bu yolda her zaman inanan tüm gizli kahramanlara minnettarlığımı belirtmek isterim.

Son olarak, hayatımdaki en özel kişiye, annem Nilgün Güleşir'e teşekkür ediyorum. Acı tatlı, mutlu üzgün birçok günümüz oldu. Dualarını hep yanımda hissettim. Bu doktora tezi kendisine armağanımdır.

ABSTRACT Adipose tissue has significant roles in whole body energy homeostasis, systemic insulin sensitivity, and lipid metabolism. Increased food intake, physical inactivity, and genetic predisposition lead to over-expansion of adipose tissues. Under constant energy surplus, adipocytes become hypertrophic and adipose tissues undergo hyperplasia. These tissue modifications lead to recruitment of preadipocytes and preadipocyte progenitors (mesenchymal stem cells) into adipogenic lineage, thereby increases the lipid storage capacity of adipose tissues. This keeps circulating blood glucose and fatty acids below toxic levels; however, adipocytes have a saturation point where they cannot store more lipids; when adipocytes are completely engorged with lipids, they start expressing stress signals to recruit inflammation into the tissue. While the mechanisms involved in recruitment of adipose inflammation remain largely unknown, some findings point to "extensive adiposity" as the responsible factor. This thesis focuses on persistent adipose inflammation and its relationship with metabolic comorbidities such as insulin resistance, type 2 diabetes, and particularly, non-alcoholic fatty liver disease (NAFLD) and non-alcoholic steatohepatitis (NASH).

A theme of this research is that adipose tissue is not inert, but as closely linked functional "mini endocrine organs" distributed throughout the body. The current literature regarding structural and functional differences in different adipose tissues is reviewed with a focus on morphometric changes (under energy surplus), and systemic effects of adipose inflammation and dysfunction (development of insulin resistance, NAFLD, etc.). The contributions of muscle activity in bodily energy homeostasis and the close interaction between muscle, adipose, liver and insulin metabolism are discussed, and the implications of "adipose failure" for lipid partitioning into the liver, a key pathway to pathogenesis of NAFLD/NASH is highlighted. The low yield of cellular material and the excessive lipid contamination make it harder to work with adipose compared to liver. The candidate developed experimental protocols for this study,

which were optimised, including adipose morphometric analysis, that were used to describe the development and progression of adipose tissue inflammation and fatty liver disease in a mouse model of NASH. We examined the effects of feeding an atherogenic diet (23% fat, 45% carbohydrate, 0.19% cholesterol) on adipose morphometry and the recruitment of inflammatory cells. We studied *Alms1* mutant *foz/foz* mice, which have a profound disturbance of hypothalamic appetite regulation. *foz/foz* mice fed an atherogenic diet developed adipocyte hypertrophy, adipose inflammation, hyperglycemia, and evidence of NASH. Wildtype (*WT*) mice fed the same diet developed milder metabolic phenotype compared to *foz/foz* mice.

The phenotypic switch towards a proinflammatory phenotype in enlarged adipocytes, this increasing cellular stress causes recruitment of macrophage crown-like structures (CLSs) into adipose tissue and a higher rate of adipocyte injury/necrosis. Toll-like receptors (TLRs) are innate immune system receptors activated by danger-associated molecular patterns (DAMPs). Necrotic cellular debris contains DAMPs which can stimulate TLR9 signalling. Activation of TLR9, particularly in macrophages, exacerbates adipose inflammation. Other works support a role for TLR4 in adipose inflammation, but the roles of other pattern recognizing receptors are less clear. In this study, we used *Tlr9*$^{-/-}$ mouse to investigate the contribution of TLR9 signalling, if any, to adipose inflammatory recruitment. Increased calorie intake with atherogenic feeding for 24 weeks, led to inflammation in adipose tissue. TLR9 deletion abolished this effect. Correspondingly, NASH prevalence was much less in *Tlr9*$^{-/-}$ mice.

The farnesoid X receptor (FXR) agonist obeticholic acid (6-ECDCA) improves steatosis in patients with NASH, but protective mechanisms remain unresolved. We therefore investigated the effects of 6-ECDCA (1mg/kg/day) on glucose metabolism, multiple adipose compartments and liver in atherogenic diet-fed *foz/foz* and *WT* mice. 6-ECDCA reduced body weight, liver mass and hepatic lipid partitioning with striking

improvement of glucose tolerance in *WT* but not *foz/foz* mice, in which it had no effect on liver histology. 6-ECDCA limited expansion of adipose tissues in atherogenic diet-fed *WT* but not *foz/foz* mice. In addition, 6-ECDCA treatment altered macrophage polarization towards a more anti-inflammatory phenotype in *WT* mouse adipose compartments but not *foz/foz* mice. To conclude, 6-ECDCA improves glucose metabolism, adiposity and adipose inflammation in animals with a milder metabolic phenotype. Conversely, 6-ECDCA fails to improve adipose inflammation or hepatic lipid partitioning in profoundly obese mice, and there is no reversal of NASH. These results help explain why 6-ECDCA treatment against human NASH improves steatosis but fails to reverse NASH pathology.

Physical inactivity contributes to adverse effects of overnutrition. We studied the effects of an exercise intervention on adipose and liver pathology. From weaning, mice were provided with an in-cage exercise wheel, in which they were calculated to run over 4 km/day. In this study, voluntary exercise protected mice against the metabolic effects of high calorie intake and atherogenic dietary feeding by reducing adipose inflammation and maintaining systemic insulin sensitivity, the latter principally with its effects on muscle. Improvements in fatty liver pathology appear to be one of the benefits conferred by exercise. In the final chapter, the most important findings of earlier experiments are discussed in relation to and how they extend the knowledge in the field. Dysfunction of adipose tissue related to stress and inflammation is of pathologic importance. Limited lipid storage capacity and pro-inflammatory factors released from adipose depots can disrupt normal functioning of other organs. Circulating lipids increase when adipose is inflamed and leading to adverse effects on other tissues, primarily the liver. Meanwhile, inflammation in adipose tissue becomes persistent. Obesity-associated NAFLD/NASH, type 2 diabetes and metabolic syndrome are closely linked to persistent adipose inflammation.

PUBLICATIONS, PRESENTATIONS and AWARDS

Publication in Process

Haczeyni F, Barn V, Mridha AR, Yeh MM, Estevez E, Febbraio MA, Nolan CJ, Bell-Anderson KS, Teoh N, Farrell G. Exercise improves adipose function and inflammation and ameliorates fatty liver disease in obese diabetic mice. *Obesity* 2015

Conference Presentations

Haczeyni F, Barn V, Larter CZ, Teoh N, Farrell G. Effects of exercise on fatty liver, adipose inflammation and obesity complications in high-fat fed wildtype (*WT*) and hyperphagic *foz/foz* mice. Australian Gastroenterology Week, Adelaide, SA, Australia. Shortlisted as finalist (top 4) for June Halliday's **Young Investigator Award** (2012).

Haczeyni F, Toohey P, Lam W, Mridha AR, Teoh N, Farrell G. Changes in adipose tissue in high fat-fed *foz/foz* mice: Relationship to adipose inflammation. Canberra Health Annual Research Meeting, Canberra, ACT, Australia (2012).

Haczeyni F, Mridha AR, Yeh MM, Teoh N, Farrell G. Activation of TLR9 and MyD88 is required for adipose and liver inflammation in diet-induced obesity-related NASH. Australian Gastroenterology Week, Melbourne, VIC, Australia. Presented at **Medical & Surgical Papers of Distinction** session (2013).

Haczeyni F, Delghingaro-Augusto V, Dagpo T, Khan A, Teoh N, Farrell G. Changes in Adipose inflammation, but not changes in adipocyte size, appears linked to excess ectopic lipid accumulation in liver of NASH prone *foz/foz* NOD.B10 mice in comparison to NASH resistant *foz/foz* Balb/c mice. Australian Liver Association, Hepatology Research Workshop, Gold Coast, QLD, Australia (2013).

Haczeyni F, Mridha AR, Yeh MM, Teoh N, Farrell G. Activation of TLR9 and MyD88 is required for adipose and liver inflammation in diet-induced obesity-related NASH. Canberra Health Annual Research Meeting, Canberra, ACT, Australia. **Winner of Best Poster Award** (2013).

Haczeyni F, Mridha AR, Yeh MM, Teoh N, Farrell G. TLR9 mediates adipose and liver inflammation in metabolically obese murine models of non-alcoholic steatohepatitis. EASL's International Liver Congress, London, UK. **EASL Young Investigator, Full Bursary** (2014).

Haczeyni F, Barn V, Mridha AR, Haigh G, Yeh MM, Estevez E, Febbraio MA, Teoh N, Farrell G. Reduced adipose inflammation through exercise improves insulin sensitivity and confers hepatoprotective effects in hyperphagic obese mice. American Diabetes Association, 74th Scientific Sessions, San Francisco, CA, USA. Granted for The Australian National University, **Vice-Chancellor's HDR Travel Grant** (2014).

Table of Content

CHAPTER 2

CHAPTER 3

CHAPTER 4

CHAPTER 5

CHAPTER 6

CHAPTER 7

REFERENCES

APPENDICES

List of Figures

CHAPTER 1

CHAPTER 3

CHAPTER 4

CHAPTER 5

CHAPTER 6

CHAPTER 7

List of Tables

Abbreviations

6-ECDCA	6-ethylchenodeoxycholic (OCA)
A-AM	Alternatively-activated macrophage
ACLY	ATP-citrate lyase
ACOX1	Peroxisomal acyl-coenzyme A oxidase 1
ACT	Australian Capital Territory
ACTB	Beta-actin
AdipoR	Adiponectin receptor
ADP	Adenosine diphosphate
ADRP	Adipose differentiation-related protein
AEC	Animal Ethics Committee
AG1	Arginase 1
AKT	Protein kinase B
ALT	Alanine aminotransferase
AMPKα	AMP-activated protein kinase α
ANU	Australian National University
aP2	Adipocyte protein 2
APPL1	Activation of DCC-interacting protein 13-α
AS160	AKT substrate of 160 kDa
ASC	Apoptosis-associated speck-like protein containing a carboxyl-terminal CARD
AST	Aspartate aminotransferase
ATGL	Adipose triglyceride lipase
Ath	Atherogenic
ATP	Adenosine triphosphate
AUC	Area under curve
B2M	β-2 microglobulin
BAT	Brown adipose tissue
BMI	Body mass index
BMI	Bone marrow
BMR	Basal metabolic rate
bp	Base pair
BSA	Bovine serum albumin
C/EBP	CCAAT/enhancer binding protein
C-AM	classically-activated macrophage
cAMP	Cyclic adenosine monophosphate
CAP	CBL-associated protein
CAV	Caveolin
c-CBL	Casitas B-lineage protein
CCL2	See MCP1
CCL5	Chemokine (C-C motif) ligand 5 (RANTES)
CCR2	MCP receptor
CD	Cluster of differentiation (as in CD36)
CD36	Cluster of differentiation 36
CE	Cholesteryl ester
CGI-58	1-acylglycerol-3-phosphate O-acyltransferase
CHOP	C/EBP homologous protein
ChREBP	Carbohydrate-responsive element-binding protein
CLS	Crown-like structures
COL1A1	Type 1 collagen alpha 1
COL3A1	Type 3 collagen alpha 1
CREB	cAMP response element-binding protein
CTS	Cathepsin
CVD	Cardiovascular disease
CXCL10	Chemokine (C-X-C motif) 10 (IP10)
DAG	Diacylglyceride

DAMP	damage/danger-associated molecular pattern
DC	Dendritic cell
DNA	Deoxyribonucleic acid
ECM	Extracellular matrix
ELISA	Enzyme-linked immunosorbent assay
eNOS	Endothelial nitric oxide synthase
ER	Endoplasmic reticulum
ERK	Extracellular signal-related kinase
ETC	Electron Transport Chain
EtOH	Ethyl alcohol
F4/80	EGF-like module-containing mucin-like hormone receptor-like 1
FA	Fatty acid
FAS	Fatty acid synthase
FATP	FA transport protein
FBG	Fasting blood glucose
FC	Free cholesterol
FFA	Free fatty acid
Fig	Figure
FIZZ1	Antigen resistin-like molecule α
FOXC2	Forkhead box protein C2
FOXO	Forkhead box O
FXR	Farnesoid X receptor
GAPDH	Glyceraldehyde 3-phosphate dehydrogenase
GC	Gas chromatography
GH	Growth hormone
GM-CSF	Granulocyte-macrophage colony-stimulating factor
GSK3	glycogen synthase kinase 3
H&E	Hematoxylin and eosin
H_2O	Hydrogen dioxide (Water)
H_2O_2	Hydrogen peroxide
HCC	Hepatocellular carcinoma
HDL	High-density lipoprotein
HFD	High fat diet
HIF	Hypoxia-inducible factor
HMGB1	High-Mobility group protein 1
HMG-CoR	3–hydroxy-3-methyl-glutaryl-CoA reductase
HMW	High molecular weight
HPLC	High-performance liquid chromatography
HSC	Hematopoietic stem cell
HSL	Hormone-sensitive lipase
HSP	Heat shock protein
ICAM	Intercellular adhesion molecule
IFN	Interferon
Ig	Immunoglobulin
IGF1	Insulin-like growth factor 1
IHC	Immunohistochemistry
IKK	Inhibitor κB kinase
IL-1R1	Interleukin 1-R type 1
IL6	Interleukin 6
IMS	Intermembrane space
IpGTT	Intraperitoneal glucose tolerance test
IRF	Interferon regulatory factor
IRF7	Interferon regulatory factor 7
IRS	Insulin receptor substrate
ISS	Innate immune system
JCSMR	John Curtin School of Medical Research

JNK	c-Jun N-terminal kinase
KLF	Kruppel-like factor
KO	Knock-out
LAS	Leica Application Suite
LCFA	Long-chain fatty acid
LD	Lipid droplet
LMP	Lysosomal permeabilization
LXR	Liver X receptor
MAPK	Mitogen-activated protein kinase
MCP1	Monocyte chemoattractant protein 1
MEK	Mitogen-activated protein kinase kinase
Mes	Mesenteric
MHO	metabolically obese healthy
MIF	Macrophage migration inhibitory factor
MIP1α	Macrophage inflammatory protein 1α
MLKL	Mixed lineage kinase domain-like protein
MMP	Matrix metalloproteinase
MSC	Mesenchymal stem cell
Mt	Mitochondrion
mTORC1	Mammalian target of rapamycin complex 1
MyD88	Myeloid differentiation primary-response protein 88
MYF5	Myogenic factor 5
NAD(P)H	Nicotinamide adenine dinucleaotide phosphate
NAFLD	Non-alcoholic fatty liver disease
NAS	NAFLD activity score
NASH	Non-alcoholic steatohepatitis
NC	Normal chow
NCBI	National Center for Biotechnology Information
NEFA	Non-esterified fatty acid
Nfe2l2	Nuclear factor [erythroid-derived] 2-like 2
NF-κB	Nuclear factor kappa-light-chain-enhancer of activated B cells
NGO	Non-governmental organization
NHPA	National Health Performance Agency
NLRP3	NOD-like receptor family, pyrin domain containing 3
NO	Nitrite oxide
NRF2	Nuclear factor-erythroid 2 p45-related factor 2
OCA	Obeticholic acid
ORO	Oil-red-O
OXPHOS	Oxidative phosphorylation
PAMP	Pathogen-associated molecular pattern
PAT	PLINs-ADRP-TIP47 protein complex
Pax7	Paired box protein 7
PDK1	Phosphoinositide-dependant kinase 1
PGC1α	PPARγ coactivator 1α
PI3K	Phosphatidylinositol 3-kinase
PKA	Protein kinase A
PLIN	Perilipin
PNPLA2	Patatin-like phospholipase domain containing 2
pO_2	Oxygen partial pressure
Pov	Periovarian
PPARγ	Peroxisome proliferator-activated receptor γ
PPR	Pattern-recognition receptor
PRDM16	PR domain containing 16
PTEN	Phosphatase and tensin homolog protein
RIP	Receptor-interacting protein kinase
ROCK	Rho-associated kinase

ROS	Reactive oxygen species
RPL13A	Ribosomal protein L13a
RUNX2	Runt-related transcription factor 2
SHP	Short heterodimeric partner
SOD	Superoxide dismutase
SOP	Standard Operation Procedure
SPF	Specific pathogen free
SRC1	Steroid receptor coactivator 1
SREBP	Sterol regulatory element binding protein
ssDNA	Single strand DNA
SVF	Stromal vascular fraction
T2D	Type 2 diabetes
TAG	Triglyceride
TEE	Total energy expenditure
TIP47	Tail-interacting protein of 47 kDa
TLR9	Toll-like receptor 9
TNFα	Tumor necrosis factor α
TRIF	TIR-domain-containing adapter-inducing interferon β
UCP1	Uncoupling protein 1
UHDL	Ultra-high-density lipoproteins
UPR	Unfolded protein response
VCAM1	Vascular cell adhesion protein 1
VEGF	Vascular endothelial growth factor
WAT	White adipose tissue
WHO	World Health Organization
WT	Wild-type
WT1	Wilms' tumor
α-SMA	α-smooth muscle actin
β-MCD	β-methyl-cyclodextrin

CHAPTER 1

INTRODUCTION

1.1 Obesity: An Overview on Australia as a Reflection of the Epidemic

The National Health Performance Agency (NHPA) is an Australian independent agency which aims to improve the general health of Australians and the Australian health system in cooperation with state governments, non-governmental organizations (NGOs), and other agencies. As described on its website, NHPA's goal is to provide nationally consistent, locally relevant, and comparable information about Australia's health system to inform consumers, and to stimulate and inform improvements and increase transparency and accountability. Since 2009, NHPA has published an important series of reports under the title of "Australia: The Healthiest Country By 2020" (1). The first technical report was assigned to obesity.

1.1.1 Obesity in Australia: A Need for Urgent Action

With the development of industrialization, agrarian cultural norms have switched to a more consumption-based sedentary lifestyle in Australia. Industrialized technologies for food production and transportation have introduced cheaper but more calorie-dense (obesogenic) nutrients to the markets for daily consumption. This has escalated obesity to epidemic levels in Australia, like any other industrialized country in the world. Australia's relatively small population, prosperous natural resources, and cultural background allowed the country to complete its industrialization in the early 1970s. Since then, obesity has been steadily increasing. Today, over 60% of Australian adults are obese or overweight; in November 2014, it was reported that more than 30% of Queenslanders are obese. Likewise, there is an increasing trend for early-onset childhood obesity (2).

CHAPTER 1: Introduction

In 2012, the Australian population was approximately 22.3 million people, of which 4.2 million were aged below 15 years (~3 million children between 0-9 years old) (3). Thus, the adult population (aged older than 15) was around 18.1 million. In NHPA's obesity report, 10.8 million adults were classified as overweight or obese in 2012 (based on body mass index [BMI]) (1). This makes the prevalence of overweight and obesity ~60% in adults. In all, 4.7 million adults suffered from obesity, which was equal to 26% of the adult population in 2012 (Fig. 1.1) (4). According to the World Health Organization (WHO), the prevalence of overweight and obese people in Australia was 67% in 2007 (5). Although values can vary slightly in different reports, it is undeniable that Australia today faces a very serious population health issue in that more than 12 million people are overweight or obese.

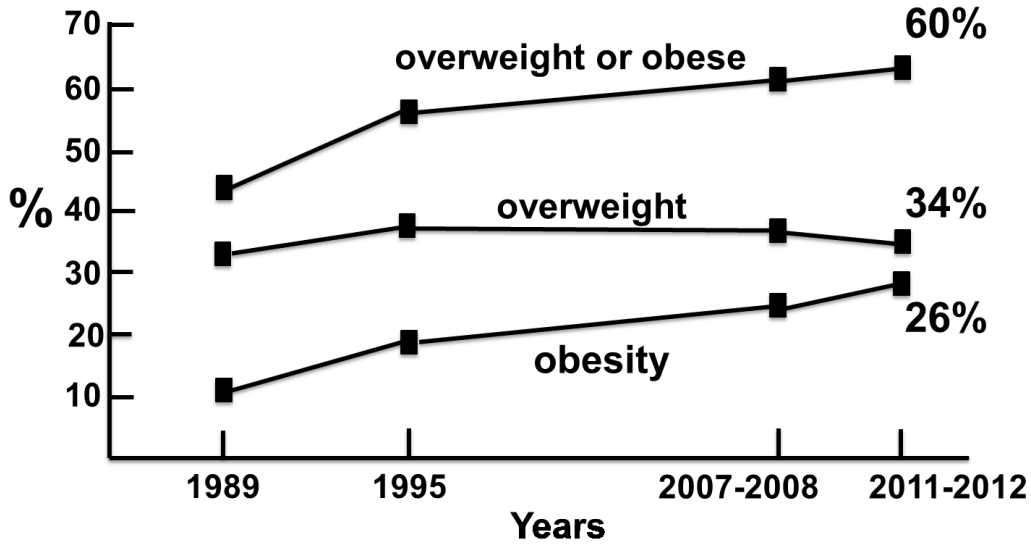

Figure 1.1: National overweight and obesity trends in Australia. Adjusted from the original article (4).

It has been projected that these rates may progressively worsen; by one estimate, the Australian population will be 28 million by 2030, but obesity trends in adults are escalating faster than the population growth rate.

1.1.2 Obesity is Not Just Fatness: It Affects Wellness

As discussed later, obesity is a complex disorder. Decades of research have clearly linked it to other severe acute or chronic diseases such as type 2 diabetes (T2D), cardiovascular disease (CVD), non-alcoholic fatty liver disease (NAFLD), and more than 10 common cancer types (6). The overall burden of obesity treatment and prevention to the Australian economy was estimated as ~$58.2 billion in 2008 (1). Other research conducted in 2005 showed that obesity contributed to 4 million days of work lost in 2001 (7), higher than any specific illness. Another concern for the welfare of the Australians is the perception of increasing discrimination against overweight or obese people. For instance, job discrimination against obese people has become a topic of debate in social media, and several articles have been written about it. Therefore, obese individuals may not only suffer physically, but also psychologically, contributing to depression and mental illnesses (8). A similar picture can easily be drawn for many other countries or the global level. By 2025, 335 million people worldwide are expected to have “diabesity”, obesity with the complication of T2D (9). Today, obesity with T2D and CVD kills twice as many people as the total deaths caused by inherited disorders and infectious diseases.

1.2 Obesity and Adipose Tissue

According to PubMed Health Online Platform (A.D.A.M. Medical Encyclopaedia), obesity means “having too much body fat”. This description should not be confused with weighing too much because for instance, an individual engaged in body building can also weigh “too much” (much more than average for height) because of expanded lean body mass (muscle); this is one example where BMI fails to properly identify obesity. Some researchers have also describes obesity as a state of low-grade

inflammation. In addition, some public health authorities might define obesity as a global epidemic, whereas other clinicians think of obesity more narrowly is a medical disorder. Each of these explanations is only partially true. In this PhD thesis, we will address the concept, admittedly a speculative one, that obesity, or more specifically metabolic (unhealthy) obesity, is dysfunction or failure of adipose tissue to accommodate positive energy imbalance.

1.2.1 "Adipose" Biology

Adipose is a highly dynamic, energy (fat) storing tissue that can readily adapt to changing environmental circumstances. For example, if there is nutrient abundance in the habitat of a vertebrate (human, rodent etc.), there is a net increase in the total number and size of adipocytes in the body to store as much fat as possible (10). This process appears to have evolved in order to assist survival of animals when it is not possible to find nutrients. The first "anatomically modern" human body appeared around 200,000 years ago during the second subdivision of the Palaeolithic age. Archaeological findings indicate that the first farmers existed in the last quarter of the Neolithic age, around 8000 BC. Accordingly, for about 190,000 years, human activity was confined to hunters and gatherers. In this context, the unique dynamic capacity of adipose tissue to expand and store fat would give the host the ability to survive during lack of food, such as when humans could not find animals to hunt or fruit, vegetables or nuts to gather.

The importance of body weight regulation on human health has been referenced back to Hippocrates of Kos, Ancient Greece. The commonly accepted idea since then was that a physiological feedback loop regulates energy homeostasis. Modern adipose biology, perhaps a new era in medical research, began with the discovery of a peptide hormone, leptin. The Jackson Laboratory had developed a severely obese mouse model

(*ob*/*ob* mice) in 1949 by genetic manipulation (11). In 1966, Doug Coleman and his colleagues identified a new mouse colony called *db*/*db* mice, with similar severe obesity (12). Breeding (parabiosis) of these mice with wild-type counterparts and observation of their phenotypes revealed fascinating results. When *ob*/*ob* mice were joined with wild-type mice, there was a significant reduction in their calorie intake. Likewise, wild-type mice stopped eating when joined with *db*/*db* mice. Accordingly, Coleman asserted that the *ob* gene produces a hormone, and *db* protein, which they proposed was selectively localized in hypothalamus, recognizes this molecule. This endocrine system could be adjusted by fat reservoirs to control the satiety/hunger feelings and overall body weight gain (13).

In the early 1990s, Jeffrey Friedman set out to identify the *ob* gene product. Instead of the widely-used traditional hormone purification technique, he managed to clone the *ob* gene. Friedman's group published their discovery in 1994 in *Nature* (14). Friedman named the peptide "leptin" and suggested that leptin, exclusively produced by adipose tissues, regulates the balance of food intake and energy expenditure of the body. Coleman's and Friedman's discoveries were important in three ways:

- The use of advanced molecular biology techniques, such as genetic approaches and positional cloning fascinated a new generation of researchers,
- The newly discovered cross-talk between fat and brain through an endocrine system could be valid for other physiological systems,
- Adipose tissue could no longer be regarded as an inert tissue; it must be a functional endocrine organ.

From the anatomical or structural view point, adipose tissue is a specialized form of loose connective tissue (15). The discovery of leptin as a hormone revealed that the functions of adipose tissue are considerably more than just "connecting" tissues. This initial discovery in 1994 triggered an avalanche of productive research. Many other

hormones, adipose-derived cytokines and chemokines (adipokines) were discovered within the next decade. Adipokines are exclusively or selectively produced by adipose tissues, and are important for many metabolic pathways. Today, adipose tissue has become accepted as the biggest (most extensive) endocrine organ in the body (16).

Adipose tissue is essentially formed of fat-containing adipocytes embedded in a stroma (this will be discussed later). Over-eating, calorie-overload, genetic predisposition, early development, and physical inactivity contribute to energy imbalance (input > output) of an individual. In the presence of excess kjoules, already mature adipocytes start to enlarge, store more fat and undergo "cellular hypertrophy" (17). If the excess calorie imbalance is not reconciled by increased energy dissipation or utilization, cellular hypertrophy leads to the development of adipose tissue hyperplasia. Accordingly, large adipocytes secrete a set of hormones and cytokines which increase recruitment of preadipocytes, as well as promoting their development into mature adipocytes.

As mentioned above, adipose tissue is comprised of adipocytes and a stromal vascular fraction (SVF) (Fig. 1.2). The latter consists of preadipocytes, preadipocyte progenitors (mesenchymal stem cells), fibroblasts, endothelial cells, and immune cells (18). These cells are surrounded and connected (enmeshed) by a fibrillary structural extracellular matrix (ECM) – the components of this material also influence adipose functions (19). Adipose tissue is the primary energy storage compartment in the body. In addition, adipose located under the skin dampens mechanical impacts from the outer world and provides thermal insulation (20).

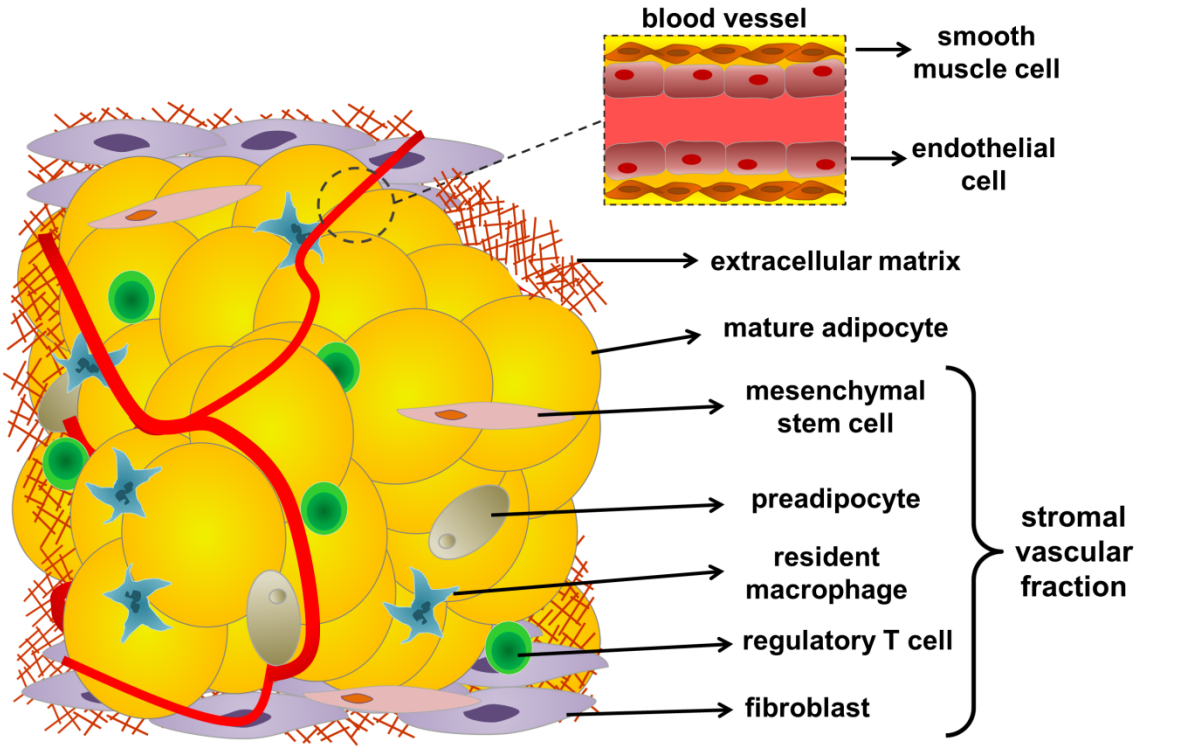

Figure 1.2: Adipose tissue cellular heterogeneity. In addition to mature adipocytes, adipose tissue contains a stromal vascular fraction that is composed of tissue-resident mesenchymal stem cells, partially-committed preadipocytes, fibroblasts, immune cells such as resident macrophages and regulatory T cells, vascular endothelial cells, pericytes (not shown), and smooth muscle cells.

1.2.2 The Origins of Adipose Tissue

The increasing prevalence of obesity and obesity-related metabolic morbidities has aroused enormous interest in the developmental origins of adipose tissue. One critical finding has been the "heterogeneity" of body fat (21). The locations of adipose tissues can be divided into two types: visceral and subcutaneous adipose tissue (abbreviated as WAT for white adipose tissue). Subcutaneous WAT is located under the skin or in external "pads", like fingers and the heel, whereas visceral WAT is located around the internal organs, such as the kidney, gonads, and intestines. These two adipose types originate from different sources during development, and they exhibit different structural integrity as well as different functions in adulthood (22). The predominant location of the fat deposition impacts on the severity of obesity and its complications,

and these are particularly linked to expansion of visceral WAT (visceral adiposity or central obesity).

Using transcriptomic analyses, it has been shown that the gene panels activated in adipocyte progenitors during development can vary between different fat depots (23). Mesoderm is a germ layer formed in the gastrulation stage of embryonic development. The Wilms' tumor 1 (*Wt1*) gene product is a transcription factor responsible for the development of the gonads and kidneys from their mesodermal origins (24). WT1 expression is limited to the layer between paraxial mesoderm and the lateral plate (Fig. 1.3). Visceral fat depots arise from the layer responsible for the development of kidney, gonads, omentum, and spleen. In 2014, Nick Hastie and his colleagues reported that WT1 expression is restricted to visceral adipose pads; they could not find WT1 expression in either subcutaneous or brown adipose tissue (BAT) (25). Further analyses have revealed that only SVF cells express WT1 in visceral fat, not mature adipocytes. In addition to this finding, heterogeneous progenitors have been found for each individual visceral adipose pad according to their physical attachment to the various visceral organs, but all of these progenitors develop from WT1-expressing mesothelium during embryonic development.

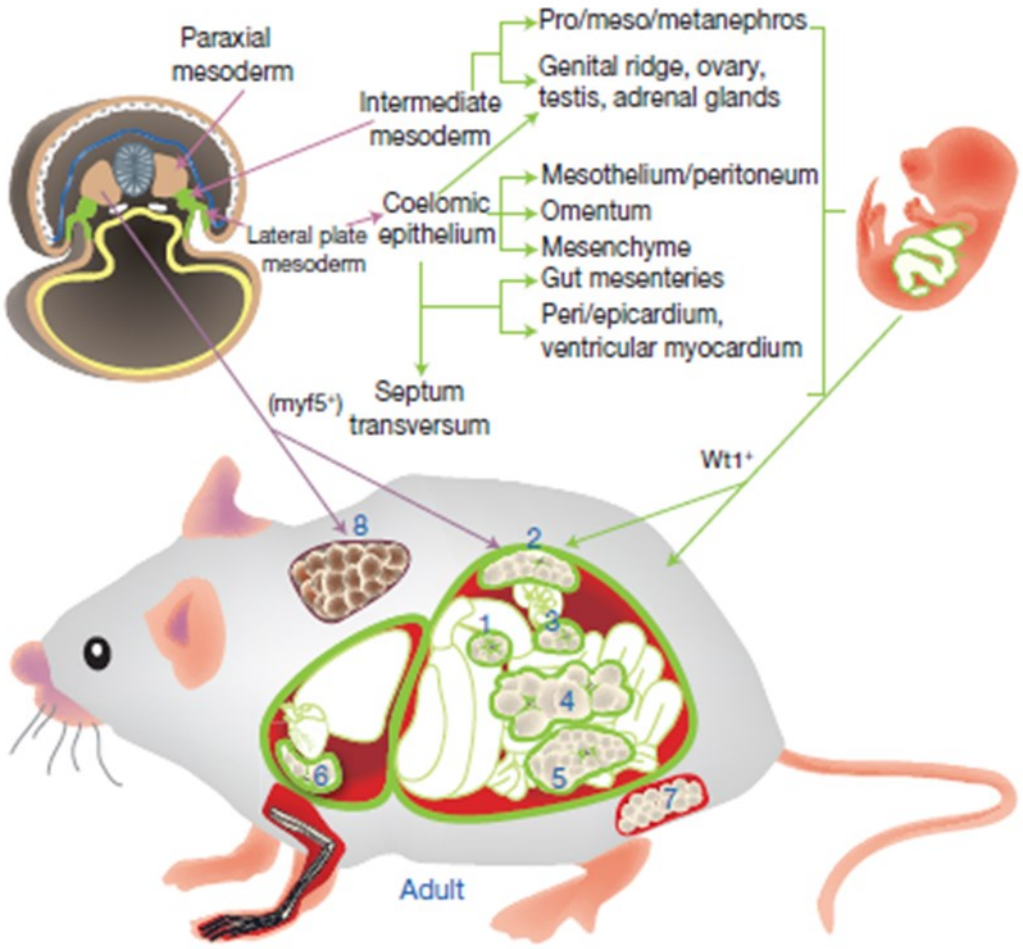

Figure 1.3: Mesodermal layers forming adipose tissues during development. Adjusted from the original article (25)**.** WT1 is primarily expressed in the intermediate and lateral plate mesoderm layers. These mesenchymal stem cells (MSCs) form internal organs such as ovary, testis, adrenal glands, kidney, and gut (mesothelial layers in all of internal organs). In addition to that, visceral adipose tissues include (1) omentum, (2) perirenal, (3) mesenteric, (4) epididymal, (5) abdominal cavity, and (6) thoracic cavity. Unlike visceral pads, (7) subcutaneous and (8) brown adipose tissues develop from the paraxial mesoderm and the neural crest (shown blue between paraxial layers).

Subcutaneous WAT and BAT are not formed by WT1-expressing cells. Unlike visceral pads, subcutaneous adipose tissue arises from the paraxial mesoderm as well as the neural crest (25). These germ layers are relatively closer to the ectoderm which forms the skin during development (Fig. 1.3). Thus, there are ontogenetic differences between subcutaneous and visceral fat pads and these developmental differences may partly explain functional variations between fat pads.

1.2.3 Adipose Development

"Genesis" derives from Greek word "Gignesthai", which means "coming into being". Accordingly, genesis refers to creation or generation in biological sciences. Adipogenesis includes two main events: proliferation (or migration) of progenitor cells, and adipogenic differentiation. As mentioned earlier (section 1.2.2), different adipose depots arise from mesodermal origin (25). BAT develops roughly at the second half of the gestation period, whereas WAT formation follows later. The amount of BAT reaches its apogee 3 months after birth, and some of it vanishes (or is replaced with WAT) after another 3 months (26).

The ultimate source for adipocyte development is MSCs (27). These are multipotent, self-renewable clonogenic cells derived from the mesoderm. Stem cell biology has expanded greatly following the discovery of bone marrow (BM)-residing hematopoietic stem cells (HSCs), the main source for blood components. Soon after that (1960s), the potential of BM stroma to generate important other tissues such as bone, cartilage, and adipose was discovered (28). The recognition of another subset of BM cells which could differentiate into these tissues stimulated interest in their nature. Early studies defined them as fibroblast-like cells (colony-forming unit fibroblasts), but their ability to proliferate *in vitro* and transform into multilineage daughter cells eventually led to the term "mesenchymal stem cells". Some studies have shown adipocyte development is possible from HSCs, but this seems to be a rare event (29).

MSCs are largely uncommitted multipotent stem cells (30). They possess a great capacity to differentiate into other cells. MSCs are thin and elongated (fibroblast-like morphology) with a small cell body. They tend to reside in the stroma of yellow BM, so called because of the presence of fat (31). Some cell types which can be constituted from MSCs residing in yellow BM are adipocytes, osteoblasts, pancreatic islet β cells, hepatocytes, and some immune cells, including macrophages. The common origin of

adipocytes and immune cells is another possible link between excess adiposity, adipose inflammation (discussed in Section 1.5), and development of metabolic obesity.

Although MSCs are primary progenitor cells for adipocyte development, recent studies have demonstrated that adipose tissue itself is another rich source of MSCs (32, 33). In 2006, Karen Bieback and her colleagues compared MSCs from 3 different sources; BM, umbilical cord blood, and adipose tissue (34). Although MSCs from the three different sources exhibited minor differences, those researchers found that MSCs from each source possessed considerable differentiation potential. They also concluded that adipose tissue is an attractive source of MSCs for potential therapeutic/clinical use. These data suggest a direct link between BM stroma and adipose tissue; as a result, adipose tissue is packed with multipotent stem cells.

1.2.4 Adipose Differentiation

Adipogenesis is the biological process by which mature adipocytes are formed (35). Adipose development is highly complex because mature adipocytes do not possess proliferative capability (36); fresh adipocytes (or preadipocytes) must arise from progenitor cells. Considering the fact that adipocytes are highly dynamic cells that can turnover rapidly (37), the supply of adipocyte progenitors is a tightly-regulated advanced system.

Enlargement of adipose tissue involves both increasing the volume of adipocytes and increasing their number by generation of new adipocytes. In 2010, Erik Arner and his colleagues reported that the relative death rate of adipocytes is ~10% and the mean adipocyte age is up to ~10 years in adult humans, regardless of gender (38). During nutrient overload (energy surplus), this balance is impaired, and this has negative impacts on the body (adipocyte degeneration, discussed later). On the other hand, cholesterol and lipid molecules are not just structural components of adipocytes, they

have functional significance as discussed later (Section 1.4). Thus, regulation of cholesterol and lipid metabolism is also closely related to "adipocyte turnover".

1.2.4.1 Commitment of Stem Cells into Adipogenic Lineage

Fat tissue is highly heterogeneous. When considering the differing ontogenetic, morphogenetic and functional properties of various depots, it is relevant to conceptualize different adipose pads as separate "mini-organs" (39). These mini-organs appear to arise from distinct progenitor cells. Further the distinctive structural, developmental, and functional characteristics of preadipocytes and adipocytes in subcutaneous and visceral adipose depots involve hundreds of genes (40). These genes are engaged in adipogenic determination and development, and also in cellular cholesterol and lipid metabolisms. Accordingly, depot-specific gene expression patterns designate the regional heterogeneity of fat, and link this regional heterogeneity to differences in functional characteristics between different adipose tissues (41). These distinctive (depot-specific) gene expression patterns assist (pre)-adipocytes to attain the individual cellular instruments for different cellular tasks, such as lipid synthesis, intracellular transport, thermogenesis, insulin signalling and secretion of adipokines. However, "the core" of adipogenesis is identical for all adipocyte types and proceeds through activation of the CCAAT/enhancer binding protein (C/EBP) and peroxisome proliferator-activated receptor γ (PPARγ) signalling pathways (42).

Adipose tissues are packed with stem cells committed at different levels into the adipogenic lineage (43, 44). Vascular stem cells are multipotent. They can therefore give rise to a variety of cell types, including preadipocytes or fibroblasts. Some studies have also reported that adipose stem cells can differentiate into macrophages (45). Nevertheless, adipose multipotent stem cells possess the same considerable potential to differentiate as their close relatives, BM-derived MSCs.

The first step in adipogenesis is commitment of multipotent stem cells into preadipocytes. This requires modification of the gene expression profile of the cell, but at this stage there is no morphological change. Thus, preadipocyte progenitors and preadipocytes show similar morphology (46). Determination of multipotent stem cells into adipogenic lineage is a very complex process; many researchers have focused on the second (mitotic clonal expansion) or third (terminal differentiation) steps of adipogenesis, leaving this initial, critical transition unresolved.

MSCs adopt a different phenotype depending on both intrinsic and extracellular factors. Examples of extrinsic factors include tissue fluid flow, pressure, compression, tension, matrix stiffness, and cellular shapes (47). These considerations are because adipose tissue is highly dynamic, and adipocytes rendered hypertrophic by nutrient overload can easily cause mechanical changes in the tissue which may recruit (further occupy) more stem cells into the adipogenic lineage. Other changes that are the consequences of adipocyte hypertrophy, such as an increase in pericellular matrix, surface cadherin molecules, and changing cytoskeleton can provide signals that augment predisposition of stem cell commitment into adipogenic lineage.

Another important determinant of stem cell fate is cross-regulation by differentiation factors (35). Multipotent stem cells express low levels of factors specific to several different lineages. Factors characteristic of one lineage can suppress differentiation into another type. For example, adipogenic factor PPARγ suppresses runt-related transcription factor 2 (RUNX2) expression, which belongs to the osteogenic lineage (48). Likewise, Rho-associated kinase (Rho-kinase/ROCK) is an anti-adipogenic agent which promotes myogenesis in stem cells. The balance between these factors is delicate and, depending on the stimuli, easily changes the stem cell fate.

1.2.4.2 An Exceptional Phenomenon - Mitotic Clonal Expansion

Preadipocytes are recruited from a pool of multipotent or pluripotent (49) stem cells which reside in the SVF of adipose tissue. They are unipotent and exhibit self-renewal properties similar to multipotent stem cells, but they can only differentiate into one cell type, adipocytes (50).

The cell cycle is a term used to encompass all the events culminating in cellular division (51). During interphase, a cell grows in size, perhaps undergoes morphological changes, replicates its deoxyribonucleic acid (DNA) and assembles its cellular machinery (division proteins etc.) to prepare for mitosis. Mitosis happens after passing a checkpoint control (G_2), when the cell employs its energy and structural sources solely for cell division (Fig. 1.4). There are several checkpoints in the cycle, and these are responsive to the cell sensing the relevance of the conditions for its division, as well as the integrity of its DNA and cellular machinery, as to whether it is ready for division or not (52). There is a restriction point in the cell cycle (leading to growth arrest) where the cell makes a determination to become quiescent (G_0). As such this restriction point suppresses the preparations for cellular proliferation, and allows continuation of cell growth and phenotypic transformation/differentiation (53). Accordingly, cell division and differentiation do not happen synchronously; however, mitotic clonal expansion of preadipocytes poses a possible exception to this rule (54).

As mentioned, the fundamental instruments for adipogenic differentiation are the PPARγ and C/EBP protein families of transcription factors (42). Their activity confers the cellular equipment required for acquisition of the adipocyte phenotype. PPARγ is the master regulator (orchestra conductor) of adipogenic differentiation. It is obligatory for adipocyte differentiation, as, in its absence, no other factor has been identified which can orchestrate adipogenesis (55, 56). PPARγ is also important to maintain the differentiated state of adipocytes. C/EBPβ and C/EBPδ are pro-adipogenic transcription

factors which stimulate the expression of C/EBPα and PPARγ by binding the C/EBP regulatory elements in the promoters of related genes. However, C/EBPβ molecules expressed upon hormonal stimuli lack the ability to bind DNA. Initially, therefore, C/EBPβ cannot function to accelerate the adipogenic cascade (40). Upon hormonal induction (shown *in vitro*), the DNA-binding ability and activity of C/EBPβ occur after approximately 14 hours, and it reaches its full capacity at 24 hours. In this 24 hours, although preadipocytes commit to differentiate, they can only divide one or two more times until C/EBPβ acquires its DNA binding activity and activates transcription of *C/EBPα* and *PPARγ* genes. C/EBPα and PPARγ have anti-mitotic properties, thereby ensuring that preadipocytes escape from the cell cycle and focus entirely on terminal differentiation.

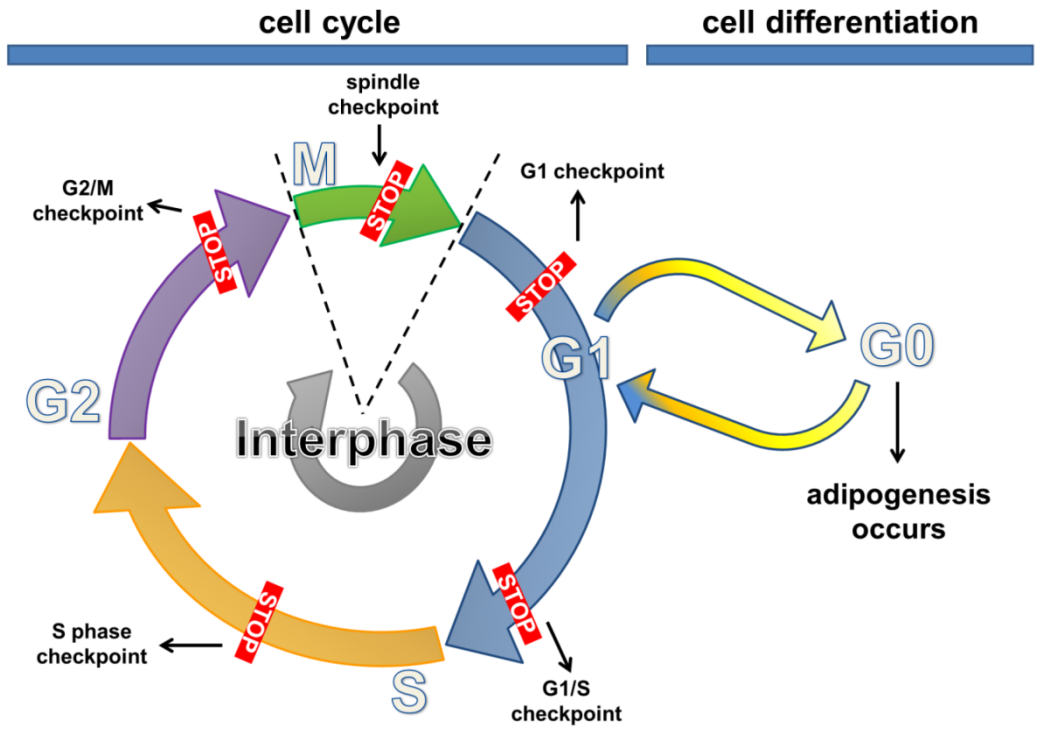

Figure 1.4: Overview of the cell cycle. In mammalian systems, tissues grow by the division and differentiation of various cell types. There is a delicate balance between these two indices, and cells do not differentiate when they have entered the cell cycle.

This "post-confluence mitosis" is a very rare phenomenon in eukaryotic organisms and the reason for it is still not clear. Unresolved issues are whether it is an essential part of the terminal adipogenic differentiation, or whether it is a delay caused by the slow maturation period of C/EBPβ molecules.

1.2.4.3 Terminal Differentiation of Preadipocytes

After their clonal expansion, late-stage preadipocytes commit to terminal adipogenic differentiation. This process is mainly orchestrated by PPARγ activity. Although brown-, beige- and white-adipocytes do not share the same ontogenetic and functional characteristics, both types of adipocytes share similar transcriptional machinery that leads to the terminal differentiation into adipocytes. As stated earlier, the transcript profile of adipogenesis is regulated by combination of C/EBPα and PPARγ. Brown/beige adipocytes (more details in Section 1.2.6) express all genes which are expressed in white adipocytes, but in addition they express distinctive genes that give them the brown characteristics (Fig. 1.5) (57, 58). Forkhead box protein C2 (FOXC2) is a key browning transcription factor. It stimulates the response to adrenergic stimuli, and initiates browning of the adipocyte phenotype. The factors leading to the white-to-brown adipocyte switch are co-activators, such as steroid receptor coactivator 1 (SRC1), PPARγ coactivator 1α (PGC1α), and PR domain containing 16 (PRDM16)**.** Pro- and anti-adipogenic factors regulate overall adipogenic differentiation. Some of these factors are Kruppel-like factors (KLFs), ancient signalling pathways such as WNT-, hedgehog- or notch-signalling, the mitogen-activated protein kinases (MAPK) pathway, and insulin and insulin-like growth factor 1 (IGF1) signalling.

Studies on gene knock-out mice have revealed important details about adipogenic differentiation, for instance liver X receptor (LXR). LXR is a transcription factor family that interacts with several nuclear receptor molecules, such as the PPARs, farnesoid X

receptor (FXR), and sterol regulatory element binding protein 1 (SREBP1). Together with these factors, LXRs play a pivotal role in the regulation of cholesterol, fatty acid (FA), and glucose homeostasis (59). In 2005, Isabelle Gerin and her colleagues reported that *Lxrα* and *Lxrβ* double knock-out (KO) mice develop normal adipose tissue, but show impaired capacity to increase adipocyte size and tissue mass with nutrient overload or during aging. A similar study has been conducted with *Srebp2* KO mice (60). SREBP2 is a key transcription factor for regulation of cholesterol metabolism, and plays regulatory roles in terminal adipogenic differentiation. Regulation of adipogenesis is also subjected to with different molecular mechanisms, such as miRNAs, epigenetic regulations (matrix interactions, angiogenesis etc.), and transcription factor/co-activator interactions.

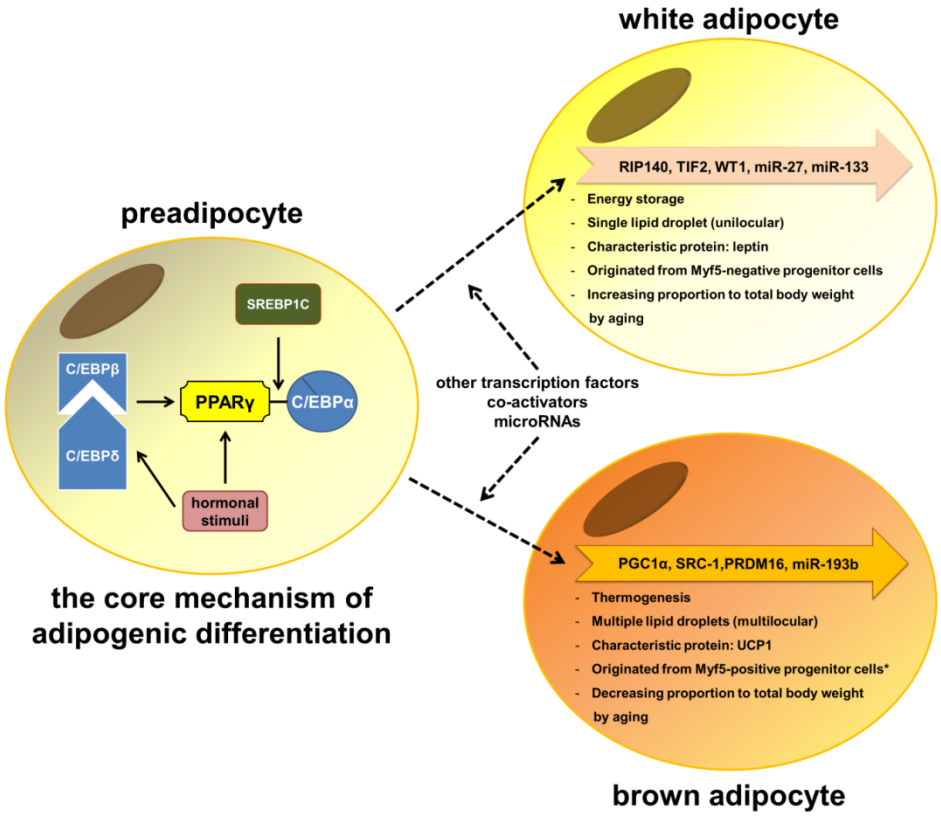

Figure 1.5: The differing characteristics of white and brown adipocytes. The core mechanism of adipogenesis is similar for both adipocyte types, but the assisting co-activators, microRNAs, and other transcription factors determine the cell fate. White adipocytes have evolved essentially to store lipids, whereas brown adipocytes use lipids for thermogenesis.

1.2.5 Adipose Structural Characteristics and Functional Differences

Mammalian adipose is traditionally sub-grouped into two physiological classes: WAT and BAT (61). According to this classification, both visceral and subcutaneous pads are considered WATs. WATs can be found in different parts of the body. Surrounding the heart, heels, hips, periorbital region, kidney and omentum are a few locations where fat is deposited. A considerable number of adipose pads serve only as a structural scaffold in the body, as a cushion against mechanical impact.

The most characteristic histological feature of WAT is the presence of unilocular adipocytes (62). A single large lipid droplet (LD) occupies most of the cell, and other cellular contents, including the nucleus, are squeezed into an outcropping at the periphery. These cells have minimum numbers of mitochondria. White adipocytes are highly dynamic; they can readily enlarge and shrink depending on the metabolic state, via lipogenesis vs. lipolysis (63). Among important extracellular and intracellular receptors which are located on these adipocytes, insulin and growth hormone receptors have special importance for sustaining systemic energy homeostasis. In addition, adipocytes can secrete and recognize diverse hormones which regulate a wide range of physiologic process, from immune responses to haemostasis, from sex determination to blood pressure control (64).

Compared to WAT, BAT gains its brown colour from mitochondria-rich multilocular adipocytes as well as from its rich vascularization (65). BAT is highly abundant during the neonatal period and in hibernating animals; it provides enough heat for survival (66). In adults however, BAT distribution in the body is quite limited.

Uncoupling protein 1 (UCP1) is transmembrane protein located between the mitochondrial matrix and intermembrane space (IMS) (67, 68). Energy stored in molecular bonds is termed “chemical energy”. By UCP1 activity, brown adipocytes can transform chemical energy into thermal energy, in other words, produce heat. The exact

function of UCP1 remains largely unknown; however, long-chain fatty acid (LCFA) anions activate UCP1 to transport protons-(H^+) from the IMS to the mitochondrial matrix. Such proton leak causes mitochondria (therefore the cell) to produce heat instead of generating high-chemical energy molecules in the form of adenosine triphosphate (ATP).

Adaptive thermogenesis is a well-documented phenomenon, especially in rodents, and it contributes to energy homeostasis by consuming energy. Adaptive thermogenesis helps maintain the optimal body temperature at a tightly regulated level; cold is the main inducer of adaptive thermogenesis (69). In addition, some studies have reported that adaptive thermogenesis can also be induced by certain nutrients/diets (70); however, this phenomenon has not yet been fully elucidated.

Beta (β)-oxidation is the chemical reaction where FA molecules are catabolized to smaller compounds (71). β-oxidation in BAT is abundant and contributes substantially to the body's total energy expenditure. Acetyl-CoA, an end product of β-oxidation, enters the Kreb's cycle (citric acid cycle) in mitochondria. The Kreb's cycle is a series of enzyme-catalyzed chemical reactions that eventually create a proton gradient that can be used by other protein complexes to produce ATP molecules (72). As stated above, UCP1 provides an alternative route for these protons in brown adipocytes (67). β-oxidation is a common form of mitochondrial oxidative phosphorylation (OXPHOS) (73). BAT needs a liberal supply of oxygen; this is why BAT has a greater blood supply (larger number of capillaries) than WAT. The blood circulation of BAT also serves to transfer heat from where it is generated to other areas where it is needed.

Aggregation of mitochondria confers the brown colour to BAT cells under light microscopy, but having high numbers of mitochondria has other consequences for cell fate. Thus, mitochondria are an important source of reactive oxygen species (ROS) leakage (74). ROS are highly toxic molecules. For this reason, there are some tightly-

regulated protective mechanisms against ROS in eukaryotic systems, such as superoxide dismutase enzymes, that serve as an anti-oxidant defence (75). Nevertheless, ROS still contribute to many "defects" in the body, such as cell senescence (aging) or DNA damage in cancer initiation. In 2010, Rebecca Oelkrug and her colleagues reported that UCP1 reduces superoxide production in brown adipocyte mitochondria (68). Considering the above aspect, BAT is clearly a beneficial tissue that has great potential to contribute to energy homeostasis and to general health by reducing the burden of oxygen metabolites.

1.2.6 Beige Tones in White Adipose

While the relationship between visceral adiposity (visceral obesity) and metabolic comorbidities, such as insulin resistance and T2D, has been mentioned, subcutaneous adipose tissue has been accepted as a "metabolic sink". Thus subcutaneous adiposity appears to be relatively less harmful, and potentially beneficial to the body (76). Considering the fact that adipose in both sites is white, the question arises on to why visceral adiposity should be hazardous whereas subcutaneous adiposity is relatively benign. The essential problem is the narrow breadth of the question, because subcutaneous adipose tissue is actually not a "pure" white tissue; it can reveal different shades of "beige" depending of adjustment to whole body energy homeostasis.

Temperature control is tightly regulated in the human body. Different times of the day or different parts of the body can exhibit slight changes, but core body temperature is fixed around 37^0C. Humans can survive in a wide range of climates, indicating that there are thermoregulatory mechanisms which provide easy adaptation for humans (and rodents) to a variety of different climatic states. Depending on the temperature, these mechanisms can be shivering, sweating, vasoconstriction, and uplifting hair follicles (pilo-erection). In cold weather, human skin-subcutaneous adipose tissue forms an

important barrier for heat insulation; recently, researchers have started to understand that this complex tissue is not only responsible for heat insulation, but is also responsible for heat production (similar to BAT). This phenomenon is a good example of beneficial effects of subcutaneous adipose tissue because during the human evolution, the existence of beige adipocytes under the skin has conferred the great advantage of a heat-producing thermo-regulative capability. By this capability, the human body could adapt to colder climates and protect itself from the dangerous consequences of hypothermia.

Beige adipose in subcutaneous sites owes its colour to a third kind of adipocyte that has been recently identified, in addition to unilocular white and multilocular brown adipocytes. An alternative term is “brite” adipocytes (77). Beige adipocytes are highly abundant in subcutaneous adipose tissue. They show a distinct gene expression pattern, and their origins are different from white adipocytes (78). Beige adipocytes express characteristics of both white and brown adipocytes. For instance, like brown adipocytes, they are thermogenic cells. On the other hand, although they are often not unilocular like white adipocytes, they can contain quite large LDs (79). Beige adipocytes are anti-obesogenic cells; as in brown adipocytes, they express UCP1 although at a comparatively lower basal level. However, stimulation by cold or other factors can strikingly increase UCP1 levels in beige adipocytes, conferring to these cells thermogenic capability (80).

Increasing the number of beige adipocytes in subcutaneous adipose tissue is called “browning”. A cold stimulus, activation of β-adrenergic pathways, and some hormone stimuli can induce browning of subcutaneous fat (79). The process of browning involves mitochondrial aggregation and cellular proliferation/differentiation of beige adipocytes. Subcutaneous adipose tissue is prone to browning, whereas browning is rare

in visceral WAT. Why browning is less at this site has aroused curiosity on the origins and development of beige adipocytes.

1.2.6.1 Brown vs. Beige Adipocytes

Brown fat is located in the interscapular region of human newborns. There are data supporting the existence of brown adipose in the perirenal area in adults (81). In rodents, brown fat is widely dispersed throughout the body (82). Nonetheless, determining the localization of brown fat has not yet been fully resolved.

Non-shivering adaptive thermogenesis is driven by a set of genes that are regulated by a β-adrenergic receptor/cyclic adenosine monophosphate (cAMP) dependant pathway in both brown and beige adipocytes (83). Despite the similar properties, brown and beige adipocytes show a different gene expression pattern in cell culture (79). In addition, the response of beige adipocytes to genetic manipulations and hormonal stimuli differs from that of brown adipocytes.

Several studies have demonstrated that brown adipocytes arise from a skeletal muscle origin (84, 85). Myogenic factor 5 (MYF5) is a regulator of myogenesis (muscle cell differentiation) that is essential for skeletal muscle development. Brown adipocytes and myocytes both express MYF5, whereas white and beige adipocytes do not (Fig. 1.6). This observation suggests different developmental origins for brown and beige adipocytes. In 2014, Bruce Spiegelman and his colleagues suggested a smooth muscle-like origin for beige adipocytes (78).

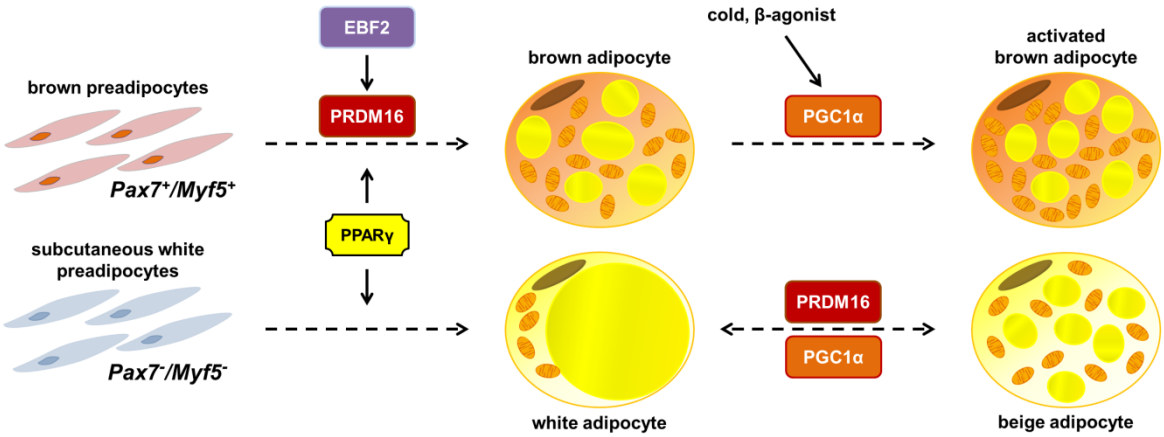

Figure 1.6: Transcriptional regulation of brown and beige adipocyte development. *Pax7*$^{+}$/*Myf5*$^{+}$ preadipocytes give rise to brown adipocytes, whereas white adipocyte progenitors do not express these genes. In addition to the machinery central to adipogenesis, PRDM16 orchestrates promotion of the brown phenotype in *Pax7*$^{+}$/*Myf5*$^{+}$ preadipocytes. Induction of PGC1α by external stimuli, such as cold exposure and β-agonists, activates brown adipocytes to produce more mitochondria and generate heat. Abbreviations: *Myf5*, myogenic factor 5; *Pax7*, paired box protein 7; PGC1α, PPARγ-co-activator 1 alpha; PPARγ, peroxisome proliferator-activated receptor gamma; PRDM16, PR domain containing 16.

As previously mentioned, adipose tissue contribution to metabolic comorbidity depends on its localization (visceral vs. subcutaneous). For example, visceral adipose tissue has been accepted to be more prone to inflammatory recruitment than subcutaneous fat. The present limited knowledge cannot explain the main reasons behind these functional and physical differences between visceral vs. subcutaneous compartments; however, browning in subcutaneous adipose tissue provides a strong clue for the functional differences.

1.2.6.2 A "Browning" Transcription Co-Regulator: PRDM16

There is an important factor for adipose browning: PRDM16. PRDM16 is a transcription co-regulator that controls the muscle/brown differentiation switch in early embryologic development (84). In adults, PRDM16 is expressed in some WATs, and so too is UCP1 expressed under certain stimuli. These data suggest the involvement of PRDM16 in beige adipocyte development.

Prdm16$^{-/-}$ mice are prone to develop profound visceral obesity (86). This could reflect the important role that PRDM16-driven beige adipocytes plays in whole body energy expenditure, since these are "mitochondria-rich" cells. A striking discovery was that PRDM16 and WT1 are reciprocally regulated. WT1 expression is exclusively specific to visceral adipose, and reciprocal regulation of these factors determines the visceral vs. subcutaneous gene expression program. PRDM16 regulates UCP1 accumulation (23). Bruce Spiegelman and his colleagues have shown that absence of PRDM16 results in ablation of beige cells, triggers more subcutaneous adiposity, and switches on "visceralization" of adipose characteristics, even cells located in subcutaneous sites (86). In this way, *Prdm16* gene is effectively a "switch button" between visceral and subcutaneous adipose phenotype. However, the mechanisms by which PRDM16 production and activity are regulated remain largely unknown. Cold is a main stimulus. In addition, β-adrenergic agonists induce PRDM16 activity. Given the fact that β-adrenergic receptor stimulation expands the lung (bronchodilation) and prepares the body for exercise (increased blood flow) (87), increased physical activity may also influence PRDM16 expression and the number of the beige adipocytes. This possibility was a focus for the experiments described in Chapter 6. The important metabo-protective effects of PRDM16 expression in beige adipocytes also provide a target for drug development, holding great potential as a new class of therapeutics to combat obesity-related disorders.

1.2.7 Subcutaneous vs. Visceral Adiposity: An Ergonomic Issue

The central theme of this research in that adipose function is a key factor in metabolic health, but due to several reasons (discussed later), adipose tissue can fail to function optimally. In terms of comprising an efficient reservoir of stored energy, such dysfunction or failure is responsible for metabolic obesity.

A sustained disequilibrium in energy balance (energy intake vs. expenditure) can initiate adipose tissue expansion. However, adipose tissue has a limited capacity to expand. Particularly visceral fat, which is packed inside the body cavities and links internal organs, and therefore it has a more restricted potential for enlargement. Within body compartments, visceral adipose depots are usually connected and surround other tissues and organs. The abdomen, formed by the abdominal muscles, pelvis, and the ribcage, is a firm structure and relatively inflexible to accommodate anatomical changes effectively. Therefore, over-expansion of visceral adipose pads in the abdomen is potentially harmful to other organs; it needs to be kept under control.

Compared to the semi-rigid constrains of body compartments, the skin is a soft tissue organ which covers ligaments, muscles, and bones (88, 89). The epidermis is an outer layer of the skin, forming the major barrier which protects the body from mechanical and other physical external impacts (90). Dermis is the middle layer of the skin. It contains functional units such as sensory receptors or sweat glands. It is also rich in ECM components, and this ECM framework provides mechanical strength to the dermis (and therefore the skin), as well as an almost unlimited flexibility to this soft tissue (91). The dermis also contains a significant number of stem cells to sustain the high rate of skin turnover required for its renewal (92). Hypodermis is not really a part of the skin, but it lies immediately beneath the dermis. It is in this layer where subcutaneous adipocytes reside (Fig. 1.7) (93). Considering these details, it can be appreciated that subcutaneous adipose tissue beneath the skin has more space to enlarge than do visceral fat depots.

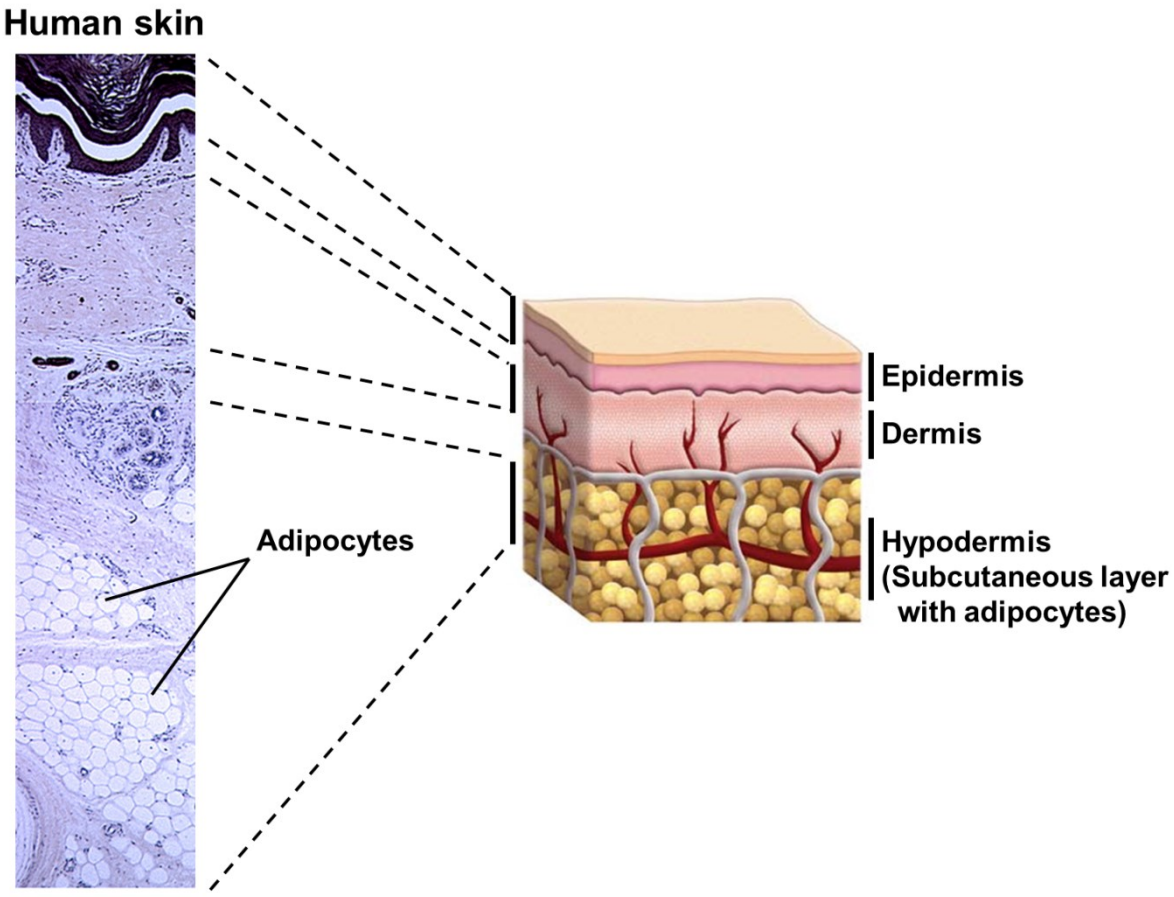

Figure 1.7: Human skin layers and adipocytes in the subcutaneous layer (hypodermis). Illustration taken from ©iStockphoto.com/James_Steidl.

At this stage, the question arises: what factors determine the particular adipose tissue for storage of excess energy? Unfortunately, the mechanisms guiding/directing excess energy into adipose pads remain largely unknown. Distinct gene networks regulate the development of adipose tissues. These transcriptional programs can be reprogrammed over an individual's life, for example during the menopause in women (94). Particular programs could be inherited within families, as noted by anecdotal observations of body shape within families, but this requires more formal study. The topology of regional fat deposition is yet to be understood, but it could provide an important tool to understand the nature of obesity. For example, numerous clinical studies have reported that some individuals with severe adipose expansion seem to exhibit normal physiology or hormonal profiles. Such healthy but highly overweight people are classified as

"metabolically healthy obese" (MHO). They exhibit increased subcutaneous adiposity (95), and show limited expansion of visceral fat (less abdominal obesity). It is still debated whether calling metabolically healthy people "obese" or "overweight" is appropriate. In this thesis, obesity is discussed as an unhealthy state.

1.3 Regulation of Energy Homeostasis and Insulin Sensitivity

Adipose tissue contributes importantly to whole body energy homeostasis (96). It can take up, store, and release such nutrients as glucose (converted to FA in lipogenesis) and FAs, as well as structural molecules like cholesterol. Adipose also releases lipids for use as an energy molecule for other tissues. By releasing certain hormones, adipose tissue(s) also programs the hypothalamus to organize "appetite" regulation (97). As with other organs in the body, adipose tissue has a unique developmental, structural, and functional pattern and physiological limits as outlined in section 1.2. Different mechanisms and genes regulate expansion of the adipose storage capacity; however, details about these gene cassettes and their regulation remain largely unknown. What is known that adipose tissue of some individuals exhibit higher capacity to expand than other individuals, and in such "protected" individuals, some depots appear able to store fat without showing any abnormal signals. Such overweight/obese individuals may be said to be "metabolically obese healthy" (MHO) (section 1.2.7).

1.3.1 Energy Homeostasis

There is no universality in the capacity of human organ systems. Mutations, polymorphisms, and epigenetic alterations such as genomic imprinting or histone modification predicate the capacity and limits of organ functions. Accordingly, some individuals can have a "better quality" adipose tissue which retains its normal functioning despite the physiologically unusual circumstances of consistent nutrient

overload and minimal energy expenditure. Conversely, others, even under circumstances of relatively minimal energy surplus, have adipose tissue that readily emits stress signals (or "S.O.S.") (restricted lipogenesis, increased lipolysis, stress and inflammation etc.). These stress signals are discussed in later sections of this chapter, and are the subject of research throughout this thesis. In sum, the phenomenon of adipose stress (or dysfunction) indicates the potential harmfulness of obesity.

In humans and the mammals (such as rodents), food intake is regulated by specific appetite hormones (98). The appetite traffic control centre resides, principally in the hypothalamus (99). Brain signals (such as neuropeptides), the gastrointestinal endocrine tissue, and the systemic circulation converge on the hypothalamus to regulate energy homeostasis (food intake vs. energy expenditure). The amount and pattern of release of appetite-regulating hormones differs between normal weight and obese individuals.

1.3.1.1 "Eating"

Hunger is a subjective motivational state. In the physiological sense, hunger (feeling) increases when the body needs fuel. As mentioned above, this feeling is orchestrated via appetite hormones, such as leptin, adiponectin, insulin, and ghrelin. Hunger signals are initiated from the gastrointestinal system and increase as the circulating blood glucose concentration falls. Moreover, blood levels of other molecules such as amino acids, peptides, and FAs can also provide direct and/or indirect information or feedback to the brain, which coordinates feeling of hunger and food intake in response to this feeling. The brainstem, adjacent to the hypothalamus, is another important part of the central nervous system responsible for controlling ingestion behaviours (100). Eating is an ingestion process that is directly related to the energy balance in the body. Hunger, eating, and satiety are regulated by a neuronal circuit between the endocrine system (located in the gastrointestinal tract, pancreatic β cells and adipose tissue),

hypothalamus, and brainstem. Mutations and polymorphisms in this circuit alter behaviours in ways that lead to the development of obesity (101, 102).

Regulation of feeding behaviours is complex; for instance, there is emerging evidence that circadian rhythm is an important determinant in the development of obesity and insulin resistance; the circadian rhythm of an individual can assign or establish specific times for eating events during the 24h day (103). Prior to these certain time periods, the body initiates insulin secretion, so causing a decrease in blood glucose levels and a resultant "pre-meal hunger" feeling. For instance, irregular shift-workers or long-flight pilots may be inclined to gain weight more easily than regular shift workers because of the disruption of their circadian rhythm-adjusted insulin secretion pattern.

1.3.2 Insulin

Insulin is a peptide exclusively produced by pancreatic β cells (104). It controls energy homeostasis by promoting glucose uptake by cells (adipocytes, myocytes, neurons etc.) from the circulation, and by suppressing hepatic glucose production. Accordingly, the amount of insulin produced and secreted by β cells is proportional to the blood glucose levels, teleologically because very high glucose levels are toxic for the body and insulin helps to keep blood glucose levels in a "nontoxic" range. Besides its circulating glucose lowering effect, insulin has diverse anabolic and catabolic effects on other metabolic pathways and in several cell types (105, 106, 107). In light of all these functions, insulin is an important regulator of whole body energy homeostasis.

At the postprandial stage, glucose is taken up by β cells of the pancreatic islets (108). Within these β cells, glycolysis generates ATP which further triggers a chemical cascade resulting in the release of insulin (Fig. 1.8). While other factors contribute to insulin secretion or its inhibition, increasing blood glucose is a constant stimulus for insulin release. Insulin release is episodic (109). Several compounds and neuronal

signals provide a feedback network to the pancreas and, depending on the individual's metabolic rate, the quantity of insulin released, and the periodicity of oscillations in the pattern of insulin release can change.

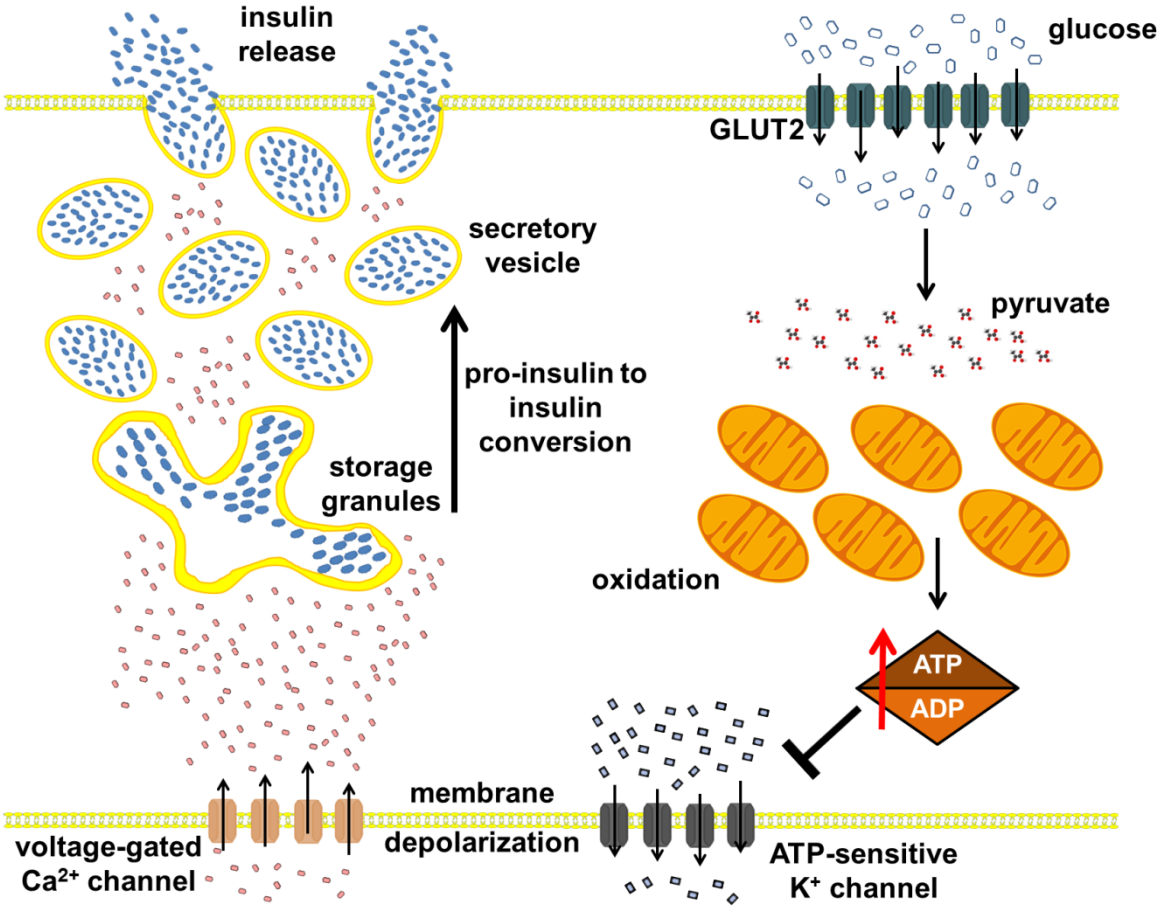

Figure 1.8: Insulin secretion from pancreatic β cells. Increased ATP levels close ATP-sensitive K^+ channels and open voltage-gated Ca^{2+} channels via membrane depolarization. Increasing cellular Ca^{2+} levels regulate movement and fusion of insulin-containing vesicles to the plasma membrane for the exocytosis of insulin molecules.

Healthy adipose tissue responds promptly to low concentrations of insulin. The first response is rapid clearance of glucose from the circulation. Conversely, an obese individual with a sedentary lifestyle can have stressed adipose tissue (discussed later) that resists responding to the insulin stimulus, and thereby, shows impaired or delayed glucose clearance from the circulation. Accordingly, the insulin responsiveness of

tissues such as adipose and muscle determines overall whole body insulin sensitivity (110); the contribution of muscle is higher than adipose depots (111).

1.3.2.1 Bodily Response to Insulin

Bodily (systemic) "insulin sensitivity" is defined by the duration of the clearance profile of postprandial blood sugar from the circulation (110). Insulin-sensitive individuals show a rapid increase in blood insulin levels upon feeding until the blood glucose is restored to certain lower levels.

Insulin resistance starts, at least initially, in response to lifestyle imbalance, and this is compounded by aging. Thus, it occurs when individuals take unhealthy habits, such as over-eating, irregular sleeping habits (altered circadian rhythm), and sedentary lifestyle. The severity ranges from mild insulin resistance to pre-diabetes (with increased fasting blood glucose [FBG]) and type 2 diabetes (112). Insulin resistance results in glucose intolerance which has potentially harmful consequences on the body. In humans, blood glucose concentrations between 7.8 – 11.0 mmol/L at 2 hours after a meal or glucose challenge (oral glucose tolerance test) indicate glucose intolerance, which is attributed to insulin resistance. In a recent study in mice, FBG levels between 10 – 15 mmol/L were defined as pre-diabetic, whereas levels higher than 15 mmol/L were accepted as the diabetic phenotype (113).

In mild insulin resistance, pancreatic β cells release more insulin molecules into the circulation in an attempt to overcome the relative lack of responsiveness of tissues to insulin (114). Herein lies a key issue: insulin resistance, as defined, pertains uniquely to carbohydrate metabolism, not to other of the biological effects of insulin. Specifically, insulin is an important anabolic/catabolic agent, and a prolonged increase in blood insulin level itself has important metabolic consequences, particularly on lipid turnover, as will be discussed later. In addition, the sustained effort of β cells to produce, store,

and release more insulin may cause cellular stress to those β cells, thereby impairing their function and eventually causing their deletion by apoptosis (the interesting cell biology behind this is beyond the scope of the present review) (115, 116). At this stage, blood insulin levels will be less increased because the stressed and damaged β cells become dysfunctional and the β cell mass decreases. β cell dysfunction, together with the severity of systemic insulin resistance, determines the incidence and severity of T2D (117). Unlike type 1 diabetes (autoimmune destruction of β cells), T2D is established on the severity of the insulin resistance; therefore T2D is associated with obesity and can be prevented or glucose tolerance improved by a more active daily life and healthier-eating (118, 119).

1.3.3 From Tissue to Whole Body Insulin Resistance

Different tissues contribute differently to systemic (overall) insulin resistance. Myocytes (muscle cells) are one important regulator of body energy homeostasis and an important target for insulin. Cardiac and smooth muscle (in intestines, blood vessels etc.) contract unconsciously whereas skeletal muscle works voluntarily (120). By the contraction of myofibrils, muscle provides motion to the organism, and this requires work; therefore, muscle cells utilize large amounts of ATP molecules as their energy source.

1.3.3.1 Muscle and Exercise

Oxidation of carbohydrates is the main energy source in myocytes. In muscle, glucose is stored as glycogen molecules. An 80 kg young male (normal BMI) has an average of total 0.6-1.2 kg glycogen mass (average over a day), nearly all of it is stored in skeletal muscle cells (a small quantity is in liver) (121). Nevertheless, muscle cells use far more

glucose than they store. Muscle is a leading tissue for energy consumption. As a result, myocytes gain a special importance in the regulation of total body insulin sensitivity.

Physical activities such as running, pulling, pushing or jumping result from the contraction of muscles. There are different types of muscle contractions depending on several parameters (muscle shortening vs. muscle lengthening etc.) but the common factor is that every muscle requires energy for contraction (122). The source of energy for contraction is ATP molecules, but the molecules that are used to generate ATP vary in myocytes, as discussed next.

1.3.3.2 Energy Expenditure in Muscle and Insulin

According to the sliding filament theory, ATP hydrolysis to form adenosine diphosphate (ADP) molecule reorients myosin heads and binds them to neighbouring actin filaments; this event forms myosin cross-bridges (123). With the removal of ADP, myosin cross-bridges rotate, and when myosin heads bind new ATP molecules, the cross-bridges release the actin filaments and cause one unit motion along the filament. When secondary ATP molecules are hydrolyzed to ADP, myosin heads become reoriented to the initial position (124). The repetition of this event requires large amounts of ATP. In addition, the reduction of ATP during physical activity (contractions) activates other cellular pathways in myocytes, in order to generate more ATP molecules.

A higher AMP/ATP ratio in myocytes increases the phosphorylation of AMP-activated protein kinase α (AMPKα) (125). In turn, phospho-(P)-AMPK reorganizes cellular metabolism. It modulates increases in mitochondrial biogenesis, FA oxidation, and glucose transport (uptake). In myocytes, GLUT4 is the main glucose transporter and P-AMPK controls its effective function (126). It does this by phosphorylating AKT substrate of 160 kDa (AS160) proteins that facilitate the localization of GLUT4 vesicles

into the plasma membrane. This event increases cellular glucose uptake into the cytoplasm, offering a direct link between muscle activity and glucose clearance from the circulation (127).

Insulin has multi-dimensional effects on muscle tissue. The anabolic effects of insulin on muscle have been long debated in both medical and sports circles. Some scientists suggest that insulin increased the protein synthesis of myocytes, whereas others claim the opposite (128). Nonetheless, recent studies have shown that insulin can increase or decrease the metabolic rate of myocytes in a dose-dependent manner (129, 130). It seems likely, therefore, that insulin is an important regulator of myogenesis (131).

Insulin initiates signal transduction in myocytes by binding to insulin receptors. Insulin-stimulated phosphorylation of its receptors induces signal transduction through the insulin receptor substrates (IRS)-1,2 and phosphatidylinositol 3-kinase (PI3K) proteins (132, 133). The effects of regular muscle activity on all these molecules can vary. Different studies have reported upregulation or downregulation of insulin receptors, as well as on the adapter molecules (IRSs and PI3K), depending on the duration and intensity of the exercise (134, 135). Effectively, insulin signalling travels through a cluster of molecules resident on the intracellular surface of the cell membrane until it results in the activation of protein kinase B (AKT) by its phosphorylation. Phospho-(P)-AKT is a serine/threonine-specific kinase that regulates such key metabolic mechanisms as cell survival (inhibition of apoptosis), cell division (escape from G1 cell cycle arrest), glycogen synthesis (increased), and upregulation of GLUT4 production and localization on the cellular surface (136, 137).

While muscle insulin sensitivity correlates positively with the extent of physical activity, there are other effects of exercise training on myocytes that need to be considered. For instance, it is apparent that exercise enhances myocyte insulin sensitivity by improving intracellular insulin signalling, while activation of AKT and

AMPK results in increased glucose uptake from the circulation into myocytes (138, 139). Moreover, factors improved by insulin signalling, such as enhanced cell survival, stimulated cell proliferation, and increased mitochondrial biogenesis favour muscle development (140, 141). A characteristic feature of T2D is skeletal muscle with impaired insulin signal transduction (142). Exercise improves muscle (and therefore systemic) insulin sensitivity, with the obvious implication that exercise is a possible intervention to prevent development of T2D, as well as to improve glycemic control.

1.3.3.3 Aerobic vs. Anaerobic Respiration in Myocytes

A sedentary lifestyle substantially decreases the energy consumption rates of an individual. As previously mentioned, easy access to food and over-eating cause high calorie intake. One of the best ways to balance the excess energy intake is to increase energy expenditure with an active lifestyle. However, increased physical activity is not the ultimate solution for the prevention of obesity and T2D development because myocytes have a finite capacity for contraction. This is partly because they require a maintenance period/break between sessions of physical activity.

Myocytes harvest ATP molecules by glycolytic activity; glycolysis can happen either in the presence or absence of oxygen molecules (143). Aerobic (oxidative) respiration is an efficient way of producing ATP from glucose, and the end product, pyruvic acid, can be used in other reactions. The problem with oxidative respiration is that it is slow, and it is not able to provide sufficient energy to myocytes during short-burst or long-lasting exercise (144). When myocytes require higher amounts of energy than is contained within the ATP reserves (demand > supply), they undergo anaerobic respiration. Even though this is a faster way of producing ATP molecules, it is less efficient (145). Further, the end (waste) product of anaerobic respiration is lactic acid (lactate), the accumulation of which is toxic to myocytes (146, 147).

1.3.4 Effects of Energy Surplus on Muscle

When energy intake overwhelms the amount of energy that an individual can spend by physical activity (which depends on the muscle/exercise capacity), weight gain becomes inevitable. Despite this, an individual may prefer a sedentary lifestyle. As a result of such a lifestyle, myocytes could be inactive, not oxidize energy molecules, and become engorged with glycogen (later fat) molecules. If this is the case, they do not have further capacity to take up or process glucose from the circulation (148). This triggers down-regulation of the insulin response in myocytes, so as, teleologically, to protect themselves from the energy surplus. As a consequence, systemic insulin resistance increases (149).

1.3.4.1 Molecular Modifications in Myocytes

In order to tolerate energy surplus, muscle cells undergo substantive metabolic modifications. As mentioned in section 1.3.2, nutrient response is mainly regulated by insulin (and IGF1). Insulin orchestrates cellular metabolism mainly by activation of AKT; the phosphorylation status of AKT predicts its activity. AKT can be phosphorylated on either threonine (T)308 or serine (S)473, and these phosphoproteins may have antagonistic effects on each other (150, 151). Phosphatase enzymes, such as the phosphatase and tensin homolog protein (PTEN) also regulate AKT kinase activity (152, 153). Recent studies indicate that ATP-binding stabilizes the phosphorylated sites of AKT molecules by preventing phosphatase access (154, 155). Using AMPK-activating drugs, it has been shown that P-AMPK, which can be also produced by a high AMP/ATP ratio, can regulate dephosphorylation and inactivation of AKT enzymes (156). These findings suggest that energy dynamics (AMP/ATP or ADP/ATP ratios) are

important regulators of AKT activity, and, hence, of the insulin responses in myocytes (Fig. 1.9).

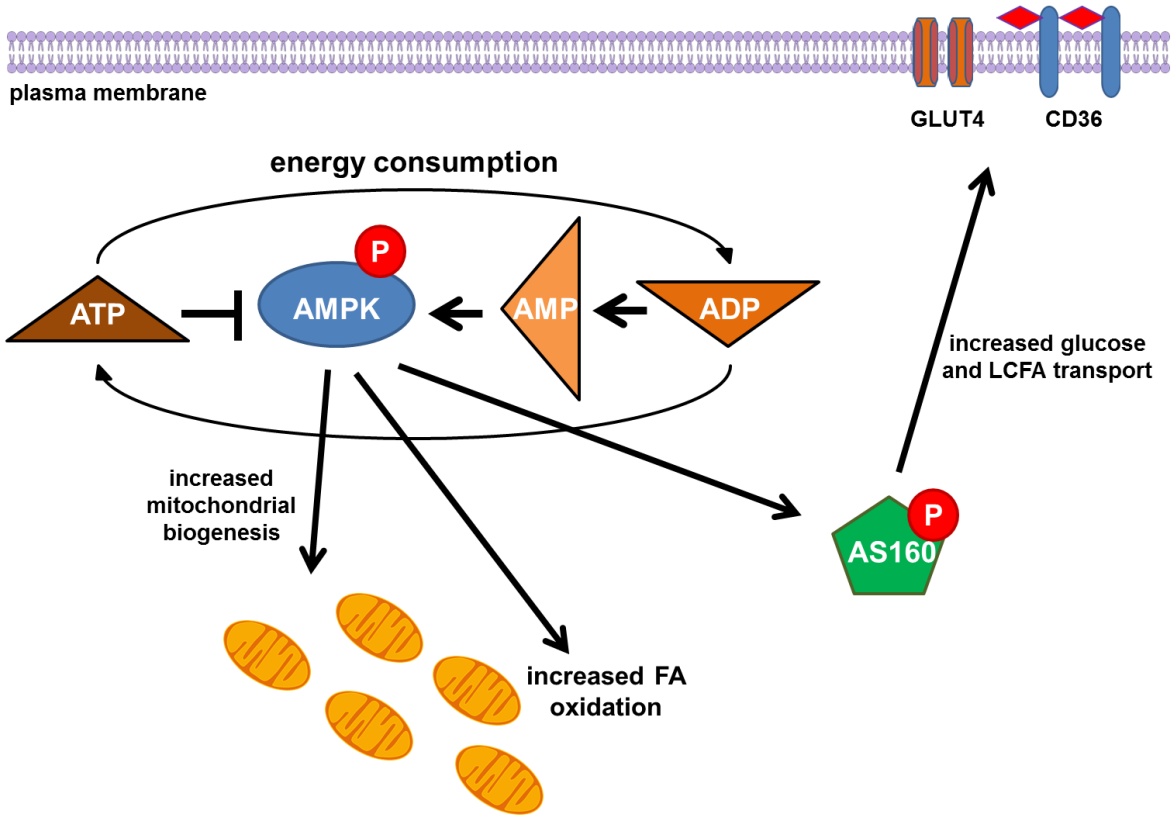

Figure 1.9: Changes in the ATP/ADP/AMP gradient in myocytes effect glucose and fatty acid uptake. Energy consumption increases AMP levels, which activate AMPK. AMPK phosphorylates AS160, which facilitates fusion of GLUT4 and CD36 vesicles into the plasma membrane so as to increase glucose and LCFA transport into the cell. In addition, active AMPK increases mitochondrial biogenesis and FA oxidation to produce more ATP. Abbreviations: AMPK, AMP-activated protein kinase; AS160, AKT substrate of 160 kDA; CD36, cluster of differentiation 36; LCFA, long chain fatty acid.

Insulin-dependent AKT activation inhibits forkhead box O (FOXO) transcription factors. This downregulates expression of IRSs and enzymes that catalyze gluconeogenesis (157). Energy surplus also activates mammalian target of rapamycin complex 1 (mTORC1), a sensor of cellular nutrient/energy levels. In turn, activation of mTORC1 prevents assembly of the mTORC2 complex (152). mTORC2 is the molecule which mediates S473-phosphorylation of AKT molecules; inactivation of mTORC2 prevents further transduction of the insulin response and prevents AS160

phosphorylation. As previously mentioned (Section 1.3.3.2), P-AS160 activity is required for the localization of GLUT4 on the cell surface; therefore, energy surplus eventually renders GLUT4 molecules dysfunctional as they are not targeted to plasma membrane even though they may be present in the cell. Under conditions of calorie restriction, cellular ATP/AMP levels remain lower; this inhibits mTORC1, assembly of mTORC2 and maintenance of insulin sensitivity in myocytes.

As stated, muscle tissue is the greatest site of energy expenditure in the body. Inadequate activity levels impair muscle efficiency for energy expenditure. Physical inactivity causes a "deceleration" in muscle activity. In this context, adipose tissue (and a lesser extent the liver) becomes an important site to process the energy surplus evident in circulating metabolites (especially glucose and FAs).

In summary, food means energy and survival. For this reason, human bodies have evolved to store as much energy as possible when food is present. In fact, most animals, not only mammals, have evolved to store energy (fat) in their bodies (10). Adipose tissue is the main storage organ for such energy. An increase in muscle insulin resistance results from impairment of muscle metabolism, and this targets adipose tissue to process the circulating glucose and balance glucose intolerance. Muscle inefficacy, together with over-eating, creates a considerable burden on the adipose. Adipose tissue responds to this imbalanced energy homeostasis by increasing the size and the number of adipocytes. However, due to its limited capacity to expand further to accommodate continuing energy surplus, adipose stress occurs which results in inflammation and dysfunction of the tissue, as discussed later (Section 1.4.4.5) in this review.

1.4 Relationship between Adipocyte Size and Function

Systeomics is a multidisciplinary approach to biology and medical sciences, which incorporates several sub-disciplines, such as genomics, computational and mathematical

biology, and molecular experimental approaches. Using this systematic approach investigates conditions holistically instead by reductionism. Systeomics is gaining special importance in obesity research. This is because development of obesity and its relationship to metabolic comorbidities involves composite investigations of cell signalling, metabolic networks and environmental interactions. “Obesity” offers an excellent example to study the relationship between phenotype and genotype, as well as interactions between environmental factors and genotype in determining disease phenotype. Finally, it is important for investigators and clinicians to keep in mind that metabolic obesity is not the result of dysfunction of a single tissue, it is a failure of a multifactorial, interactive system that involves several tissues.

1.4.1 The Pathway to Adipocyte Hypertrophy

The genetic program that determines bodily energy storage is tightly regulated. Accordingly, some individuals find it difficult to lose weight whereas others find it extremely hard to “gain” weight (158). The human body tends to maintain consistent body weight and energy homeostasis; to a certain extent, it resists the tendency to gain or lose weight. Certain factors such as early development in life, genetic predisposition, over-eating, and physical inactivity impair this balance, thereby initiating a series of processes that lead to weight gain and development of obesity. As stated previously (section 1.3), the first tissues to react to circulating excess nutrients (energy) are (arguably) pancreatic β cells and muscle; however, muscle energy storage capability is quite small and restricted. Moreover, if the individual prefers a sedentary lifestyle with minimum use of muscles, adipose tissue is the next “in line” to undergo modifications. With adipose tissue, reaction to the presence of excess energy starts from the most identical structural units, mature adipocytes.

The word “hypertrophy” is derived from the two Greek words, “hyper”, which means exceeding, beyond (excess) and “trophia” as in feeding, nourishment. This explanation for the origin of the word is particularly appropriate to describe how adipocytes become over-expanded as the result of excess “circulating” energy (nutrients). In medical terminology, hypertrophy is used to describe the increasing volume of a cell type or tissue (159). In the presence of circulating excess energy, existing adipocytes take up glucose from the circulation and convert it into neutral lipids, essentially, this involves synthesis of LCFAs and their package into triglycerides (TAGs) – this process is termed lipogenesis. TAGs, and to a lesser extend other lipids, are stored in LDs, a specialized lipid storage organelle, which are abundant in adipocytes.

1.4.2 Adipocyte Lipogenesis

Lipogenesis is important in adipocytes for two reasons: Firstly, adipocytes help regulate glucose tolerance, orchestrated by insulin. Secondly, adipocytes store lipid molecules for use during a later state of nutrient deprivation.

Glucose is the starting molecule in respiration to produce ATP. The molar mass of glucose molecule is 180.16 g/mol, and one gram contains 16 kJ energy. The most common glucose polymer in the mammalian body is glycogen (160). Except in the brain, where glucose is the only energy source, glucose (and glycogen) provides short-burst energy to the system. Although glucose molecules contain relatively less energy than other energy sources (lipids, protein etc.), its metabolization is considerably faster. Presumably this is why muscle cells store energy as glycogen. Adipose tissue does not need a “short-burst” source of energy. It is comprised of adipocytes that sustain their life cycle with a minimum number of mitochondria, except for the beige and brown adipocytes, which are metabolically more active, as discussed earlier. In all, the response of adipocytes to stimuli and bodily needs is slower but longer-lasting.

The main function of adipocytes is to store energy. Such storage is useful for other tissues when needed in times of energy demand (increased physical activity) or nutrient deprivation (starvation). Adipocytes store energy in lipid molecules (mostly as in TAG). Mass per mass, the same amount of lipid contains double the energy of glucose (or amino acids); one gram lipid contains approximately 38 kJ (161). Moreover, TAGs are hydrophobic, virtually insoluble in water. This is because the polar hydroxyls of glycerol and the polar carboxylates of the FAs form ester linkage, with eversion of the non-polar acyl chain. The hydrophobic character of TAGs allows cells to store lipids in greater amounts.

Lipogenesis, thereby, involves two main events: LCFA synthesis (*de novo* lipogenesis) and formation of TAGs. TAGs are comprised of one glycerol molecule with 3 fatty acyl side chains (161). In adipocytes, monosaccharides, such as glucose, can also be used as starting molecule for lipogenesis. Depending on the type of FAs, TAGs can be saturated or unsaturated. Unsaturated lipids have lower melting points and are more likely to be in liquid form at room temperature. Recent studies have demonstrated that the type of the LCFA (saturated vs. unsaturated) can influence the development of tissue insulin resistance and inflammation, in particular effecting on PPARγ function (more details in Section 1.5) (162, 163).

1.4.3 Digestion and Absorption of Energy Molecules

After eating, the digestion of carbohydrates requires the hydrolysis of complex (starch) or simple (maltose) carbohydrates into their component monomers (monosaccharides). Intestinal villi absorb monosaccharides by active transport across the cellular membrane (164, 165). Carbohydrate digestion takes place from the saliva (minimal) to the upper small intestine (maximal), and large intestines (metabolism by bacterial flora).

Lipids cannot be absorbed from the intestines in form of TAGs (166). The digestion and absorption of lipids is promoted by bile (167); a metastable, alkaline solution produced and secreted by hepatocytes into bile duct. Bile is stored in the gallbladder, where it goes under secondary modifications by bile duct epithelial cells. It consists of bile salts, pigments (bilirubin etc.), neutral lipids, phospholipids, cholesterol, and electrolytes. Bile salts are produced by the oxidation of cholesterol molecules (168).

The oxidation of cholesterol molecules to produce bile acids is a multistep process that occurs only in hepatocytes (169, 170). Bile acids can "self-limit" their own production by signalling in a feed forward process; accordingly, bile acids can act as a steroid hormone through the activation of FXR (171). FXR is a nuclear receptor which binds to DNA upon activation, where it regulates the hepatic expression of many other transcription factors, such as short heterodimeric partner (SHP), SREBP2, and PPARα in liver (172). FXR activation can indirectly reduce hepatic lipogenesis, suppress cholesterol *de novo* synthesis of cholesterol and increase the β-oxidation of LCFAs (173, 174). FXR is not only expressed in hepatocytes but also in adipose and some other tissues, such as the intestine. It seems likely that FXR activation has different effects on different tissue types (discussed later for adipose tissue) (175, 176).

Within enterocytes, FAs are reassembled onto glycerol molecules to form TAGs, which in turn are packed into chylomicrons in the endoplasmic reticulum (177). Chylomicrons are the largest lipoproteins, being composed of proteins, TAGs, and cholesterol esters (Fig. 1.10) (178). Chylomicrons are synthesized by the mucosal cells of intestinal villi, and are secreted into the lymphatic system, eventually reaching the systemic circulation. From there, they target other tissues such as cardiac and skeletal muscle, adipose tissue and liver. When its lipid load has been delivered, the chylomicron remnant (with residual traces of lipids) is directed to liver for catabolism (179).

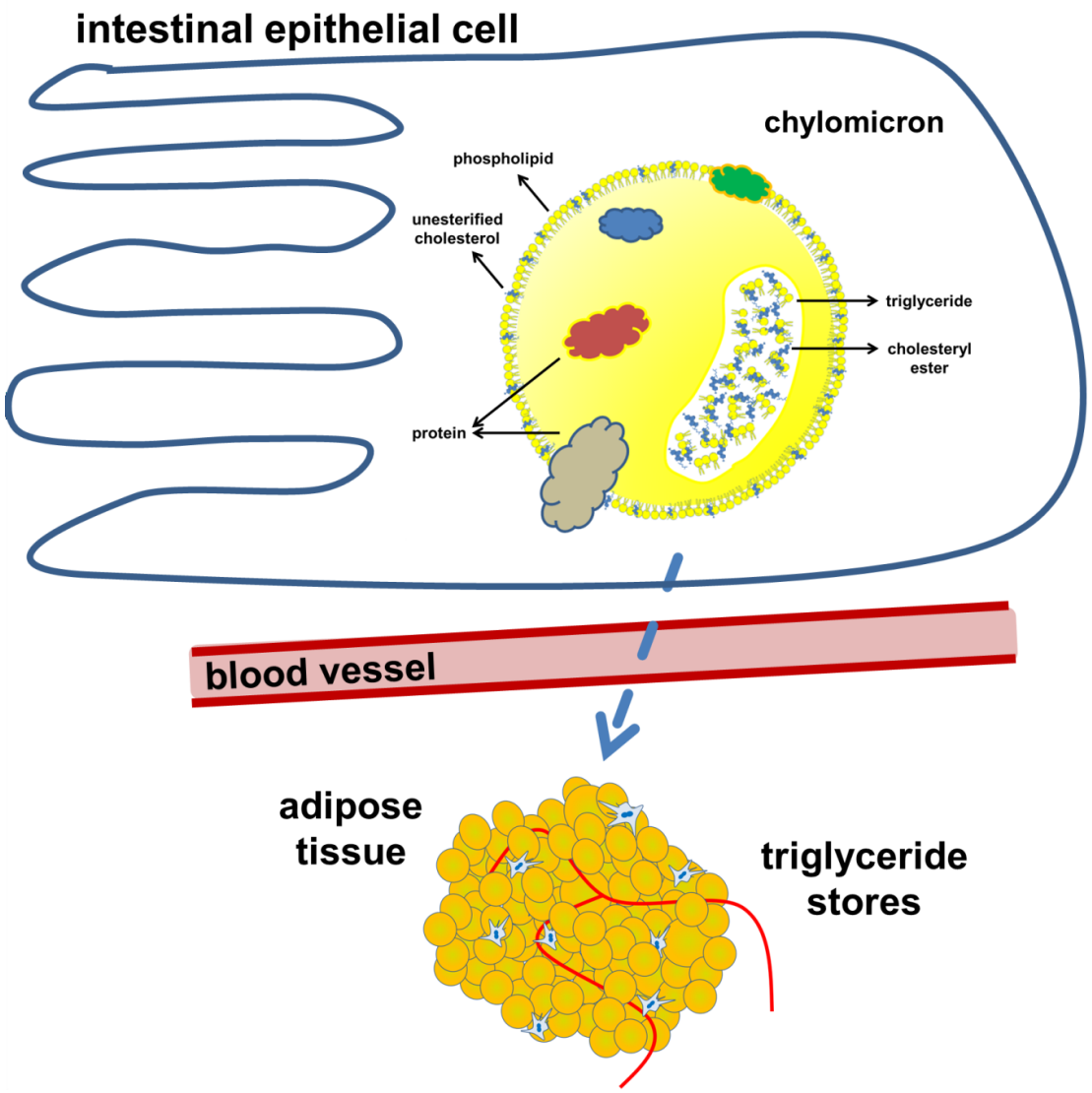

Figure 1.10: Formation of chylomicrons. Chylomicrons are the largest lipoproteins. They contain triglycerides, phospholipids, unesterified cholesterols, cholesteryl esters, and proteins. Chylomicrons are assembled in intestinal epithelial cells by dietary lipids absorbed from intestines, and deliver their cargo to adipose tissue via blood circulation.

1.4.4 Insulin and Adipocytes

Adipocytes can take up both sugars and lipids from the circulation. As pointed out earlier (section 1.3.2), insulin regulates glucose entry to adipocytes. In this respect, adipocyte insulin signalling has a distinctive pattern compared to other cell types, and insulin is critical for the control of adipocyte metabolic reactions (discussed later).

1.4.4.1 Glucose Uptake

In adipocytes, as in myocytes, GLUT4 is the main glucose transporter (180, 181). Recent studies have shown that hippocampal neurons can also produce GLUT4, and lack of GLUT4 activity in these cells causes memory impairment and behavioural changes, with a tendency towards depression (182, 183). When circulating insulin levels are low, GLUT4 molecules are retained as vesicles in the interior of cells (184). At this stage, GLUT4 molecules remain inactive. Insulin binding to its receptors activates a signal cascade which results in the relocation of GLUT4 into the cellular membrane. Accordingly, insulin dictates the rate of the movement of GLUT4 molecules in adipocytes, but there are also data which indicate possible insulin-independent mechanisms for translocation of GLUT4, for instance, in conditions of acute, extensive exercise.

1.4.4.2 Lipid Uptake

Cluster of differentiation 36 (CD36) is a class B scavenger receptor present in many cell types (185). Besides its several other functions, it is an important FA translocator in adipocytes and skeletal muscle cells. CD36 can bind LCFAs. Thus, it is required for lipid utilization in myocytes and energy storage in adipocytes (Fig. 1.11). Similar to GLUT4 relocation into the cellular surface, vesicles carrying CD36 molecules can be translocated to the cell membrane upon insulin stimulation (186). In muscle cells, muscle activity (contraction) can also promote CD36 translocation to increase LCFA uptake from the circulation (187). The mechanism of insulin-induced CD36 translocation resembles that of insulin-induced GLUT4 translocation (186). Besides CD36, other FA translocators have been identified in adipocytes which mediate FA-uptake from the circulation, such as members of FA transport protein (FATP) family.

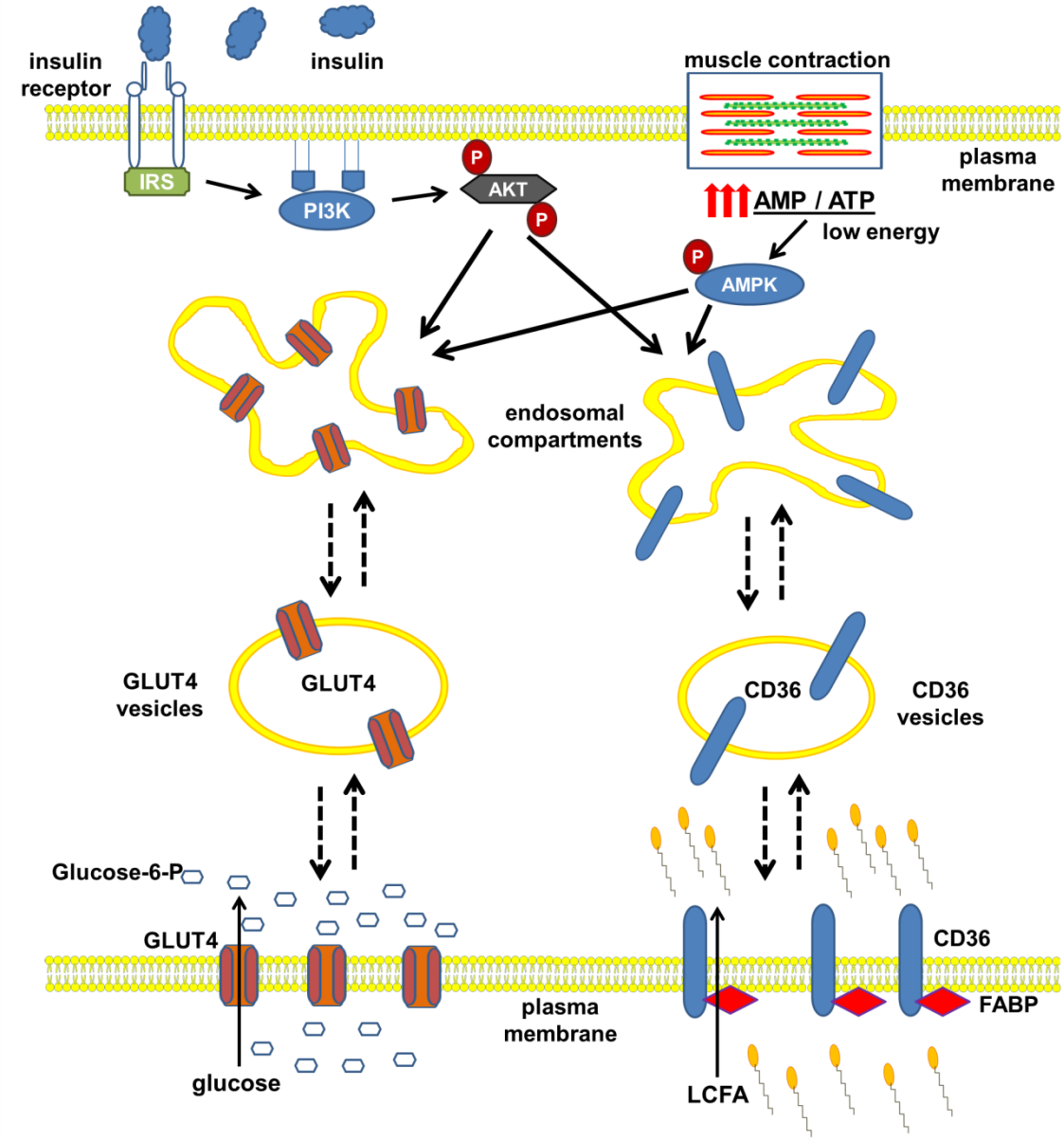

Figure 1.11: Cross-regulation of GLUT4 and CD36 vesicles. Increasing AMP levels activate AMPK, whereas insulin signalling activates AKT molecules. Both these pathways regulate GLUT4 and CD36 vesicles, orchestrating their movement and fusion to the cellular plasma membrane. Abbreviations: AMPK, AMP-activated protein kinase; AKT, protein kinase B; CD36, cluster of differentiation 36; FABP, fatty acid binding protein; IRS, insulin receptor substrate; LCFA, long chain fatty acid; PI3K, phosphoinositide 3-kinase.

1.4.4.3 "Caveola" and Insulin Signalling in Adipocytes

Lipid rafts are structural units of plasma membrane which consists of glycosphingolipids, proteins and cholesterol molecules (188). Lipid rafts provide the perfect "docking sites" for receptor signalling and membrane transport proteins. Caveolae are non-planar lipid rafts composed of caveolin proteins. They are abundant in

adipocytes, where they are formed by caveolin 1 (CAV1) and CAV2 (189). CAV1 is also present in some other cell types, such as fibroblasts, but its highest expression is observed in adipocytes.

CAV1 and CAV2 form high-molecular-mass complexes. Expression of CAV2 depends on CAV1, because without CAV1, CAV2 is trapped within the Golgi (190). Cholesterol deprivation in adipocytes causes disassociation of CAV1 proteins and disassembly of the caveola structure. As the result of these interactions, abundant cholesterol content is vital for adipocyte metabolism, particularly for adipocyte insulin signalling (191).

Insulin receptors have tyrosine kinase activity. Insulin binding causes their auto-phosphorylation so as to initiate the insulin signalling cascade (140). On adipocytes, insulin receptors reside on caveolae, which function as specialized signalling compartments. Recent studies have shown that CAV1 proteins not only provide anchors or scaffolding for these receptors, but also enhance insulin signal transduction via protein interactions (189, 190). In recent studies, insulin has been found to cause phosphorylation of CAV1 proteins.

1.4.4.4 Caveola and Glucose Uptake

Caveolae units are also thought to be important for GLUT4 translocation into plasma membrane, although the mechanisms are not yet fully understood. Konstantin Kandror and his colleagues have demonstrated that caveolae and GLUT4 vesicle membranes have distinctive structures (192). Further, cholesterol deprivation from caveolae (achieved using agents such as β-methyl-cyclodextrin [β-MCD]) downregulates GLUT4 internalization (193). In other words, without functional caveolae, GLUT4 proteins remain locked into the plasma membrane and their endocytosis is impaired. In addition, Alex Cohen and his colleagues have shown that CAV1-null mice express three- to four-

fold higher levels of GLUT4 protein in adipocytes to compensate for the impairment of GLUT4 translocation (190). Moreover, some data suggest that insulin induces tyrosine phosphorylation of casitas B-lineage protein (c-CBL). In turn, phospho-c-CBL interacts with CBL-associated protein (CAP) and flotillin, to bring GLUT4 vesicles to the cellular surface and attach them into the plasma membrane. Accordingly, CAV1 is needed for stabilization of the CAP/Flotillin/P-CBL complex. A 21 kDa small GTPase molecule, TC10, is also involved in this mechanism (194).

1.4.4.5 Effects of Insulin on Adipocyte Metabolism

As described in the preceding two sections, post-prandial insulin stimulation causes relocation of glucose and lipid translocators to the adipocyte plasma membrane to initiate uptake of these molecules. Meanwhile, insulin-stimulated AKT phosphorylation has other consequences in adipocytes, additional to the significant increase in glucose and LCFA uptake. In this sense, insulin is remarkable: most anabolic reactions are activated by only insulin in adipocytes.

Insulin stimulates adipogenic activity via increasing PPARγ expression (195). FOXO1 negatively regulates adipogenesis by binding PPARγ transcription sites. Insulin-stimulated P-AKT phosphorylates FOXO1. Phosphorylation of FOXO1 results in the release of this protein from DNA, as well as an increase in cellular expression of PPARγ (Fig. 1.12) (196, 197).

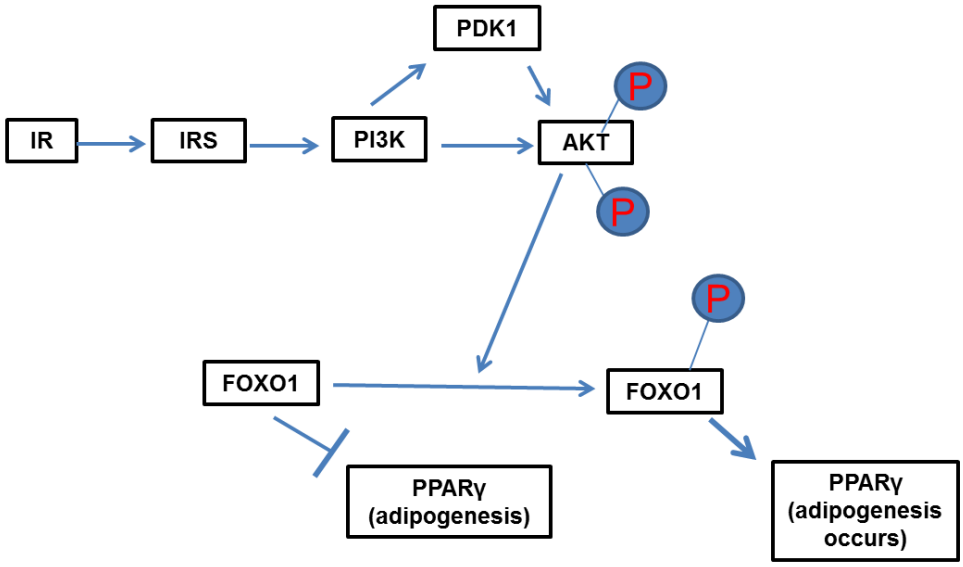

Figure 1.12: Phosphorylation of FOXO1 via insulin signalling activates adipogenesis by increased expression of PPARγ. Abbreviations: AKT, protein kinase B, FOXO1, forkhead box protein; IR, insulin receptor; IRS, insulin receptor substrate; PDK1, phosphoinositide-dependant kinase 1; PI3K, phosphoinositide 3-kinase; PPARγ, peroxisome proliferator-activated receptor gamma.

In lean adipocytes in the fed state, active P-AKT causes a decrease in cellular cAMP levels (198). In contrast, during fasting, activation of adrenoreceptors activates adenyl cyclase, thereby increases cellular cAMP levels. In turn, increased cellular cAMP activates protein kinase A (PKA) by its phosphorylation. PKA is an enzyme that phosphorylates perilipin (PLIN) proteins as well as hormone-sensitive lipase (HSL), and at the same time inhibits lipogenesis and stimulates lipolysis, thereby suppressing adipogenesis (199). HSL is a key enzyme that catalFyzes adipocyte lipolysis; it becomes activated when other compartments in the body need to mobilize energy. Insulin inhibits lipolysis in adipocytes by suppressing HSL activity. It does this indirectly, both by inhibiting phosphorylation of PLIN (lipid droplet) molecules, and by inhibiting PKA. Insulin can also inhibit *de novo* FA synthesis by suppressing ATP-citrate lyase (ACLY) by inhibiting glycogen synthase kinase 3 (GSK3) activity (200, 201).

In the presence of excess food, surplus carbohydrates are primarily oxidized instead of being converted into LCFAs (202). Nevertheless, when sedentary lifestyle minimizes the use of energy by muscles, conversion of carbohydrates into FAs can increase in adipocytes. On the other hand, *de novo* synthesis of certain LCFAs is continuous in adipocytes. This is, at least partly, because some bioactive LCFAs used by adipocytes are distinct from those taken from nutrients or "recycled" from other tissues. These specialized LCFAs (particularly poly-unsaturates) often serve as structural or messenger molecules (203).

1.4.5 Lipid Storage in Adipocytes

The *sn*-glycerol-3-phosphate pathway is the dominant biosynthetic pathway for producing TAGs in adipocytes and hepatocytes (204). The reaction is catalyzed in the endoplasmic reticulum. The pre-cursor molecule, *sn*-glycerol-3-phosphate, is used to produce mono-, di-, and triglycerides (respectively abbreviated in this thesis as MAGs, DAGs, and TAGs) by esterification of FAs. The glycerol backbone is traditionally assumed to be derived from glucose catabolism. However, there are increasing data to suggest that *de novo* glyceroneogenesis in adipocytes can occur from pyruvate (205). TAGs produced by this machinery are stored in LDs.

1.4.5.1 A Controversial Organelle: Lipid Droplets

LDs are cellular organelles which regulate the storage and hydrolysis of neutral lipids; they are formed in every cell of the body and in all eukaryotic organisms, indicated very basic and "primitive" functions (206). Lipid droplet is the accepted nomenclature, but these organelles are far from an inert cellular storage vehicle. In fact, the function of such LDs is better viewed as a protective mechanism by which cells such as adipocytes and hepatocytes protect themselves from lipotoxicity. LDs do play a special role in

some secretory epithelia, such as mammary gland, and in monocyte-macrophage, but these are beyond the scope of the present review.

1.4.5.2 Lipid Droplet Proteins

Several specialized protein families are important for LD structure, function (lipolysis), and regulation (Table 1). One important family is comprised of the PLIN proteins (207). Their expression is regulated by the key adipogenic transcription factor, PPARγ. Dynamic interactions between PLIN molecules and PPARγ determine the size of the LD, as well as its rate of lipolysis (208, 209). For instance, phosphorylation of PLIN1 allows 1-acylglycerol-3-phosphate O-acyltransferase (CGI-58) to interact with adipose triglyceride lipase (ATGL [Desnutrin]). CGI-58 enhances ATGL activity 20-fold, which initiates the breakdown of TAGs stored in LD (210). Lipolysis is more critical for BAT. It is not surprising, therefore that the protein composition and regulation of LDs differs in brown and white adipocytes (211). Another important protein is tail-interacting protein of 47 kDa (TIP47); this functions in the maturation of LDs (212). Early data suggested a role of TIP47 in the biogenesis of LDs, but recent findings have shown that suppression of TIP47 blocks maturation of LDs, not their production. PLINs and TIP47 are usually co-located on the surface of LDs with adipose differentiation-related protein (ADRP) (213). In preadipocytes, an increase in *Plin* and *Adrp* mRNA levels is a good indicator of adipocyte differentiation. Protein crystallography studies have shown that PLINs-ADRP-TIP47 (PAT) proteins might function in analogous fashion with apolipoproteins; they consist of helical repeats that interact with lipids, as well as C-terminal subunit interacting proteins (214).

1.4.5.3 Cholesterol in Adipocytes

LDs are surrounded by a phospholipid (mono)-layer (206). Unlike its presence in other tissues, most of the cholesterol in adipocytes is in the non-esterified (free) form and located within the LD membrane (215). Free cholesterol (FC) also exists in the core of LDs, but this comprises a lesser quantity; the core of LDs is mainly comprised of TAGs and cholesterol esters. Recent studies have suggested that the structure of LDs resembles the inner structure of an onion bulb rather than that of an orange (216). This analogy reflects the multiple "scale membranes" inside of a LD rather than existence of a single surface membrane (Fig. 1.13). Considering the fact that FC is packed in the membrane of LDs, such an "onion bulb" phenomenon would explain why adipocytes are very rich in FC without undergoing lipotoxicity; FC is bioactive and toxic to hepatocytes (217).

TABLE 1
Mammalian lipid droplet proteins.

Protein grouping	Members	Protein name	Size (kDa)	UniProt accession
PAT family	ADRP	Adipose differentiation-related protein	50	Q99541
	TIP47	Mannose-6-phosphate receptor-binding protein1	47	O60664
	S3-12	S3-12	131/141	O88492
	Perilipin	Perilipin	65	Q9BSC3
Chaperones	Endoplasmin	Endoplasmin	94	P14625
	BiP (GRP78)	Heat shock protein 90 kDa β member 1	78	P11021
	HSPA1A	Heat shock 70 kDa protein 1A	70	Q61696
Lipid metabolism	ACCα	Acetyl-CoA carboxylase α	280	Q13085
	CGI58	CGI58	39	Q8WTS1
	LSS	Lanosterol synthase	83	P48449
	HSL	Hormone sensitive lipase	84	P54310
	PNPLA2 (ATGL)	Adipose triglyceride lipase	55	Q96AD5
	OXPAT	Lipid-storage droplet protein 5	50	Q8BVZ1
	CIDEC/FSP27	Fat-specific protein 27	27	Q96AQ7
Membrane trafficking	GAPDH	Glyceraldehyde-3-phosphate dehydrogenase	40	P04406
	RABs	Ras-related proteins	-	-
	VAT1	Synaptic vesicle membrane protein VAT1 homolog	42	Q99536
Cytoskeleton	Actin	Actin	42	P60709
	Vimentin	Vimentin	54	P08670
Signalling	CHP	Calcium-bindin protein 22	22	Q99653
	Caveolin1	Caveolin1	22	Q03135
	AAM-B	Methyltransferase-like protein 7A	28	Q9H8H3

Over 200 mammalian LD proteins were reported. In this table, proteins that are confirmed with at least 3 proteomic studies are mentioned.
UniProt: Universal Protein Resource/Database.

During the expansion of LDs, caveolin molecules from the plasma membrane are directed to their surface (218). Thus, LD expansion requires large amounts of cholesterol and caveolin proteins. Cholesterol is an essential structural unit of caveolae, and similar to the plasma membrane, caveolae have important structural and functional (lipolysis) duties within LD membrane (Fig. 1.14). It has been shown that CAV1 assists PKA-mediated phosphorylation of PLIN proteins (219). Phosphorylation dissembles PLINs from the LD surface and provides "open-spots" for ATGL activity.

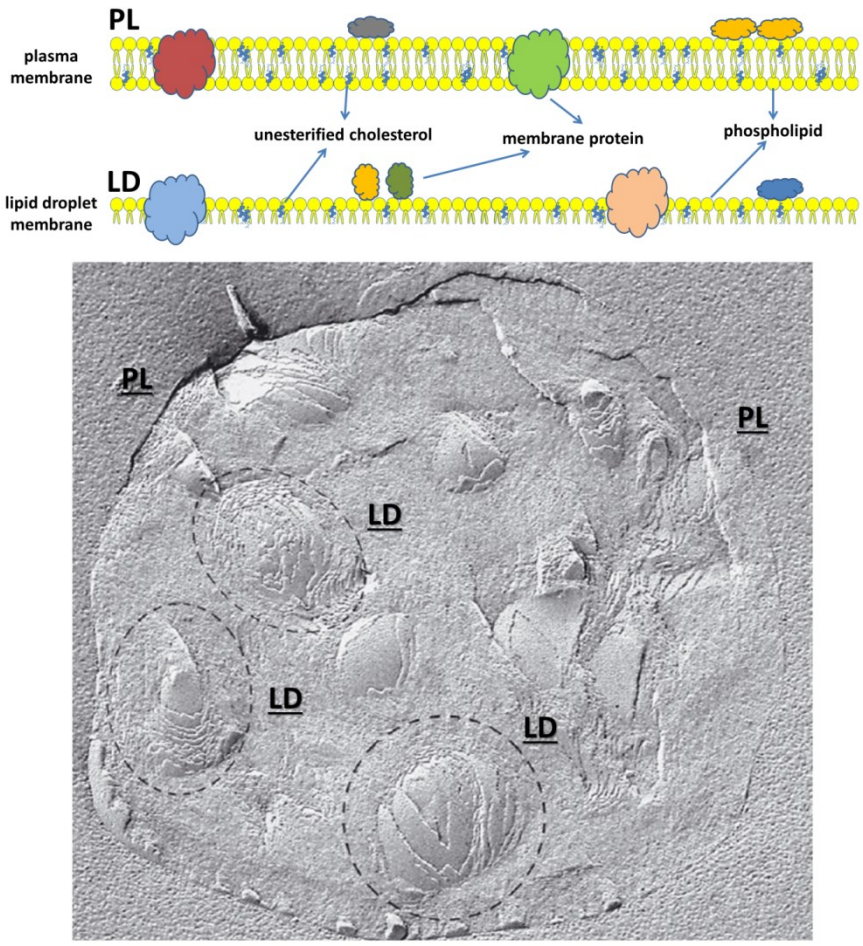

Figure 1.13: Onion bulb-like structure of lipid droplets. Adjusted from the original article (216). Unlike plasma membrane, lipid droplet membrane is composed of a single layer of phospholipids and unesterified cholesterols. As shown in the section, lipid droplets (encircled) contain multiple membrane layers amalgamated, which make them perfect cholesterol storages. Bar: 0.5 µm. Abbreviations: LD, lipid droplet; PL, plasma membrane.

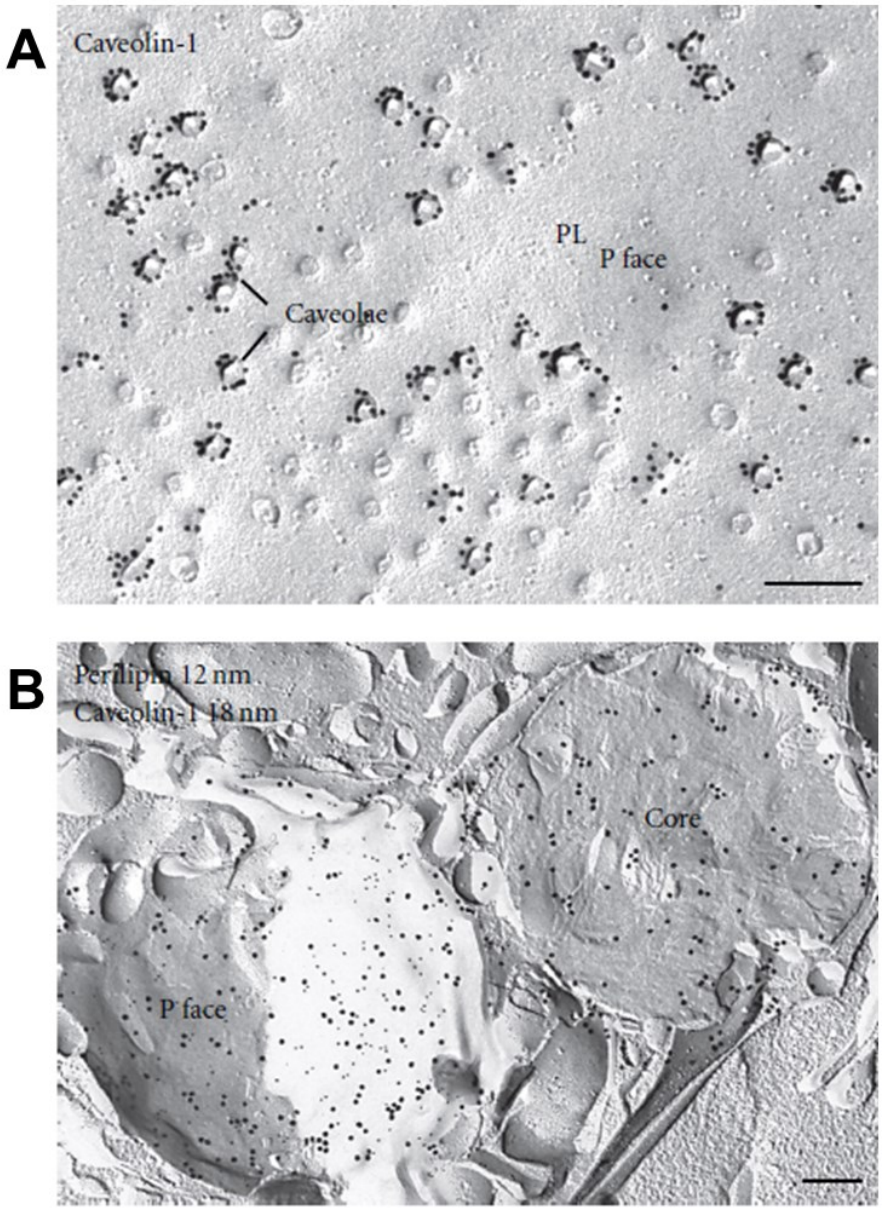

Figure 1.14: Distribution of caveolin-1 and perilipin in adipocytes. Adjusted from the original article (218). (A) Caveolae appear on the surface of adipocytes (PL, plasma membrane). Gold particles show caveolin-1 in the caveolae. (B) Apart from PL, caveolin-1 is abundant both on the surface and in the core of lipid droplets. The droplet on the left side shows co-localization of perilipin (12 nm gold particles) and caveolin-1 (18 nm gold particles) on the lipid droplet surface. The core of lipid droplet on the right side contains only caveolin-1 labels. Bar: 0.2 μm. P face – outer surface.

1.4.5.4 Cholesterol as a Messenger Molecule in Adipocytes

Recent studies indicate that cholesterol plays a messenger role in adipocytes. As described already (section 1.2.1), continued disequilibrium in energy homeostasis results in large hypertrophic adipocytes, and this results in cholesterol accumulation in adipocytes. While intracellular cholesterol transport is not yet completely understood, it

has been shown that expansion of LDs increases adipocyte size and redistributes cholesterol from the plasma membrane to LD membranes (215). This process decreases the cholesterol content of the adipocyte plasma membrane. As a consequence, the fluidity of the plasma membrane increases. At the same time, the enlargement in LD surface area causes an increase in auto-lipolysis of the droplet TAGs resulting from the increased CAV proteins on the LD surface.

In adipocytes, 30% of FAs produced by lipolysis are re-esterified with glycerol. In other words, the FA efflux pathway works with 70% efficiency in adipocytes. This increases the cellular concentration of FAs (220). The combination of increased cellular FAs and cholesterol deprivation selectively induces SREBP2 as a transcription factor in hypertrophic adipocytes (221). In other words, a peculiar "unhelpful" consequence of overnutrition in adipose tissue is that, although, the system is loaded by dietary cholesterol as a result of over-eating, adipocyte hypertrophy evokes a fake "cholesterol depletion" signal. This induces cholesterol biosynthesis in adipocytes through induction of SREBP2 and its target genes, e.g. 3–hydroxy-3-methyl-glutaryl-CoA reductase (HMG-CoR). This sequence of maladjustment opens the gate to a series of metabolic changes in adipose tissue and the whole system. This is because hypertrophy in adipocytes is related to recruitment of hyperplasia in adipose tissue. However, the link between enlarged adipocytes and the increase in preadipocyte proliferation/adipogenic differentiation remains largely unknown (discussed later).

1.4.5.5 Adipocyte Hypertrophy and Critical Cell Size

To recapitulate, the perception of cholesterol depletion in enlarging adipocytes is detected by SREBP2. The moment when SREBP2 stimulation is switched on might be critical for fat cell size, the time when cellular machinery is activated to induce neighbour and surrounding preadipocytes to proceed to adipogenesis. Such adipocytes

also express paracrine factors (discussed later) which result in recruitment and proliferation of adipocyte progenitors. According to this concept, cholesterol molecules may not only be structural units in adipocytes, but also take on important functional tasks in cellular metabolism. Finally, when adipocytes reach their critical cell size, the formation of hyperplastic adipose tissue is initiated as a "system" adjustment to over-nutrient/energy imbalance.

As stated previously, FXR can inhibit SREBP activity in hepatocytes (222). FXR is also expressed in adipocytes, and FXR activation can exhibit positive effects on adipogenesis and adipose insulin sensitivity (223); however, full mechanism in adipose tissue has not yet been clarified. In this context, FXR activation can delay or reorganize the metabolic modifications in adipocytes via their effects on SREBP2 when lipid loading leads to adipocytes reaching the critical size. This interesting concept requires further investigation for its clarification. The possible anti-inflammatory role for FXR activation in adipose tissue as well as the metabolic improvements could be related to improved adipose functions (discussed in Chapter 5). This concept allows for a pivotal role of FXR activity for treatment of metabolic disorders, not only fatty liver disease.

1.4.6 Hyperplasticity of Adipose Tissue

Fat cell size is directly related to the development of hyperplasticity in adipose tissue. Thus, adipocyte expansion results in increased adiposity. Enlargement also changes the hormone and peptide expression and secretion profiles of adipocytes (224). Two types of effects flow from the changes in adipose-derived hormones, cytokines and chemokines that result from the adipocyte phenotypic switch due to enlargement. The first effects on adipose tissue are the re-organization, and the second are effects on energy homeostasis. As one example, a decrease in adiponectin production resulting from adipocyte hypertrophy results in hyperplasia of adipose tissue, but it is also

associated with decreased systemic insulin sensitivity because adiponectin is an important insulin-sensitizing agent, particularly in the liver (225).

1.4.6.1 Preadipocyte Proliferation

Paracrine growth factors are important for the development of adipose tissue hyperplasticity. Paracrine signalling is a form of communication between adjacent cells that results either from their direct interaction or is affected by local mediators. Hypertrophic adipocytes produce paracrine growth factors which stimulate an increase in preadipocyte number (226, 227). In 2013, Valerie Chaves and her colleagues reported patients with isolated growth hormone (GH) deficiency regarding adipose tissue changes (228). These patients were found to have enlarged adipocytes, but the average fat cell number was actually less compared to matched (GH producing) controls. Treatment of GH-deficient patients with growth hormone had two interesting consequences: it increased the number of adipocytes, but it decreased adipocyte volume. Interestingly, there was a particular reduction in abdominal (visceral) fat mass because of growth hormone-stimulated lipolysis. Another interesting finding was the small amounts of growth hormone produced in obese individuals without GH deficiency from hypothalamic or pituitary disease.

1.4.7 Relationship of Adipocyte Size to Function

Adipocyte phenotype is directly related to its size. For example, the proliferative capacity of adipocytes, their β oxidation capacity and hormone/cytokine expression rates all differ in subpopulations of small, medium and large adipocytes. Accordingly, small (lean) adipocytes exhibit a more insulin-sensitive phenotype with a lipogenesis / lipolysis ratio that is correspondingly higher (229). Conversely, large adipocytes are insulin-resistant cells with an increased basal rate of lipolysis.

Recent findings have shown even greater complexity, as there are different populations of small adipocytes (230). Accordingly, some of these small subpopulations are healthy and anti-inflammatory, whereas others can be highly cytotoxic, and contribute thereby to recruitment of inflammation into the tissue, particularly into visceral adipose.

Besides the changes in hormone and cytokine secretion, subcutaneous adipocyte hypertrophy paradoxically reduces TAG storage, which in turn increases FA and cholesterol over-flow to the muscles, visceral adipose depots, and liver (231, 232). This "spill-over" from large adipocytes into ectopic sites (tissues like muscle and liver that are not designed primarily for lipid storage) triggers systemic insulin resistance. The contribution of different adipose depots to the free FA (FFA) and cholesterol leakage varies between different pads. For example, although visceral adipocytes are generally smaller than subcutaneous adipocytes, their transmembrane FFA efflux is higher. Considering the fact that only adipocytes can release FFA to the circulation, visceral adipocytes assume special importance in systemic and portal FA flux, a process that increases systemic insulin resistance. In a recent study, the size distribution of omental adipocytes was found to be more closely correlated to measures of adiposity and metabolic parameters in Asian Indians than subcutaneous adipocyte size (233). In another study, Laura Gathercole and her colleagues found depot-specific differences in lipogenesis enzymes; subcutaneous adipocytes exhibited enhanced lipid storage capacity (234). However, it remains unclear whether visceral and subcutaneous adipocytes share the critical fat cell size (mentioned earlier) or not, and it is also unclear what causes the difference in the capacity of these adipose tissues to expand.

In the fasting state, plasma non-esterified FAs (NEFAs [same with FFAs]) are produced by adipocytes via TAG hydrolysis. In the obese state, such fat mobilization from adipocytes is impaired (204). Insulin-resistant hypertrophic adipocytes accumulate

increased amounts of cellular cAMP. This higher cellular cAMP concentration stimulates PKA, resulting in phosphorylation of PLIN and HSL. In turn, this increases lipolysis. In other words, swollen adipocytes in obesity exhibit increased lipolysis and NEFA efflux. A paradoxical finding in obesity is that the increase in basal lipolysis rates of hypertrophic adipocytes is largely unrelated to the increased plasma NEFA levels. As yet, the reason is not clear (uptake of NEFA by hepatocytes via CD36 may play a role) but hypertrophic adipocytes develop resistance to lipolysis and do not respond appropriately to such stimulants as catecholamines (235).

Longer periods of energy surplus and impaired energy homeostasis prolong the extension of hypertrophy and hyperplasia in adipocytes, causing an irreversible phenotypic switch in their cellular phenotype. These large adipocytes develop severe insulin resistance and produce pro-inflammatory factors such as chemokines (e.g., monocyte chemoattractant protein 1 [MCP1], chemerin) or tumor necrosis factor α (TNFα) and interleukin 6 (IL6), with resultant inflammatory recruitment into the tissue. The pro-inflammatory cytokines themselves stimulate ongoing lipolysis in these adipocytes, and also impair cellular anabolic pathways.

1.5 Adipose Tissue Inflammation

If reaching to the critical cell size is the “first hit” leading to adipocyte dysfunction, the second hit could be the presence of ultrastructural abnormalities in hypertrophic adipocytes; but the second “hit” is a spectrum of events rather than one isolated incident. In this section, energy surplus-related abnormalities on adipocytes (and SVF cells) and their consequences on local and systemic levels are explained. Identification and regulation of these abnormalities remains a great challenge in adipose biology, but has the potential to explain the pathogenesis of adipose inflammation and dysregulation.

1.5.1 Vascularization in Expanding Adipose Tissues

Adipose readily undergo tissue reformation. It can easily shrink or expand, and adapt to the changing environmental and physiological conditions. Vascularization (macro or micro), therefore, is one important factor in adipose biology. In theory, vascularization should be well-regulated in parallel to adipose formational changes; however, in practice, it does not reflect the expansion rates of adipose tissue. Cardiac output does not increase sufficiently to provide enough oxygen and other components to growing adipose. As a result, a dysregulated adipose tissue blood flow occurs in metabolic obesity (236).

As stated previously (section 1.2.1), adipose tissue functions as an endocrine organ. It requires a well-established "delivery" system to receive resources and deliver factors to realize its regulatory (and endocrine) duties. A capillary network, therefore, is an important part of adipose tissue. Reduction in the density of this network resulting from adipose over-expansion can cause "vascular insufficiency" and contribute to the events that eventually lead to development of adipose inflammation and dysregulation.

Adipose expansion depends on angiogenesis, the process of forming new vessels from pre-existing vessels (237). Adipose tissue orchestrates its own neo-vascularization (angiogenesis) by expressing angiogenic factors such as leptin, apelin, and vascular endothelial growth factor (VEGF). This orchestration also includes anti-angiogenic factors that are produced by adipocytes and SVF cells such as endostatin, angiostatin and thrombospondin.

Obesity results in hypoperfusion of blood constituents, especially oxygen, into adipose tissue (236). As mentioned above, capillary density in various adipose depots can dramatically decrease during obesity development. Lower capillary density is usually accompanied by larger vessels in mesenteric fat formation (Fig. 1.15). In

addition, the diffusion distance between hypertrophic adipocytes and capillaries increase compared to that for lean adipocytes.

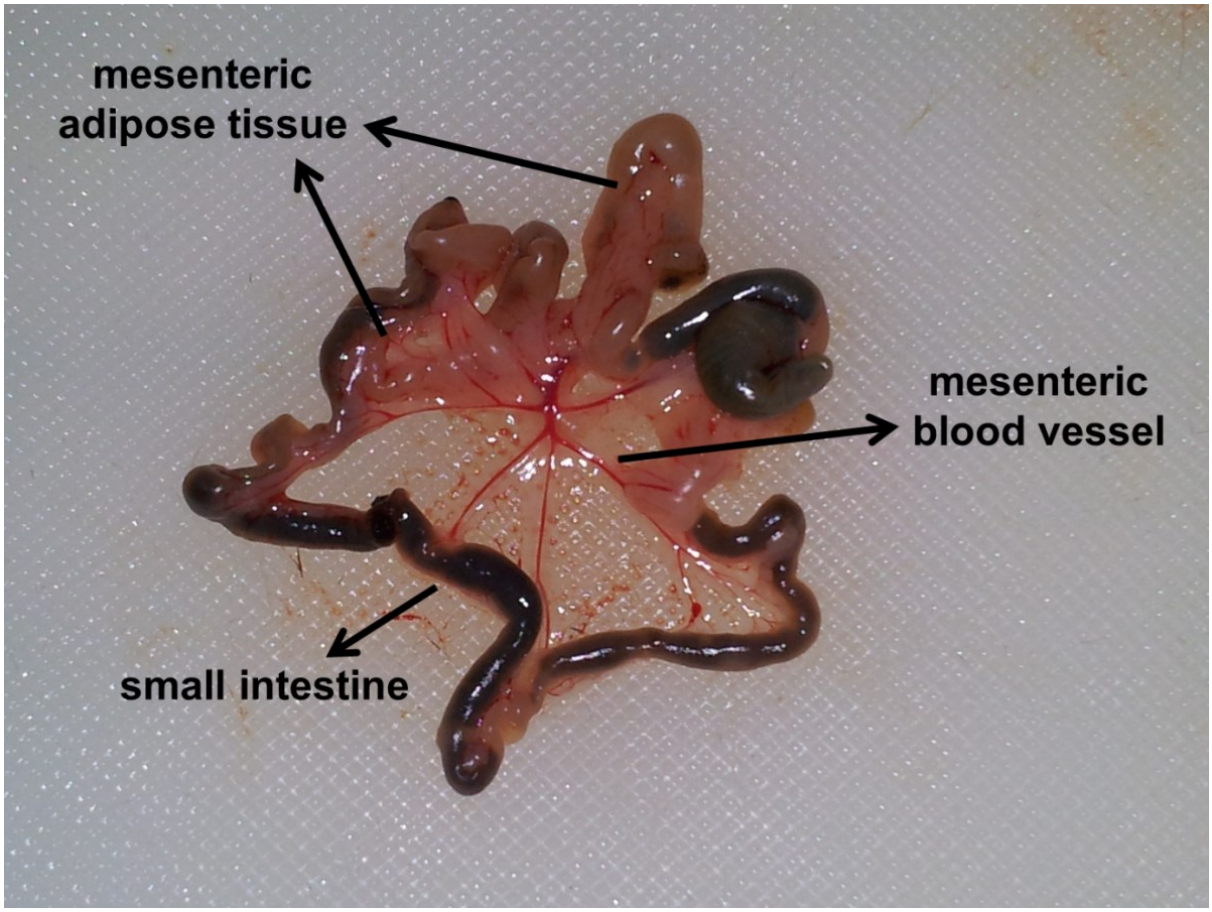

Figure 1.15: Mesenteric fat and large blood vessels. Obtained from diabetic obese mice following the standard tissue harvest protocol in the host lab.

A lower capillary density and increased diffusion distance reduce the oxygen partial pressure (pO_2) around adipocytes to cause tissue/cellular hypoxia. Some scientists believe that such reduced pO_2 predicates the inflammatory response in adipose tissue (Fig. 1.16). In this context, experiments with cultured adipose explants have shown that expression of over 1000 genes changes in hypoxic conditions (236). Most of these changes cause hypoxic stress on adipocytes**.**

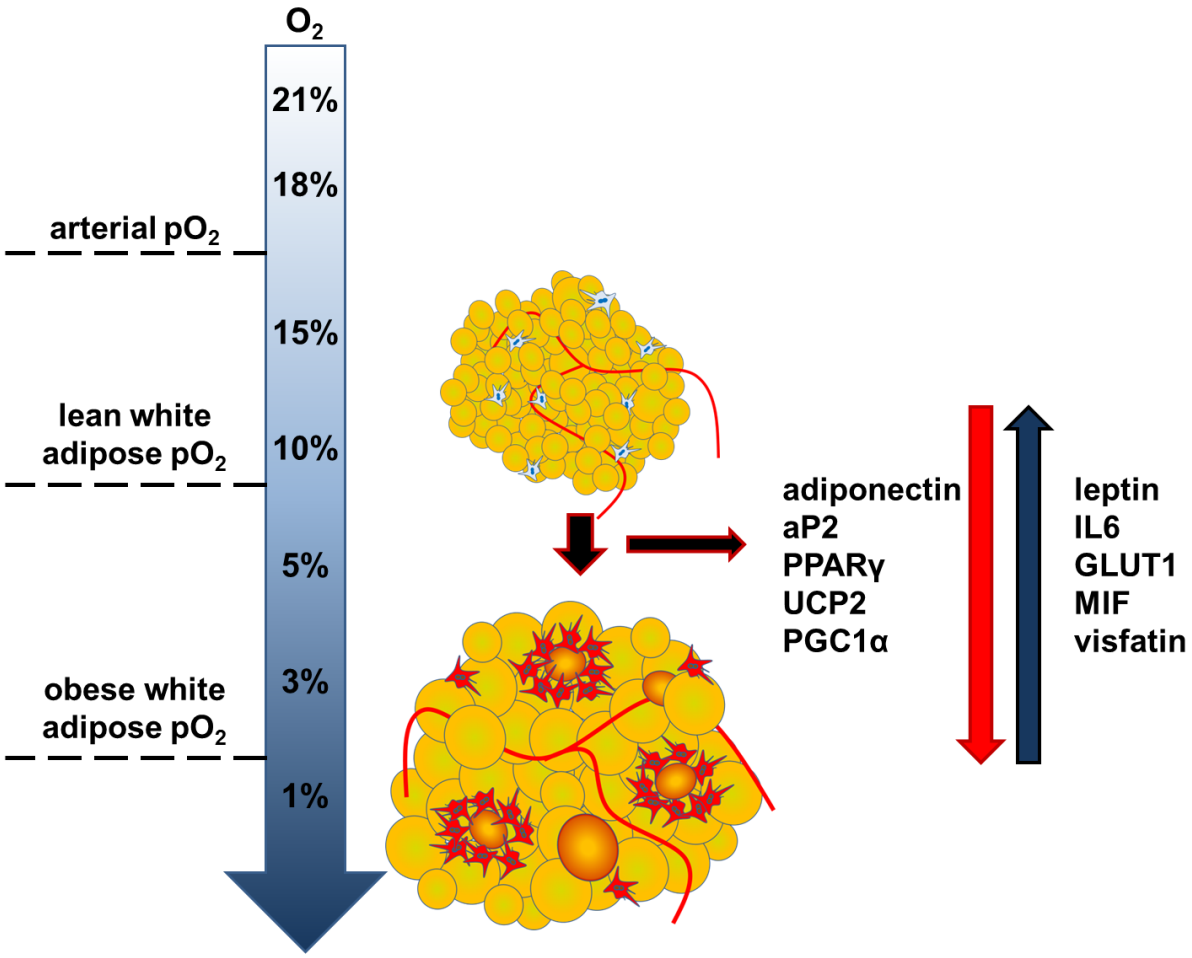

Figure 1.16: Changes in gene expression of adipocytes under different oxygen concentrations. Over-expansion of adipocytes leads to development of hypoxia in the tissue micro-environment. This results in significant changes in gene expression. Abbreviations: aP2, adipocyte protein 2; IL6, interleukin 6; MIF, macrophage migration inhibitory factor; PGC1α, PPARγ-co-activator 1 alpha; PPARγ, peroxisome proliferator-activated receptor gamma; UCP2, uncoupling protein 2.

1.5.1.1 Depot-Specific Differences in Adipose Vascularization

Angiogenic potential of different adipose depots is unclear. Nevertheless, it has been shown that actively-expanding adipose tissues contain more blood vessels than relatively stable ones. This is important because there are physiological and ergonomical limitations on visceral adipose growth whereas subcutaneous WAT can expand further without causing any metabolic problems (MHO individuals). Accordingly, a higher angiogenesis potential and denser capillary network is more likely in subcutaneous WAT (especially in humans) compared to visceral compartments. Visceral (intraabdominal) fat depots drain directly into the portal vein. Production of hypoxic stress-derived factors from adipocytes may therefore have direct and potentially harmful effects on other parts of the body, particularly liver.

1.5.1.2 Other Factors Effecting on Adipose Vascular Capacity

The increase in postprandial (glucose-induced) adipose tissue blood flow is impaired for any level of glucose intolerance (238). This is a result of increased leptin levels in obese individuals. Leptin inhibits nitrite oxide (NO) production (239). The presumed reason is to oppose apoptosis (e.g., NO induces β cell apoptosis), but, decreased NO production results in dysregulation of endothelial cells, the inner-lining of blood vessels. Dysregulated endothelial cells negatively effects vascularity.

There are other factors influencing adipose vascularization, such as insulin, the sympathetic and parasympathetic nervous systems, gastrointestinal peptides, and vasodilators. For example, moderate exercise has been shown to improve vascular cell functions (240). As discussed in chapter 6, voluntary exercise improves adipose function in obese mice; improvements in vascularization through exercise may partly explain this improvement.

Vascularization effects adipose function not only by preventing hypoxia, but also via functions of endothelial cells. Thus endothelial cells and adipose tissue control the permeability of adhesion and chemotactic factors and this effects infiltration of preadipocytes and immune cells into the tissue (241, 242). In this way, vascular insufficiency can act as the source and accelerator of adipose inflammation. The property of visceral adipose to be more prone to vascular insufficiency could also explain why visceral adipose depots are more likely to develop inflammation compared to subcutaneous WATs.

1.5.2 Extracellular Matrix, Adipose Tissue, and Hypoxia

ECM is a protein layer in the connective tissues (243). ECM proteins such as collagen, laminin, and fibronectin are secreted from matrix forming cells by exocytosis. In adipose, there are two different forms of ECM: first form is known as "basement membrane" (244). This large fibrillary structure lies under the epidermis layer of subcutaneous WAT. The outer layers of several organs and blood vessels share similar structured feature with basement membrane (advanced fibrillary protein pool).

Secondly, the "interstitial matrix" is a filling material that provides a physical working environment for cells to conduct chemical reactions. Production of a flexible interstitial matrix is crucial for healthy adipose function because it enables cell-to-cell communications (autocrine and paracrine). The interstitial matrix is composed of two components: ECM proteins and interstitial fluid. Water is the important solvent in all living systems on earth and most chemical reactions take place in water-based interstitial fluid. The aquatic solvent contains ions and solutes such as glucose, FAs, cellular metabolites, hormones, cytokines and chemokines. A significant proportion of studies about "hypoxia and adipose tissue" have focused on changes in gene expression levels of adipokines rather than investigating the actual production and secretion of

adipose-derived peptides. Interstitial fluid offers sample of ever greater relevance to study the effects of hypoxic stress on adipose-derived factors.

Maintenance of the interstitial matrix bears a complex relationship to adipose function. Rapid expansion of adipose tissue impairs the composition and flexibility of interstitial matrix, possibly because of hypoxic stress on adipose cells, and especially on hypertrophic adipocytes. A defective interstitial matrix can itself distort the structure of adipose tissue and thereby contribute to adipose dysfunction (19).

1.5.2.1 Activation of Hypoxia-Inducible Factors

Hypoxia-inducible factors (HIFs) are members of a transcription factor family that is responsive to changing oxygen levels (O_2 homeostasis) (245). Oxygen deprivation in the adipose cellular microenvironment stimulates an increase in HIF expression. HIF1-α is an important member of the family both in humans and rodents (246). Its stimulation by hypoxia promotes tissue vascularization by increasing expression of endothelial nitric oxide synthase (eNOS) (247). However, activated HIF1-α in adipose tissue, unlike its action in tumour tissues, may fail to initiate a proper angiogenesis response (discussed later).

Other HIFs, such as HIF2-α or HIF3-α, are not as well-studied as HIF1-α. Nevertheless, limited data show that other HIFs are more like tissue-specific factors. HIF2-α appears to have anti-inflammatory properties, such as inducing an anti-inflammatory phenotype in macrophages by increasing arginase 1 (AG1) expression (248). There are also other master regulators of the hypoxia response. Some of these are nuclear factor kappa-light-chain-enhancer of activated B cells (NF-κB) and cAMP response element-binding protein (CREB) (249, 250). Activation of these factors during hypoxia has been shown. However, it is not clear whether they are a part of the hypoxia response in adipocytes, and whether they enhance hypoxic stress-related inflammation.

1.5.2.2 Hypoxia-Related Oxidative Stress

Oxygen is a highly reactive element. It is the third most abundant atom in the universe (by mass) and most organic molecules include oxygen as a constituent. As mentioned earlier (section 1.2.5), oxygen is central to ROS generation. ROS can arise from different are both important sources of ROS. Reduction of molecular oxygen (O_2) to H_2O requires 4 electrons (e^-) in the Electron Transport Chain (ETC). During these redox reactions (transportation of e^- from donors to recipients), electron leakage can generate ROS, thereby causing irreversible damage to biomolecules, especially macromolecules (251, 252). These macromolecules include amino acids (peptides, proteins), nucleic acids, and lipids. For example, lipid peroxidation is a well-studied form of ROS damage to unsaturated LCFAs, from which cellular and organelle membranes are damaged with serious consequences (253, 254). In hypertrophic adipocytes, chronic lipolysis (section 1.4.7), driven by inflammation, is an important source of ROS in hypertrophic adipocytes.

A seemingly paradoxical finding is that ROS have been found in hypoxic lesions (255). Hypoxia-dependent increase in HIF1-α activates anaerobic metabolism and glycolysis in adipocytes, but this does not stop is from activating the Kreb's cycle and ETC in adipocytes, which occurs by using the residual oxygen in the tissue. On the other hand, eNOS can also generate ROS by its reductase function (256, 257). A delicate balance can shift from NO to ROS production. Peroxynitrite ($ONOO^-$) is a strong oxidant that occurs with the interaction of O_2- and NO. Growth factors and cytokines can also result in ROS production, for example, TNFα can stimulate nicotinamide adenine dinucleaotide phosphate (NAD(P)H) oxidases that can result in ROS production. These factor-dependant pathways of ROS production are well-documented for vascular smooth muscle cells, but there are increasing data for other cell types and tissues.

In light of the above considerations, it is apparent that oxygen is both vital and deadly for adipocytes; hypoxia and oxidative stress can cause serious cellular injury or death. There are several anti-oxidant molecules (e.g., superoxide dismutases [section 1.2.5]) that confer cyto-protective effects against ROS (258). Nuclear factor-erythroid 2 p45-related factor 2 (NRF2) is an important transcription factor in the regulation of such anti-oxidants. NRF2 binds both anti-oxidant and electrophile responsive elements (A/EpRE) in the nucleus after stimulation by ROS exposure (259). This initiates/accelerates expression of downstream anti-oxidant molecules such as glutathione *S*-transferase and glutathione peroxidase 2 (260). Mitochondrial (SOD2) or extracellular (SOD3) superoxide dismutases catalyze the transformation of ROS into less harmful derivatives, such as hydrogen peroxide (H_2O_2) and O_2 (261). The cellular levels of SOD2 and SOD3 differ depending on whether oxidative stress is acute (increases expression) or chronic (decreases expression).

1.5.2.3 Hypoxia-Related Lactate Accumulation in Adipocytes

Hypoxia-induced changes in cellular metabolism have some other deleterious consequences on hypertrophic adipocytes. As stated previously (section 1.3.3), anaerobic respiration causes cellular lactate accumulation that is toxic to the cell (238). A direct correlation between adipocyte size and cellular lactate production has been shown (262). Up to 70% of cellular glucose is metabolized to lactate in hypertrophic adipocytes (263). Moreover, recent studies have shown that lactate is an important extracellular messenger that can stimulate inflammatory responses in macrophages, as well as promote tissue insulin resistance (264, 265). This may indicate an indirect link between hypoxia and insulin resistance in obesity.

1.5.2.4 Hypoxia-Related Dysregulation of Adipose ECM

Increasing HIF1-α levels dictate an alternative transcriptional program on adipocytes that involve over-expression of some ECM proteins (Fig. 1.17) (266). Expression of such genes associated with ECM production as type 1 collagen alpha 1 (COL1A1) and type 3 collagen alpha 1 (COL3A1) increase in hypoxic conditions (10% pO_2). More than 50 genes are upregulated by HIF1-α (236). Expression of matrix metalloproteinases, MMP2 and MMP9, changes in hypoxia; these enzymes are important for tissue remodelling and ECM turnover.

Changes in interstitial matrix protein composition, caused by hypertrophic adipocytes, impair cellular communication and redox reactions (enzyme functions) in adipose tissue. Some studies also indicate an "early-phase fibrosis" in adipose tissue. This fibrosis induces adipose derangements, thereby linking adipose over-expansion to inflammatory recruitment and tissue insulin resistance (267).

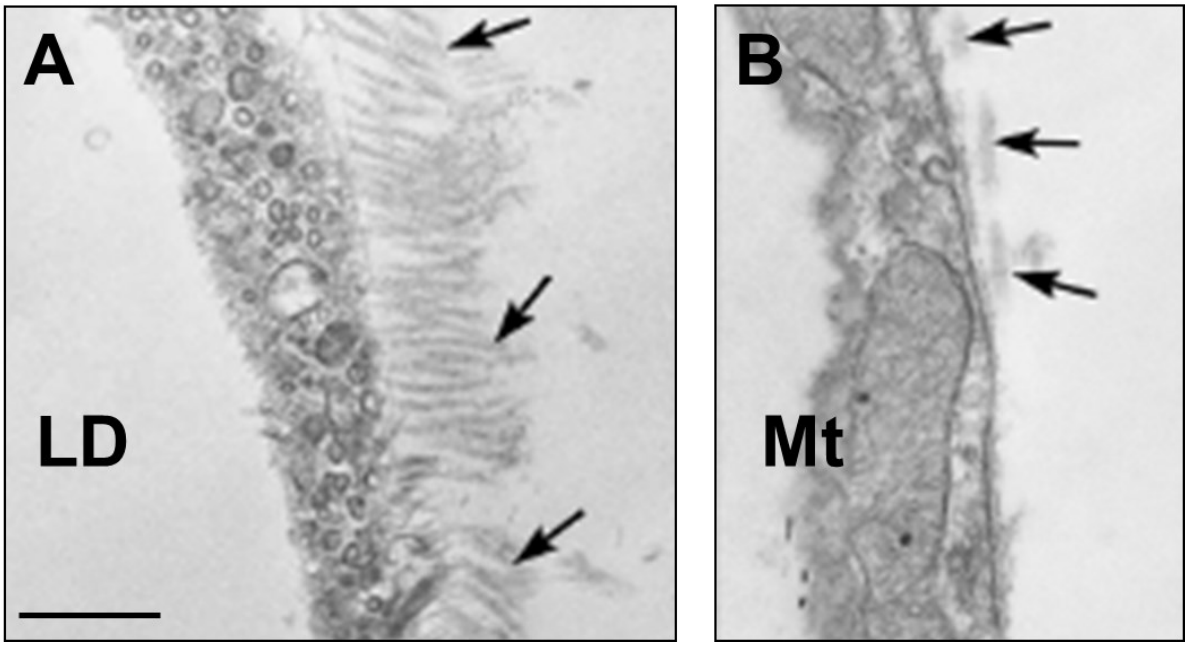

Figure 1.17: ECM of a hypertrophic vs. lean adipocyte. Adjusted from the original article (266). (A) Large hypertrophic adipocytes display abnormal enlarged ECM which appears expanded, whereas (B) small adipocytes express less ECM proteins. Scale bar: 30 μm. Abbreviations: LD, lipid droplet; Mt, mitochondrion.

1.5.3 Adipose Stress

Hypertrophic adipocytes and hyperplastic adipose tissues face serious problems because of the factors given below:

- Vascular insufficiency-related hypoxic stress
- Lactate accumulation
- Distorted ECM formation
- Fibrosis
- Development of cellular and tissue insulin-resistance
- Restricted lipogenesis,
- Increased chronic lipolysis,
- Excessive cholesterol production (activation of SREBP2)
- Abnormal release of FAs and cellular lipotoxicity
- Production of ROS and oxidative stress

Hypertrophic adipocytes exhibit substantial cellular stress or trauma and the consequences can be fatal. As evidence of this, several adipocyte ultrastructural abnormalities have been reported. Most of these abnormalities have been found to be more abundant in visceral depot adipocytes compared to subcutaneous depots. Hypertrophic adipocytes displaying ultrastructural abnormalities have been referred to as “degenerating” adipocytes (266).

1.5.3.1 Adipocyte Ultrastructural Abnormalities

One of the first consequences of adipocyte stress is the appearance of organelle abnormalities. As reported by Gokhan Hotamisligil and his colleagues, endoplasmic reticulum (ER) stress is an important defect for the intersection of adipose inflammation and metabolic disease (Fig. 1.18) (268). ER is the major cellular component for the folding required during protein maturation and for intracellular trafficking. ER

dysfunction results in an unfolded protein response (UPR) that is critical for continued function of cellular metabolism. Exposure to ROS can promote UPR and ER stress in adipocytes, and/or alternatively conflicting data that ER provides a highly relevant environment for the generation of ROS. Nevertheless, continuous oxidative stress and accumulation of misfolded/unfolded proteins (and dilation of the ER lumen) has toxic effects on hypertrophic adipocytes. Increased activity of anti-ROS enzymes can also instigate ER stress (269). Hypertrophy of mitochondria and the Golgi complex are among other organelle abnormalities in hypertrophic adipocytes (Fig. 1.18) (270, 271).

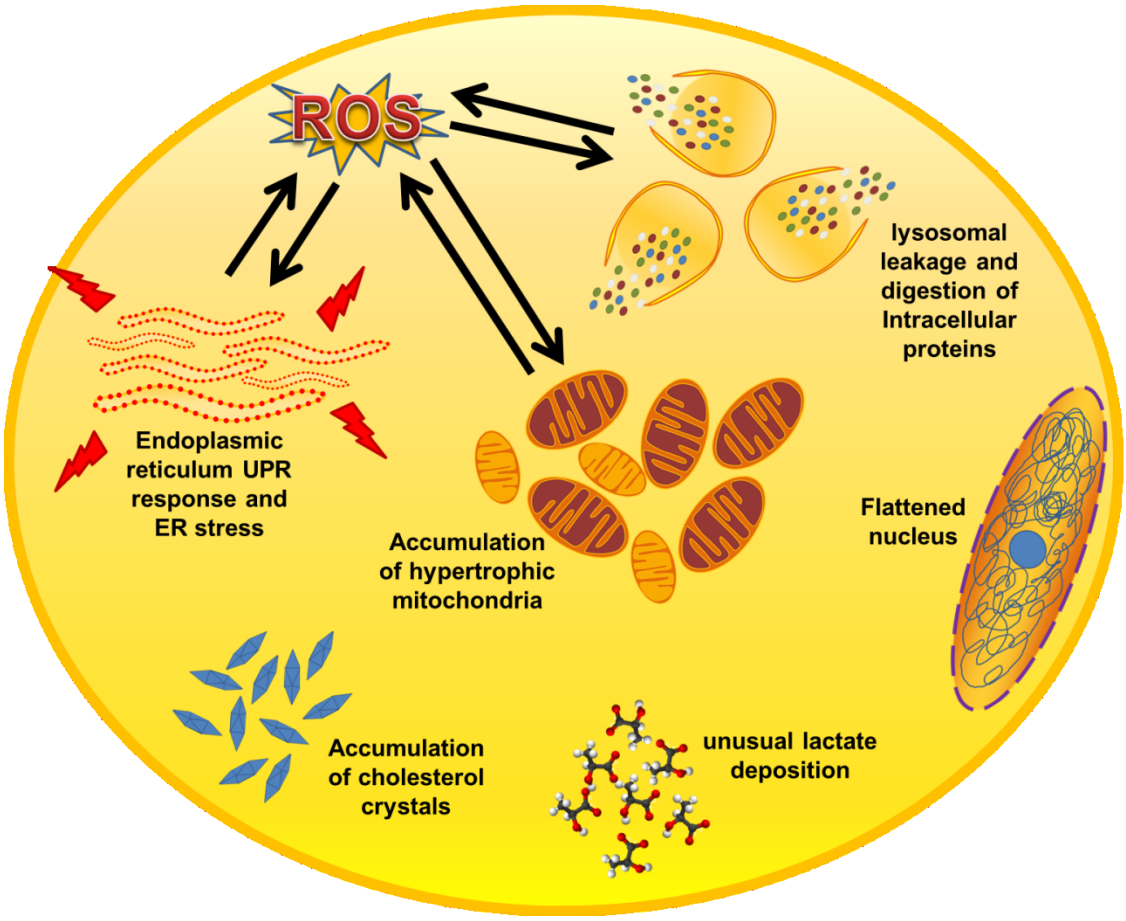

Figure 1.18: A hypertrophic adipocyte displaying ultrastructural abnormalities. As described in section 1.4.5, adipocytes stimulate SREBP2 activity after reaching to a critical cell size, to produce cholesterol, although hypertrophy initiates a "mistaken signal" of cholesterol deprivation in adipocytes (221). Excess amounts of cholesterol results in the formation of cholesterol crystals in hypertrophic adipocytes (Fig. 1.18) (266, 272). These cholesterol crystals are thought to activate NOD-like receptor family, pyrin domain containing 3 (NLRP3) inflammasome in adipocytes and force them to die by "pyroptosis" (discussed later in the section).

Lysosomal permeabilization (LMP) appears to occur in the late stages of adipocyte degeneration. It is mainly driven by chronic oxidative stress (Fig. 1.18). LMP is highly lethal as the release of lysosomal enzyme content results in digestion of intracellular proteins (273). This triggers a series of events that result in cellular degeneration and death. On the other hand, other changes noted in hypertrophic degenerating adipocytes include unusual glycogen deposition, increased cAMP and Ca^{++} accumulation, a flattened nucleus and a thinner cytoplasmic rim (266).

1.5.4 Adipokines

Adipose tissue is an active participant of bodily (energy) processes. As a secretory organ, it responds to stimulants by producing adipokines. Leptin, adiponectin, resistin, visfatin, and adipsin are the adipokines specifically/exclusively produced by adipocytes. There are publications reporting the production of some of these factors by other cell types, however, these observations were made after non-physiological manipulations. Other factors are produced by both adipocytes and SVF cells, such as IL molecules (e.g., IL6, IL10), TNFα, and MCP1. Lipid-engorgement of adipocytes and presence of ultrastructural abnormalities have adverse effects on adipose adipokine production (expression and secretion). These changes intensify stress on adipose cells and eventually recruit inflammation into the adipose tissue.

1.5.4.1 Leptin

As described in section 1.2.1, leptin was the first adipose-derived hormone to be discovered (274). It is produced by mature adipocytes, mostly in subcutaneous WAT. Leptin has a central regulatory role on appetite control by binding its receptors that are highly expressed in the hypothalamus (275). Leptin levels increase after feeding, especially when the amount of nutrients (fat) stored in adipocytes reach as a certain

level. In addition, lower circulating leptin levels associate with suppression in insulin release from β cells; this also increases feeling of hunger. Obese individuals are prone to develop resistance to leptin stimulation in their brain (276). The relationship between hyperleptinemia and leptin resistance is similar to the "chicken and egg" phenomenon; therefore, the mechanism of leptin resistance is yet not clear but leptin resistance leads to a constant feeling of hunger in individuals that results in increased food intake and possibly obesity.

Hyperleptinemia is an important cause of immune cell dysmodulation, adipose dysregulation, and hyperinsulinemia in obese individuals (277). Hypertrophic adipocytes increase their leptin production. Leptin can inhibit apoptosis of β cells indirectly by decreasing systemic NO levels (278). The decreased NO levels and upregulation of adhesion molecules in adipose endothelial cells that result from increased leptin levels increase oxidative stress in these cells and cause their dysfunction. Moreover, leptin has direct effects on thymus function; it induces T lymphocyte proliferation and activation (279, 280). Some studies have reported that leptin-deficient *ob*/*ob* mice showed reduced inflammation but increased susceptibility to infections and to endotoxin (281).

1.5.4.2 Adiponectin

Adiponectin is a 30 kDa adipokine. Low- (LMW [trimer]), middle- (MMW [hexamer]), or high- (HMW [dodecamer]) molecular weight forms are found in the circulation and the HMW form is accepted to be the main and biologically most effective form (282, 283). Adiponectin is found in microgram levels in a millilitre of blood whereas leptin is in nanogram amounts by mass; adiponectin is the most abundant hormone in the human circulation.

Adiponectin levels are increased in MHO individuals. A recent study reported a direct correlation (association) between hyperadiponectemia and a MHO phenotype in obese African Americans (284). These subjects also showed lower circulating insulin levels, smaller waist circumference and higher circulating high-density (HDL) cholesterol. Obese subjects with hypoadiponectemia were diagnosed with metabolic syndrome. On the other hand, hypoadiponectemia triggers neovascularization which is necessary for the expansion of adipose mass. However, as stated previously (section 1.5.2), vascularization usually is not sufficient to accommodate the oxygen needs of expanding adipose tissues.

As mentioned earlier (section 1.3.2), eating causes activation and insulin secretion of β cells. The post-prandial insulin response results in increased lipid and glucose uptake in adipocytes. This stimulates PPARγ to produce more LD proteins. Meantime, PPARγ also upregulates adiponectin production from adipocytes as an insulin-sensitizing hormone (285, 286). PPARγ agonists (and its endogenous activation) induce adiponectin production in adipocytes. However, this is not the ultimate response in the regulation of adiponectin. Accordingly, increasing adiposity has been shown to reduce tissue and circulating adiponectin levels. For example, increased ROS levels cause a reduction in adiponectin expression during excessive adiposity (287, 288). Lipid-engorgement in hypertrophic degenerating adipocytes also results in decreased adiponectin production (225, 289).

Adiponectin actions are exerted through two different receptors, AdipoR1 and AdipoR2. These are expressed differently in different tissues, resulting in different cellular and metabolic effects (290). Activation of DCC-interacting protein 13-α (APPL1) and the ratio of AdipoR1/2 determine the fate of human macrophages in adipose tissue, and is an important regulator of lipid metabolism, inflammation and

foam-cell formation from macrophages. Moreover, APPL1 is also involved in adiponectin/insulin-signalling cross-talk.

Another key function of adiponectin is that it is an important anti-inflammatory adipokine (291). Its globular domain structurally, but not sequentially, resembles that of TNFα. Adiponectin and TNFα have reciprocal inhibitory effects on each other. Thus, cellular indices leading to adiponectin downregulation stimulate TNFα expression in adipocytes. Conversely, adiponectin inhibits the pro-inflammatory NF-κB signalling (292, 293). Absence of adiponectin, therefore, has a permissive effect on inflammatory recruitment in adipose tissue.

As stated in Section 1.5.4, there are other important adipose-derived factors such as resistin, visfatin, and adipsin. Some of these have positive some of these have (relatively) negative effects on adipose and whole body homeostasis. For example, adipsin is an adipokine that connects healthy adipose function to sustaining pancreatic β cell function (294). Development of obesity suppresses expression of this adipokine (295).

1.5.5 Adipose-Derived Inflammatory Factors

Caloric overload perturbs adipokine secretion in adipocytes. Constant lipid load switches healthy adipocytes (in those exhibiting increased adiponectin and IL10 expression) to an "aggressive" (inflammatory) phenotype. Insulin is another player that contributes to promotion of an inflammatory response in adipocytes. Eventually, several inflammatory kinases become activated, such as c-Jun N-terminal kinase (JNK) and inhibitor κB kinase (IKK) in hypertrophic adipocytes and initiate secretion of such pro-inflammatory factors as TNFα and MCP1 (296). The main "rationale" for these cellular reactions would seem to be to protect the cell from lipid-engorgement and lipotoxicity

(dyslipidemia); however, local protective mechanisms cause problems in systemic levels.

1.5.5.1 TNFα

TNFα has attracted significant attention from scientists over the last two decades. It was first found in patients with cachexia. Cachexia is a disorder characterized by irreversible adipose and muscle waste in the body (297). Inflammatory responses in cachexia led scientists to discover TNFα, and it was no surprise to them that TNFα is also involved in the pathogenesis of obesity (298, 299). Accordingly, TNFα arises from tissue inflammatory responses, and further promotes tissue degradation.

An important reason for TNFα expression in enlarging adipocytes appears to be downregulation of cellular lipid and glucose uptake, thereby attempting to inhibit the constant stream of nutrients into nutrient-overloaded cells. How does this happen? TNFα inhibits intracellular insulin signalling by phosphorylation of IRS1 serine residue (300). IRS1 is unable to function as a signalling kinase when phosphorylated at serine instead of tyrosine residues. Meanwhile, TNFα also stimulates pro-inflammatory IL6 and MCP1 production in adipocytes through activation of NF-κB (301, 302). Although adipocytes initiate the TNFα production in adipose tissue, pro-inflammatory (M1) macrophages augment TNFα production to a higher level. This results in chronic lipolysis of hypertrophic adipocytes. Accordingly, TNFα produced by macrophages (paracrine) and adipocytes themselves (autocrine) increases intracellular cAMP levels via activation of mitogen-activated protein kinase kinase (MEK) and extracellular signal-related kinase (ERK) pathway (303). As stated in section 1.4.4, increased intracellular cAMP stimulates PKA that results in hyperphosphorylation of lipid droplet perilipins and subsequently infiltration of HSL into LD and increase lipolysis. To summarize, TNFα abrogates lipid and glucose uptake in hypertrophic adipocytes, and

meantime, reverses lipid overload by activating lipolysis. These indices confer protective effects on adipocyte metabolism, but also promote peripheral (ectopic) lipid accumulation and systemic insulin resistance, linking obesity to metabolic syndrome. Conversely, individuals with MHO exhibit lower levels of TNFα and a reduced inflammatory profile (304).

1.5.5.2 MCP1

MCP1 (also called CCL2) participates in adipose inflammation by chemo-attraction of immune cells, primarily monocytes and/or macrophages (305). MCP1 is mainly produced by mature adipocytes; there is a positive correlation between MCP1 and leptin expression. It is also thought that MCP1 expression starts with the expression of growth factors in hypertrophic adipocytes (section 1.4.6) (306). Monocytes are the macrophage progenitor cells, originated from BM. They can also differentiate into dendritic cells (DCs). MCP1 mediates chemotactic recruitment of monocytes into adipose tissue after binding to its receptor, CCR2, on these cells. Moreover, there are some studies showing that MCP1 triggers a pro-inflammatory phenotype transformation in monocytes (307, 308). However, it is still not clear whether monocytes migrate to adipose tissue before their differentiation into macrophages or they start their transformation towards a pro-inflammatory phenotype even in the circulation (pro-inflammatory monocytes).

Overall, elevated plasma level of MCP1 results in a systemic inflammatory response that is sufficient to initiate inflammation and insulin resistance, not only in adipose tissue, but also in liver and muscle (309). Researchers have shown that adipocyte-specific over-expression of MCP1 is capable of causing systemic insulin resistance and hepatic lipid accumulation (310). In contrast, experiments on *Ccr2*$^{-/-}$ mice have showed that absence of MCP1 results in reduced numbers of macrophages despite excessive fat accumulation; these mice exhibit a MHO-like phenotype (311). In conclusion, the

MCP1 – CCR2 axis is an important module in the initiation and acceleration of adipose inflammation.

Many other adipose-derived factors are important in the genesis of adipose inflammation and its relationship to systemic dysregulation, such as insulin resistance and atherosclerosis. Chemerin is a recently reported chemotactic adipokine; serum circulation of this novel adipokine was demonstrated to associate with metabolic syndrome (312). Some others are IL6, resistin, visfatin, and adipsin. Phenotype comparison of unhealthy (metabolic) obese individuals to MHO subjects has great potential to understand the pathophysiology these factors. An improved understanding of adipose-derived factors has therapeutic potential to combat obesity-related metabolic comorbidities.

1.5.6 Adipose Tissue Macrophages and Inflammation

The origin of adipose tissue macrophages has been a major question until recently. Some studies reported important similarities between adipocytes and macrophages (313), and indeed other work has shown that preadipocytes, under certain stimuli, can differentiate into macrophages (314). Nevertheless, adipose tissue macrophages have generally been found to derive from the BM *in vivo* (315). In Chapter 4, we will discuss the origins of adipose tissue macrophages through the experiments performed with BM chimeric *Tlr9*$^{-/-}$ and *WT* mice.

1.5.6.1 Macrophage Crown-Like Structures

Although the exact reason is not clear, there are resident macrophages in adipose tissue. These macrophages exhibit an anti-inflammatory (M2) phenotype (316). Adipocyte hypertrophy and degeneration cause a phenotypic switch in these macrophages towards a pro-inflammatory (M1) profile (317). Although research in the

last few years has revealed much greater diversity of "flexibility" in macrophage subtypes, M1 and M2 phenotypes are used here for clarity. M1 macrophages start to express pro-inflammatory markers such as cluster of differentiation molecule 11b and 11c (CD11b, CD11c), EGF-like module-containing mucin-like hormone receptor-like 1 (F4/80), and etc (318, 319). Intercellular adhesion molecule (ICAM) is a pro-inflammatory adhesion molecule that is produced upon stimulation by TNFα. Pro-inflammatory M1 macrophages are the main source of ICAM production in inflamed WATs (320). Nevertheless, macrophage phenotypic switch is not sufficient to initiate an inflammatory response in adipose tissue. In this respect, installation of adipose tissue inflammation happens by the formation of "macrophage crown-like structures" (CLS) (230). Classically-activated (pro-inflammatory) M1 macrophages form CLSs by congregating around small adipocytes (Fig. 1.19). The close proximity of these macrophages intensifies their pro-inflammatory response by effecting on each other, via intercellular communication, paracrine signalling, etc. At times, these processes culminate in cellular fusion to form a giant multinucleate cell (referred as foam cells).

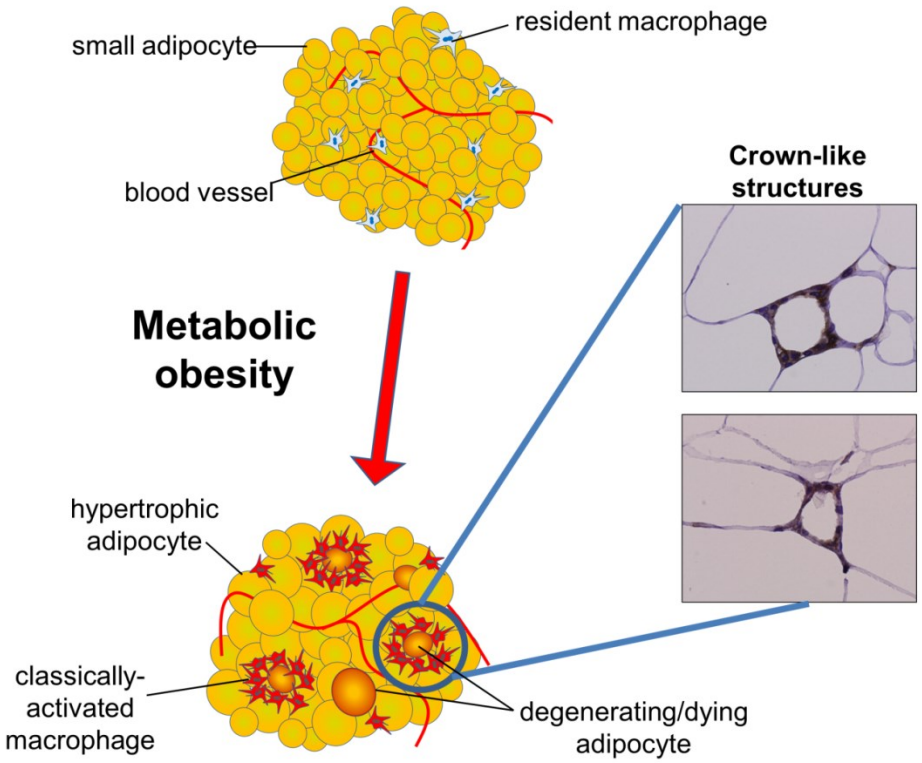

Figure 1.19: Adipose crown-like structures (CLSs) form around small injured or dead adipocyte. Classically-activated (M1 – F4/80 positive) pro-inflammatory macrophages recognize degenerating/dead adipocytes and coalesce around them to form CLSs, presumably so as to minimize the toxic effects of the cellular debris to the adipose tissue.

1.5.6.2 Small Dead Adipocytes in the Centre of CLSs

In inflamed adipose tissues, 90% of macrophages are found in CLSs (321). At this stage, the vital question is that what induces/triggers macrophage accumulation to coalesce around small adipocytes. Scientists have suggested this is "adipocyte death". However, it is still not clear by which mechanisms macrophages can sense and migrate to degenerating or dead adipocytes. In this PhD thesis, we discuss the activation of damage/danger-associated molecular pattern (DAMP)-recognizing toll-like receptor 9 (TLR9) in adipose tissue macrophages as one potential mechanism regarding the formation of CLSs (Chapter 4). Upon activation by signalling from one or more pattern recognition receptors (e.g., TLRs 4 and 9, NLRP3), M1 macrophages localize to dead adipocytes in order to clear (phagocytosis) toxic cellular debris and remnant LDs. Thereby, lipid-laden macrophages form "foam cells" during adipose inflammation

(321). In addition, M1 macrophages can also sense hypertrophic degenerating (injured) adipocytes and cause their death by extracellular signalling, such as by producing high concentration of TNFα after surrounding the cells (321, 322). These processes are presumably performed in the first instance, to maintain adipose structure and function. In other words, macrophages protect the whole tissue from degeneration and death by sacrificing individual adipocytes. In constant energy surplus, macrophage-mediated tissue remodelling becomes permanent and adipose tissue inflammation becomes "persistent".

Until recently, small adipocyte subpopulations have been referred as healthy modulators in adipose tissue. Accordingly, large adipocytes were hypertrophic, pro-inflammatory, and degenerating, whereas small-to-medium adipocytes were healthy and anti-inflammatory. This belief has been changing with the discovery of the remnants of adipocyte deaths in inflamed adipose tissues. A significant number of adipocytes die via pyroptosis and these cells are similarly small in size as are the new, healthy adipocytes. For this reason, detailed adipose morphometry analyses should also discriminate the types or "locale" of adipocytes (e.g., in relation to surrounding macrophages), not just their size.

1.5.6.3 The Mechanisms of Adipocyte Death

Small adipocytes that are surrounded by CLSs exhibit characteristics of necrotic cell death (230). Some studies, however, reported apoptotic cell death after stimulation with high fat diet (HFD) (323). Both of these proposals are true but there is no single mechanism for adipocyte death. Hypertrophic degenerating adipocytes are sometimes forced to death by macrophages by a mechanism called "necroptosis". Necroptosis is forced (inflammatory) cell death, primarily induced by TNFα (324, 325). Induction of TNF receptor activates the receptor-interacting protein kinase 3 / mixed lineage kinase

domain-like protein (RIP3/MLKL)-dependent necrosome and results in regulated (forced) necrosis (326). Nevertheless, most of these degenerating adipocytes die through pyroptosis and trigger the formation of CLS around them.

Progress in electron microscopic techniques has unravelled many subcellular abnormalities in hypertrophic adipocytes. As mentioned previously (section 1.5.3), these abnormalities are directly linked to adipocyte stress and they cause degeneration of the cells (266). These abnormal features and increased cellular stress can result in activation of NLRP3 inflammasome, which assembles with apoptosis-associated speck-like protein containing a carboxyl-terminal CARD (ASC) to cause a pro-inflammatory dimerization of pro-caspase 1. This activates caspase 1 catalytic cleavage of these molecules to their active form (327). There is likely a direct association between generation of ROS derivatives and activation of NLRP3 (Fig. 1.20) (328).

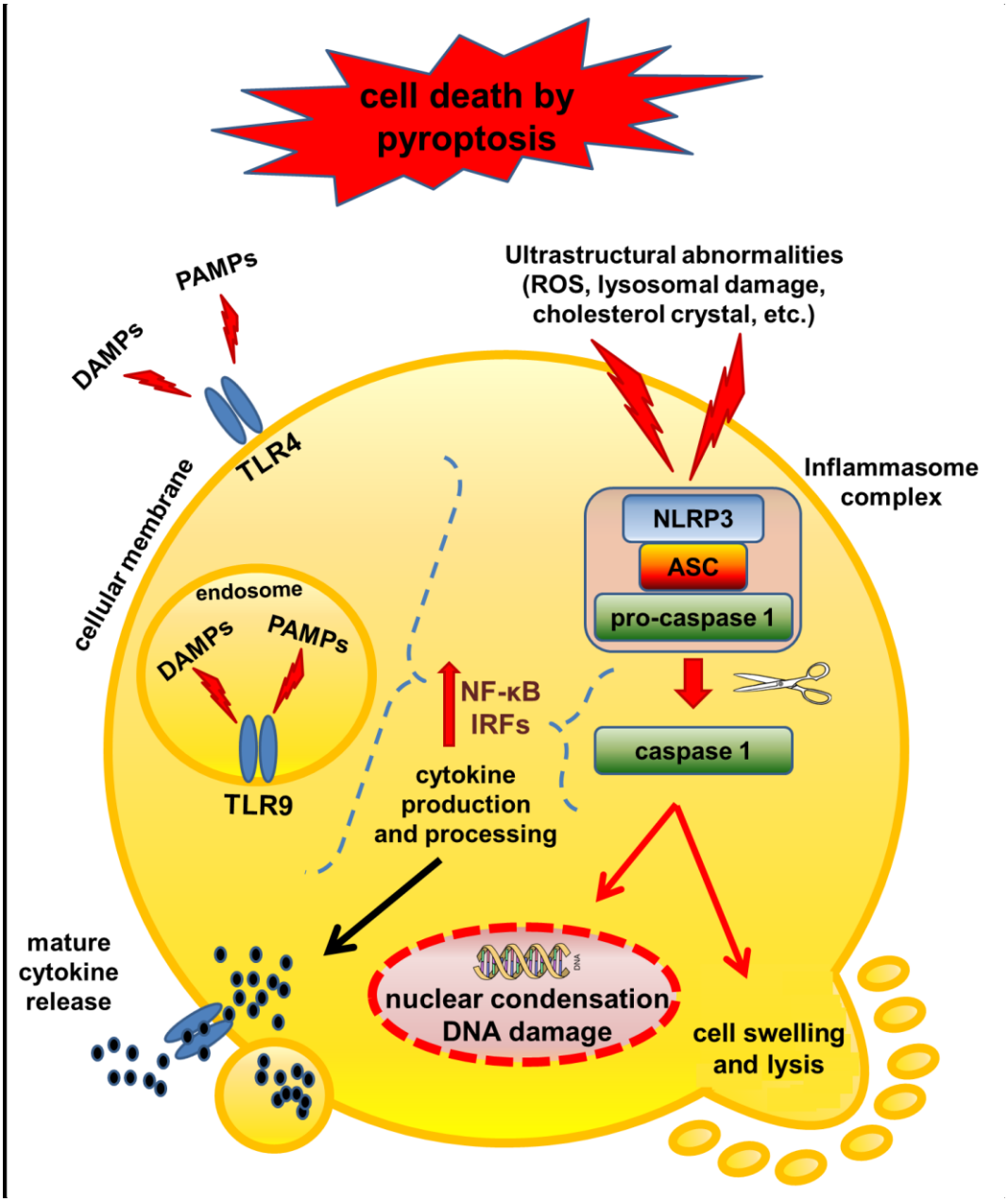

Figure 1.20: Lipid-engorged adipocytes die of pyroptosis. Stress-related ultrastructural abnormalities activate the inflammasome complex in hypertrophic adipocytes. This leads to cleavage of pro-caspase 1 and induction of the pyroptotic cascade in the cell. Induction of TLR4 and/or TLR9 by external stimuli and oxidative stress contribute to this process. Abbreviations: ASC, apoptosis-associated speck-like protein containing a carboxyl-terminal CARD; DAMPs, damage/danger -associated molecular patterns; IRFs, interferon regulatory factors; NF-κB, nuclear factor kappa B; NLRP3, NOD-like receptor family, pyrin domain containing3; PAMPs, pathogen-associated molecular patterns; ROS, reactive oxygen species; TLR, toll-like receptor.

Caspases have protease activity; these enzymes are regulated by inflammasome and they can lead to cell death. Accordingly, caspase 1 is a highly pro-inflammatory cellular agent and it can kill the cell by an inflammatory form cell death, pyroptosis (327, 329). There are several characteristics of pyroptosis, such as water influx, osmotic lysis,

plasma membrane degradation, and release of pro-inflammatory cellular content (330). Like apoptosis, pyroptosis is also associated with DNA laddering, caused by DNase cleavage into ~200 bp oligonucleotides. Release of adipocyte cytokines and chemokines attracts other macrophages to locate around the cell.

There are similarities and differences between apoptosis, necrosis and pyroptosis, but they occur by different mechanisms. Pyroptosis requires formation of inflammasome (also called pyroptosome) and resulting caspase 1 activity, unlike apoptosis which requires cellular energy and caspase 3/7 activity (326, 329). Some characteristics of necrosis (and necroptosis) occur in pyroptosis, such as cellular swelling and pore formation in the plasma membrane. On the other hand, necrosis is generally not a programmed mechanism and does not require either caspase 1 or caspase 3/7 activity.

There are also other mechanisms identified with adipocyte death. For example, LMP in degenerating adipocytes results in activation of cathepsins (331, 332). Cathepsin B (CTSB) induces mitochondrial dysfunction whereas cathepsin D (CTSD) can induce pro-apoptotic protein activation. This results in cytochrome C release and activation of caspases in the cell. However, LMP can lead to cell death earlier than caspase activation in cells displaying characteristics of necrosis (333).

1.5.7 Recruitment of Adipose Inflammation

Pyroptosis or pro-inflammatory forced death (necroptosis) causes cell lysis. This includes liberation of cellular lipid content. If lipid release is not controlled in the tissue, it causes lipotoxicity even to surrounding healthy adipocytes (266). For this reason, macrophages phagocytos the lipid extracts. This results in formation of the “foam cell-like macrophage syncytia” in adipose tissue.

Granulocyte-macrophage colony-stimulating factor (GM-CSF) is an important glycoprotein that functions as a cytokine and modulates immune responses (334). It is produced by a variety of cell types, including immune cells, fibroblasts, and endothelial cells. Although it is produced locally, it has paracrine and endocrine effects on the maturation and migration of macrophages. In 2011, Daorong Feng and her colleagues performed an experiment on *Gm-Csf*-null mice to show whether adipocyte death was linked to macrophage infiltration (335). The results were striking. *Gm-Csf*-null mice fed a HFD displayed similar numbers of adipocyte deaths compared to HFD-fed controls. However, macrophage infiltration into adipose tissue was markedly reduced. Likewise, disabling of macrophages by using liposome-clodronate did not display much effect on adipocyte death although there was a significant decrease in adipose inflammatory recruitment. These findings imply that the death of hypertrophic degenerating adipocytes is independent of macrophage recruitment.

Perhaps the most interesting finding in this study was the improvement in systemic insulin resistance in HFD-fed *Gm-Csf*-null and liposome-clodronate macrophage-ablated mice (335). This finding needs to be supported by future investigations. Nevertheless, it points to adipose inflammation being more hazardous than adipocyte dysregulation in terms of effecting on whole body energy metabolism.

1.5.8 "Persistency" in Adipose Inflammation and Adipose Restriction

Constant energy surplus, continuous adipocyte death and adipose inflammatory recruitment cause permanent changes in adipose tissues (336). Inflammation becomes persistent and chronic inflammation results in chronic metabolic changes. Persistent adipose inflammation is a local reaction comparable to infection or trauma-induced immune responses. This is why obesity is called a low grade (sterile) inflammatory disease.

In one study, C57 male mice fed a HFD lost 40% of their epididymal WAT mass between 12 and 16 weeks of age. From 16 to 20 weeks, epididymal WAT weight become fixed and did not change (337). During 12 – 20 weeks, whole body insulin resistance increase at a constant rate and hepatomegaly occurred. Macro-steatosis became evident after 12 weeks. On the other hand, there was a reduction in circulation MCP1 levels after 12 weeks. The reason for the latter change may be that a balance between macrophage saturation and relatively healthier adipocytes eventually is established in persistently inflamed adipose tissues.

Similar to the above findings, most adipose depots become dysregulated in unhealthy obese individuals. Macrophages in persistent adipose inflammation behave like "guardians" and regulate adipocyte metabolism. Most hypertrophic degenerating adipocytes die, but they are not fully replenished by new adipocytes. In addition, other already-existing adipocytes become insulin-resistant so that their glucose and lipid uptake is limited. Overall, these mechanisms protect adipose tissues (and the system) from adipocyte mass destructions, toxic effects of cellular lysis and further tissue atrophy; however, adipose tissues decrease in size and develop effectively a "growth restriction".

Adipose restriction is a chronic problem. Perhaps, the most important physiological process of adipose tissue is buffering the acute lipid fluxes in the circulation during the post prandial phase. When the lipid/energy storage capacity is impaired in adipose tissues, ectopic deposition of lipids happens, primarily in the liver and skeletal muscle. The details of the ectopic lipid accumulation and the progression of non-alcoholic fatty liver disease will be discussed in Chapter 3, which the effects of adipose dysregulation and inflammation on myocyte insulin sensitivity and activity are the subject of further consideration in Chapter 6.

1.6 Overall Hypothesis and Aims of This Reseach

Systemic insulin resistance, NAFLD and NASH is the outcome of complex interactions between nutrient supply, blood glucose, and adipose lipid storage capacity reflected by adipose morphology and inflammation. We therefore investigated the effects of alterations in adipose function on glucose metabolism and liver, as well as mechanisms of adipose inflammatory recruitment and adipose dysfunction in murine models of dietary obesity and/or metabolic obesity with NASH. Specifically,

a) Examine the effects of adipose expansion and morphometry as well as adipose inflammation in relation to NASH pathogenesis (Chapter 3).
b) Elaborate adipose morphometry in terms of adipocyte size changes and distribution in metabolic obesity with adipose inflammation; test whether TLR9 signaling plays a role in adipose inflammatory recruitment and investigate whether adipose inflammation is related to liver inflammatory recruitment in NASH (Chapter 4).
c) Test whether 6-ECDCA confers metabolic improvements in diabetic obese mice as well as in mice with diet-induced obesity; compare adiposity, inflammation and macrophage phenotypic polarization in different adipose compartments from obese, 6-ECDCA-treated vs. untreated mice (Chapter 5).
d) Test whether provision of an exercise wheel prevents adipose inflammation and dysfunction as well as insulin resistance, diabetes, hepatic steatosis and NASH (Chapter 6).

CHAPTER 2

CHAPTER 2: MATERIALS AND METHODS

The laboratory equipment used in this study is listed in Appendix A. The compounds and commercial kits used are also listed in Appendix A. Detailed protocols for biochemical and molecular techniques are provided in Appendix B.

2.1 Animal care

2.1.1 Mice

2.1.1.1 Ethics and Animal Housing

Experimental procedures were approved by the Animal Ethics Committee (AEC) of The Australian National University (ANU) under the animal ethics protocol number A2012/22. Experimental mice were bred, maintained and housed at the animal facility in Hugh Ennor Building of The ANU or The Canberra Hospital. Unless stated otherwise, mice were grouped 2-5 per cage, with *ad-libitum* access to water and food, under 12-hour day/night cycle and constant temperature of 22^0C. Cages were filled with bedding material as well as an igloo, wooden sticks, and other enrichment materials.

2.1.1.2 Mice Strains and Backgrounds

Several lines of mutant or gene-deleted mice and different background strains have been used during this PhD project; specific information is provided regarding the choice of animal model in each Chapter. The mouse strains are NOD.B10, Balb/c, and C57B6. As a genetic model of obesity and non-alcoholic steatohepatitis (NASH), we used *foz/foz* mice (338). These mice have profoundly disordered appetite regulation due to a mutation of the *Alms1* gene (susceptible to murine equivalent of Alström syndrome). They develop early-onset hyperphagic obesity with later development of insulin

resistance, diabetes, and dyslipidaemia associated with low serum adiponectin (339). In addition, *Tlr9*, *Tlr4*, *MyD88* gene-deleted mice on C57B6 strain were used for specific experiments outlined in this thesis.

2.1.2 Diets

2.1.2.1 Atherogenic Diet

After weaning, mice were fed standard rodent chow diet (Gordon's Speciality Stockfeed, Sydney, Australia) unless otherwise stated. As a dietary model of obesity, we used an atherogenic diet which contains 23% fat, 45% simple carbohydrate, and 0.19% cholesterol (4.78 kcal/g digestible energy; Speciality Feeds, Glen Forrest, Australia). Food intake was assessed by weighing added and residual food on a weekly or fortnightly basis.

2.1.2.2 Obeticholic (6-ethylchenodeoxycholic) Acid "Cupcakes"

To understand whether cholesterol overloading is relevant to adipose inflammation, we used an FXR agonist, obeticholic acid (OCA), administered orally (the rationale is presented in Chapter 6). 10 mg OCA was dissolved in 0.5 ml 50% ethyl alcohol (EtOH) and further in 50 ml distilled H_2O. Drug solution was sprayed on 1 kg atherogenic diet (equally distributed) and the food was allowed to dry at 37^0C for 2 hours and kept in a commercial cupcake tray at 4^0C until complete evaporation. Final EtOH concentration in the diet was < 0.05%. The firm cupcakes were stored at 4^0C until used.

2.1.3 Anaesthesia and Tissue Collection

At the end of experimental procedures, mice were fasted for a standard 4 hour unless otherwise stated. Prior to the harvest, all mice were weighed and anaesthetized using 100 mg/kg ketamine and 16 mg/kg xylazine, administered intra-peritoneally. Blood was

collected by intra-cardiac puncture, and serum separated by centrifugation of the blood sample at 10 min, 3500 rpm. Depending on the study, liver, visceral (epididymal/periovarian and/or mesenteric) WATs, subcutaneous WATs (lumbar and/or dorsal), BAT, pancreas, colon, and gastrocnemius muscle were removed by standardized procedures to ensure reproducibility. Tissue segments were fixed in 10% neutral buffered formalin and in cryofixative compound (frozen) for staining/histology purposes. The remainder of the tissues was snap-frozen in liquid nitrogen and stored at -80^0C until used for analyses.

2.1.4 Exercise Protocol

From weaning (4 weeks age), half the cages were fitted with mice in pairs and an exercise wheel for *ad libitum* physical activity, which was monitored by recording wheel rotations with a cycle computer every week. Body weight was assessed weekly. Basic read-outs from the cycle computer were maximum speed (km/h), average speed (km/h), distance (km), and running time (h-min). Measurements were divided into two for each cage and read out (body weights were checked firstly to ensure that both mice had used the wheel evenly or close in the cage).

2.1.5 *In vivo* Determination of Insulin Sensitivity

At the predetermined age, mice were fasted 14 hours, anesthetized and administered insulin (1 U/kg body weight), by intra-aortic injection. Liver, visceral and subcutaneous WAT and gastrocnemius muscle samples were collected by a standard protocol both before (from right side) and 3 minutes after (from left side). To prevent excess bleeding during the 3 minutes period, the pedicle of the resected liver segment was ligated.

2.1.6 Mouse Irradiation and Bone Marrow Transplantation

8 week old mice were used for BM transplantation experiments. The irradiation process was conducted in John Curtin School of Medical Research (JCSMR) building at the ANU Acton campus, using a Standard Operation Procedure (SOP). Mice were exposed to a total dose of 900 cGy in 2 sessions (one in the morning, one in the afternoon). For BM reconstitution, we used histocompatible wildtype or mice of the designated mutation or gene-deletion of interest. All processes were conducted under sterile conditions. Irradiated mice were administered 10^6 BM cells (in normal saline) via lateral tail vein injection. After irradiation and BM transplantation, BM chimeric mice were transferred to AEC-approved specific pathogen free (SPF) animal facility at JCSMR. For 6 weeks after irradiation, mice were administered antibiotics ($8.5x10^5$ U/L polymyxin-B-sulphate, 1.1 g/L neomycin sulphate). Thereafter, they were fed atherogenic diet for 14 weeks. At the end of experiments, mice were harvested under the standard harvest procedure (section 2.1.3).

2.2 Biochemical Methods

2.2.1 Blood Analyses

2.2.1.1 Serum Analyses

Serum samples were sent to Australian Capital Territory (ACT) pathology department for analysis (by multichannel autoanalyzer) of alanine aminotransferase (ALT), aspartate aminotransferase (AST), total cholesterol, total triglyceride, and ultra-high-density lipoproteins (ultra HDL).

2.2.1.2 Enzyme-Linked Immunosorbent Assay

Commercially available enzyme-linked immunosorbent assay (ELISA) kits were used to determine the circulating concentrations of specific proteins such as adiponectin,

insulin, and MCP1. For individual assays, serum samples were diluted in a range of 1:1 to 1:1000, as needed. Sample absorbance values (at 450 – 570 nm wavelengths) were assessed by a spectrophotometer. When r^2 was 0.98 and higher (optimally 1), the value of absorbance (Y axis) was used to calculate the sample concentration (X axis) by a formula.

2.2.1.3 Fasting Blood Glucose and Intraperitoneal Glucose Tolerance Test (IpGTT)

One week before the end of experiments, mice were fasted for 4 hours, then glucose tolerance determined after intraperitoneal injection of glucose (2 g/kg lean body mass; in saline). Blood glucose measurements were determined at 0, 15, 30, 60, 120, and 180 minutes post-injection using a glucometer. This glucometer indicates as "HI" any glucose level higher than 33.4 mmol/L. To accommodate this restriction on accuracy, we introduced negative bias by using the lower value of 33.4 mmol/L in such instances to calculate group data.

2.2.2 Tissue lipid Content

2.2.2.1 Oil-red-O Staining

Tissue lipid content was assessed using oil-red-O (ORO) staining. Frozen tissue samples were gently homogenized using a plastic disposable homogenizer, stained with ORO solution. Incorporated ORO content was assessed by measuring the absorbance by a spectrophotometer. The detailed protocol is provided in Appendix D.

2.2.2.2 Lipid Analyses by Gas (GC) and High-Performance Liquid (HPLC) Chromatography

Tissue TAG, DAG, FC, cholesteryl ester (CE), total and free FAs were measured by a collaborator, Dr Geoff Haigh from University of Washington, Seattle USA, using chromatographic techniques (340).

2.2.3 Histological Analyses

2.2.3.1 Immunohistochemistry

Liver and adipose tissue samples were fixed in formalin and embedded in paraffin blocks. Sections cut from these samples (4-8 μm thick) were analyzed by immunohistochemistry (IHC) for specific antibodies. Antibodies are provided in Appendix A, and detailed protocols for immunohistochemical staining are given in Appendix B.

2.2.3.2 Liver Histology and Assessment of Liver Fibrosis

Hematoxylin and eosin (H&E)-stained liver sections were scored blind by an experienced liver pathologist (MMY) according to the system devised for human NASH (scoring based on NAFLD activity score [NAS]; 0 – 3 = not NASH, 4 = borderline, 5 – 7 = definite NASH) (341). A different rotation based on pathologist's global assessment was also used (0 = normal, 1 = definite NASH, 2 = simple steatosis, 3 = borderline for NASH). To quantify liver fibrosis, we performed densitometry of liver sections stained for collagen with Masson's trichrome, using ImageJ software.

2.2.3.3 Adipose Morphometry Analysis

Formalin-fixed adipose tissue samples were embedded in paraffin and 4 μm thick sections cut. Morphometry was performed on H&E-stained adipose sections using Leica

Application Suite software. Morphometric analyses were done on a minimum of 10 fields (1 mm^2 area). The number of CLSs was calculated by analyzing 10 fields of H&E-stained adipose sections for each mouse, with results normalized to 100 adipocytes.

2.3 Molecular Methods

2.3.1 Gene Expression via mRNA Levels

2.3.1.1 Combined Method for Total RNA Isolation

Isolation of total RNA from frozen samples was performed with a combined protocol of TRI Reagent and commercial SV Total RNA Isolation System. This strategy increased the yield and the quality of RNA, as assessed using a NanoDrop Spectrophotometer. The detailed protocol is provided in Appendix B.

2.3.1.2 cDNA Synthesis

cDNA was synthesized from 0.5 to 1 µg total RNA using High-Capacity cDNA Reverse Transcription Kit (Life Sciences, Carlsbad, CA). The detailed protocol is given in Appendix B.

2.3.1.3 Primer Design for SYBR®-Green Based Quantitative Polymerase Chain Reaction

Commercially available primers from Sigma-Aldrich have been used for experiments described in this PhD. For rare genes, primers were designed considering the right gene, product length, the exon-exon boundaries, no mis-match, GC content (50-60 %), secondary structure and Tm 65^0C. To achieve this, a diversity of online tools, such as National Center for Biotechnology Information (NCBI) website, PerlPrimer, Primer 3, and uMelt HETS was used. Primer working solutions (10 µM) were diluted from primer

stock solutions, measuring the precise concentration by NanoDrop using single strand DNA analysis. The detailed protocol for primer design is provided in Appendix B.

2.3.1.4 SBYR®-Green and Reaction Mix

Real-time polymerase chain reaction analyses were performed to detect tissue-specific mRNA levels using iQ™ SYBR® Green Supermix, conducting reactions in an iQ™5 real-time thermal cycler. Data normalization was performed using geometric mean of 3 house-keeping genes, specifically ribosomal protein L13a (RPL13A), beta-actin (ACTB), and glyceraldehyde 3-phosphate dehydrogenase (GAPDH) (342). The detailed protocol for SBYR®-Green qPCR is provided in Appendix B.

2.3.2 Determination of Protein Levels

2.3.2.1 Tissue Protein Extraction

2.3.2.1.1 Liver Protein

Frozen liver samples were homogenized in 9X ERK buffer, using the protocol detailed in Appendix B.

2.3.2.1.2 Muscle Protein

Frozen muscle samples were homogenized in muscle lysis buffer (at Appendix B).

2.3.2.1.3 Adipose Protein

Frozen adipose samples were homogenized in a detergent-free lysis buffer unless otherwise stated (343). In some parts of the PhD project, the muscle protein extraction protocol was applied to adipose. The detailed protocol is provided in Appendix B.

2.3.2.1.4 Protein Estimation

Total protein concentrations were estimated by the Bradford assay (344), using bovine serum albumin (BSA) as standard. The detailed protocol is provided in Appendix B.

2.3.2.2 Western Blotting

Proteins were resolved with SDS-PAGE, and immunoreactivity visualized by chemiluminescence detection. Heat shock protein 90 (HSP90) was used as the protein loading control unless otherwise specified. Protein bands were quantified by densitometric analysis. Phosphorylation was expressed as phospho- to total protein ratio. A list of target proteins and primary antibodies is provided in Appendix C, and the details of western blot protocols are given in Appendix B.

2.3.3 Adipose Flow Cytometry

2.3.3.1 Isolation of Mature Adipocytes

Adipose tissue is a connective tissue composed of terminally differentiated adipocytes and SVF cells. Mature adipocytes are very fragile cells, largely as a consequence of their distension by lipid. Therefore, isolation of live adipocytes is a delicate process. Cell strainers with 150/200 μm pore size were used to isolate adipocytes, by the detailed protocol detailed in Appendix B.

2.3.3.2 Isolation of Adipose Stromal Vascular Fraction

Adipose tissue SVF contains preadipocytes, preadipocytes progenitors, fibroblasts, vascular endothelial cells and a variety of immune cells. SVF cells are smaller and less fragile compared to mature adipocytes. We, therefore, used 70/100 μm cell strainers for SVF isolation. The detailed protocol is provided in Appendix B.

2.3.3.3 Cell Counting and Flow Cytometer

Cells were prepared as single cell suspensions at a concentration of 10^6 cells/ml. Cell counting was performed by using a hemocytometer. In addition to the routine flow cytometry protocol for cell surface proteins, we used a Tween-20-based protocol for intracellular staining. Antibody combinations for flow cytometry are provided in Appendix A, and the adipose flow cytometry protocol is detailed in Appendix B.

2.4 Statistical Analyses

Data are presented as means ± SEM. All group sizes were between 6 to 20 mice, and techniques were performed on 6 or more mice, per condition. Estimations by western blots and qRT-PCRs were conducted in duplicate. Significance of data was assessed by Prism 6 and SPSS Statistics 22 software, using the Student's t-test for single comparisons and one-way or two-way analysis of variance (ANOVA) (interaction absent vs. interaction present), followed by Bonferroni's *post hoc* analysis for multiple comparisons. Group differences were considered significant when $P < 0.05$.

CHAPTER 3

CHAPTER 3: Adipose Over-Expansion and Inflammation Appear Linked to Hepatic Lipid Partitioning in Diabetic Obese Mice

3.1 Introduction

There is an association between adipose inflammation and obesity complications such as T2D and NAFLD, but why adipose inflammation occurs and how it influences pathogenesis of these disorders is less clear. Obesity and diabetes are associated with hepatic steatosis in at least 80% of cases (345). Diabetes and metabolic syndrome are particularly associated with severer forms of NAFLD, such as the necro-inflammatory disorder of NASH with resultant liver fibrosis (346). This is clinically important because cirrhosis and hepatocellular carcinoma (HCC) do not occur with simple steatosis (345, 346). Interest therefore surrounds the mechanism for transition of simple steatosis to NASH and liver fibrosis, and how this could be related to the severity and other complications of metabolic obesity (discussed in Section 1.2.7).

3.1.1 Adipose Tissue Function and Fatty Liver Disease

It is now better understood that functional adipose tissue is a *sine qua non* for mammalian health. Conversely, dysfunctional adipose tissue causes several significant health problems in humans. There are two main aspects: *First*, there is a relationship between persistent adipose inflammation and obesity-related disorders such as insulin resistance and NAFLD. Cytokine and chemokine production and secretion from inflamed adipose tissue not only perpetuate adipose inflammation, but can affect other tissues and cell types in the body (347). This triggers modifications in these tissues that influence their normal function and/or provoke “alarm” signals (for detailed review, see Section 1.5). *Second*, insufficient energy storage capacity of adipose tissue has

pathologic significance (348). Accordingly, if adipose tissue is not able to channel all pre-cursors (glucose, FAs, etc.) into TAG lipogenesis, this leads to an increase in circulating FFAs. The consequences include insulin resistance and fatty liver. In turn, a consequence of insulin resistance is failure to suppress HSL; this allows continuous lipolysis with further release of FFAs from TAG.

NAFLD is the term used to describe a wide range of liver pathology related to hepatic lipid accumulation (storage of >5% triglyceride by weight, or >5% of hepatocytes stain positive for triglyceride). It has been proposed that when the liver is exposed constantly to high circulating levels of NEFA, uptake of FAs combined with lipogenesis (driven by insulin via SREBP1) and glucose (carbohydrate-responsive element-binding protein [ChREBP]) to cause hepatomegaly by a process that starts with simple steatosis. This can advance until hepatocyte injury and liver inflammation occur with NASH. NASH is a pro-fibrotic condition that can lead to hepatic cirrhosis and liver cancer (HCC) (Fig. 3.1). In developed countries, 9-26 % of NAFLD cases progress to NASH (349, 350).

The earlier ("two hit") concept that metabolic predisposition to steatosis and NASH transition are unrelated processes has been replaced by the idea that lipid molecules themselves can induce hepatocyte injury ("lipotoxicity") (Fig. 3.1) (351). Such injury is observed histologically as ballooned hepatocytes and circulation of liver enzymes (e.g. ALT) and markers of both necrosis and apoptosis (346). Suggestion of the term "liver lipotoxicity" for NASH, cements the centrality of hepatic lipid partitioning in NASH pathogenesis (352). The capacity of adipose sites for lipid storage might therefore be expected to play an indirect role in NASH pathogenesis, as we and others suggested earlier (232, 353). Whether adipose inflammation is also relevant to NASH pathogenesis remains unresolved.

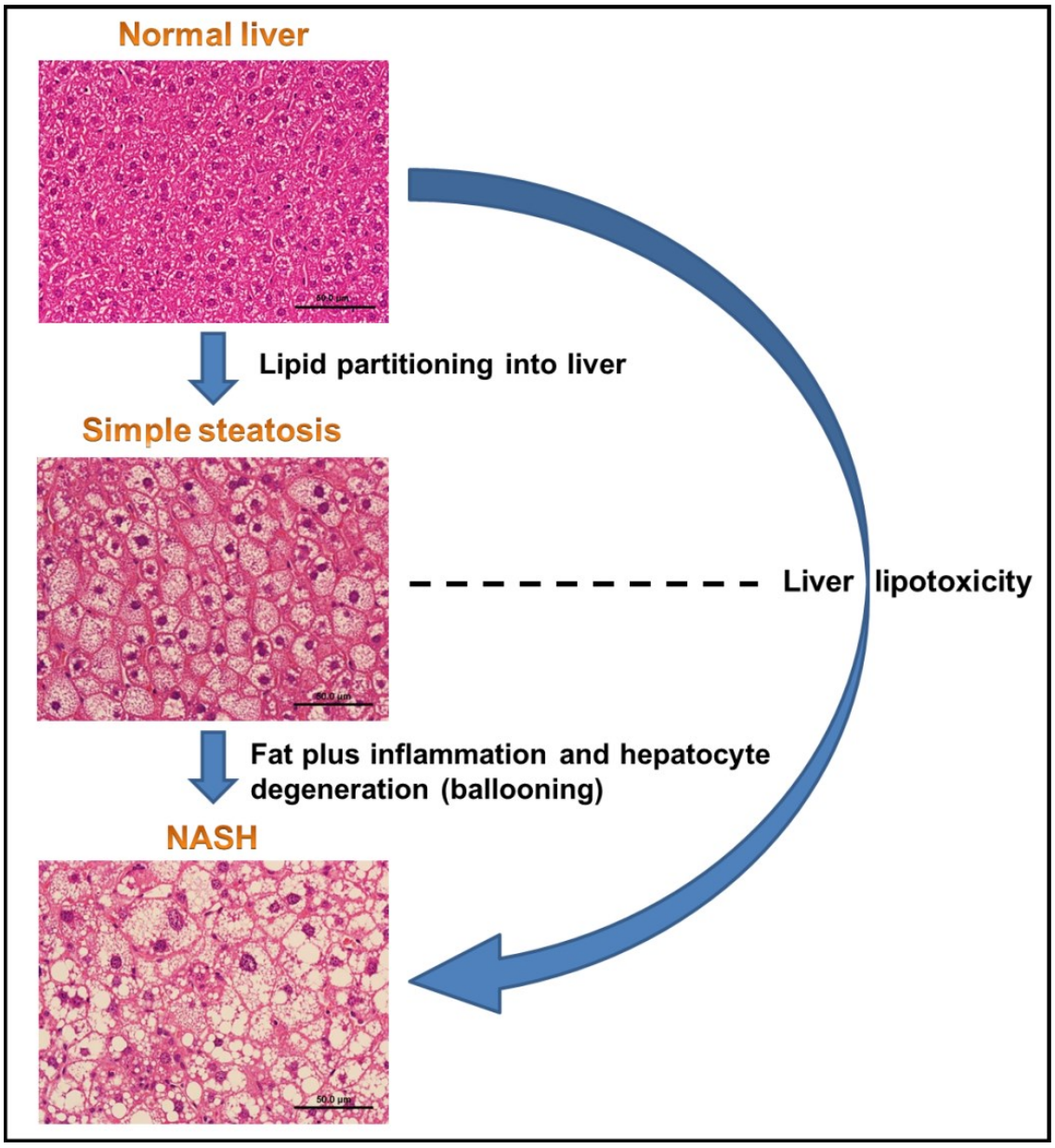

Figure 3.1: The transition from simple steatosis results in NASH. During energy surplus, lipid partitioning into liver leads to development of simple steatosis. Consistent overeating and underactivity, together with insulin resistance and genetic predisposition, increase the lipid burden on the liver. This results in liver lipotoxicity with oxidative stress and a pro-inflammatory response that lead to development of NASH.

Over 60% of patients with NAFLD and virtually all those with NASH exhibit insulin resistance (354, 355). Further, a study in which pioglitazone improved NASH pathology demonstrated enhancement of insulin-mediated suppression of lipolysis, that was consistent with improved adipose insulin sensitivity (356). Development of insulin resistance with steatosis involves muscle and liver as well as adipose (357, 358). Experimentally, macrophage accumulation in liver has been associated with

development of insulin resistance, while macrophages in adipose were associated with its persistence (359).

As reviewed in Section 1.5, in "metabolic obesity", adipose inflammation is characterized by clusters of macrophages around smaller, dying or dead adipocytes in so-called crown-like structures (CLS) (230); identical CLS focussed on lipid-laden hepatocytes are also prominent in NASH (272). However, as reviewed elsewhere (360, 361), the mechanism(s) by which inflammatory cells are recruited to adipose in obesity/diabetes remains contentious (this will be discussed in Chapter 4). One idea is that rapid-onset of over-nutrition results in adipocyte hypertrophy (as well as hyperplasia) in which some adipocytes are stressed and die (degenerate) because of lipid engorgement (337). In what can be regarded as adipose lipotoxicity is that these stressed adipocytes, secrete chemokines that attract mast cells, lymphocytes and particularly macrophages. The latter become activated and coalesced to form CLS, with secretion of macrophage chemokines, more cell recruitment and expansion of adipose inflammation (361).

3.1.2 Studies in "Fat Aussie (*foz/foz*) Mice" and its Relevance to Human NASH

Alström syndrome is a rare autosomal recessive cause of childhood obesity (362). Hyperinsulinemia, chronic hyperglycemia, neurosensory defects and obesity associated with metabolic syndrome/T2D and severe liver diseases are among the usual features. In 2002, Collin and colleagues reported that mutations in *ALMS1* gene are responsible for Alström syndrome in humans (363). During that time, it was shown that ALMS1 localizes on centrosomes and basal bodies of cell cilia; however, little was known about its function. Based on other clinical findings, it became apparent that disturbance of ALMS1 leads to ciliary dysfunction that result in pathogenic outcomes of Alström

syndrome that include male infertility (loss of cilia on sperm), deafness (loss of cilia on cochlear cells), retinopathy (loss of retinal cell cilia), and metabolic syndrome.

Collin and colleagues also investigated a novel gene in mice, called *Alms1*, which has high structural homology to human *ALMS1*. In 2006, Arsov and colleagues developed an animal model of Alström syndrome (named *Fat Aussie* (*foz/foz*) mouse) following the seminal observation of an obese mouse in a non-obese diabetic (NOD) strain (Fig. 3.2). The mutation was mapped to a loss-of-function mutation which is an 11-base pair deletion in exon 8 of the *Alms1* gene (338). Like children with Alström syndrome, *foz/foz* mice develop early-onset obesity, insulin resistance, T2D and hypercholesterolemia, changes that are accelerated by feeding them an "atherogenic" diet containing high fat (23%), high sugar (%45), and cholesterol (0.19%).

Figure 3.2: Fat Aussie (*foz/foz*) mouse compared to a *wild-type* (*WT*) counterpart. Appetite-dysregulated *foz/foz* mice develop hyperphagic obesity. Atherogenic diet-fed *foz/foz* mice have a very high body weight (86.1 g in this example vs. ~35-40 g in atherogenic diet-fed *WT* mice).

Many humans with obesity have polymorphisms of appetite-regulating proteins expressed in the hypothalamus, such as melanocortin 4 receptor, a protein expressed on the primary cilium of neurons (for more details, see Section 1.3). In 2012, a PhD student

from the host lab explored the mechanism for why a truncating mutation on *Alms1* leads to obesity development in mice (364). It was already known that ALMS1 is located at the base of cilia on hypothalamus neurons; these cilia are thought to serve as sensory antennae. Accordingly, *foz/foz* mice lose primary cilia at the time of weaning, most likely because the *Alms1* mutation affects the stability of cilial anchorage (364). Presumably because negative appetite regulators are suppressed on these cilia, this confers a powerful drive to eat in *foz/foz* mice, and consequently early development of obesity. In this way, *Alms1* mutation affects the metabolic state of liver disease "indirectly", via the drive to eat and resultant over-nutrition. Hepatocytes do not express a primary cilium so the mutation does not affect lipid handling by the liver directly (this has been confirmed by the host lab *in vitro*).

Although there are species differences in physiological indices between humans and mice, animal models can be useful to study aspects, such as liver and adipose tissue sampling that are often not possible in humans. For example, *foz/foz* mouse model is considered to address questions about the pathophysiology of adipose in relation to causation of NASH, as opposed to simple steatosis. Humans with NASH usually have more severe metabolic abnormalities (e.g., diabetes, metabolic syndrome) than those with simple steatosis. The course of metabolic changes in *foz/foz* mice over time and with diet offers the possibility to explore the relationship of these changes to development of NASH.

3.2 Aims

Using dietary manipulation in appetite-dysregulated or *WT* mice, we sought to characterize changes in different adipose tissues during development of obesity. The underlying hypothesis was that adipose over-expansion leads to inflammation in each

WAT, but particularly visceral, causing development of "unhealthy obesity" that is mechanistically linked to the pathogenesis of NASH.

Accordingly, the specific aims were to:

1 Compare adiposity rates of different adipose sites during obesity development as well as parallel weight gain in other tissues, such as BAT, muscle and liver.
2 Assess detailed adipose morphometry in atherogenic diet-fed vs. chow-fed *foz/foz* and *WT* mice in visceral WAT.
3 Establish the recruitment of CLSs as an indicator of adipose tissue inflammation in visceral WAT.
4 Test whether adipose dysfunction and inflammation are pre-conditions for development of NASH.

3.3 Experimental Details

The ANU Animal Ethics Committee approved experimental procedures in this study. Female *foz/foz* or *WT* mice on NOD.B10 strain were fed atherogenic diet (Ath in figure axis) (20% protein, 23% fat, 45% carbohydrate, 0.2% cholesterol) or normal rodent chow (NC in figure axes) from weaning to 6, 8, 10, and 12 weeks of age. All mice were kept on a 12-hour light/dark cycle in the ANU Medical School animal facility at the Canberra Hospital.

Following the methodology described in Section 2.1.3, samples of blood, liver, gastrocnemius muscle, periovarian (Pov) and mesenteric (Mes) fat (as visceral WATs), lumbar and dorsal fat (as subcutaneous WATs), and brown adipose tissue (BAT) were removed. BAT is embedded in the interscapular (dorsal) fat pad in mice. Hence, BAT samples were carefully excised from the surrounding WATs during the harvest. Blood samples were taken using intra-cardiac puncture technique at 9 am of harvest days; mice

were not fasted before taking blood samples. Blood glucose was assayed by a glucometer.

Adipose morphometry was performed on H&E-stained adipose sections by Leica Application Suite (LAS) software, which allows determination of mean adipocyte volume, cell density and size distribution (for more details, see Section 2.2.3). The number of macrophages in Pov WAT samples was determined by normalizing the number of H&E-stained cell clusters to 100 adipocytes. Liver macro-steatosis score was assessed blind by an expert pathologist (MMY). Liver lipid content was compared between *foz/foz* and *WT* mice using ORO staining, explained in Section 2.2.2.

Data are presented as mean ± SEM (n=8-18). For the analysis of data significance, Prism 6 (GraphPad, La Jolla, CA) and SPSS Statistics 22 (IBM, New York, NY) software was used, applying one-way or two-way analysis of variance (ANOVA) followed by Bonferroni's *post hoc* analysis.

3.3.1 Author Contributions

This is a collaborative study conducted together with Professor Christopher J. Nolan's group at the Canberra Hospital. Accordingly, we contributed to this study by establishing key adipose techniques, such as the removal of different adipose sites and other tissues (e.g., liver, gastrocnemius muscle), detailed adipose morphometric analyses and liver indices (e.g., histology, hepatic lipid assessment). Members of Prof Nolan's lab studied molecular elements of adipose inflammation, and pancreatic β cell structure and function. Mice of two different genotypes (*foz/foz* and *WT*), two different diets (atherogenic diet and chow), and four different age groups (6, 8, 10, and 12 week old) were studied. In light of the considerable work involved, a group of colleagues from both host labs assisted the animal harvests throughout this project, including

Tenzin Dagpo, whose study of central inflammatory cytokines formed the basis of an MPhil degree (ANU 2014).

Fahrettin Haczeyni conducted the experiments, performed data analysis, and wrote this Chapter. Viviane Delghingaro-Augusto supervised the animal work and assisted experiments. Tenzin Dagpo and Ainy Khan assisted the experiments. Matthew M. Yeh provided blind analysis of liver histology. Narcissus C.-H. Teoh contributed intellectual input and reviewed the results. Bruce Shadbolt provided invaluable advice on statistical analyses. Geoffrey C. Farrell and Christopher J. Nolan directed the study, reviewed and edited the Chapter. The authors thank the Canberra Hospital research office and animal house technicians for their highly skilled technical assistance.

3.4 Results

As stated in Chapter 1, the mechanisms determining the deposition of lipid into different adipose sites remain largely unknown. This Chapter provides an insight about adiposity rates of different adipose tissue during development of obesity, which was clearly "unhealthy obesity" in *foz/foz* mice that developed diabetes, metabolic syndrome and NASH. Moreover, adipose indices such as adipose morphometry and inflammation are analyzed in the third Results Section. In the last Results Section (3.4.3), the progression of liver weight gain and hepatic steatosis is presented together with results indicating the histological phenotype of NAFLD in these livers.

3.4.1 Adiposity in Different Adipose Sites During Obesity Development

All mice were of similar weight of weaning at 4 weeks of age (~17 g). In chow-fed *WT* mice, weight gain was slow but constant; these mice gained an average of 0.8 g every week until 12 weeks of age (Fig. 3.3). A similar but slightly faster pattern of weight gain was observed for atherogenic diet-fed *WT* mice. At 8 weeks, chow-fed

foz/foz mice gained significantly more body weight than *WT* counterparts (Fig. 3.3). The combination of atherogenic dietary feeding and increased appetite (*foz/foz* background) exerted the most profound effect on body weight, even at 6 weeks of age (2 weeks on diet). By 12 weeks of age (8 weeks on diet), atherogenic diet-fed *foz/foz* mice had developed obesity (body weight > 45 g; Fig. 3.3).

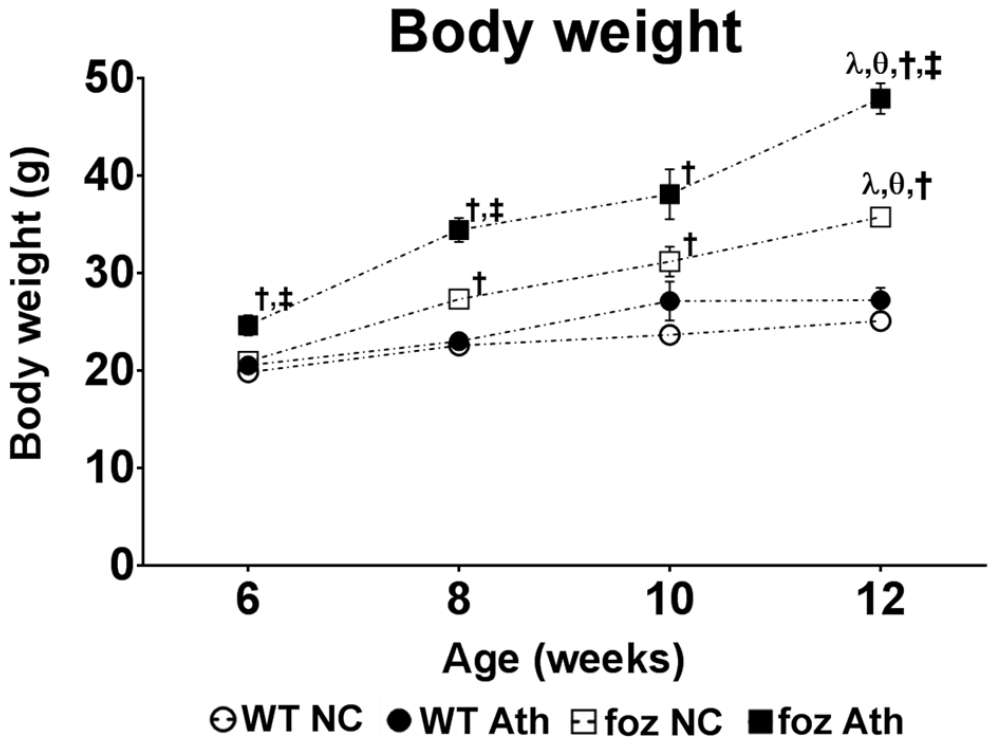

Figure 3.3: Body weight in *foz/foz* and *WT* mice fed NC or Ath from 6, 8, 10, and 12 weeks of age. Weight gain was significantly increased already in 6 week old atherogenic diet-fed *foz/foz* mice compared to diet- or genotype-matched counterparts. At 8 weeks of age, weight gain in chow-fed *foz/foz* mice was also significant (vs. chow-fed *WT*). At 10 weeks time point, body weight increase was higher in *foz/foz* mice fed either diet than corresponding *WT*, and by 12 weeks of age, body weight was nearly 2-fold greater in atherogenic diet-fed *foz/foz* mice then in similarly fed *WT*.
Data are mean ± SEM (n=8-18/gp).
† $P<0.05$ vs. diet-matched control (genotype effect); e.g., chow-fed *foz/foz* vs. *WT*
‡ $P<0.05$ vs. genotype-matched control (diet effect); e.g., atherogenic diet-fed vs. chow-fed *WT*
λ $P<0.05$ vs. 6 and 8 weeks age groups
θ $P<0.05$ vs. 10 weeks age group

The atherogenic diet exerted a strong influence on both visceral (Pov and Mes) WAT mass in 6 week old mice (Fig. 3.4A,B). This increase was more pronounced when atherogenic dietary feeding interacted with *foz/foz* genotype. After 8 weeks of age, genotype became more influential on visceral adiposity. Thereafter, expansion of both

Pov and Mes WATs remained relatively limited in atherogenic diet-fed *WT* mice (Fig. 3.4A,B). In contrast, atherogenic diet-fed *foz/foz* mice showed greater visceral adiposity by 12 weeks of age, when compared to their diet- and genotype-matched counterparts (Fig. 3.4A,B). As a proportion of body weight, these visceral compartments increased with atherogenic diet and *foz/foz* background. Thus, by 12 weeks of age (8 weeks on diet), relative Pov WAT weighed 2-fold more than Mes WAT in *foz/foz* mice fed either diet (Fig. 3.4C,D).

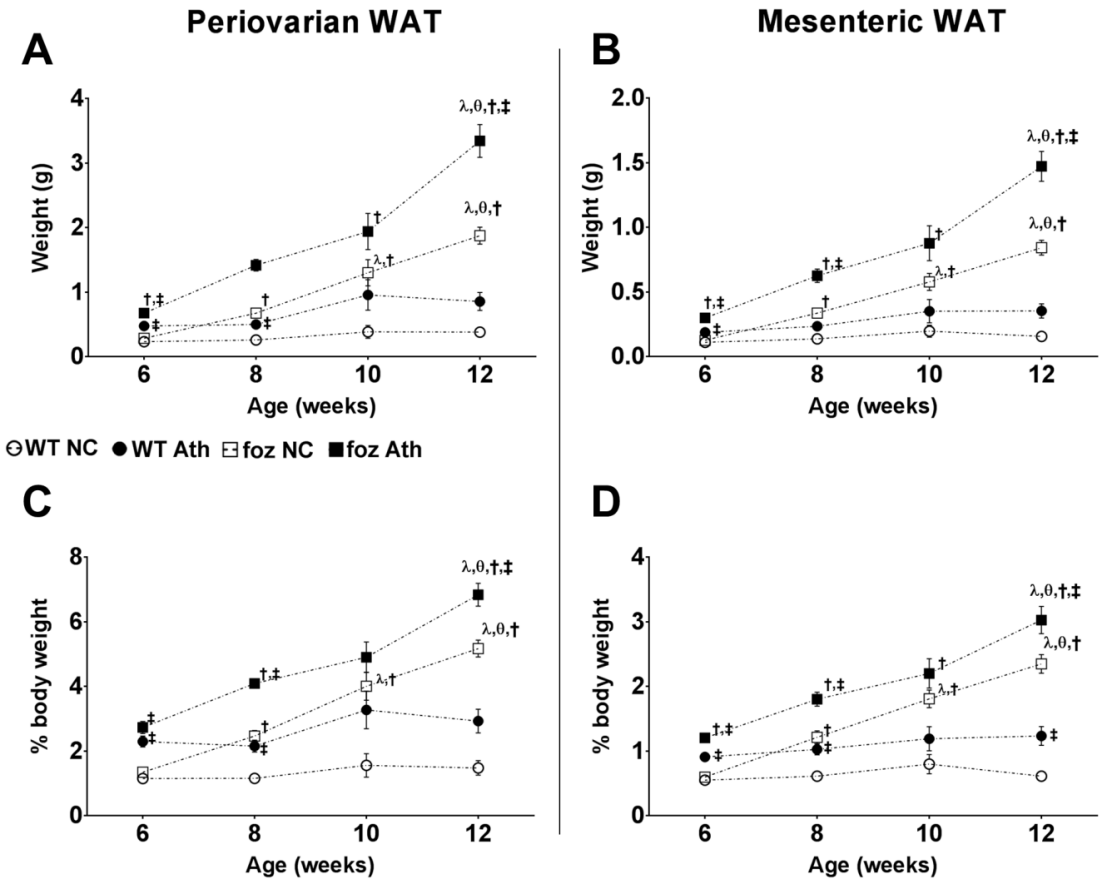

Figure 3.4: The time-dependent effect of atherogenic dietary intake and *foz/foz* genotype on visceral adiposity. (A,C) Atherogenic diet caused enlargement of Pov WAT mass in both lines (both as absolute and relative weight), with a powerful independent effect of *foz/foz* genotype at 6 weeks of age. After this time point, *foz/foz* mice showed greater adiposity than *WT* mice. At 12 weeks of age, atherogenic diet-fed *foz/foz* mice had ~3.5 g Pov WAT mass whereas chow-fed *foz/foz* mice had ~1.8 g. (B,D) Mes WAT adiposity displayed a similar pattern of increase in different experimental groups, however, there was only half as much Mes WAT as Pov WAT.
Data are mean ± SEM (n=8-18/gp).
† $P<0.05$ vs. diet-matched control (genotype effect); e.g., chow-fed *foz/foz* vs. *WT*
‡ $P<0.05$ vs. genotype-matched control (diet effect); e.g., atherogenic diet-fed vs. chow-fed *WT*
λ $P<0.05$ vs. 6 and 8 weeks age groups
θ $P<0.05$ vs. 10 weeks age group

As reviewed in Section 1.2, among different adipose sites, visceral WATs appear primarily responsible for the changes that define metabolic obesity, whereas subcutaneous WATs, by acting like a "metabolic sink", may be beneficial for general health. In the present experiment, lumbar adiposity increased with atherogenic dietary intake at an early age in both genotypes, but more so in *foz/foz* than *WT* mice (Fig. 3.5A). After 8 weeks of age, genotype effect was more prominent on lumbar adiposity. An interesting finding was that between 6 and 12 weeks of age, interaction of atherogenic dietary feeding and *foz/foz* background had a similar (parallel) expansion effect on absolute and relative Pov and lumbar WAT weights. In atherogenic diet-fed *foz/foz* mice, up to ~7% of total body weight was comprised of lumbar fat by 12 weeks of age (8 weeks on diet) (Fig. 3.5C).

Dorsal WAT is another subcutaneous depot situated behind the shoulders and neck in mice. In *WT* mice, atherogenic diet did not cause significant adiposity in dorsal WAT during development (Fig. 3.5B). In contrast, *foz/foz* mice showed a time-dependent increase in dorsal WAT mass irrespective of diet, although this increase was more pronounced in atherogenic diet-fed animals (Fig. 3.5B). Considered as a proportion of total body weight, dorsal WAT mass appeared to be more limited than lumbar WAT mass (Fig. 3.5D).

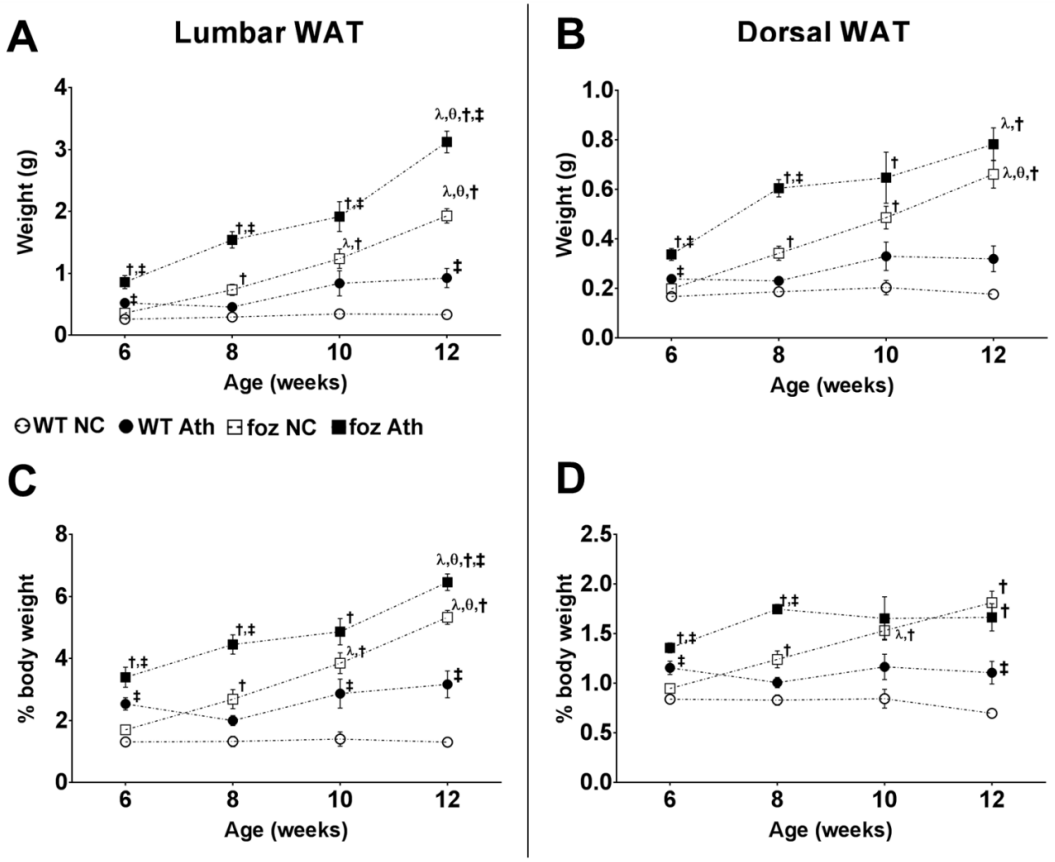

Figure 3.5: The time-dependent effect of atherogenic dietary intake and *foz/foz* genotype on subcutaneous adiposity. (A,B) Atherogenic dietary intake increased lumbar and dorsal WAT mass in both genotypes at 6 weeks of age; the combination of atherogenic diet with *foz/foz* genotype strengthened this effect. (A) After 8 weeks of age, *foz/foz* mice fed either diet showed greater adiposity in lumbar WAT than *WT* animals. (B) Likewise, dorsal adiposity was more pronounced with *foz/foz* genotype at 8 weeks of age. (C) Up to 7% of total body weight was formed of lumbar WAT in atherogenic diet-fed *foz/foz* mice by 12 weeks of age; 5% in chow-fed *foz/foz* and 3% in atherogenic diet-fed *WT* mice and less than 1% in chow-fed *WT*. (D) Unlike lumbar WAT, dorsal WAT weight as a proportion of total body weight did not increase during development in any group, except chow-fed *foz/foz* mice.
Data are mean ± SEM (n=8-18/gp).
† $P<0.05$ vs. diet-matched control (genotype effect); e.g., chow-fed *foz/foz* vs. *WT*
‡ $P<0.05$ vs. genotype-matched control (diet effect); e.g., atherogenic diet-fed vs. chow-fed *WT*
λ $P<0.05$ vs. 6 and 8 weeks age groups
θ $P<0.05$ vs. 10 weeks age group

As reviewed in Section 1.2.5., brown adipocytes are rich in mitochondria and therefore metabolically more active than white adipocytes (65, 66). In obesity, BAT loses its distinctive colour and becomes "whitish" due to infiltration of lipid-laden white adipocytes. As a result, it is technically challenging to dissect pure BAT in obese mice. In *WT* mice, BAT remained quite compact and small, with minimal increase (not significant) (Fig. 3.6A,B). In *foz/foz* mice, BAT mass increased from 6 to 12 weeks of

age, and this increase was higher in atherogenic diet-fed mice (Fig. 3.6A). However, BAT, as a proportion of total body weight, remained similar in *foz/foz* mice, irrespective of diet (Fig. 3.6B).

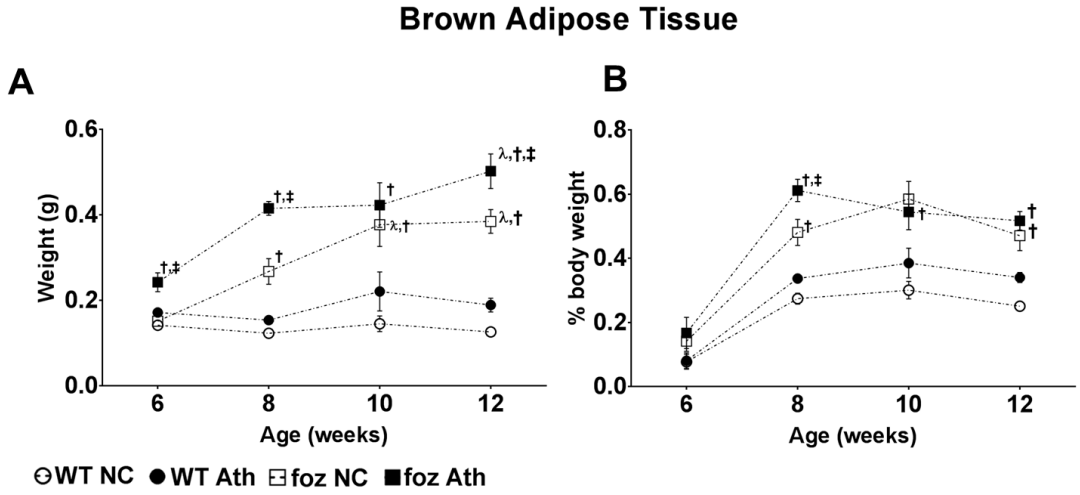

Figure 3.6: The time-dependent effect of atherogenic dietary intake and *foz/foz* genotype on expansion of BAT. (A) From 6 to 12 weeks of age, BAT mass did not change in *WT*, irrespective of diet. In chow-fed *foz/foz* mice, there was a time-dependent increase in BAT weight, and this increase was more pronounced when atherogenic dietary intake interacted with *foz/foz* genotype. (B) Nevertheless, the proportion of BAT in total body weight followed a similar pattern during development of *foz/foz* mice fed either diet.
Data are mean ± SEM (n=8-18/gp).
† $P<0.05$ vs. diet-matched control (genotype effect); e.g., chow-fed *foz/foz* vs. *WT*
‡ $P<0.05$ vs. genotype-matched control (diet effect); e.g., atherogenic diet-fed vs. chow-fed *WT*
λ $P<0.05$ vs. 6 and 8 weeks age groups

In the present study, gastrocnemius muscle mass did not change during development in *WT* mice fed either diet (Fig. 3.7A). There was a mild trend of increased muscle mass in atherogenic diet-fed *foz/foz* mice from 6 to 12 weeks of age, but this increase was not significant. Muscle mass as a proportion of total body weight was less in *foz/foz* mice at 12 weeks of age, compared to their diet-matched counterparts (Fig. 3.7B).

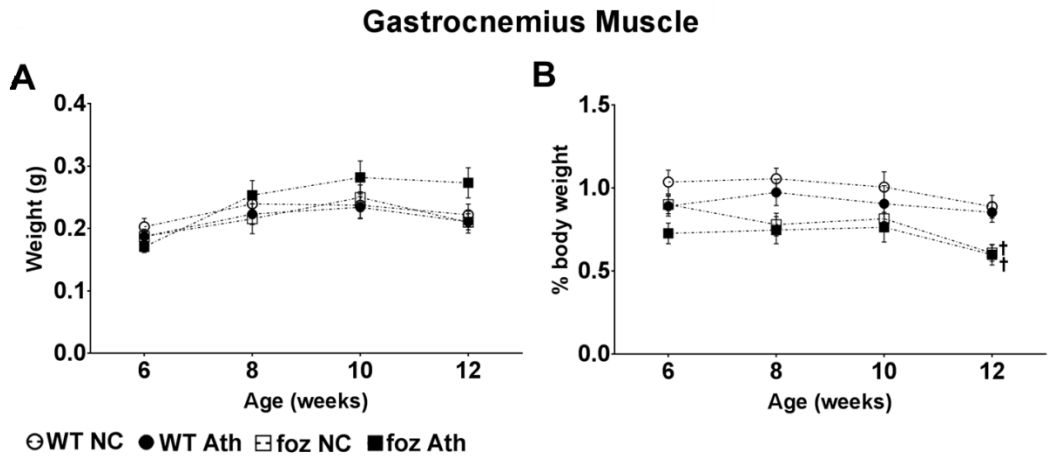

Figure 3.7: The time-dependent effect of atherogenic dietary intake and *foz/foz* genotype on gastrocnemius muscle weight. (A) Although there was a general trend of muscle mass increase in atherogenic diet-fed *foz/foz* mice, this trend was not significant and muscle weight did not change in any group from 6 to 12 weeks of age. (B) As a percentage of total body weight, muscle mass was less in 12 week old *foz/foz* mice compared to their diet-matched *WT* counterparts.
Data are mean ± SEM (n=8-18/gp).
† $P<0.05$ vs. diet-matched control (genotype effect); e.g., chow-fed *foz/foz* vs. *WT*

3.4.2 Effects of Atherogenic Dietary Intake and *foz/foz* Genotype on Adipose Morphometry and Inflammation in Periovarian Adipose Tissue

As explained in Section 1.4, there is a strong relationship between adipocyte size and function. Lipid-engorged hypertrophic adipocytes display a pro-inflammatory phenotype and assist inflammatory recruitment into adipose tissue. In the present study, we measured detailed adipose morphometry in Pov WAT from 12 week old mice.

The type of dietary intake and genotype each influenced mean adipocyte volume, with corresponding changes in adipocyte number per 1 mm^2 fixed surface area (Fig. 3.8A,B). Accordingly, both atherogenic diet and *foz/foz* background resulted in an increase in mean adipocyte volume (Fig. 3.8A). The interaction of these two factors exhibited the most powerful effect of increasing adipocyte volume in this visceral adipose compartment. As a result of this increase in cell volume, atherogenic diet and *foz/foz* genotype both reduced the average number of adipocytes observed across a fixed surface area (Fig. 3.8B). Although the combination of these two factors appeared to

further decrease adipocyte number in comparison to diet- or genotype-matched counterparts, this decrease did not reach significance (Fig. 3.8B).

Although there is no strict standardization for adipocyte size (diameter/circumference) differences, adipocytes between 500 and 4000 μm^2 are often considered to be small sized, whereas those between 5000 to 7000 μm^2 are moderate, and those larger than 8000 μm^2 are considered to be large adipocytes (results shown next).

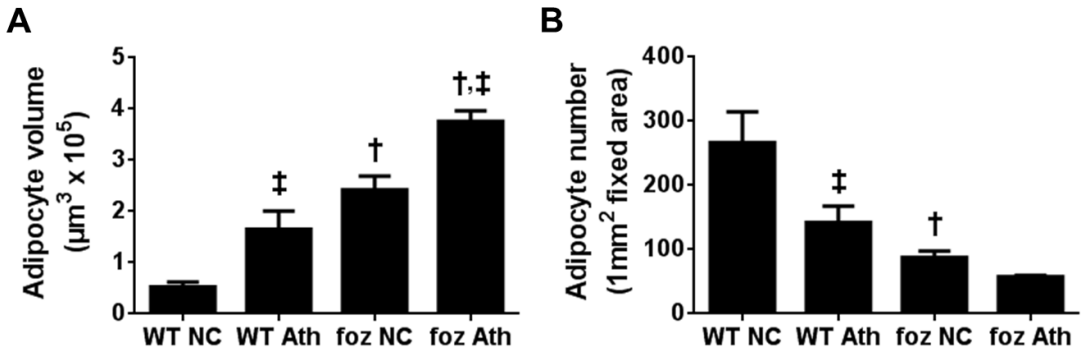

Figure 3.8: Mean adipocyte volume and density of adipocytes in Pov WAT from 12 week old *foz/foz* and *WT* mice. (A) Atherogenic diet and *foz/foz* background both increased the mean adipocyte volume in Pov WAT; the combination of these two factors exhibited the greatest influence. (B) A similar (but reverse) profile was found for mean adipocyte number. Atherogenic dietary intake and *foz/foz* genotype resulted in fewer adipocytes in a 1 mm^2 fixed area. This trend of decrease appeared more pronounced (although not significant) in Pov WAT of atherogenic diet-fed *foz/foz* mice.
Data are mean ± SEM (n=8/gp).
† $P<0.05$ vs. diet-matched control (genotype effect); e.g., chow-fed *foz/foz* vs. *WT*
‡ $P<0.05$ vs. genotype-matched control (diet effect); e.g., atherogenic diet-fed vs. chow-fed *WT*

In chow-fed *WT* mice, the majority of adipocytes were between 500 and 3000 μm^2 (Fig. 3.9A). Atherogenic dietary intake increased the proportion of moderate-sized adipocytes in *WT* mice (Fig. 3.9B), and as shown in the adipose section, the majority of adipocytes were small-to-medium. In addition, some large adipocytes (~5%) were occasionally dispersed in the Pov WAT. When fed chow, appetite-dysregulated *foz/foz* mice had an "even" distribution of different sized adipocyte populations (Fig. 3.9C). Atherogenic dietary feeding of *foz/foz* genotype led to lipid-engorgement of Pov WAT

adipocytes (Fig. 3.9D). As a result, the proportion of adipocytes larger than 8000 μm^2 (hypertrophic adipocytes) was ~30% of total adipocytes.

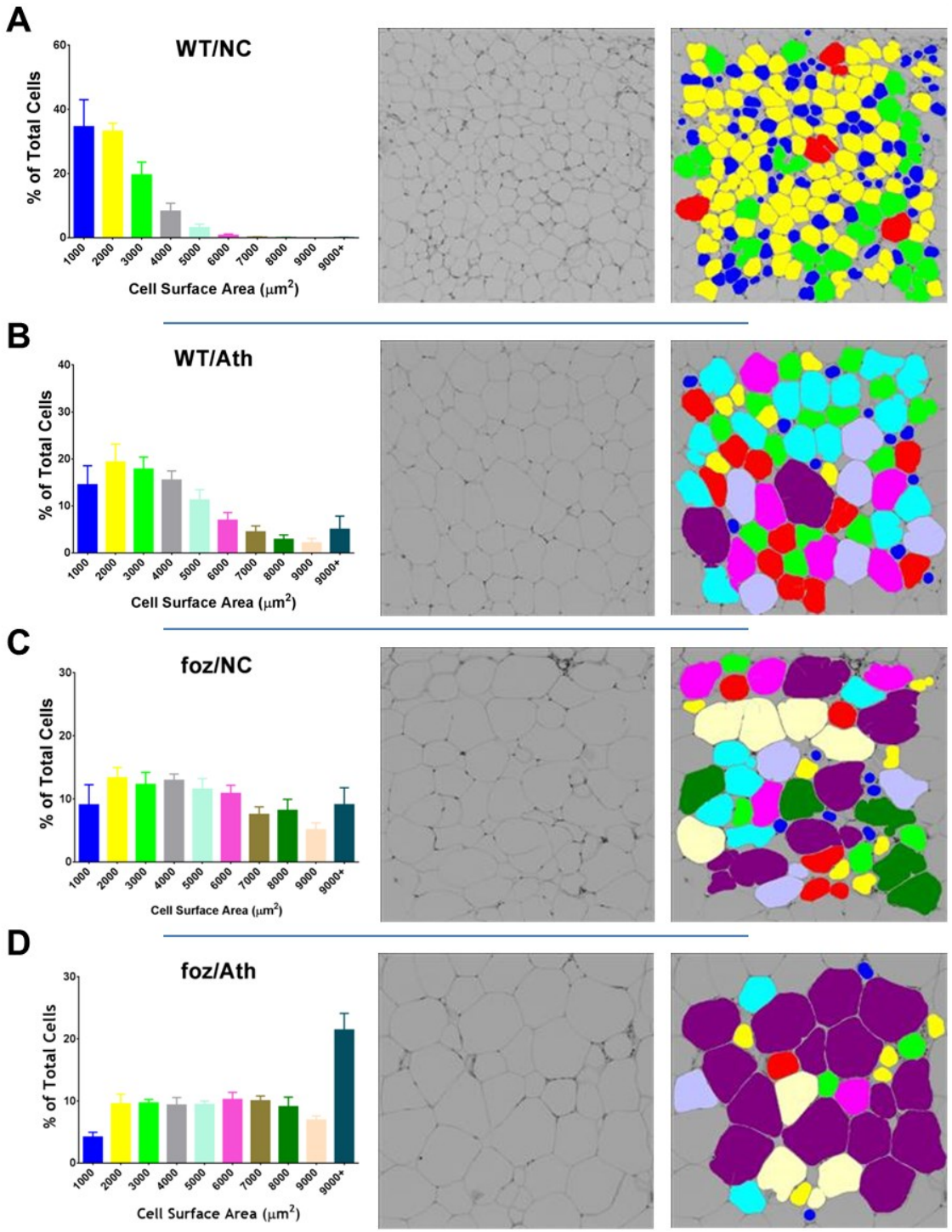

Figure 3.9: Size distribution of adipocytes in Pov WAT of *foz/foz* and *WT* mice fed NC or Ath diet for 12 weeks. H&E-stained representative adipose sections were analysed for detailed adipocyte size distribution. (A) ~90% of adipocytes were smaller than 4000 μm^2 in chow-fed *WT* mice. (B) As reflected in the adipose section, atherogenic dietary intake increased the proportion of small-to-medium adipocytes in *WT* mice. (C) In chow-fed *foz/foz* mice, Pov WAT showed an "even" distribution of adipocyte populations by size, whereas (D) in atherogenic diet-fed *foz/foz* mice, ~40% of adipocytes were larger than 8000 μm^2. The interaction of atherogenic dietary intake and appetite dysregulation (*foz/foz* genotype) resulted in markedly increased proportion of large hypertrophic adipocytes. (n=8/gp [10 sections per mouse]; 160x magnification)

Activated pro-inflammatory macrophages recognize degenerating adipocytes and congregate around them to form CLSs, as described in Section 1.5.6. This indicates operation of a pro-inflammatory response (230). CLSs are shown in a representative adipose section from atherogenic diet-fed *foz/foz* in Figure 3.10. As is evident by medium power light microscopy (160x) (Fig. 3.9) and compiled from F4/80 IHC staining (not shown), CLSs were virtually absent in chow-fed *WT* mice Pov WAT. There appeared to be a slight increase (not significant) in the number of CLSs in atherogenic diet-fed vs. chow-fed *WT* mice and chow-fed *foz/foz* vs. chow-fed *WT* mice, but in atherogenic diet-fed *foz/foz* mice, there was a major increase which was highly significant vs. chow-fed *foz/foz* mice and atherogenic diet-fed *WT* mice (Fig. 3.10). The very abundant CLS recruitment in Pov WAT in atherogenic diet-fed *foz/foz* mice is illustrated in representative adipose section (Fig. 3.10).

As another aspect of this collaborative project, analyses of pro-inflammatory molecular markers were conducted by Prof Nolan's lab (e.g., TNFα, IL6), and present CLS levels are entirely consistent with the molecular inflammatory marker levels generated by Tenzin Diagpo (unpublished data). Changes in adipocyte differentiation and cell death markers are also of great interest in this thesis. They are addressed in separate studies in Chapter 4

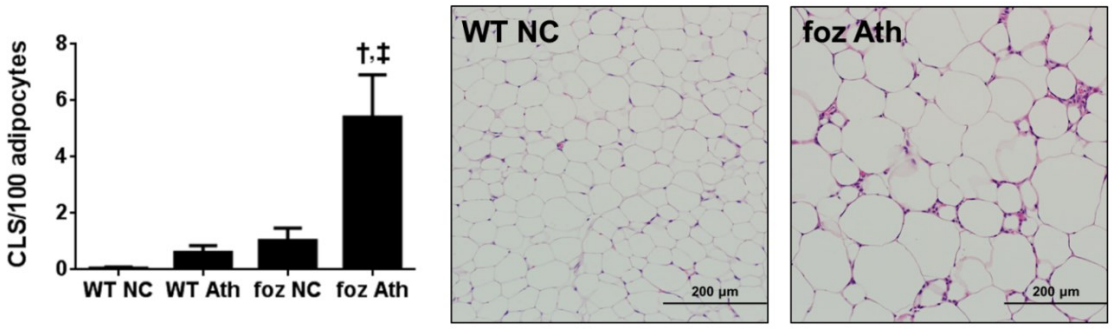

Figure 3.10: Number of CLSs in Pov WAT in 12 week old *foz/foz* and *WT* mice fed NC or Ath diet. In chow-fed *WT* mice, no CLSs were noted. There appeared to be some CLSs in atherogenic diet-fed *WT* and chow-fed *foz/foz* mice, but the apparent increase was not significant. The interaction of atherogenic dietary intake and *foz/foz* genotype resulted in marked abundance of CLSs in Pov WAT.
Data are mean ± SEM (n=8/gp [10 sections per mouse]; 160x magnification).
† $P<0.05$ vs. diet-matched control (genotype effect); e.g., chow-fed *foz/foz* vs. *WT*
‡ $P<0.05$ vs. genotype-matched control (diet effect); e.g., atherogenic diet-fed vs. chow-fed *WT*

3.4.3 Time-Dependant Effects of Atherogenic Diet and *foz/foz* Genotype on Blood Glucose, Liver Weight and Liver Steatosis

A detailed review about circulating glucose and insulin metabolism is given in Section 1.3. Because the focus of the endocrinology lab was on pancreatic islet cell histology, with whom these experiments were conducted in collaboration, blood glucose was determined on non-fasting morning samples. Surprisingly, at the time points studied here, neither atherogenic dietary intake nor *foz/foz* mutation alone significantly increased circulating blood glucose levels (Fig. 3.11). However, the combination of these 2 factors resulted in a significant increase in blood glucose as early as 8 weeks of age. By 12 weeks, atherogenic diet-fed *foz/foz* mice developed glucose intolerance (~12 mmol/L blood glucose) (Fig. 3.11).

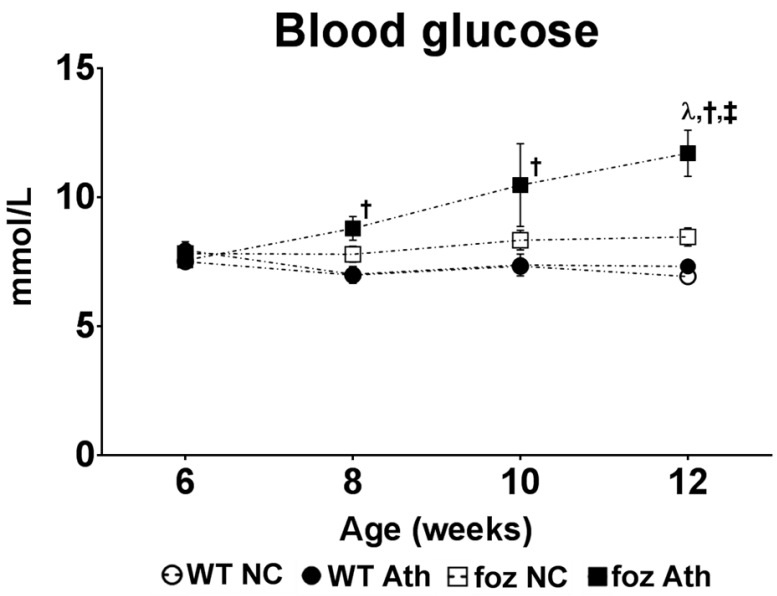

Figure 3.11: The time-dependent effect of atherogenic dietary intake and *foz/foz* genotype on circulating blood glucose. Atherogenic dietary feeding and *foz/foz* mutation did not increase morning blood glucose solely, but the combination of these 2 factors resulted in a significant increase starting from 8 weeks of age. At 12 weeks of age, atherogenic diet-fed *foz/foz* mice developed glucose intolerance (~12 mmol/L).
Data are mean ± SEM (n=8-18/gp).
† $P<0.05$ vs. diet-matched control (genotype effect); e.g., chow-fed *foz/foz* vs. *WT*
‡ $P<0.05$ vs. genotype-matched control (diet effect); e.g., atherogenic diet-fed vs. chow-fed *WT*
λ $P<0.05$ vs. 6 and 8 weeks age groups

In *WT* mice, absolute liver weight did not change from 6 to 12 weeks of age (Fig. 3.12A). Likewise, liver as a proportion of total body weight remained the same during development of *WT* mice (Fig. 3.12B). Although there seemed to be a slight increase in chow-fed *foz/foz* mice liver weight compared to chow-fed *WT* mice, this increase was significant only at 8 weeks of age (Fig. 3.12A). In contrast, changes in liver size with development were proportional to body weight gain in atherogenic diet-fed *foz/foz* mice. Hepatomegaly was present at 8 weeks of age, and liver size increased further by 12 weeks (Fig. 3.12A), so that relative liver weight was nearly ~8% of body weight vs. ~4% in all other groups (Fig. 3.12B).

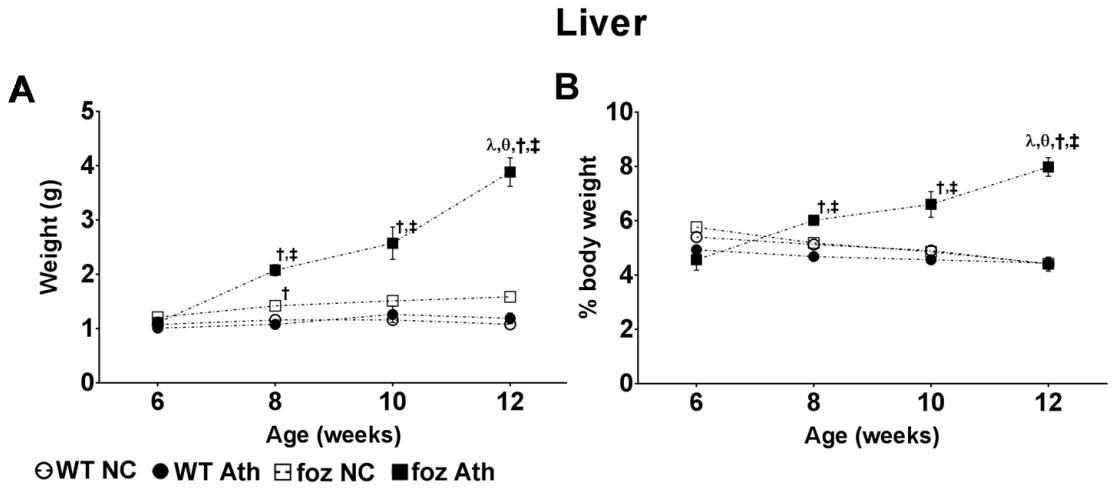

Figure 3.12: The time-dependent effects of atherogenic dietary intake and *foz/foz* genotype on liver weight. (A) Atherogenic dietary feeding and *foz/foz* mutation alone did not influence liver weight of *WT* mice during development. Chow-fed *foz/foz* mice had slightly increased liver mass, but this increase was significant only at 8 weeks of age compared to chow-fed *WT* mice. (B) As a consequence, relative liver weight (% body weight) remained unchanged in these groups. In contrast, atherogenic diet-fed *foz/foz* mice developed hepatomegaly as early as 8 weeks of age, and this was well-established by 12 weeks of age.
Data are mean ± SEM (n=8-18/gp).
† $P<0.05$ vs. diet-matched control (genotype effect); e.g., chow-fed *foz/foz* vs. *WT*
‡ $P<0.05$ vs. genotype-matched control (diet effect); e.g., atherogenic diet-fed vs. chow-fed *WT*
λ $P<0.05$ vs. 6 and 8 weeks age groups
θ $P<0.05$ vs. 10 weeks age group

Hepatic lipid content was measured only in the atherogenic diet-fed groups. Two different methods were used: total steatosis (micro + macro) by ORO staining (for methodology, see Section 2.2.2), and macro-steatosis assessed blind on H&E-stained liver sections by an expert liver pathologist (see Section 2.2.3). In atherogenic diet-fed *WT* mice, there was no evidence of hepatic steatosis at any age studied here (3.13A,B). In *foz/foz* counterparts, there was a trend of increase as early as 8 weeks of age in total steatosis (3. 13A). This increase became significant at 10 weeks, but macro-steatosis did not become apparent until 12 weeks of age (Fig. 3.13B). There are some potential technical reasons for this apparent discrepancy, as discussed later (Section 3.5).

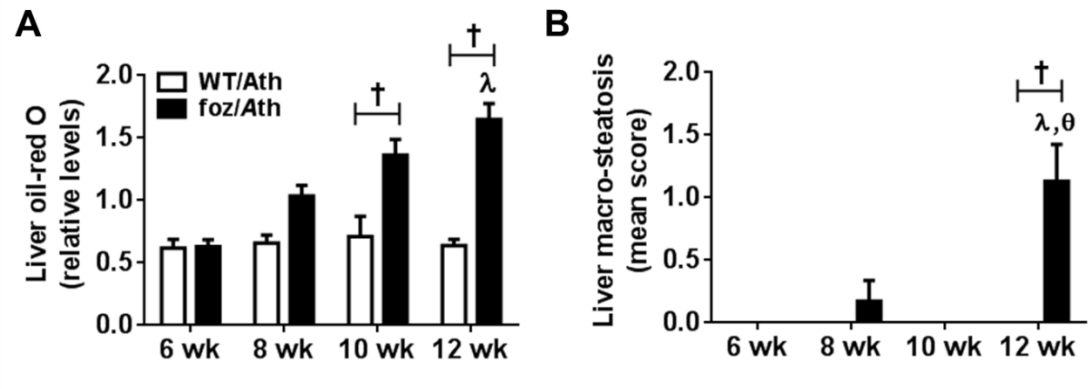

Figure 3.13: The time-dependent effects of atherogenic dietary intake and *foz/foz* genotype on hepatic steatosis. (A) By ORO staining, *WT* mice fed atherogenic diet had similar levels of liver lipids from 6 to 12 weeks of age. In *foz/foz* counterparts, liver lipids progressively increased after 6 weeks of age, to be significant at 10 weeks compared to their *WT* counterparts. (B) Atherogenic diet-fed *WT* mice did not display macro-steatosis at any age, whereas macrovesicular steatosis became apparent in livers of 12 week old *foz/foz* mice.
Data are mean ± SEM (n=8-18/gp).
† $P<0.05$ vs. diet-matched control (genotype effect); e.g., chow-fed *foz/foz* vs. *WT*
λ $P<0.05$ vs. 6 and 8 weeks age groups
θ $P<0.05$ vs. 10 weeks age group

3.5 Discussion

Constant energy imbalance favouring greater calorie intake than energy expenditure leads to energy surplus in the body, and this results in over-expansion of adipose compartments. As reviewed in Section 1.5, adipose over-expansion may result in adipose stress and inflammation, and these factors pose a serious threat to other tissues and organs. In particular, it has been shown that visceral adiposity is closely linked to adipose stress and inflammation (unhealthy obesity), whereas expansion of subcutaneous adipose compartments can be associated with metabolically healthy obesity. Despite this, relatively few studies have compared the rate of changes in adiposity in different adipose sites in a time-dependent manner and chartered how adipose stress and inflammation evolve with tissue. In the present work, we studied two visceral (periovarian and mesenteric), two subcutaneous (lumbar and dorsal) and brown adipose compartments in an experimental mouse model of obesity and diabetes. In order to be able to follow the pattern of energy storage with time, we measured changes in adiposity rate in these adipose tissues in 6, 8, 10, and 12 week old mice.

The first finding of the study is that genetic background, in this case *foz/foz* mice, exerts an important influence on adiposity of fat compartments in relation to weight gain, but the interaction of atherogenic dietary intake with genotype exhibited even greater influence on these indices. On its own, the atherogenic diet did not exert a strong influence on body weight or adipose stores compared to chow-fed *WT* mice. Although it is not statistically relevant to compare chow-fed *foz/foz* and atherogenic diet-fed *WT* mice, their body weights differed markedly at 12 weeks of age (~36 g vs. ~27 g), reflecting the more powerful obesogenic effect of this appetite defect. As shown in Chapter 6, 16 week old female *WT* NOD.B10 mice were found to weigh ~30 g whereas their chow-fed counterparts remained at 25 g. In another study, female *WT* NOD.B10 mice developed obesity (~45 g) when fed an atherogenic diet for 24 weeks (28 weeks of age). This demonstrates that aging is another important factor when combined with dietary habits in development of obesity. Atherogenic diet-fed *foz/foz* mice, on the other hand, were already obese as early as 10 weeks of age and weight gain further increased by 12 weeks of age (~ 48 g). In other studies, atherogenic diet-fed female *foz/foz* mice regularly weigh > 65 g at 24 weeks of dietary intake (232).

The main hypothesis of this Chapter was that adipose inflammatory recruitment resulting from over-expansion of adipose tissue is central to development of "unhealthy obesity". A detailed review about the developmental, structural and functional differences of visceral and subcutaneous adipose tissues was given in Section 1.2. While onset of obesity is characterized by enlargement of adipose tissues, it is not clear whether the same factors determine adipose compartment size for storage of excess energy. Unfortunately, the transcriptional mechanisms determining orientation of excess energy into adipose tissues have yet to be fully characterized. It does seem most likely, however, that topological and ontogenetic differences determine the enlargement of different adipose tissues. Accordingly, we measured adiposity in different adipose

compartments to clarify which adipose sites are targeted first to store energy surplus resulted from sustained caloric disequilibrium, and how such storage capacity changes with time and "demand".

As expected, adiposity rates differed among adipose sites during development of mice (from 6 to 12 weeks of age). At an early stage (6 weeks of age), atherogenic diet was quite influential on all adipose sites. Accordingly, atherogenic diet-fed *WT* mice showed increased adipose weights compared to chow-fed *WT* mice. This increase was more prominent with atherogenic dietary intake in *foz/foz* mice. Interestingly, appetite defect (*foz/foz* background) became more powerful on adiposity after 8 weeks of age. After this time point in chow-fed *foz/foz* mice, there was a significant enlargement of adipose compartments compared to chow-fed *WT* mice. Nevertheless, these increases remained limited when compared to those of atherogenic diet-fed *foz/foz* mice adipose sites.

The expansion of Pov and lumbar WAT was faster than Mes and dorsal WATs during mouse development. First of all, atherogenic diet-fed *foz/foz* mice showed a parallel increase in Pov and lumbar WAT mass although it was less in chow-fed counterparts. By 12 weeks of age, ~14% of atherogenic diet-fed *foz/foz* (7% + 7%) and ~10% of chow-fed *foz/foz* (5% + 5%) body weight was comprised of Pov and lumbar WAT, whereas the relative weight of Mes WAT (% body weight) was 3% in atherogenic diet-fed *foz/foz* mice and only 2% in chow-fed *WT* counterparts. The change in dorsal adipose compartment was even less in *foz/foz* mice. Atherogenic dietary feeding expanded adipose mass in all four adipose compartments in *WT* mice compared to their chow-fed counterparts, but adiposity of these tissues did not significantly increase during development. BAT mass increased marginally (but significantly) in *foz/foz* mice, but relative BAT weight remained the same after 8 weeks of age.

As discussed in details in Chapter 1, hypertrophic adipocytes are likely to develop pro-inflammatory response that leads to macrophage infiltration and formation of CLSs.

We therefore thought that it is important to study morphological changes in adipose tissue during evolution of obesity in these mice. As stated in Results Section, there is a general consensus that adipocytes between 500 and 4000 μm^2 are small sized, between 5000 to 7000 μm^2 are moderate sized, and those exceed 8000 μm^2 are large, hypertrophic adipocytes. In the present project, we studied Pov WAT in 12 week old mice to characterize any differences in adipose morphometry and number of CLSs in the tissue. Mean adipocyte volume remained very small (less than 1000 μm^3) in chow-fed *WT* mice. Both atherogenic dietary intake and *foz/foz* genotype increased mean adipocyte volume, while the interaction between these two factors markedly increased mean adipocyte volume in Pov WAT. This increase in adipocyte size correspondingly decreased the average number of adipocytes visualized a fixed surface area in atherogenic diet-fed *foz/foz* mice Pov WAT. As shown in Section 3.4.2, the even size distribution of adipocytes in chow-fed *foz/foz* mice differed strikingly for the accumulation of cells $\geq$ 8000 μm^2 to 40% of total adipocytes in atherogenic diet-fed *foz/foz* mice. Atherogenic dietary intake clearly caused lipid-engorgement of adipocytes in *foz/foz* mice.

The number of CLS increased proportional to the increase in adipocyte volume in these animals. Although traces of adipose inflammation were found for other groups, it was substantial only in atherogenic diet-fed *foz/foz* mice. Hypertrophic adipocytes become the dominant subpopulation in atherogenic diet-fed *foz/foz* mice with high number of CLSs indicating an association between adipose morphology and inflammatory status. To summarize, adipocyte size is a good indicator about the metabolic status of adipose tissues (small is good at early stages of age), and existence of large hypertrophic adipocytes can assist inflammatory recruitment into adipose tissue. In the present Chapter which addresses developmental changes, morphometry was not performed in subcutaneous WAT. In a later Chapter (Chapter 6), both sites

were studied and it became evident that there are differences between visceral and subcutaneous WATs.

As stated in Section 3.1, NASH comprises three indices: liver steatosis, inflammatory recruitment into liver, and hepatocyte degeneration (ballooning). The S.O.S. signal for the development of NASH starts with ectopic lipid partitioning, particularly into liver. In other words, excess energy that escapes from (or is not stored in) adipose tissues targets liver. Hepatocyte lipid uptake, storage and lipid trafficking within hepatocytes are not yet fully characterized. However, increasing data indicate that lipid-induced hepatocyte stress (liver lipotoxicity) and injury is central to transition of simple steatosis to NASH during histological progression.

The important liver finding in this study was that not only the amount but the intracellular pattern (type/structure) of lipid accumulation in the liver changes with the combination of atherogenic diet and *foz/foz* genotype. At 8 weeks, there were early indications of liver enlargement and hepatic steatosis (determined by liver ORO) in atherogenic diet-fed *foz/foz* mice. At 10 weeks of age, hepatomegaly was established and liver total steatosis was significantly increased compared to their *WT* counterparts. However, liver macro-steatosis was virtually absent until 10 weeks of age in liver of these mice. Absolute and relative liver weight continued to increase in 12 week old atherogenic diet-fed *foz/foz* mice. Correspondingly, liver total steatosis (micro + macro [vesicular] steatosis) also increased by ORO quantification. The finding that a significant increase in stainable liver macro-steatosis could not be observed until 12 weeks of age in atherogenic diet-fed *foz/foz* mice. This could be an important fact of lipid storage in hepatocytes during onset of NAFLD. In these initial stages, lipids (particularly TAGs) appear to be packaged in lipid droplets which form microvesicles as the "demand" for lipid storage increases, the protein composition of lipid droplets change (in favour of adipophilin over perilipin). Light microscopy of H&E-stained liver

sections is not a satisfactory method for determining minor degrees of steatosis when microvesicles predominate (365). However, once microvesicles form macrovesicles, fat (steatosis) is readily appreciated. This technical reason likely explains why the apparent pattern of hepatic lipid accumulation is gradual (between 6 to 12 weeks) when detected by ORO, but seems apparent only at 12 weeks by examination of H&E-stained liver sections.

In conclusion, interaction between "Western dietary intake" (atherogenic diet) and appetite defect-mediated over-eating (*foz/foz* genotype) results in early-onset of obesity in mice. The response of different adipose compartments to this energy imbalance differs and some tissues (Pov and lumbar WATs) have higher capacity of lipid storage than others (Mes and dorsal WATs). Atherogenic dietary intake increased mean adipocyte volume in Pov WAT during development of *foz/foz* mice and this was associated with an increase in the number of CLSs in adipose tissue. Meanwhile, the mice that showed higher number of hypertrophic adipocytes and infiltration of macrophages into adipose tissue also developed hepatomegaly and hepatic steatosis, which indicates that adipose hypertrophy and inflammation are associated with and may be a precondition for development of NASH. Next chapter provides an insight into the mechanism and significance of adipose inflammatory recruitment (role of TLR9 signaling) and adipose dysfunction.

CHAPTER 4

CHAPTER 4: Macrophages Recognise Degenerating Adipocytes via TLR9 Signalling

4.1 Introduction

In unhealthy obese individuals, fat cells die because their capacity to store lipid in the face of continuous energy imbalance is ultimately limited. During 2.5 million years of human evolution, adipocytes have developed in ways to store and provide energy to the system during periods of fasting, as in the case of nutrient deprivation in the environment. In no time in history until the last 2-3 decades, has calorie-dense food been so easy to access, and life has never been this sedentary. Evolution has not prepared human biology to adjust to these altered circumstances.

4.1.1 Adipose Dysfunction and Natural Selection

Researchers have different opinions/interpretations about the behaviour of fat cells. Some authorities think of adipocytes as being altruistic cells. For the sustainability of the system, they try their best to store as much energy as they can. Others think adipocytes are unselfish but naïve cells. They are devoted to accomplish their job under any circumstance. In addition, yet other scientists think adipocytes are simply dumb. They do not have a well-developed self-control system; they corrode themselves as a result of their "dedication", and consequently damage the whole system. Possibly all these statements are true, but they may be missing the point that vertebrate evolution continues. We take the view that adipocytes are "smart" cells; they push their limits to store energy because they are aware of the fact that constant energy imbalance is harmful for the body.

In most parts of the world, adipocytes of the 21st century are more hypertrophic and adipose tissues are more hyperplastic. Individuals who are able to control their appetite and who exercise more remain, from a relative point of view, healthier. Individuals who have "better quality" adipose (i.e., that with higher storage capacity) remain metabolically healthy obese despite conditions of energy surplus. Lastly, individuals who cannot change their lifestyle (of over-eating with sedentary behaviour) and who have adipose with a limited capacity for expansion, and/or whose adipocytes are fragile, develop serious health problems. Increased age- and gender-standardized mortality resulting from diabetes and cardiovascular problems, insulin resistance related cancers and fatty liver disease (NASH, cirrhosis, HCC) are seen mostly in the last group, who have unhealthy obesity.

Although mortality does increase with obesity and its related metabolic, vascular, neoplastic and liver complications do not usually prevent individuals from breeding (366, 367). This is because most mortality occurs after age of 40 years. For this reason, unhealthy obese individuals pass on their obesity development-related polymorphisms, perhaps mutations, as well as their cultural norms to their children. This is where Darwinist Natural Selection fails in obesity, because these alleles are not eliminated; they are inherited by the descendants. The behavioural aspects so central to over-nutrition may also be learnt during early development and passed on to subsequent generations. Unlike rarer mono-genetic disorders, obesity is highly prevalent worldwide; an exception currently being sub-Saharan Africa (368). Over the last 30 years, obesity has become the biggest challenge in medical sciences after cancer; both problems are partly lifestyle-related, partly genetically determined. These health priorities are likely to continue until biomedical science provides new drug therapy to interfere artificially with the consequences of metabolic obesity.

4.1.2 Recognition of Dead Adipocytes

As highlighted in Section 1.5, hypertrophy and ultrastructural abnormalities force adipocytes to die (266). Increasing numbers of dead adipocytes cause tissue dysfunction. The body attempts to protect adipose tissues by recruitment and activation of inflammation. In particular, there is infiltration of immune recognition and effector cells, such as DCs and macrophages, respectively. As stated earlier, 90% of macrophages in inflamed adipose tissues are found in CLSs (321). These occur around small dying/dead adipocytes. Despite the implications of such localisation, surprisingly little is known about the mechanism for inflammatory recruitment into adipose. A key question is how do macrophages recognize degenerating or dead adipocytes in order to accumulate around them. Alternatively stated: what are the recognition signals created by stressed adipose that attract inflammatory cells to the tissue?

In this Chapter, we examine the possibility that TLR9 signalling may contribute to macrophage recognition of degenerating adipocytes, with localization and formation of CLSs to initiate adipose inflammation. In order to place TLR9 in context with other pattern recognition receptors and their signalling molecules, a brief overview of TLRs will be given here.

4.1.3 The TLR Family

TLRs are one type of pattern-recognition receptors (PRRs) that form a central recognition function in the innate immune system (IIS) (369). The molecular patterns can be intrinsic (DAMPs) or from microorganisms (PAMPs). The “modern” concept for IIS research followed the discovery that B cell NF-κB is activated by the gram-negative bacterium cell wall component, lipopolysaccharide (LPS) (369, 370). NF-κB was not initially identified as a pro-inflammatory transcription factor, but was known to regulate a remarkable number of genes in inflammation. Interestingly, interleukin 1-R type 1

(IL-1R1) was found to activate NF-κB (371). Considering the fact that Toll and IL-1R1 share the same signalling domain, it was evident that these proteins may have pleiotropic NF-κB-dependant roles. This increased interest in TLR research.

The first TLR to be identified (in 1997) was called hToll (now known as TLR4) (372). One year later, five more Toll homologues were reported (373). Meanwhile, LPS was reported to signal via TLR4 through an intracellular adapter protein called myeloid differentiation primary-response protein 88 (MyD88) to upregulated NF-κB, thereby inducing expression of pro-inflammatory genes (374, 375). TIR-domain-containing adapter-inducing interferon β (TRIF) is another intracellular adapter protein, necessary for TLR4 and TLR3 signal transduction (376). These discoveries further stimulated research into the relationship of innate immunity to inflammation and tissue regeneration. For the insights gained, Bruce Beutler and Jules Hoffman were eventually awarded the Nobel Prize for Physiology or Medicine in 2011 (377).

Today, 10 human and 13 mouse TLR subtypes have been reported (378). TLR2 recognizes lipopeptides (379). TLR3 is important for viral protein recognition (380), and unlike TLR4 and TLR2, it is an endosomal (intracellular) receptor. From 2002, TLR7, TLR8 and TLR9 were also reported to recognize intracellular danger signals which are important for tissue damage-mediated inflammatory recruitment (381). The recent discovery of TLR13, which recognizes bacterial ribosomal RNA, indicates that knowledge about TLRs and IIS continues to grow. General information about TLRs is summarized in Table 4.

TABLE 4
General overview on rodent Toll-like Receptors (TLRs)

TLR	Location	DAMPs	PAMPs	Signal adapter(s)	Production
TLR1+TLR2	Cell surface	HSP60, 70; HMGB1, proteoglycans (e.g., versican)	Triacylated lipoproteins, peptidoglycans	TIRAP, MyD88/Mal	Inflammatory cytokines
TLR2+TLR6	Cell surface		Diacylated lipoproteins	TIRAP, MyD88/Mal	Inflammatory cytokines
TLR3	Endosomes	mRNA, tRNA	dsRNA (poly I:C), tRNA	TRIF	Inflammatory cytokines, type 1 IFN
TLR4	Cell surface and endosomes	HSP22, 60, 70, 72; HMGB1, proteoglycans	LPS	TRAM/TRIF,TIRAP, MyD88/MAL	Inflammatory cytokines, type 1 IFN
TLR5	Cell surface	NA	Flagellin, profilin	MyD88	Inflammatory cytokines
TLR7	Endosomes	ssRNA	ssRNA	MyD88	Inflammatory cytokines, type 1 IFN
TLR8	Endosomes	ssRNA	ssRNA	MyD88	Inflammatory cytokines, type 1 IFN
TLR9	Endosomes	ssDNA, chromatin IgG complexes, HMGB1	CpG DNA, CpG ODNs	MyD88	Inflammatory cytokines, type 1 IFN
TLR10	Endosomes	NA	Profilin-like proteins	MyD88	Inflammatory cytokines
TLR11	Endosomes	NA	Profilin (toxoplasma gondii)	MyD88	Inflammatory cytokines, type 1 IFN
TLR12	Endosomes	NA	Profilin (toxoplasma gondii)	MyD88	Inflammatory cytokines, type 1 IFN
TLR13	Intracellular	NA	rRNA	MyD88	NA

Abbreviations: dsRNA, double-stranded RNA; HMGB1, high-mobility group protein 1; HSP, heat shock protein; IFN, interferon; IgG, immunoglobulin G; LPS, lipopolysaccharide; Mal, MyD88 adapter like; MyD88, myeloid differentiation primary-response protein 88; NA, not applicable; ssDNA/RNA, single-stranded DNA/RNA; TIRAP, Toll/interleukin1 receptor domain-containing adapter protein; TRIF, TIR-domain-containing adapter-inducing interferon β.

4.1.4 "Turning on" TLR9

TLR9 signalling was first reported in 2000 as an anti-bacterial response (382). It was then shown that TLR9 could recognize CpG-rich (hypomethylated) single strand DNA (ssDNA) motifs (382, 383). TLR9 is located intracellularly in endosomes (Fig. 4.1) (384). Although there are some clinical indications that TLR9 may play a role in auto-inflammatory (-immunity) response, in general, the mechanism by which TLR9 responds to foreign DNA is under strict control (385). Such a response requires proteolytic processing of the TLR9 ectodomain in the endolysosome, a mechanism that prevents TLR9 responding to extracellular self DNA.

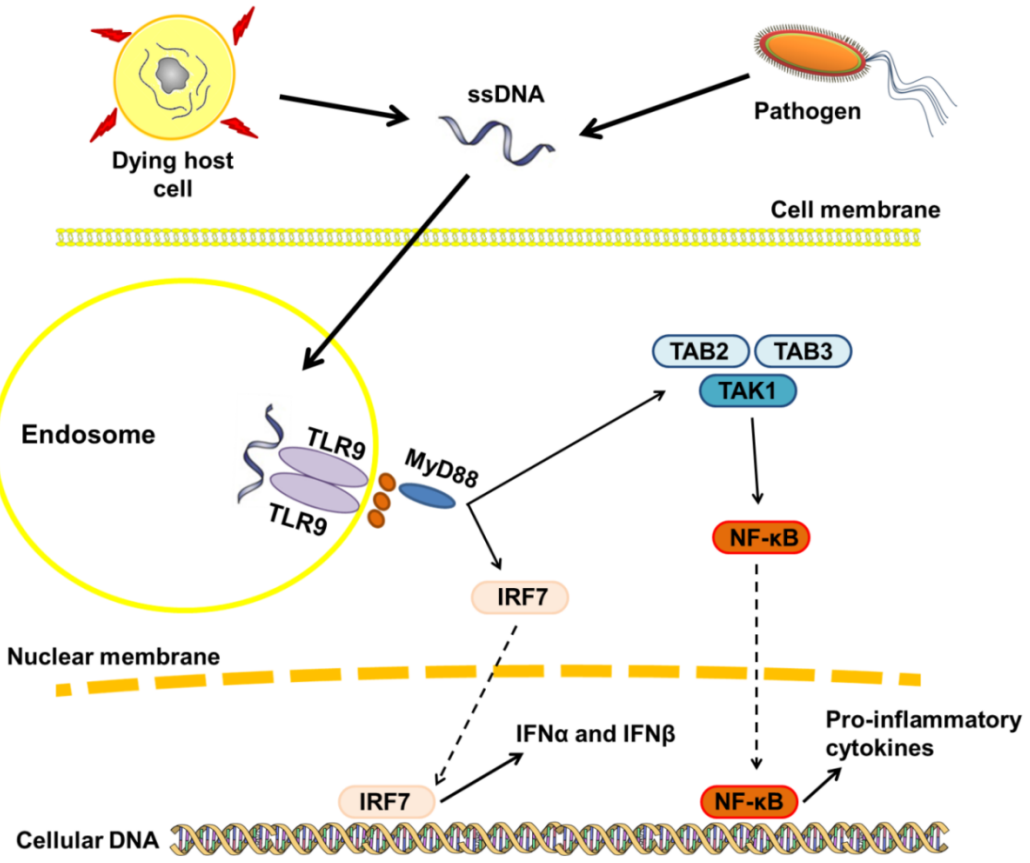

Figure 4.1: An overview of TLR9-mediated signalling pathway. Upon activation by its ligand, the cytosolic domain of TLR9 recruits MyD88. MyD88-mediated signalling cascade in turn activates interferon regulatory factor 7 (IRF7) or NF-κB to induce expression of type I IFNS (IFNα and IFNβ) or pro-inflammatory cytokines (e.g., TNFα, IL6).

4.1.5 Adipocytes and Innate Immunity

Adipose tissue is a "roundabout" that connects metabolism to the immune system. As explained in Section 1.5, adipose tissues secrete classical cytokines (TNFα, IL6, etc.), chemokines (MCP1, MIF, chemokine (C-C motif) ligand 5 [CCL5], etc.), immune-modulators, complement (adipsin, ASP, etc.), and growth factors (64). Changes in adipose morphometry, adipose macrophage infiltration, and macrophage-like differentiation of preadipocytes may affect the production of these factors. These changes are bidirectional; adipose tissues have regulatory roles in both the metabolic and immune responses. In this context, TLR9 signalling may have a special role in adipose innate immunity.

The level of TLR9 expression on adipocytes depends on the commitment level of the cell; its expression differs between preadipocytes and mature adipocytes (386). For example, the murine preadipocyte cell line 3T3-L1 does not express TLR9 under basal conditions (387). In adipocytes, there are different patterns of TLR9 expression, but there is no consensus on which cell type actually activates TLR9 signalling during adipose inflammation: is it adipocytes or is it macrophages themselves?

Interferon γ (IFNγ) plays an important role in the initiation of an adipose inflammatory response (388). The main source for IFNγ production in adipose is T cells (389). CCL5 (RANTES) is a chemokine that induces migration of leukocytes, particularly T cells, to the tissues (390, 391). Chemokine (C-X-C motif) 10 (CXCL10 [IP10]) is another small chemokine that is also described as IFNγ-induced protein 10 (392). It is produced in response to IFNγ and it can induce migration and activation of several immune cells, including monocytes/macrophages and DCs (393).

Mononuclear phagocyte leukocytes originate from BM-derived cells, circulate as monocytes and differentiate into macrophages or DCs (394, 395). While monocytes are known as circulating pre-cursors, they carry effective immune-modulatory machinery

that includes chemokine and adhesion receptors. Different subsets of monocytes can participate in immunization, conducting different tasks, such as taking up toxic molecules and producing inflammatory cytokines. Despite this appreciation, monocyte migration to sites of inflammation and their differentiation into macrophages is poorly understood.

Monocytes enter the blood from the BM and circulate until they are recruited. However, tissues also contain resident immune cells that do not originate from the BM (308). Understanding the origins of monocytes and macrophages carries potential to reveal the factors that determine adipose inflammatory recruitment. In order to understand the migration pattern of immune cells and their infiltration into tissues, BM chimeric mice are a useful model (396) and this was employed in the present research. However, it needs to be recognized that total body irradiation and BM reconstruction may present their own challenges in conducting the studies and interpretation of experimental data. Robust macrophage infiltration is the main event in persistent adipose inflammation, but it is not clear yet whether monocytes commit to a pro-inflammatory phenotype while in the circulation (before diapedesis) attributable to the presence of circulating adipose-derived chemokines, or whether they trans-differentiate after migration into the tissue. There are also few details about exactly how monocyte/macrophage infiltration into adipose occurs, except that some factors such as GM-CSF and macrophage inflammatory protein 1α (MIP1α) are present in inflamed adipose (334). This chemokine gradient is likely to favour “monocytic infiltration” into adipose tissue. If this is the case, the main source of macrophages in inflamed adipose must be the BM.

4.2 Aims

In this Chapter, we hypothesized that extensive adiposity and resultant adipocyte cell death activate TLR9 signalling in adipose tissue. Such TLR9 activation contributes to macrophage recognition of degenerating adipocytes, causing their accumulation and activation as M1 macrophages so as to form CLSs. An axiom is that the number of CLSs reflects the intensity and persistence of adipose inflammation. Accordingly, the specific aims were to:

1. Examine adipose morphometry, oxidative stress and cell death pathways in relation to adipose inflammation in our diabetic obese mouse model of metabolic syndrome and NASH; there is a particular focus on CLSs, around small degenerating or dead adipocytes.
2. Test whether TLR9 plays a role in adipose inflammation by using gene-deleted mice and diet-induced models of obesity.
3. By the combination of flow cytometry and BM chimera strategies, clarify whether adipocytes and/or macrophages are primarily responsible for TLR9 signalling.
4. Investigate the relationship of adipose dysfunction and TLR9 to the developmental origins of NASH (see Section 3.1.1 for introduction).

4.3 Experimental Details

All animal experiments were performed under appropriate ethics approval and strict adherence to these protocols (see Section 2.1.1). Unless stated otherwise, mice were grouped 2-5 per cage, with *ad-libitum* access to water and food, under a 12-hour day/night cycle and constant temperature of 22^0C. From weaning, groups (n=6-14) of female *Alms1*$^{-/-}$ mutant (*foz/foz*) C57BL/6J (B6) mice, *Tlr9*$^{-/-}$, and *WT* mice (also B6 strain) were fed either rodent chow or atherogenic (Ath) (SF03-020; Glen Forrest) diet

until 28 week old. Control mice (*WT* littermates) were established for both *foz/foz* and *Tlr9*$^{-/-}$ mice, and for the sake of clarity, these control groups were combined in data analysis. Detailed methodology about tissue harvest is given in Section 2.1.3. In the present study, fasting blood, fat pads, and liver were removed under anaesthesia for further analyses.

In this PhD project, a diverse and extensive range of molecular biology techniques was used, including serum ELISA (Section 2.2.1), mRNA quantification by qPCR (Section 2.3.1), and protein analysis by western blotting (Section 2.3.2), as detailed in the relevant sections of Chapter 2. mRNA expression levels of target genes were normalized to the mean of three "house-keeping genes": β-2 microglobulin (B2M), RPL13A, and GAPDH mRNA. Likewise, targeted protein levels in western blotting were normalized to levels of HSP90. Adipose morphometry and liver histology analyses were other techniques used in this study and have been described in Section 2.2.3. In addition to the detailed adipose morphometric analysis, the number of degenerating small adipocytes (in the centre of CLSs) was counted by analyzing 10 fields of H&E-stained adipose sections (1 mm^2 area) for each mouse. Lastly, TLR9 expression patterns of different adipose tissue cell types were analyzed by flow cytometry, as described in Section 2.3.3.

For the creation of BM chimeras, *WT* and *Tlr9*$^{-/-}$ B6 mice were irradiated (double dose 450 cGy) and received (by tail vein injection) either *WT* or *Tlr9*$^{-/-}$ BM cells, as detailed in Section 2.1.6. After 6 weeks of antibiotic treatment ($8.5x10^5$ U/L polymyxin-B-sulphate, 1.1 g/L neomycin sulphate in drinking water) to prevent systemic infections after total body irradiation, mice were fed atherogenic diet for 14 weeks. Harvest was performed following the standard procedure (Section 2.1.3).

Data are presented as mean ± SEM (n=8-18). For the analysis of data significance, Prism 6 (GraphPad, La Jolla, CA) and SPSS Statistics 22 (IBM, New York, NY)

softwares were used applying one-way or two-way analysis of variance (ANOVA), followed by Bonferroni's *post hoc* analysis.

4.3.1 Author Contributions

Fahrettin Haczeyni designed and conducted the experiments, performed all the read-out analysis, and wrote the Chapter. Auvro Robin Mridha also provided intellectual input into experimental design and assisted with the conduct of experiments. Vanessa Barn supervised the breeding and maintenance of animals. Matthew M. Yeh assessed liver histology. Narci Teoh contributed intellectual input and reviewed the experimental results. Bruce Shadbolt provided invaluable advice on statistical analyses. Geoff Farrell conceptualized and directed the study, reviewed and edited the Chapter. The Canberra Hospital research office and animal house technicians also provided highly skilled technical assistance.

4.4 Results

In order to understand the mechanism of macrophage recruitment during persistent adipose inflammation, cohorts of appetite-dysregulated *foz/foz* mice and *WT* controls were established on either the atherogenic diet (which accelerates onset of obesity, diabetes and NASH) or chow. Activation of TLR9 is the main focus of this Chapter. To study its role in adipose inflammation, a cohort of *Tlr9*$^{-/-}$ mice (with *WT* controls) was also studied to determine how absence of this immune receptor influenced physiological and pathological changes in the adipose and liver.

4.4.1 Effects of Diet and Genotype on Weight Gain and Metabolism

With atherogenic dietary feeding, *WT* mice gained more weight than chow-fed counterparts, to be ~40 g (obese) at the end of experiments (Fig. 4.2A). Chow-fed

foz/foz mice gained more weight than either chow-fed or atherogenic diet-fed *WT* mice, reflecting the powerful effect of appetite dysregulation described in Chapter 3. *foz/foz* mice developed obesity (> 50 g) on either diet. Conversely, atherogenic diet-fed *Tlr9*$^{-/-}$ mice were protected from excessive weight gain.

Atherogenic dietary feeding had only a minor (if any) effect on FBG levels in these B6 mice (Fig. 4.2B). Although there was an apparent increasing trend of FBG in *foz/foz* mice (fed either diet), these increases were not significant compared to *WT* counterparts. However, the increase in serum insulin levels was significant in chow-fed *foz/foz* mice compared to *WT* control (Fig. 4.2C). A similar increase was found in atherogenic diet-fed *foz/foz* mice vs. diet-matched counterparts, but this was not significant because of the considerable variance in this group (10 mice; range 0.3 – 18.9 ng/ml).

In chow-fed *foz/foz* mice, serum total cholesterol was ~3 times higher than chow-fed *WT* mice (Fig. 4.2D). In atherogenic diet-fed *foz/foz* mice, more profound hypercholesterolemia developed; there was 2-fold increase in serum total cholesterol compared to atherogenic diet-fed *WT* mice. On the other hand, *Tlr9* deletion did not affect serum cholesterol in chow-fed animals, and, although it was higher than in chow-fed *Tlr9*$^{-/-}$ mice, serum cholesterol levels in atherogenic diet-fed *Tlr9*$^{-/-}$ mice were still lower than for diet-matched *WT* controls.

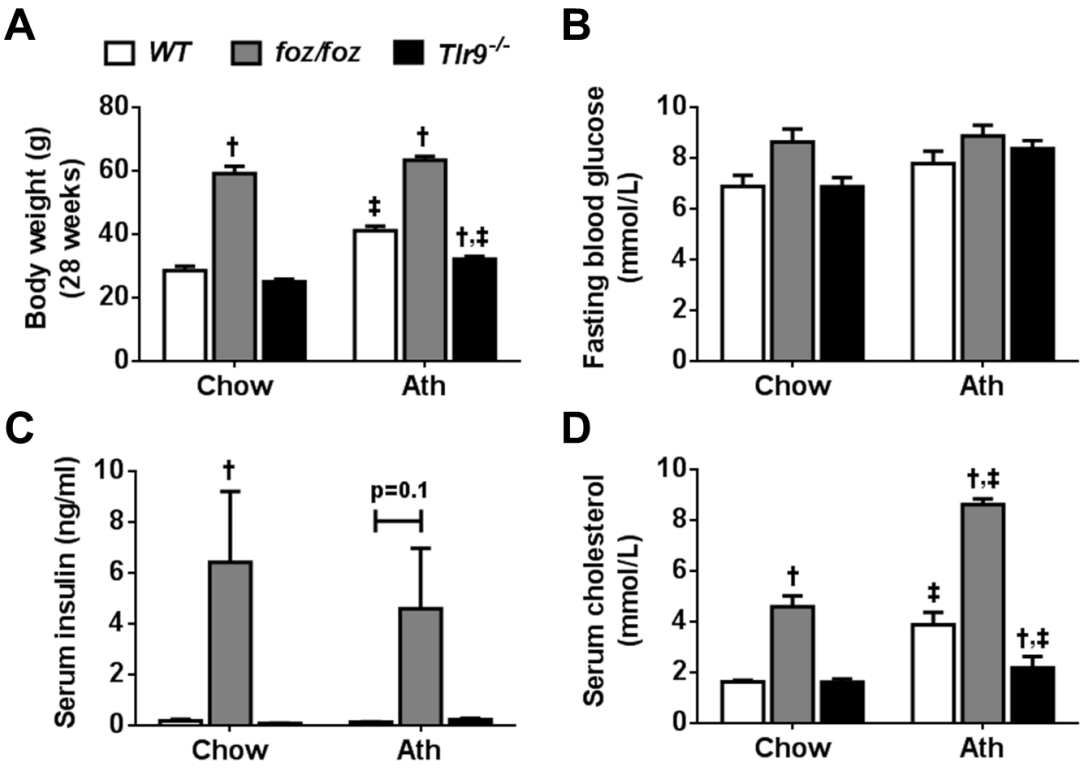

Figure 4.2: Effects of atherogenic diet on body weight, FBG, serum insulin and cholesterol in *WT*, *foz/foz*, and *Tlr9*$^{-/-}$ mice. (A) Atherogenic diet-fed *WT* and *foz/foz* mice weighed more than 40 g, whereas *Tlr9*$^{-/-}$ mice gained weight compared with chow-fed counterparts, but were protected from excessive weight gain. (B) Dietary intake and genotype did not have significant effect on fasting blood glucose. (C) However, *foz/foz* mice developed hyperinsulinemia, irrespective of diet when compared with their *WT* counterparts. There was no increase in serum insulin levels of *WT* or *Tlr9*$^{-/-}$ mice fed atherogenic diet vs. chow. (D) Atherogenic dietary intake increased serum cholesterol levels in all mice compared to their chow-fed counterparts, and *foz/foz* mice developed severe hypercholesterolemia after 24 weeks of atherogenic dietary feeding. In *Tlr9*$^{-/-}$ mice, atherogenic dietary intake increased serum cholesterol levels vs. chow-fed *Tlr9*$^{-/-}$ mice
Data are mean ± SEM (n=6-14/gp).
† $P<0.05$ vs. diet-matched *WT* (genotype effect); e.g., chow-fed *foz/foz* vs. *WT*
‡ $P<0.05$ vs. genotype-matched control (diet effect); e.g., atherogenic diet-fed vs. chow-fed *WT*

4.4.2 Effects of Diet and Genotype on Adipose Tissue Size and Function

Although multiple adipose pads contribute differently to bodily pathophysiology (see Section 1.2.7), in this part of the study we measured only periovarian adipose tissue (referred to as visceral WAT) due to the demanding (of time) morphometric analyses required. Among chow-fed mice, visceral WAT weighed more in *foz/foz* and less in *Tlr9*$^{-/-}$ mice than *WT* (Fig. 4.3A). Atherogenic dietary feeding increased visceral WAT weight (~2-fold) in *WT* mice; a similar but limited trend was found in atherogenic diet-fed *Tlr9*$^{-/-}$ mice. In atherogenic diet-fed *foz/foz* mice, adiposity was the highest among

genotypes. However, as previously reported (232), visceral WAT as a percentage of body weight was less than in chow-fed *WT* mice (Fig. 4.3B).

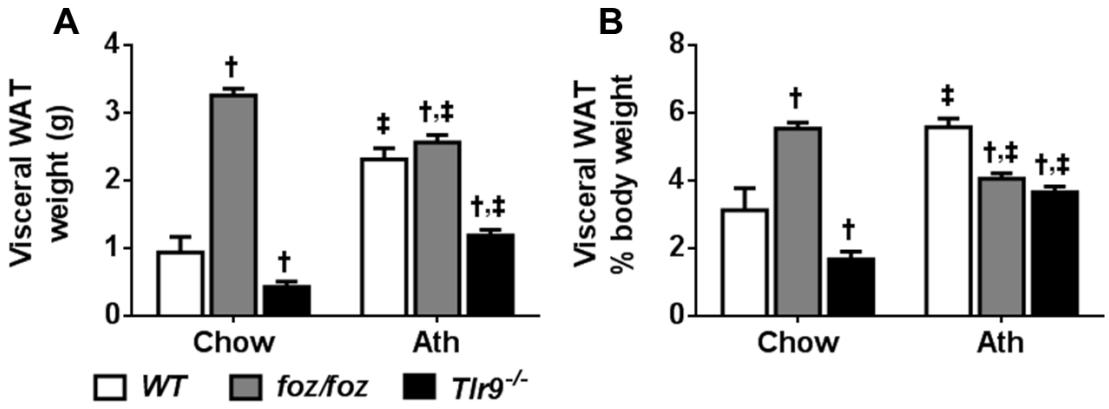

Figure 4.3: Absolute and relative visceral WAT weight in *WT*, *foz/foz* and *Tlr9*$^{-/-}$ mice.
(A) *foz/foz* mice had increased and *Tlr9*$^{-/-}$ decreased adiposity compared with *WT*, irrespective of diet. (B) However, adipose expansion as a proportion of body weight was limited in atherogenic diet-fed *foz/foz* compared to chow-fed *foz/foz* or atherogenic diet-fed *WT* mice. *Tlr9*$^{-/-}$ mice also showed limited visceral adiposity when fed an atherogenic diet compared to *WT* counterparts. Data are mean ± SEM (n=6-14/gp).
† $P<0.05$ vs. diet-matched *WT* (genotype effect); e.g., chow-fed *foz/foz* vs. *WT*
‡ $P<0.05$ vs. genotype-matched control (diet effect); e.g., atherogenic diet-fed vs. chow-fed *WT*

There was insufficient adipose in some groups (e.g., chow-fed *Tlr9*$^{-/-}$) to perform both morphometry and the full range of molecular techniques. Priority was therefore given to use tissues for morphometric and mRNA expression assays. As a result, protein analyses in this Chapter are limited by logistics. In Figure 4.4, mRNA expression levels are shown for genes concerned with adipose function. Some of them are involved in adipogenesis (and adipocyte metabolism), whereas others contribute to whole body lipid metabolism.

As described in Section 1.5.4, adipsin is an adipokine with positive effects on metabolic regulation, such as improving pancreatic β cell function (294). In atherogenic diet-fed *foz/foz* mice, levels of visceral WAT adipsin mRNA were high than in atherogenic diet-fed *WT* mice, while adipsin mRNA was lower than *WT* in *Tlr9*$^{-/-}$ mice (Fig. 4.4A). Patatin-like phospholipase domain containing 2 (PNPLA2) (ATGL)

catalyzes the first step of triglyceride hydrolysis in adipocytes (397, 398). The expression profile for *Pnpla2* mRNA was similar to adipsin (Fig. 4.4B). Perilipin 2, as explained in Section 1.4, is an important lipid droplet protein. Perilipin 2 mRNA levels were upregulated in atherogenic diet-fed *foz/foz* mice, and decreased in *Tlr9*$^{-/-}$ mice vs. *WT* counterparts (Fig. 4.4C). Caveolin 1 is a subunit in caveolae structures where insulin signalling molecules locate (see Section 1.4.4). *Cav1* mRNA levels were significantly lower in atherogenic diet-fed *foz/foz* mice visceral WAT than *WT* mice, but there was no change in *Tlr9*$^{-/-}$ mice (Fig. 4.4D).

SCD1 forms double bonds in C16 and C18 units of LCFAs that transfers saturated FAs into unsaturated ones of the same chain length (399). There was no effect of genotype on mRNA expression of this gene (Fig. 4.4E). Peroxisomal acyl-coenzyme A oxidase 1 (ACOX1) initiates FA β oxidation (400, 401). While there was a decrease in *Acox1* mRNA expression in atherogenic diet-fed *foz/foz* mice visceral WAT compared to *WT* (Fig. 4.4F), there was no change in *Tlr9*$^{-/-}$ mice. A similar trend was found for fatty acid synthase (*Fas*) mRNA levels (Fig. 4.4G). As reviewed in Section 1.3, FOXO1 is a protein regulated by insulin action (196, 197). *Foxo1* mRNA levels of visceral WAT were decreased in *foz/foz* vs. *WT* mice. In contrast, *Tlr9* deletion was associated with an increase in *Foxo1* visceral WAT mRNA levels compared to *WT* mice (Fig. 4.4H).

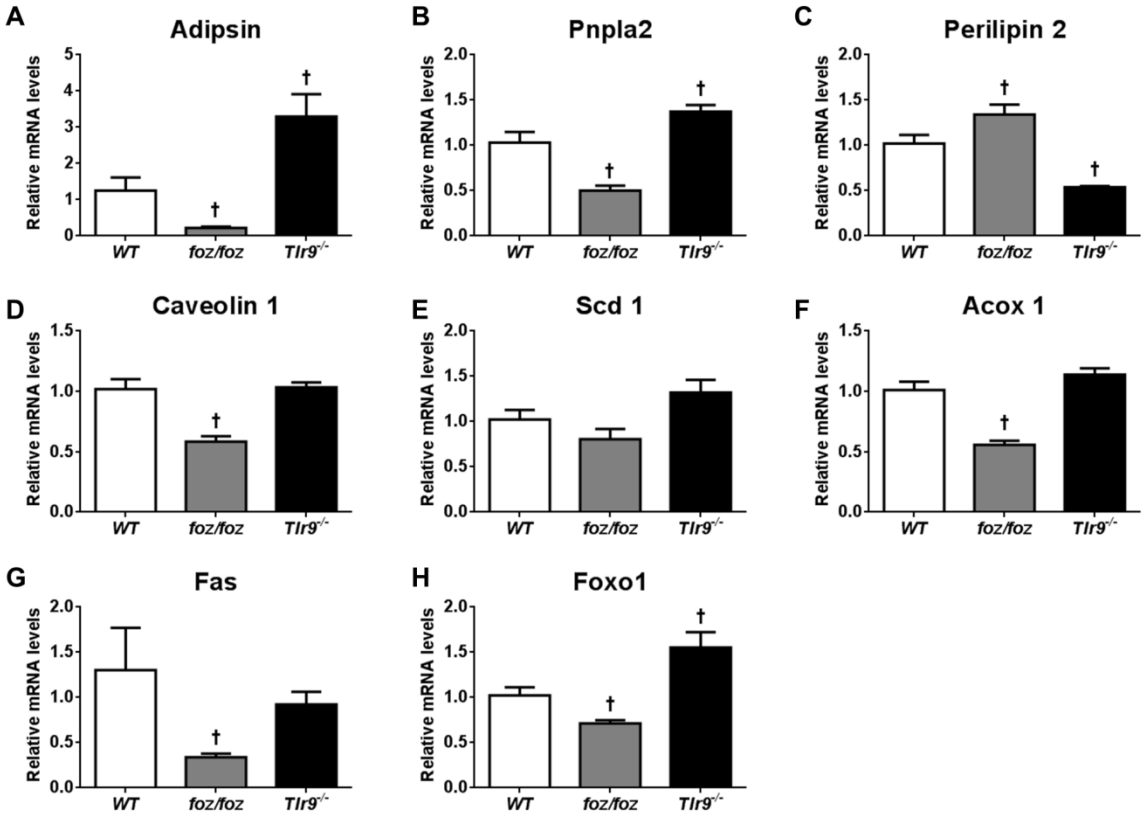

Figure 4.4: Visceral WAT mRNA expression levels for the genes indicated, which are related to adipose function, in atherogenic diet-fed mice. Note: chow-fed mice not studied here, as explained in the text. Data are mean ± SEM (n=8/gp). Values are expressed relative to *WT*, which is set at 1.0.
† $P<0.05$ vs. *WT* control (genotype effect); e.g., atherogenic diet-fed *foz/foz* vs. *WT*

A detailed overview of adiponectin as an insulin-sensitizing, anti-inflammatory hormone produced by adipocytes was provided in Section 1.5. In atherogenic diet-fed *WT* mice, circulating adiponectin levels vs. chow-fed *WT* tended to fall, but this was not significant (Fig. 4.5A). Hypoadiponectemia was found in *foz/foz* mice irrespective of diet, but this decrease was more pronounced in atherogenic diet-fed animals. Atherogenic dietary intake did not alter circulating serum adiponectin levels in *Tlr9*$^{-/-}$ mice.

Visceral (periovarian) adipose tissue is an important source of adiponectin production (see Section 1.5.4). Comparison of WAT from atherogenic diet-fed *foz/foz* or *Tlr9*$^{-/-}$ with *WT* mice showed that tissue adiponectin mRNA levels were significantly less with *foz/foz* genotype, whereas *Tlr9* deletion tended to increase (P = 0.07) adipose

adiponectin mRNA, compared to *WT* (Fig. 4.5B). Consequently, WAT adiponectin protein levels were less in *foz/foz* mice and higher in *Tlr9*$^{-/-}$ mice on atherogenic diet compared to *WT* mice (Fig. 4.5C).

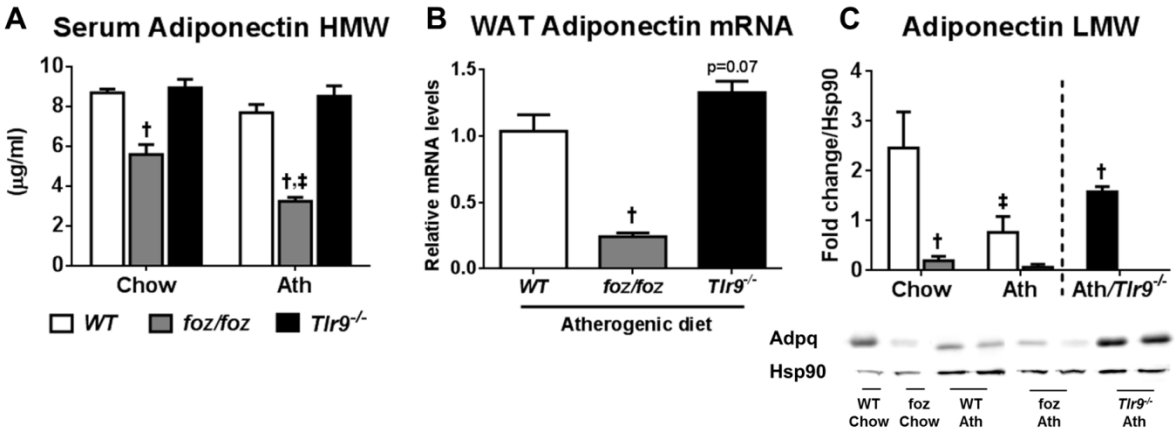

Figure 4.5: *foz/foz* mice developed hypoadiponectemia, whereas *Tlr9*$^{-/-}$ mice expressed higher tissue adiponectin compared to *WT* counterparts. (A) Serum adiponectin levels ([HMW) fell markedly in *foz/foz* mice, particularly with atherogenic diet, but values were not affected by atherogenic dietary feeding in *Tlr9*$^{-/-}$ and *WT* mice. (B) WAT adiponectin mRNA, and (C) protein expression (LMW) largely reflected serum adiponectin levels on atherogenic diet, although an effect of atherogenic diet was also evident in *WT* mice. There was insufficient tissue to assay adiponectin protein in WAT of chow-fed *Tlr9*$^{-/-}$ mice.
Data are mean ± SEM (n=8/gp).
† $P<0.05$ vs. diet-matched *WT* (genotype effect); e.g., atherogenic diet-fed *foz/foz* vs. *WT*
‡ $P<0.05$ vs. genotype-matched control (diet effect); e.g., atherogenic diet-fed vs. chow-fed *WT*

4.4.3 Effects of Diet and Genotype on Adipose Morphometry, Including Adipocyte Degeneration

A detailed review about adipocyte size is provided in Section 1.4. Adipose dysfunction and metabolic complications of obesity are associated with excess lipid partitioning into adipocytes. This lipid engorgement causes their degeneration, and degenerating adipocytes shrink due to lipid "spillage" from adipocytes. As a result of these changes, the small size of adipocytes is ambigious under different circumstances; it can reflect a healthy phenotype (as with exercise, see Chapter 6), or unhealthy (in terms of shrinking during cellular injury and death).

The mean adipocyte volume in chow-fed *foz/foz* was larger than in chow-fed *WT* (Fig. 4.6A). Atherogenic dietary intake increased adipocyte volume in *WT*, but failed to increase this parameter in *foz/foz* mice compared to their chow-fed counterparts. On the other hand, atherogenic dietary feeding (vs. chow) increased mean adipocyte volume in the visceral WAT of *Tlr9*$^{-/-}$ mice (Fig. 4.6A). Atherogenic dietary intake lowered the number of adipocytes in a fixed surface area in *WT* (not significant) and *Tlr9*$^{-/-}$ mice (vs. chow), but consistent with the lack of change in cell volume, had no effect in *foz/foz* mice (Fig. 4.6B).

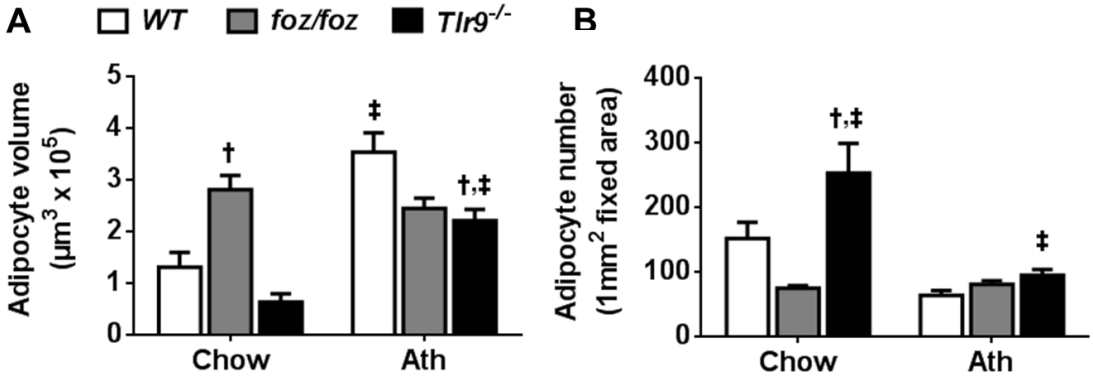

Figure 4.6: Mean adipocyte volume and number in *WT*, *foz/foz* and *Tlr9*$^{-/-}$ mice. (A) *foz/foz* mice showed increased mean adipocyte volume in visceral WAT, although this increase appeared to be more limited in atherogenic diet-fed mice compared to *WT* counterparts. Atherogenic dietary intake increased adipocyte volume ~3-fold in *Tlr9*$^{-/-}$ mice (vs. chow), but cell volume remained less than in atherogenic diet-fed *WT* mice (B) Reflecting their smaller volume, mean adipocyte numbers were lower in *foz/foz* mice than WT irrespective of diet, and larger in chow-fed *Tlr9*$^{-/-}$ mice compared with *WT*.
Data are mean ± SEM (n=8/gp).
† $P<0.05$ vs. diet-matched *WT* (genotype effect); e.g., chow-fed *foz/foz* vs. *WT*
‡ $P<0.05$ vs. genotype-matched control (diet effect); e.g., atherogenic diet-fed vs. chow-fed *WT*

A detailed explanation for adipocyte size classification is provided in Section 3.4.2. The majority of adipocytes in chow-fed *WT* mice were between 500 and 4000 μm^2 in size (small adipocytes) and the numbers of medium and large adipocytes were very low (Fig. 4.7A). In chow-fed *foz/foz* mice, the distribution of adipocyte size was greater, with the most abundant cell population between 3000 to 5000 μm^2, or 9000 μm^2 and

above (Fig. 4.7B). In chow-fed *Tlr9*$^{-/-}$ mice, the most significant proportion of adipocytes was small cells, especially between 0 and 3000 μm^2 (Fig. 4.7C).

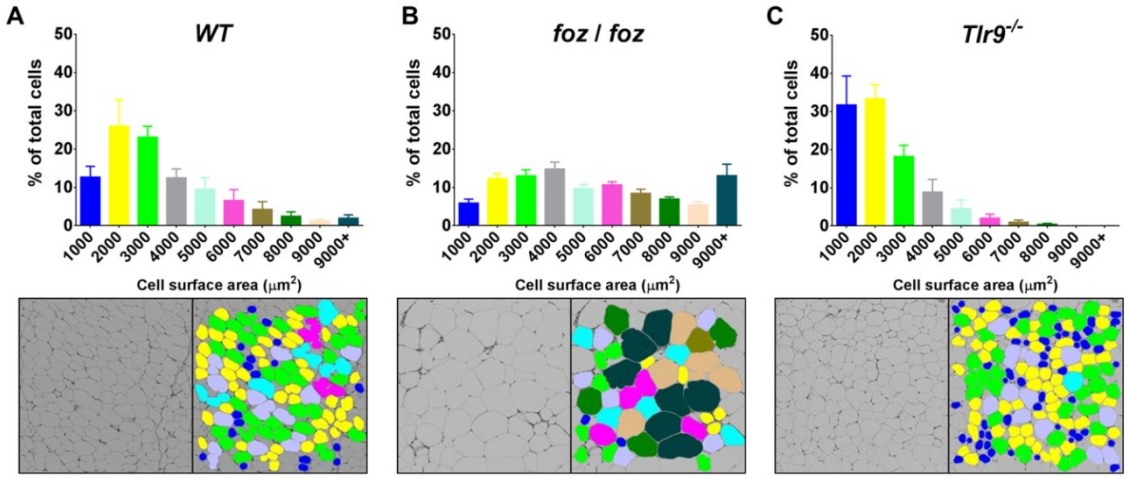

Figure 4.7: Adipocyte size distribution in chow-fed *WT*, *foz/foz*, and *Tlr9*$^{-/-}$ mice. (A) Distribution of median adipocyte size was accumulated around small to moderate adipocytes in chow-fed *WT*, (B) with no dominant size group in chow-fed *foz/foz* (> 10% cells were above 9000 μm^2), and (C) predominantly small adipocytes in chow-fed *Tlr9*$^{-/-}$ mice visceral WAT. (n=8/gp [10 sections per mouse]; H&E-staining, 160x magnification)

In atherogenic diet-fed *WT* visceral WAT, the majority of adipocytes were medium-to-large and ~20% were 9000 μm^2 and above in size (Fig. 4.8A). In atherogenic diet-fed *foz/foz* mice, the proportion of large adipocytes was less than *WT* counterparts (Fig, 4.8B). Atherogenic diet-fed *Tlr9*$^{-/-}$ mice exhibited less than 10% large adipocytes, and the majority of cells were small-to-moderate adipocytes (Fig. 4.8C). Interestingly, both atherogenic diet-fed *foz/foz* and *Tlr9*$^{-/-}$ mice showed an important proportion of small adipocytes. The possibility that the phenotype of these "small adipocytes" is different between the two genotypes is addressed by data in the next Section.

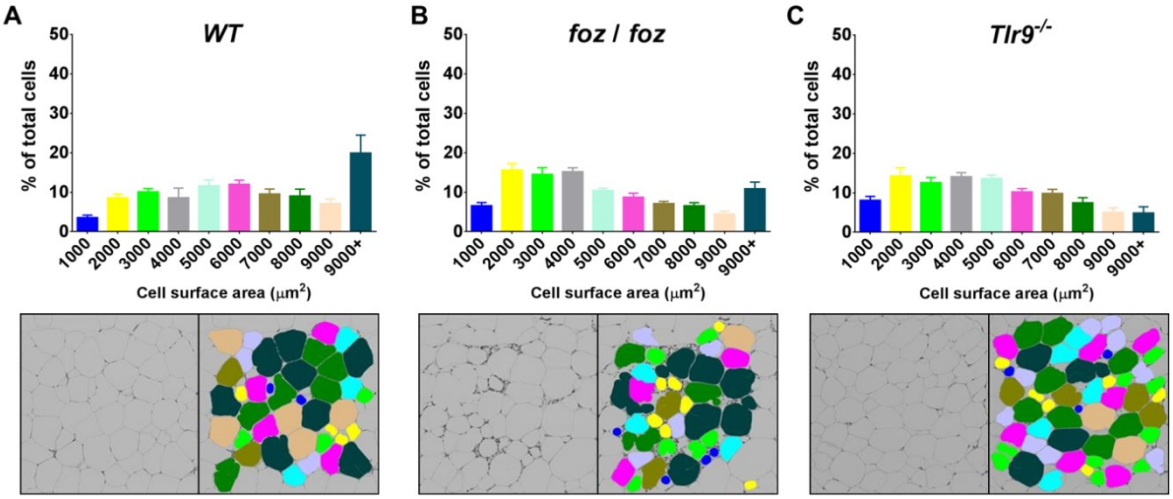

Figure 4.8: Adipocyte size distribution in atherogenic diet-fed *WT*, *foz/foz*, and *Tlr9*$^{-/-}$ mice. (A) Atherogenic diet-fed *WT* mice showed a relatively higher proportion of large adipocytes (≥8000 μm^2; ~30%) in visceral WAT compared to chow-fed *WT* (Fig. 4.7A). (B) In atherogenic diet-fed *foz/foz* mice, large adipocytes were less than *WT* mice, and there was an important proportion of cells between 1000 and 5000 μm^2. (C) In atherogenic diet-fed *Tlr9*$^{-/-}$ mice, the proportion of large adipocytes were less than ~20%, and the majority of cells were between 1000 and 6000 μm^2 with an even distribution. (n=8/gp [10 sections per mouse]; H&E-staining, 160x magnification)

As reviewed in Section 1.5, hypoxia, oxidative stress and lipid engorgement are associated with ultrastructural abnormalities in large adipocytes. These cells later shrink by release of FA and cholesterol, and degenerate by activation of programmed cell death pathways (necro-apoptotic or pyroptotic mechanisms; see Section 1.5.6). In this Section, data exploring the possible pathways for "degeneration" of adipocytes and their role in adipose inflammatory recruitment will be presented.

Hif1α mRNA expression did not change by genotype (*foz/foz* or *Tlr9*$^{-/-}$ vs. *WT*) in visceral WAT (Fig. 4.9A). However, vascular cell adhesion protein 1 (*Vcam1*) mRNA was increased in atherogenic diet-fed *foz/foz* visceral WAT compared to *WT* mice; *Tlr9* deletion did not alter *Vcam1* mRNA expression compared to *WT* mice (Fig. 4.9B). Compared to atherogenic diet-fed *WT* mice, catalase, mitochondrial *Sod2* and extracellular *Sod3* WAT mRNA levels were decreased in atherogenic diet-fed *foz/foz*, indicating the likely occurrence of chronic oxidative stress in these animals (Fig. 4.9C-E). Moreover, nuclear factor [erythroid-derived] 2-like 2 (*Nfe2l2*) mRNA levels

increased in atherogenic diet-fed *foz/foz* vs. *WT* mice, further supporting the operation of chronic oxidative stress (Fig. 4.9F). Unlike *foz/foz* mice, *Tlr9*$^{-/-}$ mice showed little evidence of WAT oxidative stress; only *Sod2* mRNA levels were significantly less than *WT*, and *Nfe2l2* mRNA was clearly not increased.

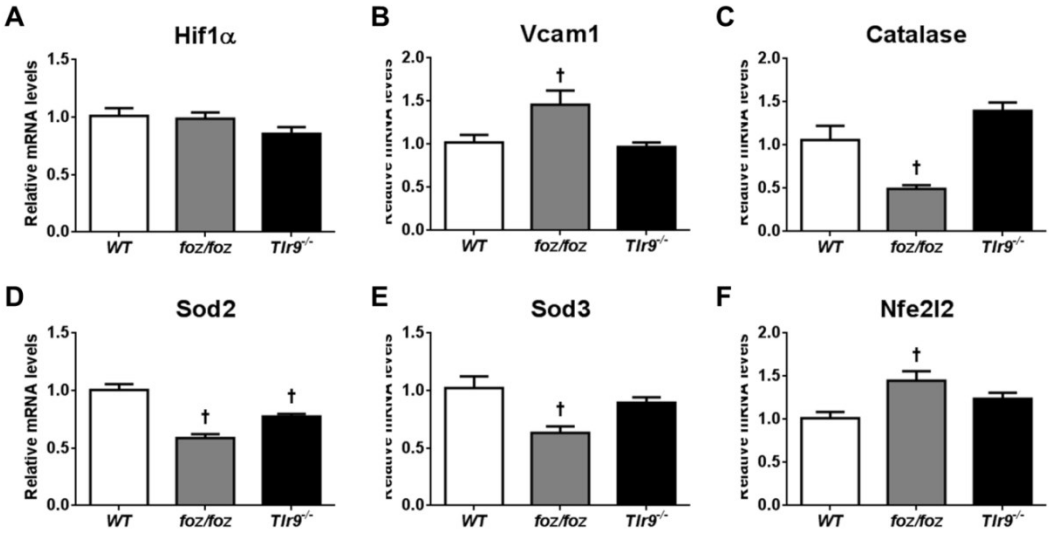

Figure 4.9: Visceral WAT mRNA expression levels for genes related to oxidative stress in atherogenic diet-fed mice. Data are mean ± SEM (n=8/gp). Values are expressed relative to *WT*, which is set at 1.0.
† *P*<0.05 vs. *WT* control (genotype effect); e.g., atherogenic diet-fed *foz/foz* vs. *WT*

C/EBP homologous protein (*Chop*) is a transcription factor that induces programmed (apoptotic) cell death in response to ER stress. There was no difference in *Chop* mRNA levels between groups (Fig. 4.10A). mRNA expression of the necroptosis (see Section 1.5.6) marker *Mklk* was decreased in *foz/foz* mice vs. *WT* (Fig. 4.10B). Compared to *WT* mice, programmed necrosis marker *Rip1* showed a decreasing trend (not significant), and *Rip3* was significantly increased in visceral WAT of *foz/foz* mice (Fig. 4.10B-D). *Tlr9* deletion did not affect WAT mRNA expression in any of these markers compared to *WT* (Fig. 4.10A-D).

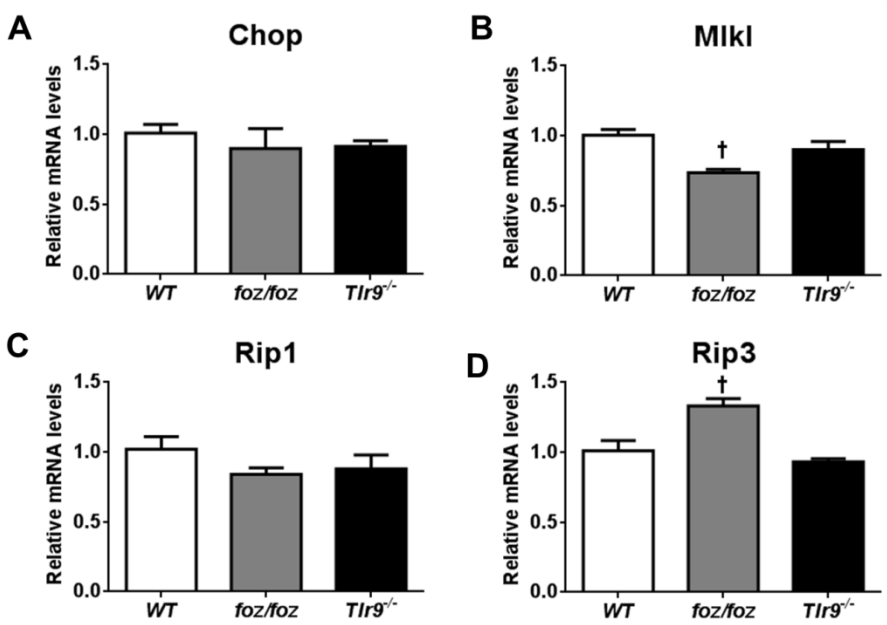

Figure 4.10: Visceral WAT mRNA expression levels for genes related to apoptosis, necroptosis, and necrosis in atherogenic diet-fed mice. Data are mean ± SEM (n=8). Values are expressed relative to *WT*, which is set at 1.0.
† $P<0.05$ vs. *WT* control (genotype effect); e.g., atherogenic diet-fed *foz/foz* vs. *WT*

As mentioned in the Introduction, interpreting the distribution of adipocytes by size can be misleading because adipocytes with the similar size can display different phenotypes. The percentage of small degenerating adipocytes in the centre of a CLS (see Fig. 4.15A for such small adipocytes) was 5% in atherogenic diet-fed *WT* mice visceral WAT (Fig. 4.11A). There was a major increase in this ratio, to 29%, in *foz/foz* mice (Fig. 4.11B), whereas it was only 1% in *Tlr9*$^{-/-}$ visceral WAT (Fig. 4.11C).

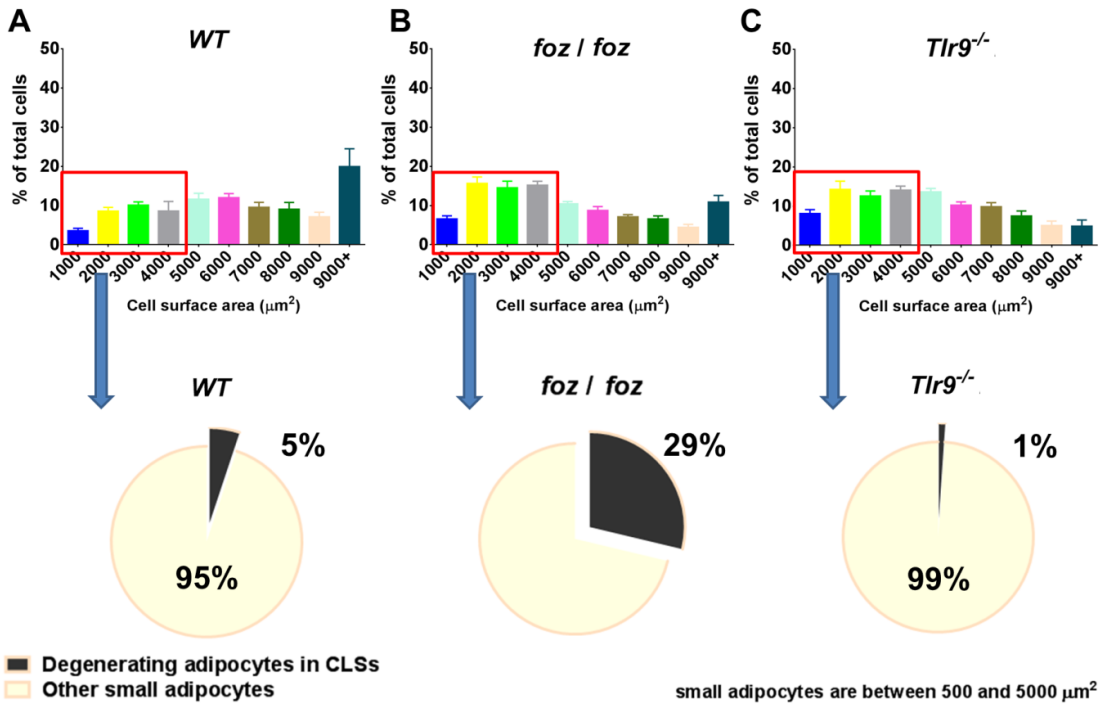

Figure 4.11: Quantification of small degenerating adipocytes in atherogenic diet-fed *WT*, *foz/foz* and *Tlr9*$^{-/-}$ visceral WATs. (A) Degenerating small adipocytes, located in the centre of a CLS (illustrated in Fig. 4.15A), were 5% of total small adipocytes (≤ 4000 μm^2) in atherogenic diet-fed *WT*, (B) 29% in *foz/foz*, and (C) only 1% in *Tlr9*$^{-/-}$ mouse visceral WAT (C). (n=8/gp [10 sections per mouse]; H&E-staining, 160x magnification)

4.4.4 TLR9 Expression and Inflammatory Recruitment in Adipose Tissue

Almost all cell types can express TLRs, but their response to TLR activation may vary. As reviewed in Section 4.1, different adipose tissue components can express TLR9. Thus some large adipocytes can display a pro-inflammatory phenotype, but the role of TLRs in this phenotypic switch has not been fully characterized. In the present study, transcript expression of TLR9 and some other TLRs and signalling molecules were measured in visceral adipose tissue and its cellular components.

As described in Section 4.1, TLR9 recognizes oligonucleotides (ssDNA fragments) from necrotic cellular debris, whereas TLR3 recognizes dsRNA and TLR4 recognizes LPS. There were increased amounts of *Tlr9* mRNA in the visceral WAT of atherogenic diet-fed *foz/foz* mice vs. *WT* (Fig. 4.12A). As expected (by definition), *Tlr9* mRNA expression was virtually absent in visceral WAT of atherogenic diet-fed *Tlr9*$^{-/-}$ mice. On the other hand, *Tlr3* mRNA expression was higher in visceral WAT of atherogenic diet-

fed *Tlr9*$^{-/-}$ compared to *WT* mice (Fig. 4.12B). There were no significant changes in *Tlr4* mRNA between any of the groups (Fig. 4.12C). There was a possible increase in *Trif* mRNA in atherogenic diet-fed *foz/foz* mice visceral WAT (not significant) (Fig. 4.12D), but *MyD88* mRNA levels were clearly similar in all genotypes (Fig. 4.12E).

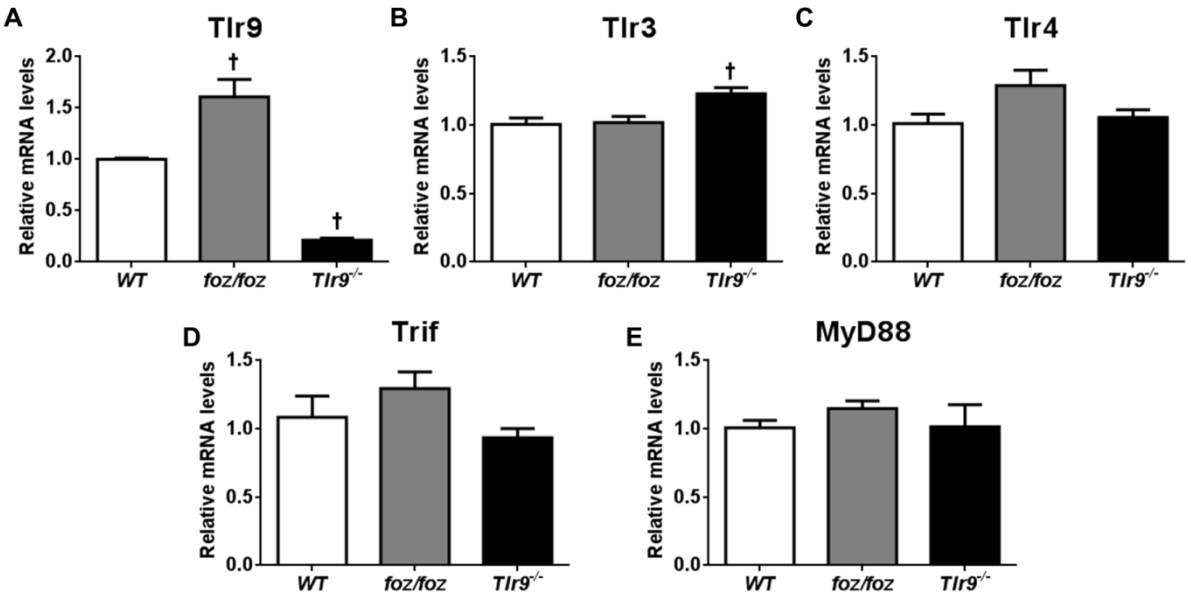

Figure 4.12: Visceral WAT mRNA expression of *Tlr9*, *Tlr3*, and *Tlr4* as well as their adapter proteins, *Trif* and *MyD88*, in atherogenic diet-fed mice. Data are mean ± SEM (n=8/gp). Values are expressed relative to *WT*, which is set at 1.0.
† *P*<0.05 vs. *WT* control (genotype effect); e.g., atherogenic diet-fed *foz/foz* vs. *WT*

The increase in *Tlr9* mRNA expression would be consistent with increased TLR9 protein levels in inflamed adipose tissue. To establish whether this is the case and to identify the cell type(s) responsible, we performed flow cytometry of mature adipocytes (Nile Red dye) and macrophages (fluorescence-labelled F4/80 antibody). As described in Section 2.3.3, cell solutions were prepared from a cohort of atherogenic diet-fed *foz/foz* mice (identical to the cohort of *foz/foz* mice studies for other read-outs). These preliminary data show that the number of TLR9-expressing adipocytes was low (~5%) in these three independent adipocyte samples (Fig. 4.13).

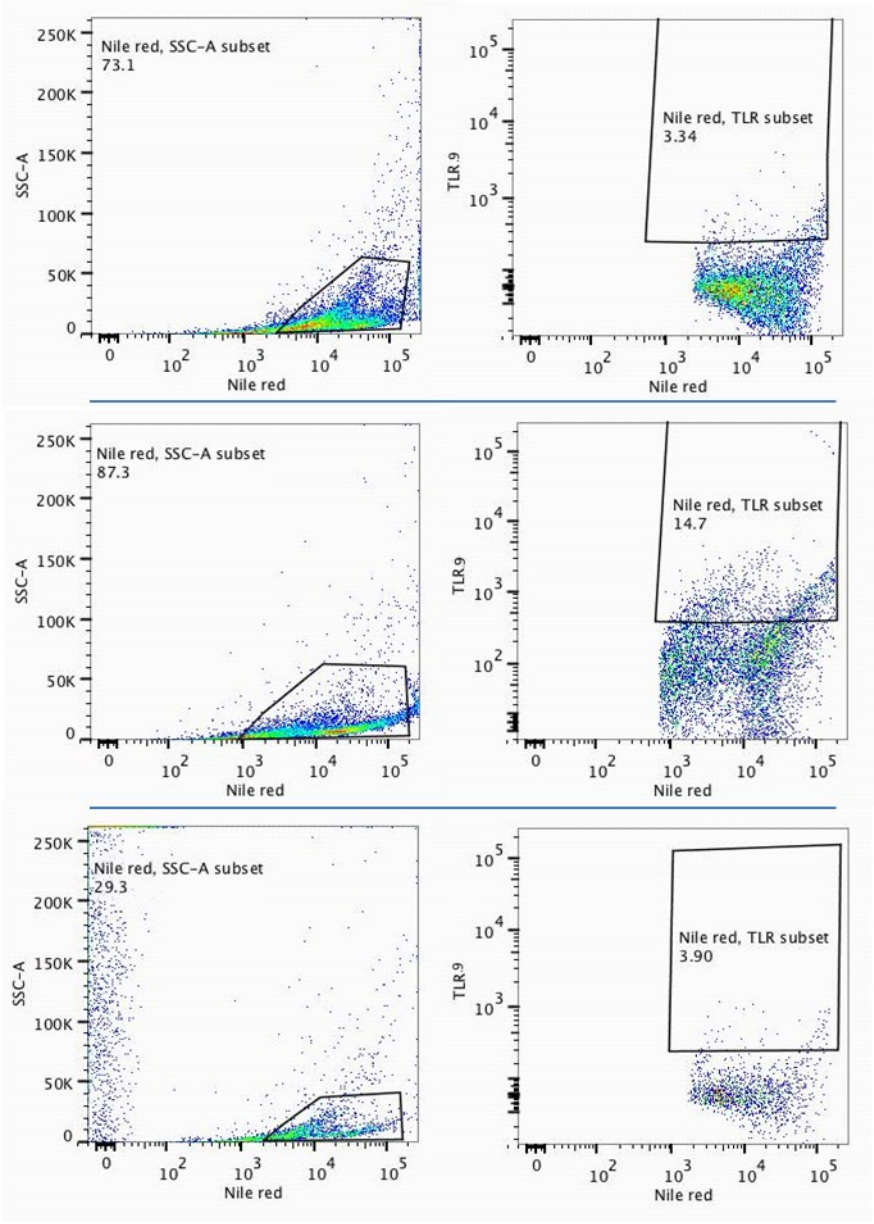

Figure 4.13: TLR9 expression in mature adipocytes from visceral WAT of atherogenic diet-fed *foz/foz* mice. Flow cytometry analysis showed that lipid-filled, mature adipocytes from visceral WAT (stained with Nile red) showed little, if any, *bona fide* expression of TLR9 protein. (SSC [side-scattered light] for single cell stream)

The same adipose tissues and a fourth sample were analysed for macrophage expression of TLR9 using a similar flow cytometry protocol. In this experiment, SVF cells were separated from adipocytes by the method outlined in Section 2.3.3. As mentioned in Section 1.5.6, pro-inflammatory (M1) macrophages express F4/80 protein on their extracellular surface. We therefore consider F4/80 to be a relevant marker to

identify macrophages in inflamed adipose tissue. Preliminary analyses of visceral WAT SVFs showed high levels of TLR9 expression on F4/80 positive cells. Accordingly, ~21 - 38% of SVF cells displayed both F4/80 and TLR9 expression (Fig. 4.14). In all, TLR9 expression levels were 4-8-fold greater in F4/80 positive macrophages than in Nile Red-stained adipocytes from visceral WAT of atherogenic diet-fed *foz/foz* mice.

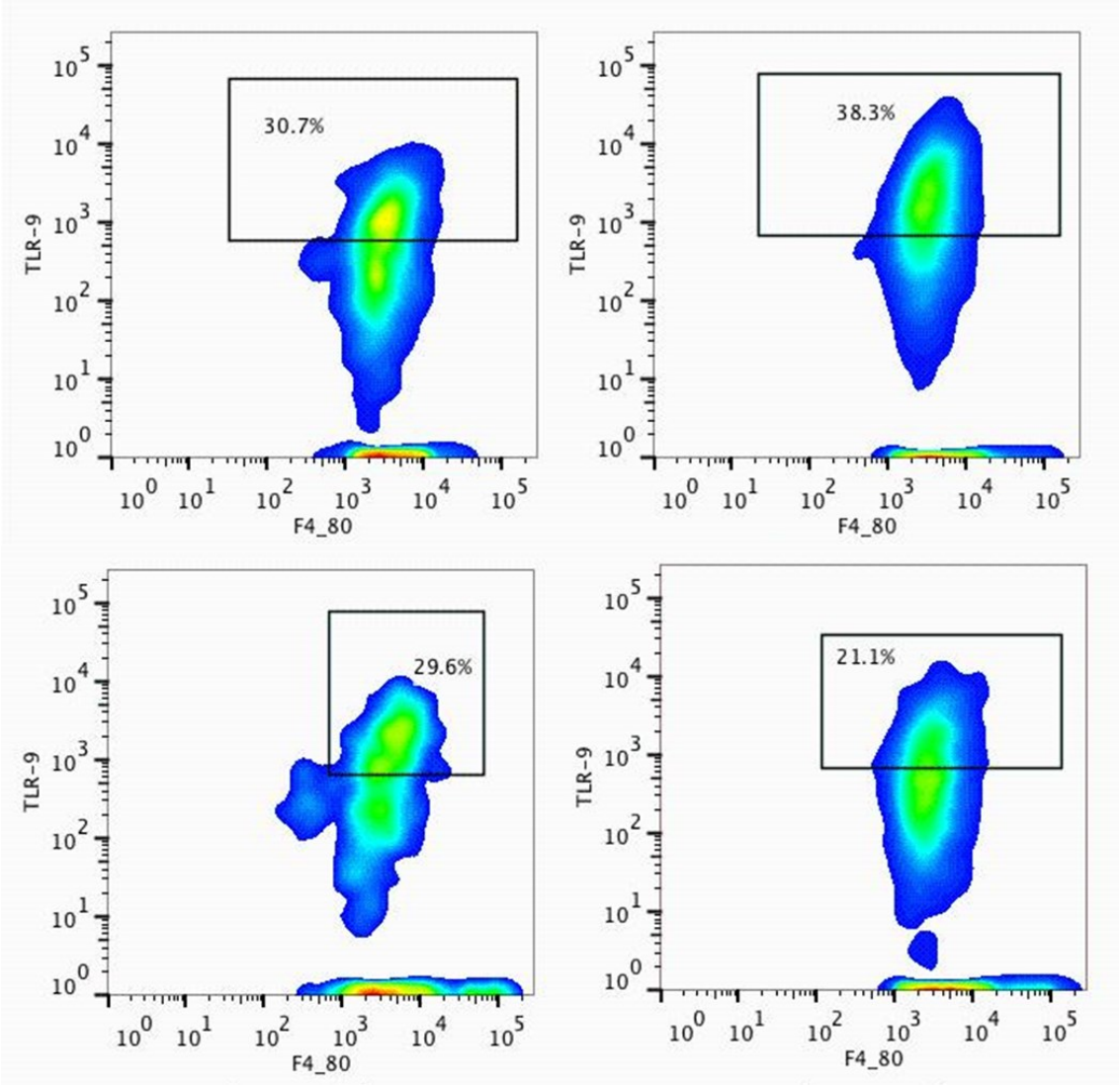

Figure 4.14: F4/80 and TLR9 co-expression in stromal vascular cells from visceral WAT of atherogenic diet-fed *foz/foz* mice. Visceral WAT stromal vascular cells expressing pro-inflammatory marker, F4/80, also often expressed TLR9 protein (~21 – 38% of all cells).

One of main hypotheses of this PhD study is that degenerating adipocytes (which are small) attract inflammation into adipose tissue. As mentioned in Section 1.5, 90% of pro-inflammatory macrophages localize around such small adipocytes (Fig. 4.15A).

Accordingly, we measured the number of visceral WAT CLSs. The number of CLSs in visceral WAT increased slightly with atherogenic dietary feeding in *WT* mice (Fig. 4.15B,C), but *Tlr9*$^{-/-}$ mice were protected from the formation of CLS, even during intake of an atherogenic diet. In *foz/foz* mice, CLS recruitment already seemed evident on chow diet (not significant vs. *WT*), and the number of sites of inflammation (such as shown in Fig. 4.13A) was significantly higher in atherogenic diet-fed *foz/foz* mice visceral WAT compared to diet- or genotype-matched counterparts (Fig. 4.15B,C).

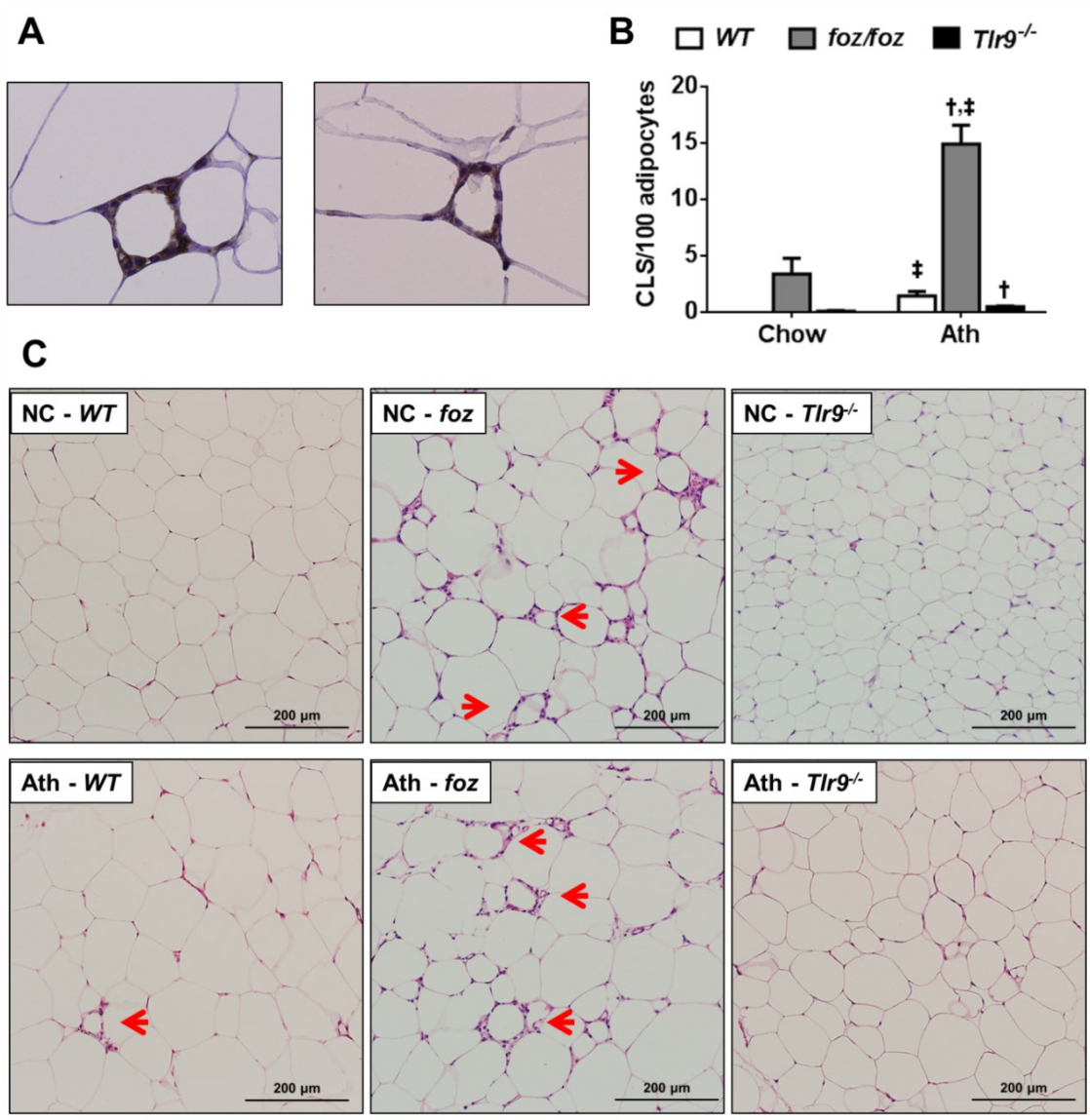

Figure 4.15: Number of CLSs in visceral WAT from *WT*, *foz/foz* and *Tlr9*$^{-/-}$ mice fed NC or Ath. (A) Numerous mononuclear inflammatory cells, abutting degenerating adipocytes to form CLSs, are illustrated. (B,C) Such CLSs were abundant in *foz/foz* mice, especially with atherogenic diet (n=8/gp [10 sections per mouse]; H&E-staining, 160x magnification). The number of CLSs was small in atherogenic diet-fed *WT* mice, and they were virtually absent in atherogenic diet-fed *Tlr9*$^{-/-}$ visceral WAT.
Data are mean ± SEM (n=8/gp).
† $P<0.05$ vs. diet-matched *WT* (genotype effect); e.g., chow-fed *foz/foz* vs. *WT*
‡ $P<0.05$ vs. genotype-matched control (diet effect); e.g., atherogenic diet-fed vs. chow-fed *WT*

As stated in Section 4.1, IFNγ and RANTES contribute to adipose inflammatory recruitment. In the present study, *Ifn*γ and *Rantes* mRNA expression were both high in visceral WAT of atherogenic diet-fed *foz/foz* (not significant for *Ifn*γ) compared to *WT* mice (Fig. 4.16A,B), with no changes in *Tlr9*$^{-/-}$ mice. *Ip10* mRNA expression appeared to be higher (not significant) in atherogenic diet-fed *foz/foz* mouse visceral WAT

compared to *WT* (Fig. 4.16C), with no difference for *WT* and *Tlr9*$^{-/-}$ mice. Compared to *WT*, there was no significant increase of *Mcp1* mRNA in visceral WAT of atherogenic diet-fed *foz/foz* mice, but *Tlr9*$^{-/-}$ mice exhibited less *Mcp1* mRNA than *WT* (Fig. 4.16D). There were no genotype differences in visceral WAT Chemerin mRNA expression (Fig. 4.16E).

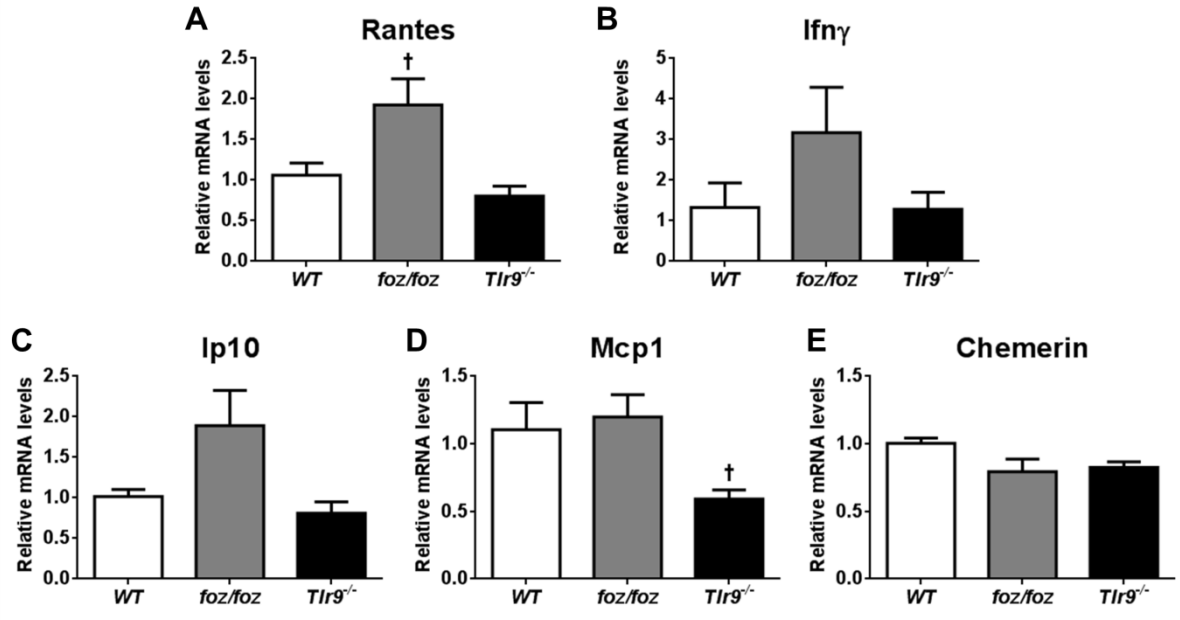

Figure 4.16: Visceral WAT mRNA expression levels for genes related to macrophage chemotaxis in atherogenic diet-fed mice. Data are mean ± SEM (n=8/gp). Values are expressed relative to *WT*, which is set at 1.0.
† $P<0.05$ vs. *WT* control (genotype effect); e.g., atherogenic diet-fed *foz/foz* vs. *WT*

As mentioned in Section 1.5.6, CD11b is an important pro-inflammatory (M1) macrophage marker (318). In the present study, *Cd11b* mRNA levels were significantly higher in atherogenic diet-fed *foz/foz* visceral WAT than *WT* mice (Fig. 4.17A). *Tlr9* deletion did not alter *Cd11b* mRNA expression levels. *Cd11c*, a marker of both macrophages and DCs (319), was increased in *foz/foz* mouse visceral WAT (Fig. 4.17B). Consistent with the vanishingly small number of recruited CLSs, *Cd11c* mRNA levels were very low in *Tlr9*$^{-/-}$ mice visceral WAT compared to *WT*. There seemed to be an increase in *Icam* mRNA in atherogenic diet-fed *foz/foz* mice visceral WAT, but this

was not significant compared to *WT* mice (Fig. 4.17C). In contrast, *Tlr9*$^{-/-}$ mice had significantly less *Icam* mRNA in visceral WAT in comparison to *WT*.

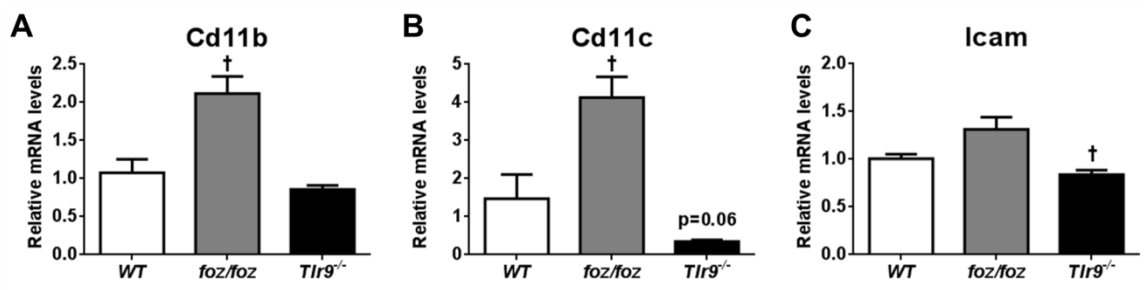

Figure 4.17: Visceral WAT mRNA expression levels for genes related to pro-inflammatory macrophage infiltration into adipose in atherogenic diet-fed mice. Data are mean ± SEM (n=8/gp). Values are expressed relative to *WT*, which is set at 1.0.
† $P<0.05$ vs. *WT* control (genotype effect); e.g., atherogenic diet-fed *foz/foz* vs. *WT*

4.4.5 Are Bone Marrow-Derived Cells Bearing TLR9 Essential for Adipose Inflammation?

As explained in Section 1.2, adipose tissue cells derive from BM. Bearing this in mind, manipulation of BM could provide insights into the function of TLR9 signalling for inflammatory recruitment into adipose tissue. Accordingly, we established cohorts of irradiated *Tlr9*$^{-/-}$ and *WT* mice with BM isolated from *WT* or *Tlr9*$^{-/-}$ mice to create chimeric mice. The detailed protocol for these experiments is given in Section 2.1.6. We anticipated that over 90% of the host BM cells would come from injected cells after total body irradiation (this has been verified in other work from the host lab).

WT mice with *WT* BM cells had the highest expression of *Tlr9* mRNA in visceral WAT (Fig. 4.18A). In *Tlr9*$^{-/-}$ mice with *WT* BM cells, *Tlr9* mRNA expression appeared somewhat less, but this was not a significant difference. Strikingly, both *Tlr9*$^{-/-}$ and *WT* mice transplanted with *Tlr9*$^{-/-}$ BM cells expressed almost no *Tlr9* mRNA in visceral WAT. To establish the specifity of this decrease in TLR9, we also measured visceral WAT *Tlr4* mRNA levels. As expected, there was no significant difference in visceral WAT *Tlr4* mRNA level between groups (Fig. 4.18B).

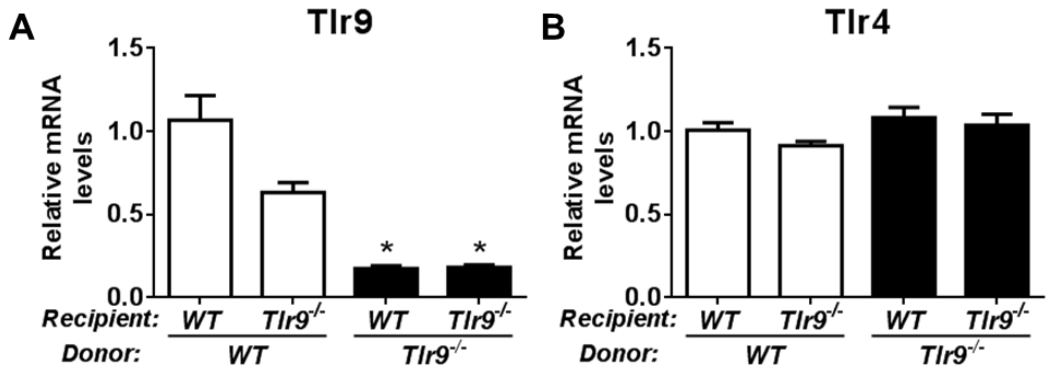

Figure 4.18: Expression levels for *Tlr9* and *Tlr4* mRNA in visceral WAT of BM chimeric mice. (A) Visceral WAT *Tlr9* mRNA expression was the highest in *WT* mice with *WT* BM cells, whereas mice with *Tlr9*$^{-/-}$ BM cells showed almost no *Tlr9* mRNA expression. (B) *Tlr4* mRNA expression was similar in all groups.
Data are mean ± SEM (n=8-9/gp).
**P*<0.05 vs. *WT* mice transplanted with *WT* BM cells.

Presumably because of the challenging effects of total body irradiation (and the subsequent antibiotic treatment), none of the mouse groups gained weight during 14 weeks of atherogenic dietary feeding (Fig. 4.19A). Likewise, there were non-significant reduction in visceral and subcutaneous WAT weights of *Tlr9*$^{-/-}$ mice compared with *WT* BM cells, and no changes in FBG between groups (Fig. 4.19B-D). Gastrocnemius muscle weight (though significantly more in atherogenic diet-fed *Tlr9*$^{-/-}$ mice with *WT* BM cells), serum cholesterol and serum alanine aminotransferase (ALT) levels did not vary importantly between groups (Fig. 4.19E-G). Interestingly, *Tlr9*$^{-/-}$ mice with *Tlr9*$^{-/-}$ BM cells showed increased levels of serum adiponectin compared to *WT* mice transplanted with *WT* BM cells (Fig. 4.19H).

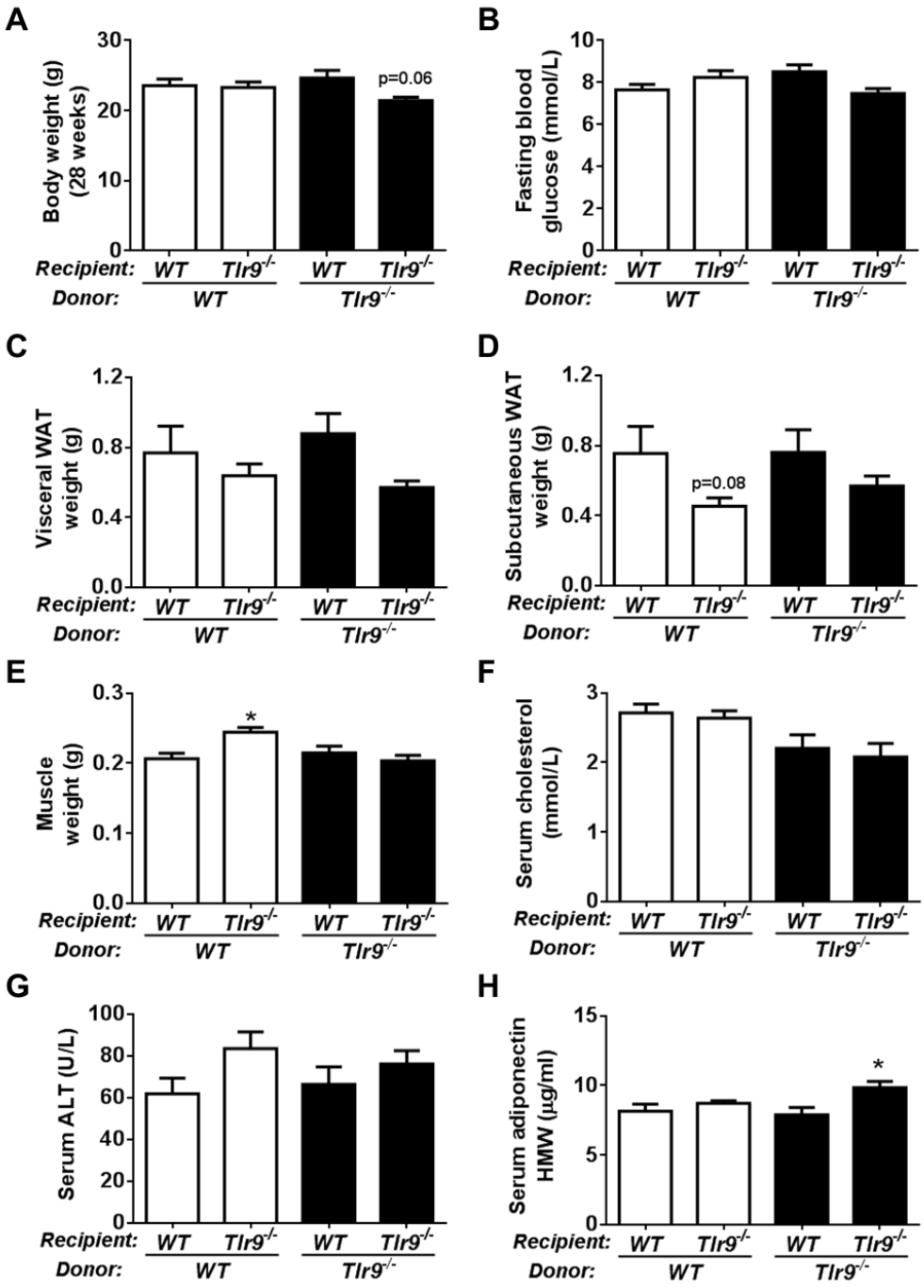

Figure 4.19: Physiological changes in BM chimeric mice transplanted with *Tlr9*$^{-/-}$ or *WT* BM cells. (A) No mice gained weight after 14 weeks of atherogenic dietary intake, while (B) fasting blood glucose, and (C,D) visceral and subcutaneous WAT weights did not vary between groups. (E) Gastrocnemius muscle mass was greater in atherogenic diet-fed *Tlr9*$^{-/-}$ mice with *WT* BM cells than other groups, (F,G) but there were no differences in serum cholesterol and ALT levels between groups. (H) Serum adiponectin was increased in *Tlr9*$^{-/-}$ mice transplanted with *Tlr9*$^{-/-}$ BM cells compared to *WT* mice with *WT* BM cells.
Data are mean ± SEM (n=8-9/gp).
*****$P<0.05$ vs. *WT* mice transplanted with *WT* BM cells.

Analysis of mRNA expression related to adipose function and inflammation did not suggest much change between groups. In a similar trend to serum adiponectin concentrations, *Tlr9*$^{-/-}$ mice with *Tlr9*$^{-/-}$ BM cells seemed to express increased levels of visceral WAT adiponectin mRNA, although this was not a significant increase compared to *WT* mice with *WT* BM (Fig. 4.20A). There was no difference between different groups in adipsin mRNA expression (Fig. 4.20B). Likewise, there was little variation in *Mcp1*, Chemerin, *Cd68* and *Cd11c* mRNA between groups (Fig. 4.20C-F).

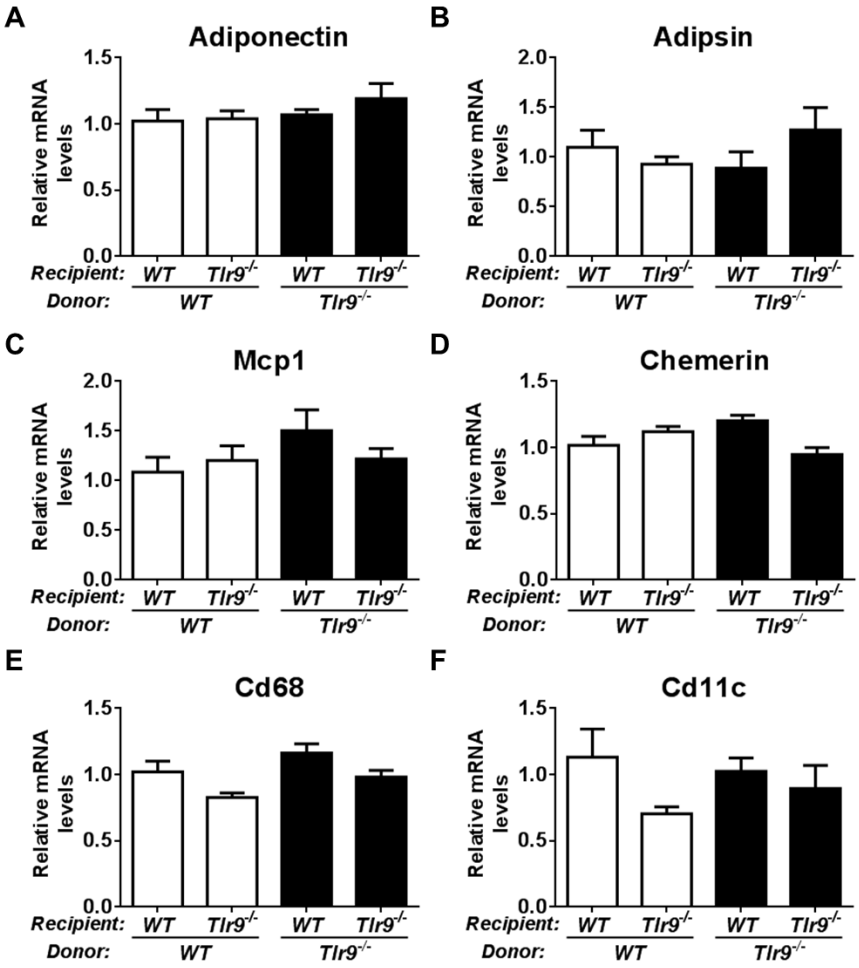

Figure 4.20: Visceral WAT mRNA expression levels of genes related to adipose function and inflammation in BM chimeric mice. (A,B) Adiponectin and adipsin mRNA levels were similar in all groups (the apparent increase in *Tlr9*$^{-/-}$ mice with *Tlr9*$^{-/-}$ BM was not significant). (C,D) There were no differences in *Mcp1* and Chemerin levels between groups. (E,F) Recipient *Tlr9*$^{-/-}$ mice, irrespective of the transplanted BM cells, appeared to express less *Cd68* and *Cd11c* mRNA in visceral WAT than *WT* mice with *WT* BM, but this trend was not significant.
Data are mean ± SEM (n=8-9/gp).
*****P<0.05 vs. *WT* mice transplanted with *WT* BM cells.

Serum MCP1 levels were decreased in *Tlr9*$^{-/-}$ mice with *Tlr9*$^{-/-}$ BM cells compared to *WT* mice with *WT* BM cells (Fig. 4.21A). Circulating serum TNFα was virtually absent in mice with *Tlr9*$^{-/-}$ BM cells irrespective of the host genotype (Fig. 4.21B). On the other hand, serum IL6 levels dependant on host genotype, so that only in *Tlr9*$^{-/-}$ mice with *Tlr9*$^{-/-}$ BM cells showed significantly lower serum IL6 than *WT* mice with *WT* BM (Fig. 4.21C).

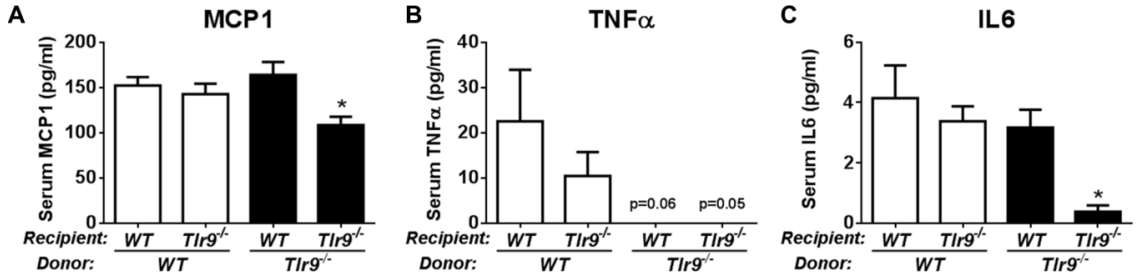

Figure 4.21: Circulating chemokine and cytokines pertinent to metabolic inflammatory responses in BM chimeric mice. (A) MCP1, (B) TNFα, and (C) IL6 levels were all reduced in *Tlr9*$^{-/-}$ mice transplanted with *Tlr9*$^{-/-}$ BM cells in comparison with *WT* mice with *WT* BM cells, whereas only TNFα levels were lower in *Tlr9*$^{-/-}$ mice with *WT* BM.
Data are mean ± SEM (n=8-9/gp).
**P*<0.05 vs. *WT* mice transplanted with *WT* BM cells.

4.4.6 Effects of Diet and Genotype on Fatty Liver Disease

All *foz/foz* mice developed hepatomegaly, and as shown earlier in the Chapter, atherogenic diet-fed *foz/foz* mouse livers weighed significantly more than chow-fed counterparts (Fig. 4.22A,B). By contrast, atherogenic dietary feeding did not cause a significant increase in liver weight of *WT* or *Tlr9*$^{-/-}$ mice.

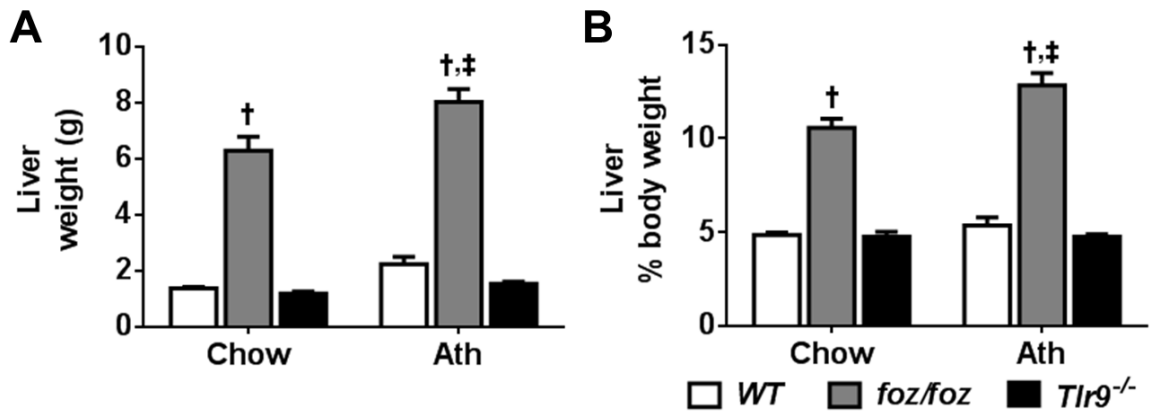

Figure 4.22: Effects of atherogenic dietary intake on liver weight in *WT*, *foz/foz* and *Tlr9*$^{-/-}$ mice. (A,B) *foz/foz* mice fed either diet developed hepatomegaly, whereas liver weights (absolute or relative) did not change in *WT* and *Tlr9*$^{-/-}$ mice after atherogenic dietary feeding. Data are mean ± SEM (n=6-14/gp).
† $P<0.05$ vs. diet-matched *WT* (genotype effect); e.g., chow-fed *foz/foz* vs. *WT*
‡ $P<0.05$ vs. genotype-matched control (diet effect); e.g., atherogenic diet-fed vs. chow-fed *WT*

Atherogenic dietary intake increased serum ALT levels in *foz/foz* mice compared to their chow-fed counterparts (Fig. 4.23A). A similar effect was found in *WT* and *Tlr9*$^{-/-}$ mice, but surprisingly, atherogenic diet-fed *Tlr9*$^{-/-}$ mice showed higher serum ALT than *WT* mice. Because TLR9 signalling seems to be important for sustaining gastrointestinal mucosal integrity, we also measured circulating endotoxin levels to search for an explanation for increased serum ALT in atherogenic diet-fed *Tlr9*$^{-/-}$ mice. Accordingly, atherogenic diet-fed *Tlr9*$^{-/-}$ mice had significantly higher circulating concentrations of endotoxin compared to chow-fed *Tlr9*$^{-/-}$ or atherogenic diet-fed *WT* mice (Fig. 4.23B).

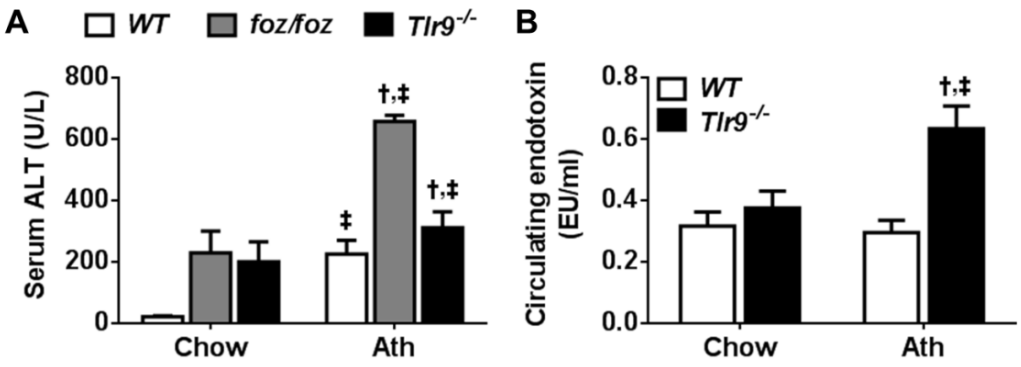

Figure 4.23: Serum ALT and circulating endotoxin levels in *WT*, *foz/foz*, and *Tlr9*$^{-/-}$ mice. (A) Atherogenic dietary intake significantly increased serum ALT levels in all mice. Surprisingly, atherogenic diet-fed *Tlr9*$^{-/-}$ mice showed higher serum ALT than their *WT* counterparts. (B) This increase was associated with an increased concentration of circulating endotoxin in atherogenic diet-fed *Tlr9*$^{-/-}$ mice in comparison with atherogenic diet-fed *WT* or chow-fed *Tlr9*$^{-/-}$ mice.
Data are mean ± SEM (n=6-14/gp).
† $P<0.05$ vs. diet-matched *WT* (genotype effect); e.g., chow-fed *foz/foz* vs. *WT*
‡ $P<0.05$ vs. genotype-matched control (diet effect); e.g., atherogenic diet-fed vs. chow-fed *WT*

Liver histology was assessed by the method outlined in Section 2.2.3. Among chow-fed mice, macro-steatosis was evident only in appetite dysregulated *foz/foz* mice. All mice fed an atherogenic diet developed moderate to severe macro-steatosis (Fig. 4.24A), but *Tlr9*$^{-/-}$ mice had less liver macro-steatosis than *WT*. Liver inflammation was highest in *foz/foz* mice, especially in those fed an atherogenic diet. It was strikingly less in *Tlr9*$^{-/-}$ mice compared to *WT* counterparts (Fig. 4.24B). *foz/foz* mice showed ballooned hepatocytes on either diet, but with atherogenic dietary intake, the number of ballooned hepatocytes was similar between genotypes (Fig. 4.24C). NAS showed that all *foz/foz* mice and atherogenic diet-fed *WT* mice developed definite or borderline NASH. Conversely, most *Tlr9*$^{-/-}$ mice exhibited mild NAFLD, indicating that they were protected from progression of steatosis to NASH (Fig. 4.24D).

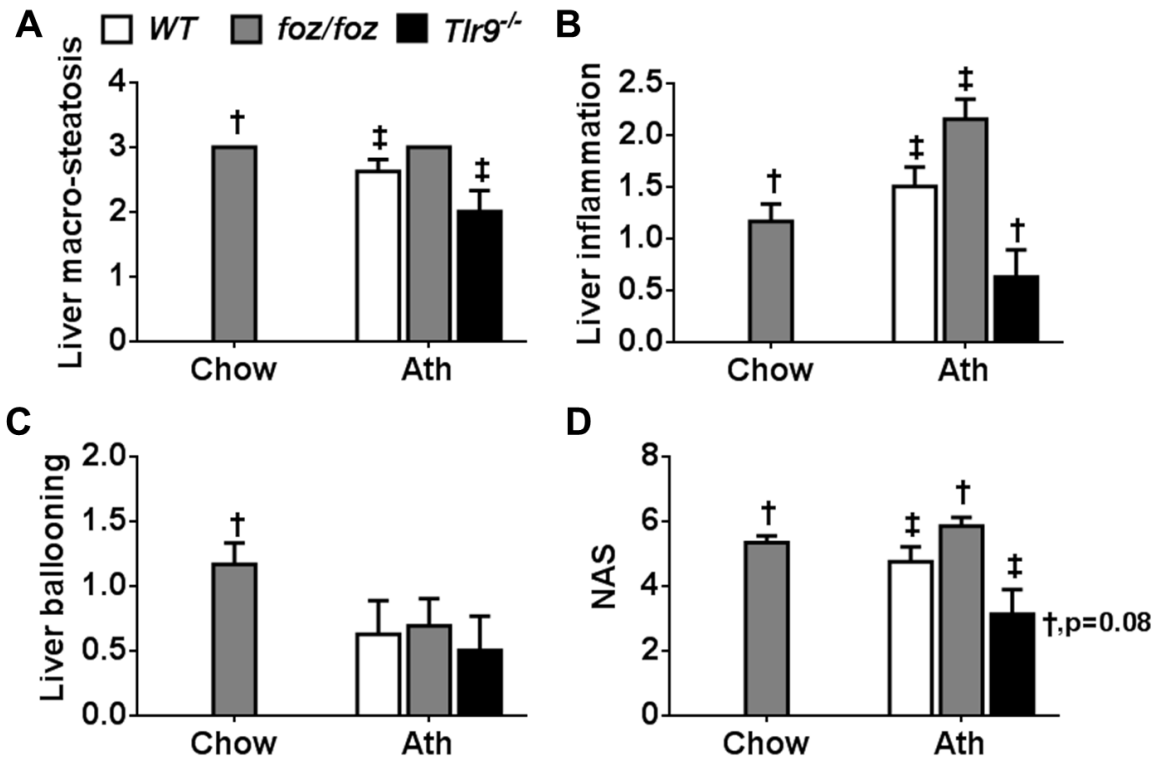

Figure 4.24: Effects of atherogenic dietary feeding on liver histology in *WT*, *foz/foz* and *Tlr9*$^{-/-}$ mice. H&E-stained liver sections were assessed blind by an expert liver pathologist (MMY) for: (A) macro-steatosis (0-3), (B) inflammatory score (0-3), and (C) ballooning score (0-2). (D) Data were compiled as the NAFLD activity score (NAS) (0-8). In chow-fed mice, all indices were significantly increased only in *foz/foz* mice. With atherogenic dietary intake, NAS increased more in *foz/foz* mice than in *WT* counterparts, whereas *Tlr9*$^{-/-}$ mice were protected from liver inflammation and NASH.
Data are mean ± SEM (n=6-14/gp).
† $P<0.05$ vs. diet-matched *WT* (genotype effect); e.g., chow-fed *foz/foz* vs. *WT*
‡ $P<0.05$ vs. genotype-matched control (diet effect); e.g., atherogenic diet-fed vs. chow-fed *WT*

4.5 Discussion

Until recently, the innate immune system was regarded as "non-specific" immunity, a rather unsophisticated part of the immune system. The discovery of TLRs changed this commonly-held belief. As stated in Section 4.1.3, a diverse range of TLR sub-types is expressed at varying levels on multiple cell types. These receptors can recognize a wide spectrum of DAMPs and PAMPs, and so activate an effective immune response via an overlapping range of different pro-inflammatory cascades. With this in mind, activation of TLRs on different cell types and tissues can result in different (relatively specific) tissue responses.

Despite there being 13 mouse TLR sub-types reported by researchers during the last 20 years, only TLR4 has been studied extensively for a putative role in adipose tissue inflammation. In the present study, we demonstrated by a range of complementary experimental approaches that TLR9 is a modulator of inflammatory recruitment into adipose tissue. In all, we believe that the data support the concept that adipose macrophages (and possibly some other immune cell types) recognize degenerating adipocytes via TLR9 signalling. The present studies also provide important details of adipose morphometry in relation to adipose inflammatory recruitment, particularly clarifying our entirely novel, important observation that small adipocytes may display different phenotypes ("good" or "bad") under varying circumstances of nutrient load.

The first new finding of the present study is that *Tlr9* mRNA was upregulated in inflamed visceral WAT sampled from mice under conditions of constant energy surplus. As shown in Figure 4.16, atherogenic diet-fed *foz/foz* mice exhibited over 1.5-fold increase of *Tlr9* mRNA in visceral WAT compared to their *WT* counterparts. An unexpected finding was that although almost virtually absent, there was detectable *Tlr9* mRNA in *Tlr9*$^{-/-}$ mice. As reviewed in Section 4.1.3, all TLRs are type I transmembrane proteins including a N-terminal leucine rich repeat (LRR) domain (where most of the structural variation occurs), a cysteine rich domain, a transmembrane domain, and an intracellular TIR domain. Although qPCR primers were designed carefully for mRNA detection experiments, some non-specific amplification may have occurred due to sequential similarities among TLRs. Accordingly, it seems likely that the minor appearance of *Tlr9* mRNA expression in *Tlr9*$^{-/-}$ mice reflected the margin of error in the assay, rather than any failure of complete genetic deletion of *Tlr9*.

The observed upregulation of *Tlr9* mRNA in inflamed WAT raises another issue: is it adipocytes or macrophages that express TLR9? In order to answer this question, we conducted flow cytometry so as to discriminate mature adipocytes vs. cells in the

adipose tissue SVF. For detection of mature adipocytes, we used Nile Red dye which stains intracellular neutral lipids (e.g., TAGs, CEs). According to the Immunological Genome Project website (immune cell database), perhaps the most relevant read-out for pro-inflammatory macrophage detection is F4/80, with very low chance of cross-reactivity with DCs or other cell types (402). We therefore used fluorescence-labelled F4/80 antibody to allow us to discriminate pro-inflammatory macrophages.

Several technical challenges for the conduct of this experiment included: formation of a foam-like solution of mature adipocytes, few cells from hyperplastic tissues, high lipid contamination, and high cell death. These difficulties mandated tight time limits for conduct of the experiments, which in turn were lengthy. For these reasons, we could not establish a full set of data from each mouse cohort. Nonetheless, our preliminary data indicate that in mice with constant energy surplus (atherogenic diet-fed *foz/foz* mice), visceral WAT contains a considerable number (~20%) of TLR9-expressing F4/80^{+} macrophages. On the other hand, a much smaller proportion of Nile Red-positive mature adipocytes showed expression of TLR9 (only ~5%). As discussed in Section 1.5.5, there is strong evidence that preadipocytes and monocytes may also express TLR9, and future investigations are required to establish if these cell types also contribute to adipose tissue TLR9 expression.

As shown in Section 4.4.5, irradiated *WT* mice transplanted with *Tlr9*$^{-/-}$ BM cells did not express *Tlr9* mRNA in visceral WAT. In other words, BM macrophages are vital for adipose inflammatory recruitment. This unambiguous finding identifies BM cells as the main source of adipose tissue macrophages. However, since total body irradiation (presumably) kills all SVF cells in adipose tissue, it is hard to clarify the likely contribution of adipose tissue-resident cells (e.g., preadipocytes, regulatory macrophages) to TLR9 expression as opposed to the dynamic role of inflammatory recruitment into adipose tissue.

While we favour the interpretation that the present data support a concept whereby macrophages enter adipose tissue to initiate and sustain the WAT inflammatory response, it remains unclear which factors drive such macrophage infiltration. The relatively high expression of TLR9 in these macrophages could reflect occurrence of DAMPs in over-expanded adipose tissues. As opposed to this idea, traditional view focuses on the role of hypertrophic large adipocytes which display a pro-inflammatory phenotype (289), thereby contributing to adipose inflammatory recruitment. However, the existence of hypertrophic adipocytes may not be enough to establish adipose tissue inflammation, and the following lines of argument support this concept.

As shown in Fig. 4.3A, atherogenic diet-fed *WT* and *foz/foz* mice showed relatively similar visceral WAT mass (~2.3 vs ~2.5 g). On the other hand, Fig. 4.8 shows that in visceral WAT of atherogenic diet-fed *WT* mice, ~40% proportion of adipocytes are larger than 8000 μm^2, whereas this proportion was only ~25% for diet-matched *foz/foz*. In light of these data, *WT* mice fed an atherogenic diet bear ~1.5 time higher number of hypertrophic large adipocytes in visceral WAT than *foz/foz* mice. Further, as shown in Fig. 4.4, adipogenic markers indicate that adipose tissue is better functioning in atherogenic diet-fed *WT* mice than in *foz/foz*. Moreover, the data in Fig. 4.8 imply increased chronic oxidative stress in *foz/foz* vs. *WT* mice. If atherogenic diet-fed *WT* mice carry greater number of hypertrophic large adipocytes in visceral WAT, how can *foz/foz* WAT be less healthy? We believe that the answer to this question is revealed by the cell death results shown in Fig. 4.10; nevertheless, this question will be subjected to further investigation as a future direction.

As discussed in Section 1.5.6.3, RIP3 expression is directly related to necroptosis, a form of programmed cell death that incorporates features of apoptosis and necrosis. In the present study, the visceral WAT of *foz/foz* mice exhibited significantly increased expression of *Rip3* mRNA compared to *WT* (Fig. 4.10D). In concordance with this

finding, the number of small adipocytes in the centre of a CLS was markedly higher in *foz/foz* mice. Presumably, these small (and possibly degenerating) adipocytes are in process of dying of necroptosis or pyroptosis (see Section 1.5.6). Thus, we believe that these small degenerating adipocytes are likely the source of DAMPs in inflamed adipose tissues. Consistent with this proposition of the existence of increased stress signals in visceral WAT of atherogenic diet-fed *foz/foz* mice. Unfortunately, to date we have not yet shown expression of these increased cellular stress and death markers in CLS-centred small adipocytes, and this will be a major new direction for these studies.

In addition to the increased number of small adipocytes in the centre of a CLS, *foz/foz* mouse visceral WATs exhibited strikingly less adiponectin expression compared to *WT* (Fig. 4.5A,B). As overviewed in Section 1.5.4, adiponectin is an important anti-inflammatory protein expressed specifically by adipocytes (282, 283). This adipose-derived hormone counters the activity of inflammatory factors, such as TNFα. It also has paracrine insulin-sensitizing and adipogenic effects in adipose tissues. Accordingly, adiponectin is mostly expressed by healthy, small and medium-sized adipocytes, and assists the maintenance of this this healthy phenotype (282). In the present study, adiponectin mRNA and protein expression were considerably less in WAT of *foz/foz* mice than *WT*. This reduction in tissue adiponectin levels could be mechanistically associated with the increase in stress signals and inflammatory recruitment in atherogenic diet-fed *foz/foz* mice, and this requires further study.

The possible interactions between different cell types in adipose inflammatory recruitment and the role of TLR9 are summarized in Fig. 4.26.

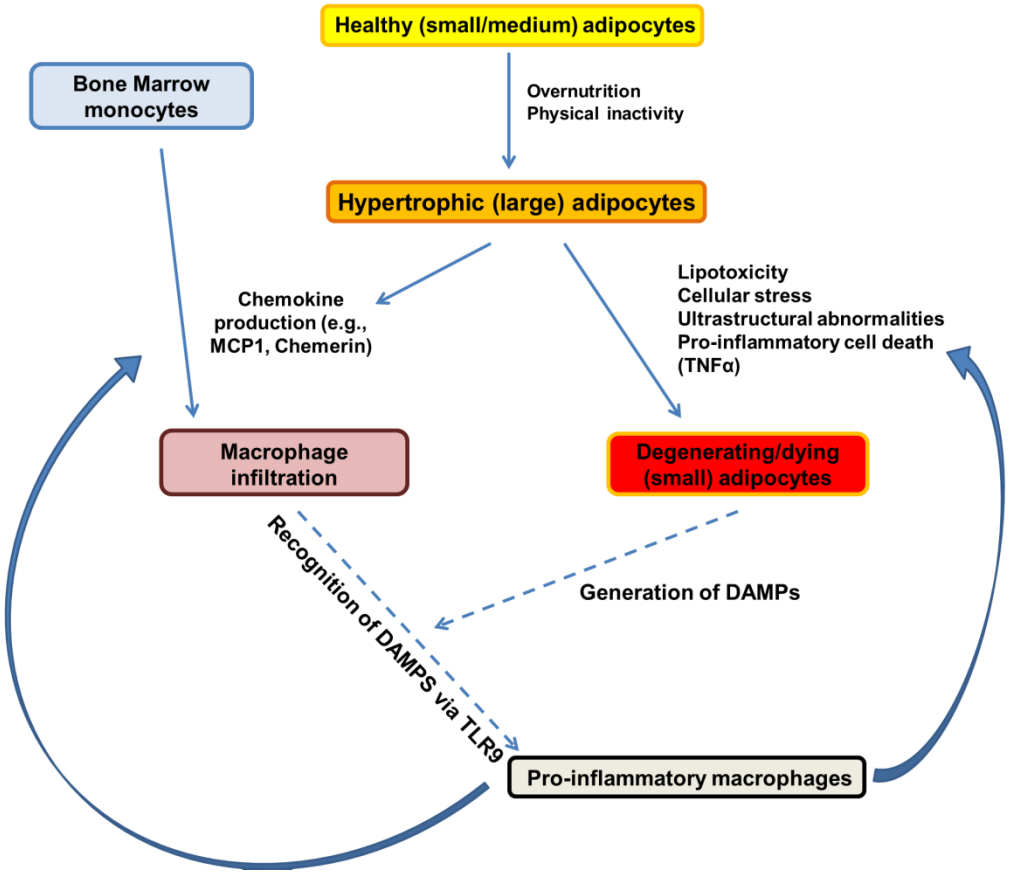

Figure 4.25: An overview on adipose inflammatory recruitment.

As mentioned in the Introduction, TLR4 was the first TLR discovered; therefore, it is the most investigated member of this immune receptor family. As overviewed in Section 1.5.3, abnormal release of FAs and cellular lipotoxicity may activate pro-inflammatory response via TLR4. In 2006, Hang Shi and her colleagues reported a possible link between TLR4 activity and adipose inflammatory recruitment (403). Accordingly, *Tlr4*$^{-/-}$ mice were partially protected from high fat diet-induced insulin resistance because there was reduced inflammatory gene expression in adipose tissue. In 2012, Rasheed Ahmad and his colleagues showed upregulation of TLR4 in WAT of obese individuals (404). As discussed in Section 1.5.3, persistent adipose stress and inflammation leads to fibrosis in WATs. In 2014, Isabelle Vila and her colleagues reported a possible association between increased TLR4 activation in adipose tissue, adipose inflammatory recruitment, and adipose tissue fibrosis (405).

Distortion of lipid droplets occurs in stressed degenerating adipocytes and as a result, these cells abnormally release FAs into the tissue microenvironment and circulation. Therefore, activation of TLR4 signalling is likely to be expected in inflamed adipose tissues. As listed in Section 1.5, chronic lipolysis in degenerating adipocytes is one example of many ultrastructural abnormalities in over-expanded WATs. Indeed, these findings support our concept that necrotic debris-derived DAMPs are primarily responsible for adipose inflammatory recruitment, and it would be incomplete to attribute the modulation of adipose tissue inflammation only on TLR4. In the present study, there was a slight increase of *Tlr4* mRNA (not significant) in visceral WAT of atherogenic diet-fed *foz/foz* mice (vs. WT). However, as shown in Fig. 4.12, the same *foz/foz* mice displayed significantly higher *Tlr9* mRNA expression compared to *WT* counterparts (Fig. 4.12). In summary, we believe TLR4 is unlikely to be the sole player for innate immune activation in metabolic obesity and TLR9 signalling is deserving of greater attention for its role in adipose inflammatory recruitment.

As shown before, all atherogenic diet-fed *foz/foz* mice develop NASH, as defined by NAS $\geq$ 5 (or 8) points (341). When fed the atherogenic diet, *WT* mice developed borderline (NAS 4,5) or established NASH (NAS > 5) whereas *Tlr9*$^{-/-}$ mice developed only simple steatosis (NAS < 4). The present data indicate that *Tlr9* deletion provides a hepato-protective effect against transition of simple steatosis to NASH. In particular, liver inflammation was markedly reduced in atherogenic diet-fed *Tlr9*$^{-/-}$ than in *WT* (or *foz/foz*) mice. However, it is less clear whether the hepato-protective effects of *Tlr9* deletion is attributable to improved adipose function or less WAT inflammation in these mice (i.e., a secondary effect), or whether it is a direct result of TLR9 absence in liver cells, such as Kupffer cells, other macrophages and hepatocytes (i.e., a direct effect). In balance, it seems likely that the less severe hepatic changes in *Tlr9*$^{-/-}$ mice than in *WT* are partly attributable to reduced weight gain and improved adipose function (and, in

turn, to less WAT inflammation), but we cannot exclude a direct effect of *Tlr9* deletion in liver cells of these mice. To resolve this issue, ***Tlr9*$^{-/-}$*.foz/foz*** mice have been created in the host lab by Vanessa Barn under supervision of Geoff Farrell, to overcome the challenge of providing a drive to eat in *Tlr9*$^{-/-}$ mice. In addition, future studies could employ an adipose-specific CRE recombinant strategy to create mice that show *Tlr9* deletion only in adipose tissues.

In summary, *Tlr9* mRNA is upregulated in inflamed visceral adipose tissue. Macrophages are the cell type most likely to explain this increase, although a few mature adipocytes seem to express TLR9. Atherogenic diet-fed *foz//foz* mice showed increased expression of cellular stress and programmed cell death markers in visceral WAT, and this increase is likely to be casually associated with the higher number of small degenerating or dead adipocytes in the centre of CLSs. Data from BM chimera mice support the conclusion that TLR9 on myeloid cells is required for inflammatory recruitment into adipose tissue. Presumably, these macrophages recognize and/or respond to unhealthy small adipocytes by TLR9 signalling. Investigation of cellular stress and death signals, particularly in small unhealthy adipocytes, poses a major target for future investigations, in addition to exploring TLR9 activity in the immune cells that form CLSs. Finally, inflamed dysfunctional adipose tissue and resultant hypoadiponectemia are associated with the worsening liver histology (transition of simple steatosis to NASH) in atherogenic diet-fed *foz/foz* mice. TLR9 provides a hepato-protective effect against transition of simple steatosis to NASH. Further research is required to establish whether this is an indirect result of improved adipose function or a direct result of *Tlr9* deletion in liver cells.

CHAPTER 5

CHAPTER 5: Effects of Obeticholic Acid on Macrophage Polarization in Metabolic Obesity

5.1 Introduction

A brief introduction about adipose tissue macrophages and their phenotypic polarization is given in Section 1.5. These phagocytic cells were discovered nearly 100 years ago, by Ilya Ilyich Mechnikov (406). His discovery started a new era (the innate immunity) in immunological sciences. Since then, macrophages have become appreciated as one of the most important "immune effector" cells. Even so, this appreciation should not allow the vital homeostatic roles of macrophages to be overlooked. During the last decade, macrophages have studied in a broader spectrum. In particular, it has been shown that tissue-resident, anti-inflammatory macrophages are as important as inflammatory macrophages. Finally, although metabolic obesity is often described as a low-grade inflammatory disorder, the factors that determine macrophage polarization in adipose tissue are still largely unknown.

5.1.1 Macrophages Display Great "Plasticity"

In the traditional view, macrophage phenotypes were established along a linear scale, with endpoints being M1 pro-inflammatory and M2 anti-inflammatory phenotypes (407). This classification was established in the years when T cell research was very popular, and immunologists tried to apply a similar classification system (cytotoxic T cells vs. helper T cells) to macrophages. M1 phenotype was somewhat convenient for macrophage classification (such cells secrete a Th1 profile of cytokines), but M2 macrophages showed greater structural and functional variety. Today, the classical linear phenotype scale has given way to a triangular system which includes 3 general

types of macrophages (Fig. 5.1): pro-inflammatory (classically-activated macrophages [C-AMs]), wound-healing, and regulatory (the latter two are both alternatively-activated macrophages [A-AMs]) (408, 409).

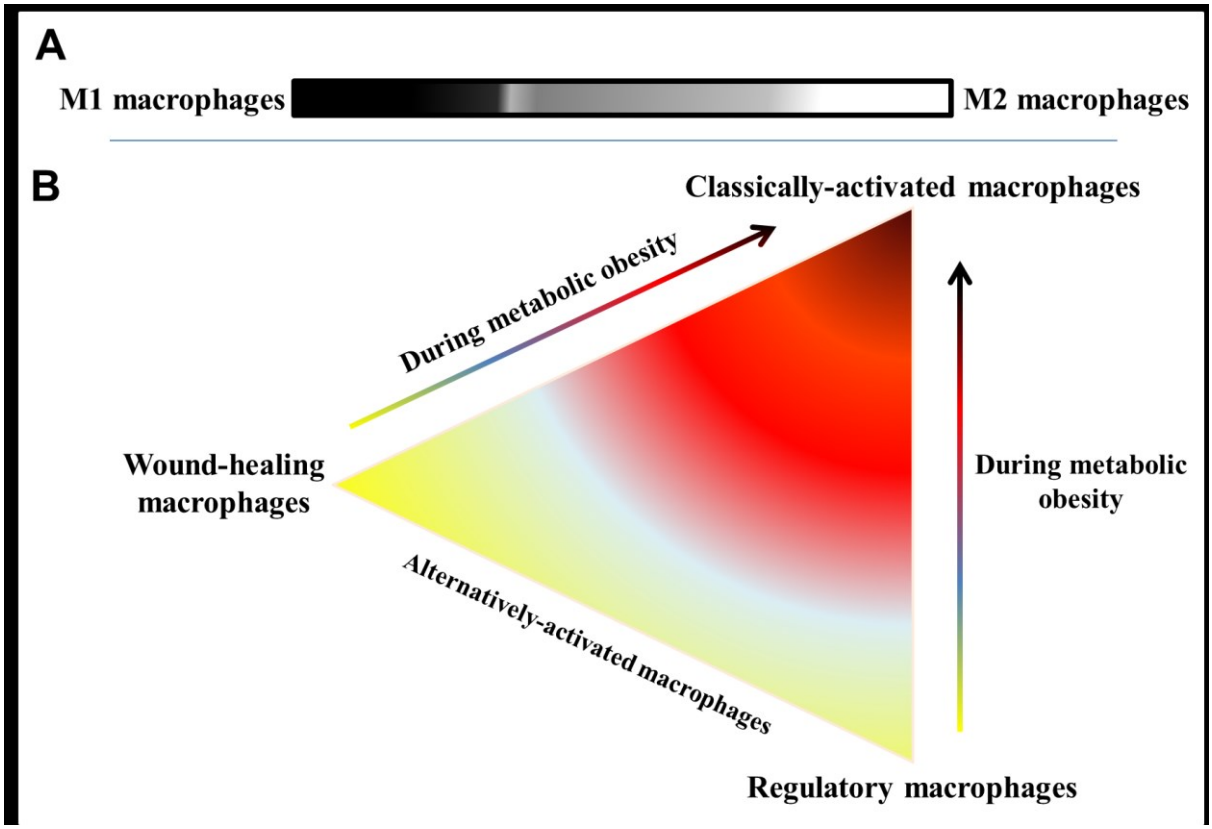

Figure 5.1: Macrophage polarization. (A) In the classical linear scale, macrophages exhibit either M1 pro-inflammatory or M2 anti-inflammatory phenotypes. (B) In the modern classification system, there are three dominant macrophage phenotypes, but there is great plasticity between phenotypes. Classical activation (pro-inflammatory [C-AM]) of wound-healing (alternatively-activated [A-AM]) macrophages is characteristic of obesity

Tissue specifity of macrophage subtypes allows a greater diversity of responses to environmental cues (410). In other words, macrophages can display different phenotypes depending on the tissue of residence. Accordingly, adipose tissue macrophages are different than Kupffer cells (liver macrophages) or microglia (central nervous system macrophages). These phenotypic variations confer optimization for recognition and degradation of pathogens or danger signals within those tissues. The findings indicate considerable "plasticity" of macrophages, by which they can exhibit

different functional and physiological/morphological properties in various environments and under varying circumstances.

5.1.2 Macrophage Phenotypes in Obesity: The Good, The Bad, and The Ugly

C-AMs are immune effector cells (408). They have higher phagocytosis capacity (microbicidal, tumoricidal, etc.) and can produce pro-inflammatory chemokines and cytokines (411). As discussed in Chapter 4, adipose macrophages can respond to endogenous danger signals. This can be related to cellular and tissue injury, as for TLR9, and the response to the signals causes physiological changes in macrophages. Moreover, macrophages can influence on their own physiology and phenotype in an autocrine fashion by producing several factors, such as TNFα (412, 413).

Two factors are essential to initiate an inflammatory response in macrophages: DAMP/PAMP induction and IFNγ production. IFNγ levels increase during tissue inflammation, but the exact mechanism is not clear (388). It has been reported that increasing leptin levels recruit natural killer T cells or CD8+ effector T cells (and possibly granulocytes) to adipose tissues; in turn, these cell types contribute to substantial IFNγ production (301, 414). Increasing IFNγ levels could possibly account for monocytic infiltration into adipose and also for macrophage polarization.

Adipose tissue resident macrophages exhibit an alternatively-activated anti-inflammatory phenotype (308, 415). Shiho Fujisaka and her colleagues showed that telmisartan, a PPARγ agonist, can selectively reduce C-AM marker expression in epididymal adipose tissue (416). However, it is not clear whether this effect was via PPARγ activation in adipocytes or a direct effect of telmisartan on macrophages, since the overall adipocyte size was also decreased in the treated group. In another study, researchers found a switch in polarization towards C-AMs in diet-induced obesity models (317). These C-AMs were found clustered in CLSs. They identified this

macrophage phenotypic alteration with the lipid spillage in adipose tissue which occurs during adipocyte degeneration. Accordingly, phagocytosis of lipids and lipotoxicity appear to transform macrophages into the classically-activated phenotype. This statement is true but incomplete, because lipid spillage and its clearance by macrophages is only one of many events that occur during extensive adiposity. There are likely to be other factors which facilitate pro-inflammatory transformation of macrophages during adipose inflammatory recruitment. As stated in Chapter 4, necrotic debris is a perfect example of DAMPs (fragmented DNA, other nucleotides, histones, mitochondrial products, etc.). Activation of TLR9 by these danger signals results in alterations of macrophage surface proteins.

Resident macrophages in adipose are not as "aggressive" as C-AMs. Adaptive signals can cause their "alternative" activation, and these changes/transformations allow macrophages to participate in homeostatic processes (415). For example, arginase 1 (AG1) producing macrophages contribute to ECM formation in order that macrophages promote wound-healing or tissue remodelling activity (417). However, as stated in Section 1.5.2.4, tissue remodelling occurs in adipose when ECM losses its integrity under hypoxic and pro-inflammatory circumstances (266, 267). With this in mind, identification of macrophages using only one single cell marker can be misleading. The expression of some markers can be persistent in macrophages; thus, these cells can display "hybrid" phenotypes. To overcome this challenge, macrophage phenotype profiling should be based on analysis of several factors. Antigen resistin-like molecule α (FIZZ1) and cluster of differentiation 163 (CD163) are other important A-AM markers (418, 419).

In obesity, the complexity of macrophage-mediated immunity in adipose tissues is considerable. In healthy adipose tissue, tissue resident macrophages exhibit a wound-healing phenotype. These cells express arginase, while pro-inflammatory markers such

as CD11b and TNFα are suppressed. PPARγ is important for regulation of these macrophages (420, 421). In obese individuals, these macrophages are classically-activated by DAMPs that arise from degenerating (necrotic) adipocytes, and peripheral blood mononuclear cells (monocytes/macrophages) migrate into adipose tissue in response to the pro-inflammatory signals.

As discussed in Section 4.5, adipose tissues develop fibrosis when there is persistent inflammatory recruitment. An interesting paradox is that adipose tissue fibrosis is mediated by macrophages that display wound-healing (ECM constructing) properties, but these macrophages actually show the A-AM phenotype. In all, the mechanisms for macrophage recruitment into adipose tissue that change healthy to unhealthy obesity remain largely unclear. Clarifying these provides potential to combat complications of obesity.

5.1.3 Activation of Farnesoid X Receptor in Adipose Tissue

Cholesterol is a steroid derivative lipid molecule that serves as a pre-cursor molecule in several biochemical pathways, such as formation of bile acids and steroid hormones (422). A detailed review about cholesterol and its relation to adipose tissue is given in Section 1.4.5. Accordingly, cholesterol may play a functional role in adipocyte metabolism in addition to its structural roles. Especially in free form, cholesterol is an active molecule for bodily regulation, but it is also toxic, as recently shown by our group in hepatocytes (217).

Cholesterol over-loading contributes to hypertrophy in adipocytes by construction of firmer cell and LD membrane. At some stage during development of hypertrophy, cholesterol acts like a messenger molecule to alarm the cell about passing a critical size. This seems to activate a pro-inflammatory phenotype in adipocytes. In this context,

cholesterol overloading is likely to be relevant to inflammatory recruitment into adipose tissue.

Bile is important for the digestion and absorption of lipids from intestines. As stated in Section 1.4.3, oxidation of cholesterol molecules is a necessary step in bile acid production. When produced in excess, bile acids inhibit their own production by activating FXR, thereby acting as a steroid hormone. FXR is a nuclear receptor that can activate several signalling pathways that are important for cellular metabolic regulation. These include reduction of (hepatic) lipogenesis, suppression of *de novo* cholesterol, and increased β-oxidation of LCFAs (173, 174). A brief discussion of FXR activation in adipose tissue is provided in Section 1.4.5.

5.1.4 Obeticholic Acid as an FXR agonist

Several FXR agonists have been subjected to clinical trials to improve hepatic and metabolic indices (423). Recent by, these include obeticholic acid (OCA [6-ethyl-chenodeoxycholic acid]), which has very high binding affinity to FXR (424). Researchers have shown that OCA treatment can attenuate body weight gain in mice and humans (176). In addition, OCA can improve whole body insulin sensitivity and NAFLD pathology (223).

The discovery of FXR expression in adipose tissue led scientists to study FXR agonists in different animal models of obesity and adipocyte cell cultures. According to these studies, FXR activation confers beneficial effects on adipocyte differentiation and function (223, 425). Giovanni Rizzo and his colleagues demonstrated that FXR is expressed in mature white adipocytes, not in undifferentiated preadipocytes (425). In cell culture, cells treated with OCA displayed larger LDs. In the same study, OCA increased *aP2*, *C/ebpα*, and *Pparγ* mRNA expression in conjunction with improved adipogenesis. Regulation of adipogenic genes was impaired in $Fxr^{-/-}$ mice. OCA

strikingly increased insulin-induced phosphorylation of AKT in *WT* adipocytes compared to *Fxr*$^{-/-}$ counterparts (425).

In a rabbit model of metabolic syndrome, OCA ameliorated diet-induced metabolic alterations and visceral adipose dysfunction (426). It was also shown that OCA improved liver steatosis in these rabbits. Yanqiao Zhang and his colleagues reported that double knock out *Ob*$^{-/-}$*Fxr*$^{-/-}$ mice were protected from excessive adipose weight gain. However, they were also susceptible to fatty liver disease and hepatic carcinogenesis (427). Skeletal muscle cells possibly do not express FXR (428). It is therefore possible to attribute these changes to FXR activation in liver and adipose tissue cells.

In all, there is growing evidence showing that FXR activation promotes adipose differentiation and improves adipose tissue function. However, we were unable to identify previous research into the effects of FXR induction on adipose inflammation. With interventions such as exercise (Chapter 6), improved adipose inflammation is usually associated with a decrease in adipose tissue weight, so the positive changes in adipose tissues could be partly attributable to reduced lipid burden on adipocytes secondary to the effects of exercise on muscle and adipose. In the present study, use of OCA offered an unusual opportunity to improve adipose function in a direct molecular way without necessarily decreasing the lipid burden on adipocytes.

5.2 Aims

Although the exact mechanism remains largely unknown, FXR agonist OCA has been shown to improve NAS in patients (429). As discussed above, it also confers beneficial effects on adipose function in animal and cell culture studies. However, it is not clear how much of the ameliorations of metabolic and hepatic changes in OCA-treated individuals is attributable to improvement in adipose tissue function, as opposed to how

much could reflect direct effects of FXR agonist on macrophage transformation. In this Chapter, we studied adipose inflammation and phenotypic switch of adipose macrophages in OCA-treated mice. The underlying hypotheses were that cholesterol overloading may be relevant for adipose inflammatory recruitment; therefore, cholesterol-lowering effects of OCA should ameliorate adipose inflammation. Secondly, improved adipose function should increase the proportion of A-AMs in adipose tissue rather than promote migration and accumulation of C-AMs.

The specific aims were to:

1. Test whether OCA treatment confers metabolic improvements in diabetic obese mice.
2. Document associated improvements (if any) in fatty liver pathology.
3. Compare macrophage polarization in different adipose sites from obese mice treated with OCA vs. non-treated.

5.3 Experimental Details

All experimental procedures were approved by the ANU Animal Ethics Committee. After weaning at 4 weeks of age, groups (n=10) of female *foz/foz* NOD.B10 mice and *WT* littermates were fed either an atherogenic diet (4.78 kcal/g digestible energy; 23% fat, 45% carbohydrate, 0.19% cholesterol; Speciality Feeds, Glen Forrest, Australia) or "OCA cupcakes" ad-libitum. As described in Section 2.1.2.2, 25 g standard OCA cupcakes (10 mg/kg diet) were prepared fresh every second week, and provided to mice for consumption (as food) in the same way as regular atherogenic diet. All mice were kept on a 12-hour light/dark cycle in the ANU Medical School animal facility at the Canberra Hospital.

As explained in Section 2.2.1, mice were fasted 4 hours one week before sacrifice (27 weeks), and a glucose tolerance was determined after intraperitoneal glucose injection

(2 g/kg body weight), using a glucometer to measure blood glucose (Accu-Chek Advantage; Roche Diagnostics, Mannheim, Germany). At 28 weeks of age, mice were fasted 4 hours, anesthetized (100 mg/kg ketamine, 16 mg/kg xylazine) and tissue harvest performed following the standard procedure (see Section 2.1.3). Liver, two visceral sites (periovarian and mesenteric) and one subcutaneous (lumbar) WAT samples were collected. Liver steatosis was measured in 3 different ways: total neutral lipids by gas chromatography (see Section 2.2.2.2) and liver ORO staining (see Section 2.2.2.1), and macro-steatosis by histology analysis of H&E-stained liver sections (see Section 2.2.3.2). Serum TAG, cholesterol, and UHDL levels were measured by a multichannel autoanalyzer at The Canberra Hospital, pathology department (see Section 2.2.1.1).

In the present study, adipose SVFs were isolated from each compartment as described in Section 2.3.3. Total RNA was extracted from periovarian, subcutaneous, and mesenteric adipose SVFs, and mRNA levels of specific macrophage markers were analyzed by qPCR (in duplicate). Data are presented as mean ± SEM. For the analysis of data significance, Prism 6 (GraphPad, La Jolla, CA) and SPSS Statistics 22 (IBM, New York, NY) softwares were used for one-way analysis of variance (ANOVA), followed by Bonferroni's *post hoc* analysis (significant when $P < 0.05$).

5.3.1 Author Contributions

Fahrettin Haczeyni designed and conducted the experiments, performed all the read-outs and data analysis, and wrote the Chapter. Vanessa Barn supervised breeding and maintenance of animals. Laurence Poekes assisted with the conduct of mRNA analyses. Matthew M. Yeh assessed liver histology. W. Geoffrey Haigh assisted with the lipidomic analysis by gas chromatography. Narci Teoh contributed intellectual input and reviewed the experimental results. Bruce Shadbolt provided invaluable advice on

statistical analyses. Geoff Farrell directed the study, reviewed and edited the Chapter. The authors thank Canberra Hospital research office and animal house technicians for their highly skilled technical assistance.

5.4 Results

We studied the effects of OCA on multiple adipose depots in mouse models of metabolic obesity and NAFLD. Accordingly, this chapter presents an outline of phenotypes of infiltrated macrophages in different adipose tissues from diabetic obese mice, and the effects of OCA on modification of these macrophage phenotypes.

5.4.1 OCA Treatment Improved Metabolic Indices in Atherogenic Diet-Fed *WT* but not *foz/foz* Mice

~10 weeks after atherogenic dietary feeding (at around 14 weeks of age), there was a "set point" after which rapid weight gain slowed in *foz/foz* mice, whereas at this time point, weight gain accelerated in atherogenic diet-fed *WT* mice. As observed in humans (429), OCA slowed body weight gain in *WT*, but there was no such effect in the appetite-dysregulated *foz/foz* mice (Fig. 5.2.A). At the end of 28 weeks, atherogenic diet-fed *WT* mice developed obesity (>40 g); OCA reduced body weight in these mice (Fig. 5.2B). On the other hand, *foz/foz* mice were significantly heavier than *WT*, and OCA had no effect on body weight.

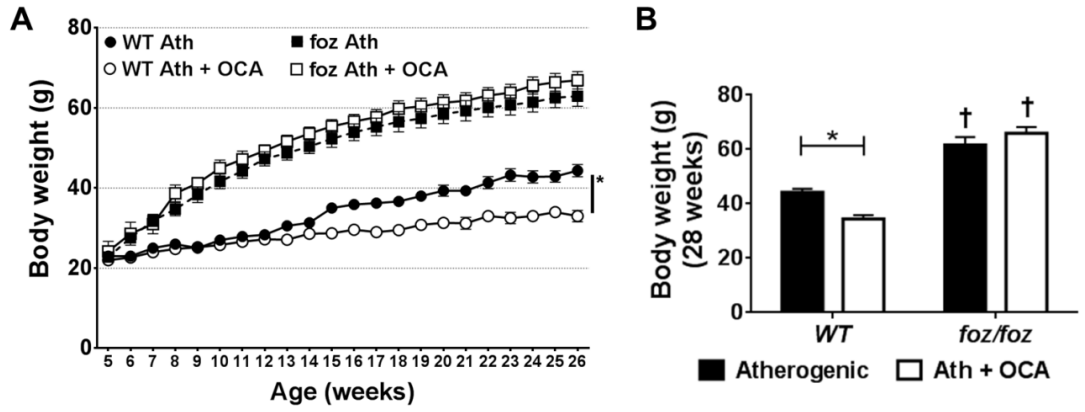

Figure 5.2: Effects of OCA on body weight gain in atherogenic diet-fed *foz/foz* and *WT* mice. (A) *foz/foz* genotype was associated with increased weight gain compared to *WT*. After 14 weeks of age, OCA significantly slowed weight gain in *WT*, but not *foz/foz* mice. (B) By 28 weeks of age, atherogenic diet-fed *foz/foz* and *WT* mice weighed more than 40 g, whereas OCA-treated atherogenic diet-fed *WT* weighed less than 35 g.
Data are mean ± SEM (n=9-10/gp).
† *P*<0.05 vs. treatment-matched control (genotype effect); e.g., OCA-treated *foz/foz* vs. *WT*.
***** *P*<0.05 vs. genotype-matched control (treatment effect); e.g., OCA-treated vs. non-treated *WT*

FBG was higher with atherogenic dietary feeding and *foz/foz* mutation; OCA did not improve FBG levels (Fig. 5.3A). A similar pattern was observed for serum insulin and HOMA-IR (insulin resistance) (Fig. 5.3B,C). IpGTT was performed using the protocol described in Section 2.2.1.3. Following glucose injection, blood glucose levels reached ~28 mmol in atherogenic diet-fed *WT* mice at 60 minutes, whereas it was ~15 mmol in OCA-treated counterparts (Fig. 5.3D). The area under the blood glucose disappearance curve (AUC) was correspondingly less in OCA-treated *WT* mice (Fig. 5.4E). In atherogenic diet-fed *foz/foz* mice, blood glucose levels remained high (~20 mmol) at 3 hours after glucose injection, and OCA treatment had no effect.

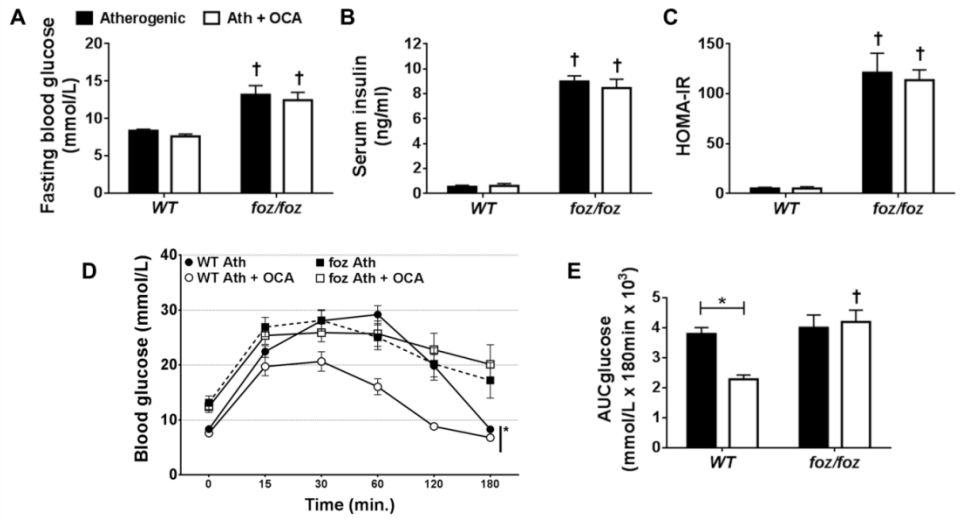

Figure 5.3: OCA significantly improved intraperitoneal glucose tolerance in *WT* mice, but failed to prevent development of diabetes in *foz/foz*. Atherogenic diet-fed *foz/foz* mice developed significant (A) hyperglycemia, (B) hyperinsulinemia, and (C) insulin resistance (HOMA-IR) compared to *WT*. OCA did not improve these indices in any genotype. (D,E) OCA improved intraperitoneal glucose tolerance in *WT* mice vs. non-treated, but failed to improve in *foz/foz* mice (remained diabetic).
Data are mean ± SEM (n=9-10/gp).
† *P*<0.05 vs. treatment-matched control (genotype effect); e.g., OCA-treated *foz/foz* vs. *WT*.
***** *P*<0.05 vs. genotype-matched control (treatment effect); e.g., OCA-treated vs. non-treated *WT*

OCA tended to lower serum TAG levels in both atherogenic diet-fed *WT* and *foz/foz* mice, but this possible improvement was not significant (Fig. 5.4A). Serum cholesterol levels were increased with *foz/foz* background, and OCA did not alter serum cholesterol (Fig. 5.4B). Serum UHDL levels tended to increase in *WT* mice after OCA administration, but this trend was not significant (Fig. 5.4C). *foz/foz* mice displayed higher UHDL levels compared to *WT*, and OCA failed to make any difference.

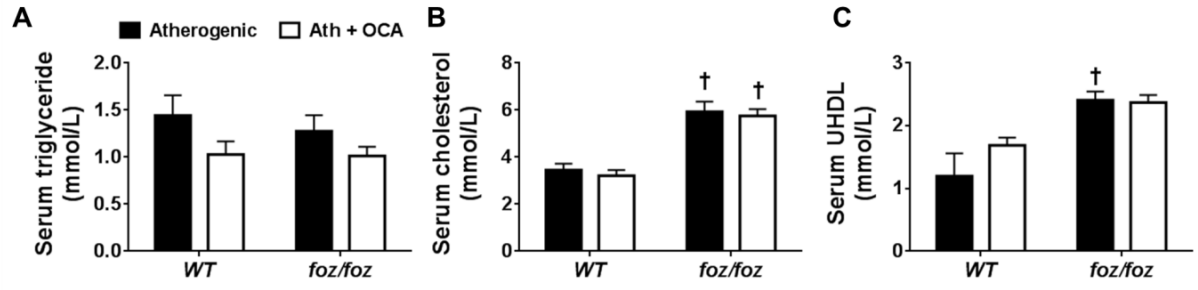

Figure 5.4: Effects of OCA on circulating serum triglyceride, cholesterol and UHDL in atherogenic diet-fed *foz/foz* and *WT* mice. (A) There was a decreasing trend (not significant) in serum triglyceride levels of OCA-treated *foz/foz* and *WT* mice vs. untreated control. (B) *foz/foz* genotype was associated with increased serum cholesterol and UHDL levels compared to *WT*; OCA did not reverse this effect.
Data are mean ± SEM (n=9-10/gp).
† $P<0.05$ vs. treatment-matched control (genotype effect); e.g., OCA-treated *foz/foz* vs. *WT*

As outlined in Section 1.5.4.2., adiponectin is an important regulatory hormone contributing to insulin sensitivity and suppression of pro-inflammatory response. Atherogenic diet-fed *foz/foz* mice developed severe hypoadiponectemia compared to *WT* (Fig. 5.5A); OCA did not ameliorate this effect. As expected, serum leptin levels were greater with *foz/foz* mutation but similarly, OCA did not cause a significant change (Fig. 5.5B). Circulating serum MCP1 levels strikingly increased in atherogenic diet-fed *foz/foz* mice (vs. *WT*). OCA treatment significantly reduced serum MCP1 in *WT*, but not in *foz/foz* mice (Fig. 5.5C).

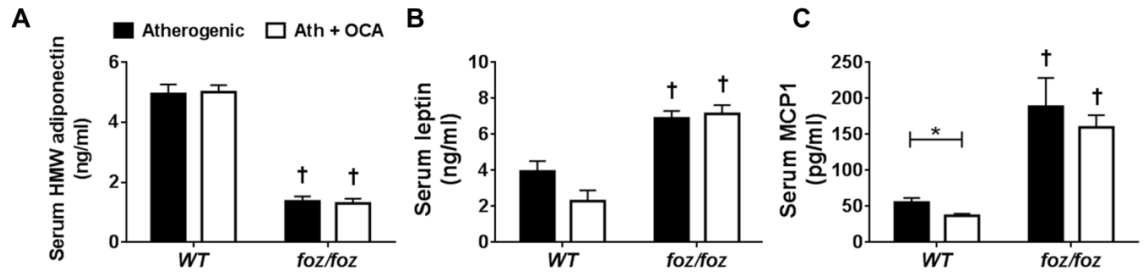

Figure 5.5: Effects of OCA on circulating serum adiponectin, leptin and MCP1 in atherogenic diet-fed *foz/foz* and *WT* mice. (A) Serum adiponectin levels were strikingly less in *foz/foz* mice compared to treatment-matched *WT* controls. OCA did not reverse this effect. (B) Serum leptin was greater in *foz/foz* mice (vs. *WT*) and OCA displayed no effect on serum leptin levels. (C) *foz/foz* genotype markedly increased serum MCP1 levels vs. *WT*. OCA treatment showed significant reduction in *WT* mice, but not in *foz/foz*.
Data are mean ± SEM (n=9-10/gp).
† $P<0.05$ vs. treatment-matched control (genotype effect); e.g., OCA-treated *foz/foz* vs. *WT*.
* $P<0.05$ vs. genotype-matched control (treatment effect); e.g., OCA-treated vs. non-treated *WT*

Liver mass was significantly less in OCA-treated (vs. non-treated) *WT* mice (Fig. 5.6A). Atherogenic diet-fed *foz/foz* mice developed hepatomegaly, and OCA did not reverse this effect. OCA appeared to cause a subtle increase in serum ALT levels of *WT* mice, but this was not significant (Fig. 5.6B). It did not significantly affect serum ALT in *foz/foz* mice. Likewise, serum AST levels were not altered by genotype or OCA treatment (Fig. 5.6C).

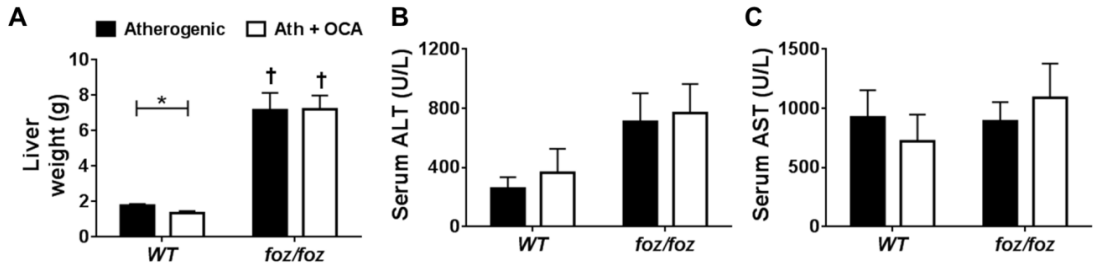

Figure 5.6: Effects of OCA on liver weight, serum ALT and AST levels in atherogenic diet-fed *foz/foz* and *WT* mice. (A) *foz/foz* mice developed hepatomegaly irrespective of OCA treatment. There was a small but significant reduction in OCA-treated *WT* mouse liver weight (vs. non-treated *WT*). (B) Serum ALT levels tended to increase by *foz/foz* genotype (not significant), and OCA did not affect on that in any group. (C) Serum AST levels were similar in all groups.
Data are mean ± SEM (n=9-10/gp).
† $P<0.05$ vs. treatment-matched control (genotype effect); e.g., OCA-treated *foz/foz* vs. *WT*.
***** $P<0.05$ vs. genotype-matched control (treatment effect); e.g., OCA-treated vs. non-treated *WT*

As shown by gas chromatography, the amount of total neutral lipids was greater in liver with atherogenic dietary intake and *foz/foz* mutation; OCA reversed this effect in *WT*, but not in *foz/foz* mice (Fig. 5.7A). The same pattern was found for total steatosis by ORO staining (Fig. 5.7B). On the other hand, *WT* mice displayed vanishingly small macro-steatosis, whereas this was clearly present (and considerable) in *foz/foz* mice; OCA did not confer any improvement on macro-steatosis, irrespective of genotype (Fig. 5.7C). Lipidomic analysis by gas chromatography showed that liver free cholesterol levels were very high in atherogenic diet-fed *foz/foz* mice compared to *WT,* and treatment with OCA did not show any significant effect (Fig. 5.7D). Cholesteryl esters (CE) are formed by esterification of cholesterol with a FA (430, 431). In the present

study, hepatic CE levels showed a strong decreasing trend in OCA-treated (vs. control) *WT* mouse liver ($P = 0.05$) (Fig. 5.7E). *foz/foz* mice showed higher levels of CE in liver, and OCA did not reverse this effect.

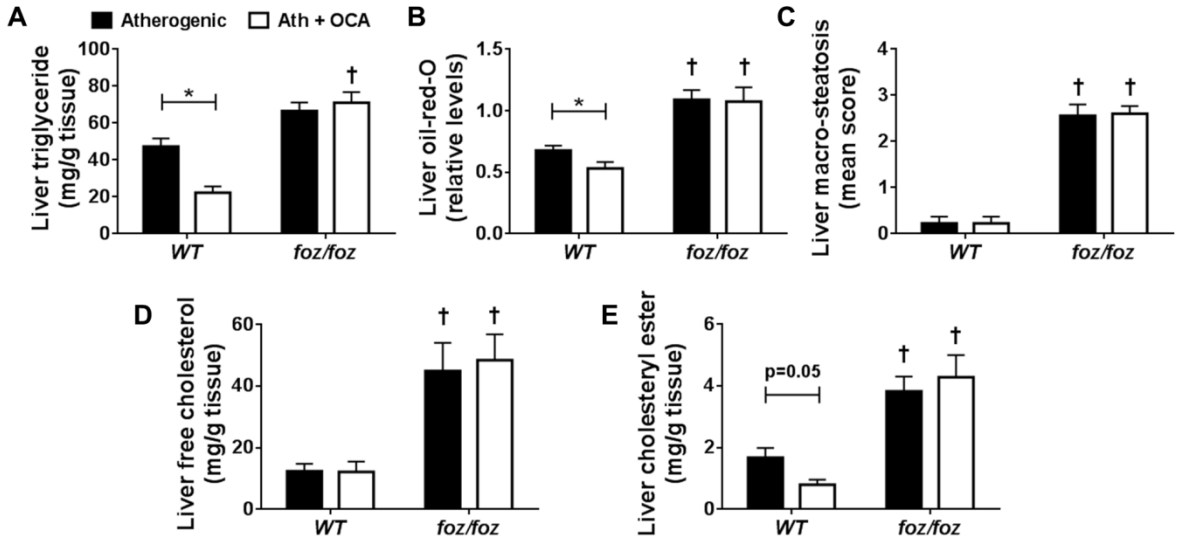

Figure 5.7: Effects of OCA on liver steatosis, free cholesterol and cholesteryl esters in atherogenic diet-fed *foz/foz* and *WT* mice. (A) OCA decreased the amount of hepatic triglyceride in atherogenic diet-fed *WT* mice. In *foz/foz* mice, OCA did not show any effect. (B) The amount of ORO-stained liver lipids showed a similar pattern. (C) Liver macro-steatosis score was very low in *WT* mice, irrespective of OCA treatment. In *foz/foz* mice, this score was strikingly higher (vs. *WT*) (3 is the maximum score), and OCA was without effect. (D) Liver FC increased in *foz/foz* vs. *WT* mice, and OCA did not reduce liver FC in either genotype. (E) Liver CE levels showed a decreasing trend in OCA-treated *WT* mice (vs. non-treated), but this did not reach significance ($P = 0.05$).
Data are mean ± SEM (n=9-10/gp).
† $P<0.05$ vs. treatment-matched control (genotype effect); e.g., OCA-treated *foz/foz* vs. *WT*
* $P<0.05$ vs. genotype-matched control (treatment effect); e.g., OCA-treated vs. non-treated *WT*

5.4.2 Effects of OCA Treatment on Liver Pathology in *foz/foz* and *WT* Mice Fed an Atherogenic Diet

In atherogenic diet-fed *WT* mice, liver inflammation was slightly less (but not significant) in OCA-treated counterparts (Fig. 5.8A). Atherogenic diet-fed *foz/foz* displayed more liver inflammation than did *WT* mice. OCA had minimal effect on liver inflammation in *foz/foz* mice. *WT* mice displayed very few ballooned hepatocytes whereas atherogenic diet-fed *foz/foz* mice showed conspicuous ballooning (2 is the maximum score) regardless of OCA treatment (Fig. 5.8B). Liver NAS score (the

composite of macro-steatosis, inflammation and ballooning score) showed that all *foz/foz* mice developed NASH (Fig. 5.8C). Unlike *foz/foz* counterparts, *WT* mice did not develop NASH. Constant with its lack of effect on macro-steatosis, inflammation and ballooning score, OCA treatment did not influence NAS in either group.

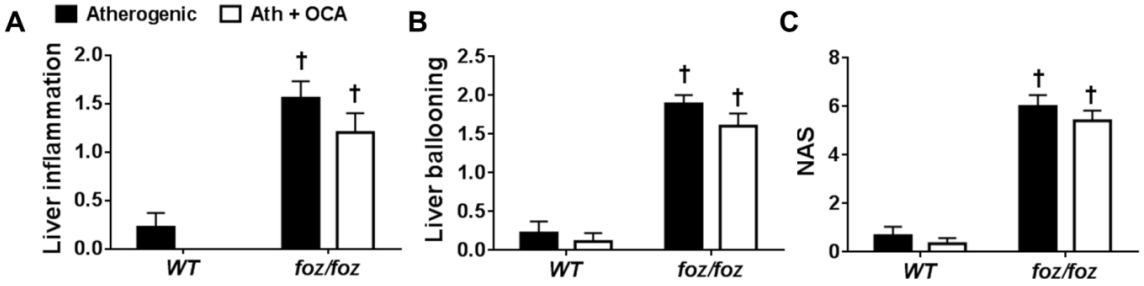

Figure 5.8: OCA treatment failed to improve liver histology in atherogenic diet-fed *foz/foz* or *WT* mice. H&E-stained liver sections were assessed blind by an expert (MMY) for (A) liver inflammation and (B) ballooning, and these scores were compiled with liver macro-steatosis (Fig. 5.7C) as (C) NAS. In atherogenic diet-fed *foz/foz* mice, NAS increased significantly compared to *WT* controls, but OCA treatment failed to improve NASH (and the overall liver histology assessed independently as absolute NASH, borderline NASH or not NASH) in any genotype.
Data are mean ± SEM (n=9-10/gp).
† $P<0.05$ vs. treatment-matched control (genotype effect); e.g., OCA-treated *foz/foz* vs. *WT*

5.4.3 OCA Treatment Limited Adipose Expansion in *WT*, but not *foz/foz* Mice

Consistent with changes in body weight gain, OCA treatment significantly reduced Pov WAT weight in atherogenic diet-fed *WT* mice (Fig. 5.9A). Surprisingly, atherogenic diet-fed *foz/foz* mice showed less Pov WAT mass compared to *WT*, and did not show a significant effect of OCA treatment. On the other hand, *foz*/*foz* genotype was associated with increased Sub WAT mass compared to *WT*; OCA did not affect significantly Sub WAT weight in *foz/foz* mice (Fig. 5.9B). Conversely, OCA reduced Sub WAT weight in atherogenic diet-fed *WT* mice. Compared to Pov and Sub WAT mass, Mes WAT weighed less in all mice (Fig. 5.9C). OCA treatment significantly reduced Mes WAT mass in *WT* mice, but not *foz/foz* mice.

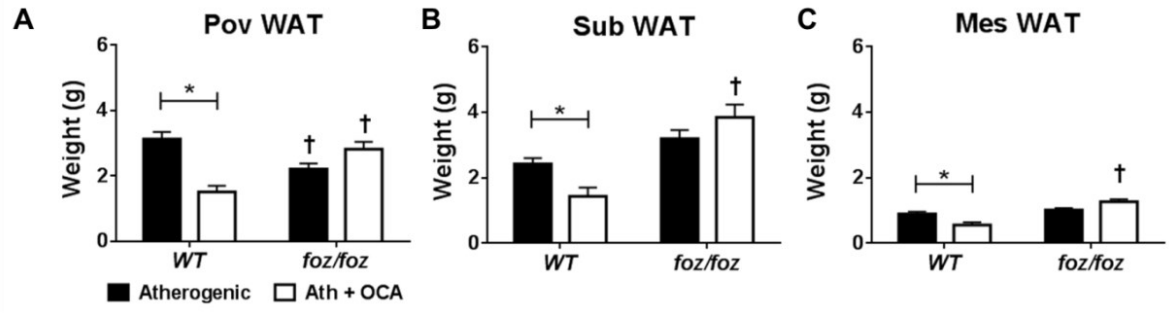

Figure 5.9: Effects of OCA on adipose weights in atherogenic diet-fed *foz/foz* and *WT* mice. (A) Atherogenic diet-fed *foz/foz* mice showed limited expansion of Pov WAT compared to *WT*. OCA reduced Pov WAT mass in *WT*, but not *foz/foz* mice. (B) Sub WAT weighed more in atherogenic diet-fed *foz/foz* than *WT* mice; OCA caused a reduction in Sub WAT mass only in *WT* mice. (C) Mes WAT adiposity was limited compared to the other compartments. OCA-treated *WT* mice showed less Mes WAT mass than non-treated animals; OCA failed to alter Mess WAT in *foz/foz* mice.
Data are mean ± SEM (n=9-10/gp).
† $P<0.05$ vs. treatment-matched control (genotype effect); e.g., OCA-treated *foz/foz* vs. *WT*
* $P<0.05$ vs. genotype-matched control (treatment effect); e.g., OCA-treated vs. non-treated *WT*

5.4.4 Effects of OCA Treatment on Macrophage Phenotype in WATs of *foz/foz* and *WT* Mice Fed an Atherogenic Diet

As discussed in Section 5.1.2, the presence of different cell types (e.g., adipocytes, pericytes) in adipose tissue could confound analyses of macrophage polarization. For this reason, macrophage mRNA detection analysis was conducted on SVF samples, following the protocol given in Section 2.3.3, to prevent any bias caused by adipocyte mRNA. In all adipose depots (SVFs), macrophage marker *Cd68* mRNA levels were greater in atherogenic diet-fed *foz/foz* mice compared to *WT* (Fig. 5.10). OCA did not affect on *Cd68* mRNA in *foz/foz* mice, but it significantly reduced this marker of macrophages in Pov WAT SVF of atherogenic diet-fed *WT* mice. Similar trends in subcutaneous and mesenteric adipose tissues (SVFs) were not significant (Fig. 5.10).

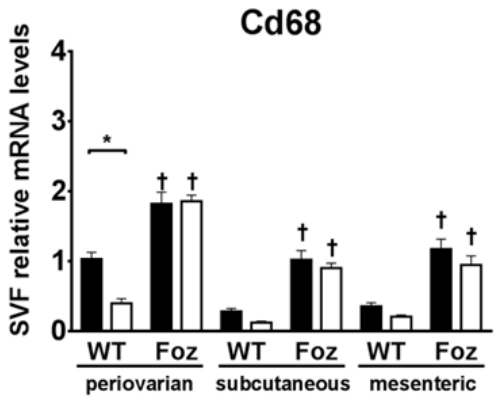

Figure 5.10: Effects of OCA on *Cd68* mRNA expression in adipose SVF samples of atherogenic diet-fed *foz/foz* and *WT* mice. In atherogenic diet-fed *WT* mice, OCA appeared to reduce *Cd68* mRNA expression in all adipose compartments, and this effect was significant in Pov WAT SVF ($P < 0.05$). Atherogenic diet-fed *foz/foz* mice showed greater *Cd68* mRNA levels in all adipose compartments compared to *WT*; OCA failed to reverse this effect.
Data are mean ± SEM (n=9-10/gp). Values are expressed relative to Pov WAT SVF of atherogenic diet-fed *WT*, which is set at 1.0.
† $P<0.05$ vs. treatment-matched control (genotype effect); e.g., OCA-treated *foz/foz* vs. *WT*
***** $P<0.05$ vs. genotype-matched control (treatment effect); e.g., OCA-treated vs. non-treated *WT*

foz/foz mice exhibited increased *Tnfα* mRNA levels than *WT* in all adipose tissue SVF samples; OCA significantly reversed this effect only in Mes WAT SVF of *foz/foz* mice (Fig. 5.11A). OCA did not affect *Tnfα* mRNA in any adipose compartment of atherogenic diet-fed *WT* mice. In all sites, adipose SVF expression of the MCP1 receptor gene, *Ccr2,* was less in *foz/foz* mice than in *WT*. OCA had no effect on *Ccr2* mRNA expression in atherogenic diet-fed *foz/foz* mice (Fig. 5.11B). In contrast, OCA treatment consistently reduced expression of *Ccr2* mRNA in all adipose tissue SVFs in atherogenic diet-fed *WT* mice. Atherogenic diet-fed *foz/foz* mice showed greater *Cd11b* and *Cd11c* mRNA expression in SVFs from three adipose compartments compared to *WT* control (Fig. 5.11C,D). OCA reduced *Cd11b* mRNA in Mes WAT SVF of *foz/foz* mice (vs. non-treated). In Pov WAT SVF of *WT* mice, *Cd11c* mRNA levels were less in OCA-treated vs. non-treated animals.

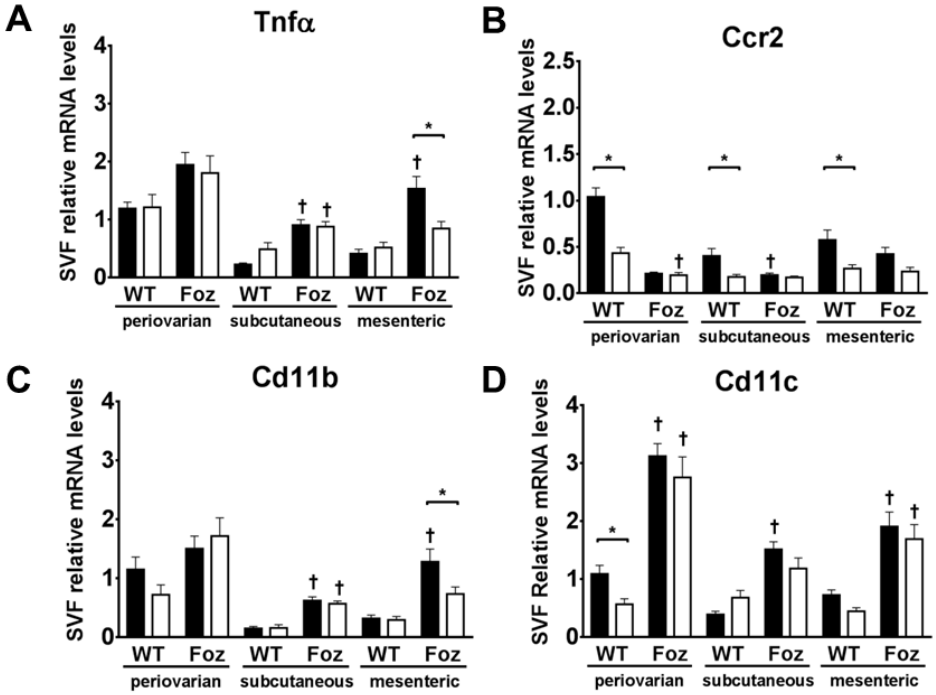

Figure 5.11: Effects of OCA on pro-inflammatory gene expression in adipose SVF samples of atherogenic diet-fed *foz/foz* and *WT* mice. (A) *Tnfα* mRNA expression was greater in Sub and Mes WAT SVFs of atherogenic diet-fed *foz/foz* than *WT* mice. OCA reversed this effect in Mes WAT SVF of *foz/foz* mice. (B) OCA treatment significantly reduced *Ccr2* mRNA expression in all adipose compartments of atherogenic diet-fed *WT* mice (vs. non-treated). *foz/foz* genotype was associated with lower levels of *Ccr2* mRNA, and OCA had no effect. (C,D) Expression of *Cd11b* and *Cd11c* mRNA was increased in atherogenic diet-fed *foz/foz* mice adipose SVF samples in comparison with *WT* control. OCA decreased *Cd11b* mRNA in Mes WAT SVF of atherogenic diet-fed *foz/foz* mice vs. non-treated counterparts but not at other sites. On the other hand, OCA-treated atherogenic diet-fed *WT* mice showed less *Cd11c* mRNA in Pov WAT SVF compared to non-treated controls, but not at other sites.
Data are mean ± SEM (n=9-10/gp). Values are expressed relative to Pov WAT SVF of atherogenic diet-fed *WT*, which is set at 1.0.
† $P<0.05$ vs. treatment-matched control (genotype effect); e.g., OCA-treated *foz/foz* vs. *WT*
***** $P<0.05$ vs. genotype-matched control (treatment effect); e.g., OCA-treated vs. non-treated *WT*

As stated in Section 5.1.2, AG1, FIZZ1 and CD163 are markers of A-AMs. The ratios of *Cd163* / *Cd68*, *Ag1* / *Cd68*, and *Fizz1* / *Cd68* ratios in mRNA expression provide evidence for the proportion of A-AMs in total macrophage population. *Cd163* mRNA was significantly less in Pov WAT SVF of *foz/foz* mice vs. *WT*; OCA had no effect in any group (Fig. 5.12A). OCA treatment increased the ratio of *Cd163* / *Cd68* in atherogenic diet-fed *WT* mouse visceral (Pov and Mes) adipose SVFs (vs. non-treated),

but not in Sub WAT in which this ratio was already high (Fig. 5.12B). In atherogenic diet-fed *foz/foz* mice, OCA treatment did not alter this ratio.

Atherogenic diet-fed *foz/foz* mice tended to have less *Ag1* mRNA in all adipose compartments (not significant) compared to *WT* counterparts (Fig. 5.12C). OCA appeared to increase *Ag1* mRNA in Pov and Sub WAT SVFs of atherogenic diet-fed *WT* mice compared to non-treated control, but this increase was significant only in Sub WAT SVF. In atherogenic diet-fed *foz/foz* mice, the ratio of *Ag1 / Cd68* were strikingly less compared to *WT* counterparts; OCA failed to reverse this effect. Conversely, OCA significantly increased the ratio of *Ag1 / Cd68* in Sub and Pov WAT SVFs of atherogenic diet-fed *WT* mice (vs. non-treated) (Fig. 5.12D). Similarly, *Fizz1* mRNA was less in all adipose compartments (SVFs) of atherogenic diet-fed *foz/foz* than *WT* mice; OCA did not alter on *Fizz1* mRNA expression in *foz/foz* mice in any compartment (Fig. 5.12E). OCA increased the ratio of *Fizz1* / *Cd68* in Pov WAT SVF (and in subcutaneous but not significant) of atherogenic diet-fed *WT* mice vs. non-treated (Fig. 5.12F). All atherogenic diet-fed *foz/foz* mice showed vanishingly low *Fizz1* / *Cd68* ratios than *WT* counterparts in all adipose SVF samples; OCA did not reverse this effect.

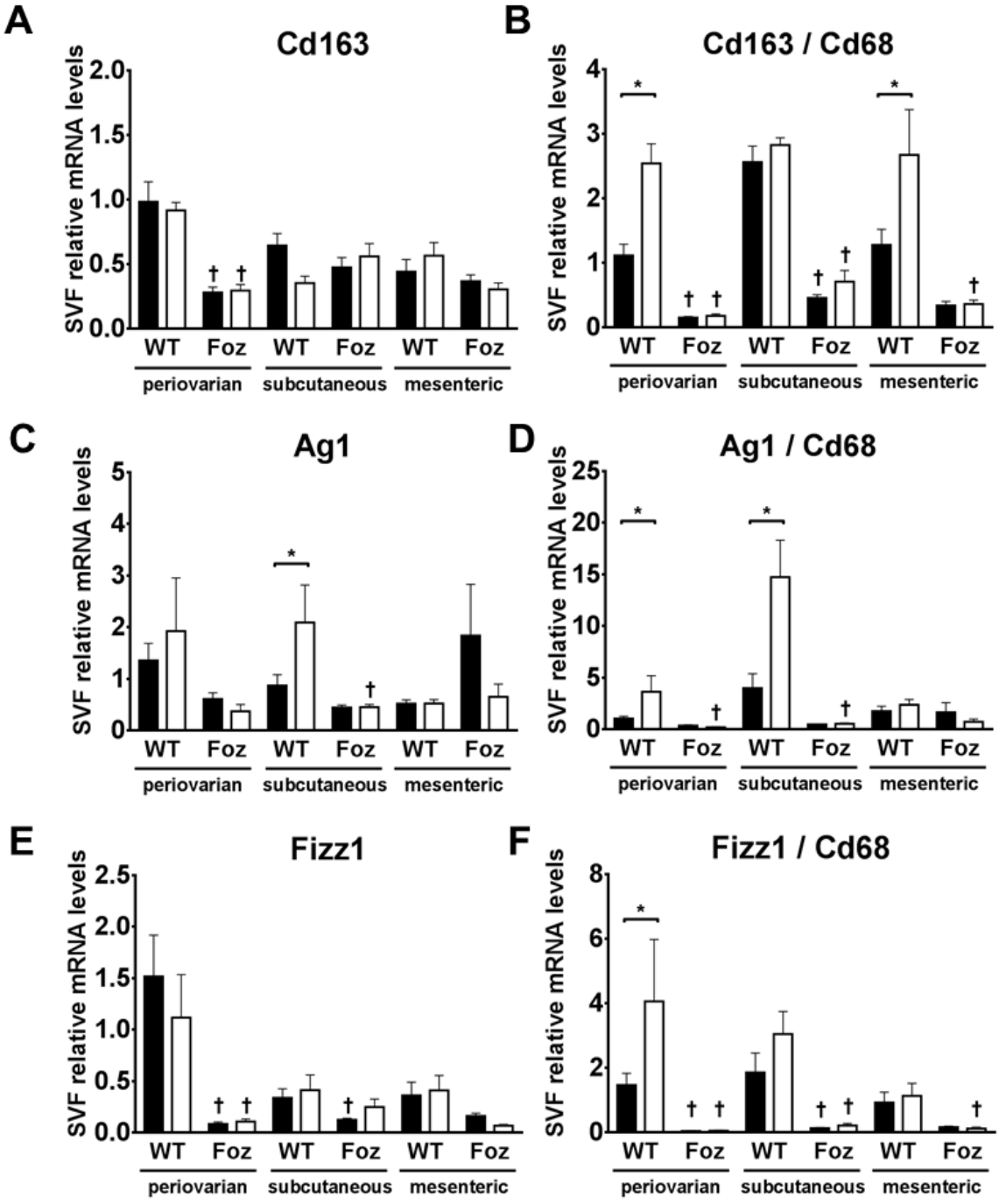
A
Cd163
SVF relative mRNA levels
2.0
1.5
1.0
0.5
0.0
WT
Foz
periovarian
subcutaneous
mesenteric
B
Cd163 / Cd68
4
3
2
1
0
C
Ag1
5
4
3
2
1
0
D
Ag1 / Cd68
25
20
15
10
5
0
E
Fizz1
2.5
2.0
1.5
1.0
0.5
0.0
F
Fizz1 / Cd68
8
6
4
2
0

Figure 5.12: Effects of OCA on mRNA levels of A-AM markers in adipose SVF samples of atherogenic diet-fed *foz/foz* and *WT* mice. (A) *Cd163* mRNA expression was less in Pov WAT SVF of atherogenic diet-fed *foz/foz* mice vs. *WT*, but there were no effect on other sites. (B) The ratio of *Cd163* / *Cd68* was strikingly higher in atherogenic diet-fed *WT* mice than *foz/foz* in all sites. OCA further increased *Cd163* / *Cd68* ratio in Pov and Mes WAT SVFs of *WT* mice vs. non-treated, but had no effect in atherogenic diet-fed *foz/foz* mice. (C) *Ag1* mRNA expression appeared to be less in all adipose compartments of atherogenic diet-fed *foz/foz* than *WT* mice; OCA failed to reverse this effect on *Ag1* mRNA levels in adipose compartments of *foz/foz* mice, but caused a significant increase in Sub WAT SVF of *WT* mice, compared to non-treated controls. (D) OCA significantly increased the ratio of *Ag1* / *Cd168* in Pov and Sub WAT SVFs of atherogenic diet-fed *WT* vs. non-treated counterparts. Atherogenic diet-fed *foz/foz* mice exhibited smaller *Ag1* / *Cd68* ratio compared to *WT;* OCA did not reverse this effect. (E) *Fizz1* mRNA was significantly less in Pov and Sub WATs of atherogenic diet-fed *foz/foz* mice compared to *WT*. OCA had no effect on *Fizz1* mRNA in any adipose compartment in either genotype. (F) The ratio of *Fizz1* / *Cd68* was lower in atherogenic diet-fed *foz/foz* mice adipose compartments in comparison with corresponding *WT* controls. OCA significantly increased the *Fizz1* / *Cd68* ratio in Pov WAT SVF of *WT* mice (vs. non-treated control), but there were no effect in other sites. OCA did not affect on this ratio in atherogenic diet-fed *foz/foz* mice in any adipose compartment.
Data are mean ± SEM (n=9-10/gp). Values are expressed relative to Pov WAT SVF of atherogenic diet-fed *WT*, which is set at 1.0.
† $P<0.05$ vs. treatment-matched control (genotype effect); e.g., OCA-treated *foz/foz* vs. *WT*.
***** $P<0.05$ vs. genotype-matched control (treatment effect); e.g., OCA-treated vs. non-treated *WT*.

5.5 Discussion

As discussed throughout this thesis, metabolic obesity is characterized by pro-inflammatory macrophage recruitment in adipose tissues. The speed, mobility, and the ability of quick reaction confer great advantage to macrophages in pro-inflammatory immune responses. In Chapter 4, we showed that activation of TLR9 signalling assists macrophages to infiltrate into adipose tissue and recognize degenerating or dead adipocytes. However, as overviewed in Section 5.1, macrophages display great plasticity and they can develop different phenotypes depending on conditions of the tissue micro-environment. These conditions can be a threat to the health of the tissue and affect the recovery period after cell damage. In this context, we studied macrophage polarization in three different adipose compartments (two visceral and one subcutaneous) in obese and lean mice, then established the effects of OCA administration to determine whether an FXR agonist could alter the phenotype of recruited adipose inflammatory cells.

OCA treatment reduced body weight gain in atherogenic diet-fed *WT*, but not *foz/foz* mice (Fig. 5.2). As discussed next, this reduction was mostly accommodated by reduced weight gain in adipose compartments, but the reason for gaining less adipose weight is not clear. Nevertheless, there is compelling evidence that this limitation on weight gain does not result from calorie restriction in mice taking OCA. For example, in 2013, Yongjie Ma and his colleagues conducted research with another FXR agonist, GW4064 (432). GW4064 delayed weight gain in high fat diet-fed *WT* mice, but food intake did not change between treated and non-treated animals. Presumably, there is a positive effect of FXR activation on adipocytes (and possibly hepatocytes) on energy utilisation in *WT* mice, and this leads to a more metabolically active phenotype. Unfortunately, we could not perform adipogenic marker analyses such as PPARγ, PRDM16, aP2, or LD proteins (Table 1, Chapter 1) in whole adipose tissue lysates as analyses in SVF samples are heavily time consuming to perform. An important future direction is to establish if and how OCA exerts direct effect on adipocyte metabolism in whole tissue lysates.

By 28 weeks of age, all atherogenic diet-fed *foz/foz* mice were diabetic, and OCA treatment did not influence this complication. Specifically, glucose clearance from the circulation after intraperitoneal glucose injection was not improved by OCA treatment in *foz/foz* mice (Fig. 5.3). On the other hand, OCA treatment strikingly improved glucose clearance in atherogenic diet-fed *WT* mice compared to their non-treated counterparts. Apparently, atherogenic diet-fed mice with appetite defect (*foz/foz*) exhibited more disordered glucose metabolism than *WT* counterparts, so that OCA was unable to affect this, unlike its positive effects in *WT* mice.

One important reason for the "limited" effects of OCA in *foz/foz* mice might be the mode of drug administration. As will be shown in Chapter 6, the average atherogenic dietary intake is ~26 g per week for *WT* and ~33 g per week for female *foz/foz* NOD.B10 mice. In the present study, cupcakes were prepared with 10 mg/kg OCA

content, allowing this for *WT* mice to take in ~0.26 mg OCA, and *foz/foz* mice ~0.33 mg OCA per week. In the literature, there is no consensus on the amount of OCA administration that is optimal in mouse studies, but the general trend appears to be daily administration of amounts used in the present study (e.g., 0.2 mg OCA for a 40 g mouse), not weekly as in the present study. On the other hand, most of studies use such regime for only 10 to 14 days; in the present study, a lower dose of OCA was used for a longer period. Nonetheless, potential limitations on *foz/foz* mice may have occurred because of the amount of OCA taken in as it was below an optimal therapeutic dose. To solve this problem, the host is currently using the more demanding gavage technique to administer OCA and other drugs.

Another important finding in this study was that the interaction between genetic predisposition to develop obesity (*foz/foz* mutation) and a high fat/sugar/cholesterol dietary intake (atherogenic diet) exerts such a strong influence on adipose tissues that beneficial effects of OCA treatment, if any, was minimal. Previous studies provided evidence that OCA treatment improves adipose tissue function by increasing the expression and activation of adipogenic markers such as PPARγ (for details, see Section 5.1). This was not measured in SVFs in the present study as direct analysis on adipose tissue is more relevant. On the other hand, as discussed in Chapter 3, adipose inflammation is associated with dysfunction of the adipose tissue; in other words, a reduction in adipose inflammatory recruitment is linked to better adipose function. With this in mind, it is assumed that OCA improved adipose tissue function in atherogenic diet-fed *WT* mice because pro-inflammatory gene mRNA levels (e.g., *Cd68*, *Tnfα*, *Cd11b*, *Cd11c*) were significantly less in adipose compartments of these animals compared to non-treated controls. Nevertheless, as discussed previously, direct effects of OCA treatment on adipose function will be clearer after conduct of experiments in whole adipose tissue lysates analyzing expression of adipogenic markers.

Most proteins in adipose tissue show cell type-specific expression patterns. For example, CD68 is expressed only in macrophages, whereas adiponectin is specific for adipocytes. However, some proteins display a cross-expression profile between different cell types. For instance, AG1 is expressed by both adipocytes and macrophages, most likely because both cell types contribute to ECM formation in adipose tissues. Moreover, AG1 is used in determination of macrophage polarization analysis; it is an A-AM marker, not one for C-AM. Adipose tissue contains both adipocytes and macrophages. For this reason, molecular analysis of AG1 in whole adipose tissue lysates can be mis-leading.

In the present study, we isolated SVFs from each adipose compartment to avoid this complexity. As discussed in Section 1.5.2, over-expanded hyperplastic adipose tissues form increased amounts of ECM, and this process is considered to be orchestrated by wound-healing (A-AM) macrophages that express AG1, not by C-AMs. However, in the present study, the *Ag1* / *Cd68* ratio indicated less infiltration of A-AMs in adipose tissues of atherogenic diet-fed *foz/foz* mice. This may be an example of the highly complex nature of inflammatory responses in obesity.

As shown in Chapter 3 and 6, macrophage infiltration is highly abundant in adipose tissues of atherogenic diet-fed female *foz/foz* NOD.B10 mice, especially in Pov WAT. In the present study, although a numerical analysis of CLS infiltration had not been completed by the time of thesis submission, greater levels of *Cd68*, *Tnfα*, *Cd11b*, and *Cd11c* mRNA reflect an increased macrophage infiltration in adipose compartments of atherogenic diet-fed *foz/foz* mice compared to *WT*. Presumably, macrophage number and phenotype remain unchanged by FXR agonist administration, since OCA did not show any effect on expression levels of these pro-inflammatory markers. An unexpected finding was the lower expression of *Ccr2* mRNA in SVF samples of atherogenic diet-fed *foz/foz* vs. *WT* mice (Fig. 5.11B). There may be two reasons for this finding: (a)

SVF cells may not be the primary target of MCP1; perhaps most of adipose macrophages arise from BM cells (as shown in Chapter 4). (b) There may be a "macrophage saturation" point in these highly inflamed adipose tissues. This subject was beyond the limited scope of the present research, but it does merit further investigation.

The increasing proportion of cells that express *Cd163*, *Ag1* and *Fizz1* mRNA indicates that OCA treatment switches the macrophage phenotypes towards a more anti-inflammatory phenotype in WATs of atherogenic diet-fed *WT* mice. The ratio of these markers to *Cd68* mRNA expression is correlates positively with infiltration of A-AMs. OCA treatment significantly increased these ratios in all of adipose SVF samples of atherogenic diet-fed *WT* mice compared to non-treated counterparts, but was without effect in *foz/foz* mice in which these ratios were very low. Mes WAT SVF of *WT* mice showed a higher ratio of *Cd163* / *Cd68*, whereas Sub WAT SVF showed a higher *Ag1* / *Cd68* ratio. In addition, Pov WAT SVF showed a higher *Fizz1* / *Cd68* ratio in atherogenic diet-fed *WT* mice (vs. non-treated). These observations strongly confirm that different adipose tissues differ in the phenotypes of infiltrated macrophages, as well as in response, somewhat, different to FXR agonist.

Atherogenic diet-fed *WT* mice developed mild NAFLD with no evidence of steatohepatitis, whereas *foz/foz* (appetite-dysregulated, diabetic/obese) mice developed absolute NASH (Fig. 5.8). In *WT* mice, OCA strikingly reduced liver steatosis compared to non-treated controls, as shown by gas chromatography and ORO staining analyses (Fig. 5.7). However, it is not clear whether this reduction in liver steatosis was attributable to reduced adipose inflammation, or to a primary effect of OCA via FXR activation in hepatocytes. This is of interest as in the recent FLINT study (429), OCA failed to reverse the pathology of NASH, despite of a significant (but relatively small) effect on steatosis and NASH. In the present study, OCA did not improve either

steatosis or necro-inflammatory score, and histology in atherogenic diet-fed *foz/foz* mice.

In summary, OCA treatment appears to confer adipo-, hepato- and metabo-protective effects in atherogenic diet-fed *WT* mice. The mechanism and inter-relation of these findings need further clarification by more direct evidence of FXR activation in the corresponding tissues. On the other hand, OCA may not be very efficient solely when overeating (*foz/foz* background) combines with atherogenic dietary intake. In mildly obese mice (between 40 and 50 g), treatment with OCA reduces mRNA expression of macrophage pro-inflammatory markers in adipose tissue, and causes a phenotypic switch towards to a more anti-inflammatory macrophage phenotype. This study also supports the concept that reduction in adipose inflammation is associated with improvements in glucose metabolism in atherogenic diet-fed *WT* mice. Pharmalogical FXR activation (by OCA) holds some potential for treatment of obesity and obesity-related complications. However, further research is required to clarify the optimal dose and treatment duration in very obese individuals in addition to clarify the exact mechanism. This is especially important on adipose compartments in which studies of FXR expression in relation to differentiation markers (e.g., PPARγ, adipsin, adiponectin) could now be of interest. In the meantime, it seems from the present research, with its limitations (e.g., possible optimal dose), and from the FLINT study (429) in NASH that this pharmalogical approach to metabolic obesity is limited. To establish the full potency of conventional lifestyle modifications, an exercise intervention in these two lines of mice would be of interest, and this is described next.

CHAPTER 6

CHAPTER 6: Exercise Improves Adipose Dysfunction in Obesity

6.1 Introduction

In Chapter 3 it was demonstrated how constant energy surplus causes enlargement of adipocytes with their eventual degeneration, and this is associated with development of adipose tissue inflammation. Visceral depot adipocytes are more susceptible than subcutaneous adipocytes for the facilitation of adipose inflammatory recruitment. As reviewed in Chapter 1 (Section 1.3), physical inactivity contributes importantly to over-nutrition and its resultant obesity complications. In T2D and NAFLD, exercise improves glycemic control and liver indices, but its effects on tissue-specific insulin sensitivity, adipose inflammation and liver histology are less clear.

6.1.1 Body Weight and Exercise

Adipose and muscle function are key factors in weight control and metabolic health. As explained in Chapter 1, continuous disequilibrium in energy balance (intake vs. expenditure) can initiate adipose tissue over-expansion and impair its normal functioning (336). In this way, a sedentary lifestyle leads to adipose dysfunction and metabolic disorders, but the mechanisms whereby physical activity protects against adipose dysfunction is less clear.

There is an inverse relationship between body weight and physical activity. A detailed review about muscle activity, energy expenditure, and insulin sensitivity is given in Section 1.3. Physical inactivity results in reduced energy expenditure, therefore, exercise appears to have beneficial effects for mitigating excessive weight gain. Paradoxically, body weight also has effects on the regulation of physical activity (433). In an initial exercise intervention study with male mice, we found that levels of

voluntary physical activity decrease after mice reach a critical body weight suggests that physical activity is partly regulated by body weight. This finding and several similar studies led us to consider whether the level of physical activity may be a response to obesity rather than a contributor to weight control (433, 434). According to this consideration, regulation of physical activity and body weight is the result of multi-factorial interactions between genetics, dietary habits, mental health (hypothalamic lesions, etc.), sex, age, and perhaps most importantly, environmental (433, 435). These factors can lead to hypoactivity of individuals.

Total energy expenditure (TEE) results from the combination of physical activity and basal metabolic rate (BMR). BMR is comprised of unconscious activities such as breathing, exercise-independent thermogenesis, maintenance of body posture, and cardiac contractions (433, 436). Besides voluntary physical activity, body weight also regulates non-volitional activity (spontaneous but purposeless movement), and this confers effects on an individual's food intake as well as the overall energy utilization from ingested food and from catabolism of that stored in adipose tissues.

6.1.2 Why Study Exercise in Mice?

The relevance of mouse exercise studies to humans is still debated; however, there are several aspects of experimental design that can prevent some of the complicating factors of human exercise studies. For example, biological determinants such as age, pharmacological and surgical interventions are easier to control in mouse studies. Moreover, it is easier to measure locomotor activity and minimize exploratory or free activity in rodents by using methods such as home cages and exercise wheels. This minimizes (or makes it easier to follow) the environmental effects.

Another important determinant that is easier to control in rodent studies is dietary habits (437, 438). The different composition of macronutrients in diets can affect energy

utilization, the thermic effects of food, and the oxidation of macromolecules (439). For example, fat is efficiently stored in adipose tissues whereas simple carbohydrates are efficiently oxidized in myocytes. Today, what is called a "Western diet" is a high-fat and cholesterol diet often with excessive simple carbohydrates (including fructose) (440, 441). Many studies have associated this atherogenic diet with excessive weight gain, inferring that dietary feeding is an important determinant of body weight and possibly level of physical activity. Nevertheless, some studies have implied there is no relationship between diet type and hypoactivity. In the present study, we addressed whether there is an influence of diet (atherogenic vs. chow) on the level of exercise in wild-type (*WT*) NOD.B10 mice.

Gender is another important determinant of exercise behaviour in mice. Female mice appeared to be more active and less aggressive than their male counterparts (442, 443). This is possibly because of hormonal differences between genders that affect mental (e.g., cognitive performance) and emotional (e.g., anxiety) states. In the present PhD project, conduct of experiments in the host lab posed a similar challenge. Accordingly, an initial (pilot) cohort of male C57.B6 mice (which are relatively aggressive), was established for 20 weeks of voluntary exercise. Serious fights between cage-mates, skin wounds, and a sharp decline in daily exercise after a certain age (critical body weight in obese mice) were probably key determinants of unsatisfactory results (variance, and incomplete effects on weight gain and related metabolic effects). Accordingly, we established a cohort of female mice, and provided an exercise wheel for the lesser time of 12 weeks.

6.1.3 Exercise, Obesity, and Non-alcoholic Steatohepatitis

The close association between obesity, adipose inflammation, and progression of fatty liver disease is reviewed in Section 1.5. In metabolic obesity, exercise lowers post-

prandial blood glucose levels with concomitant decrease in serum insulin. This slows progression to diabetes in diabetes intervention studies, and improves glycemic control in patients with type 2 diabetes (444, 445). Resolution of hepatic steatosis and improved insulin sensitivity in extra-hepatic sites have also been described (446).

In a large cohort of NAFLD patients, regular moderately vigorous exercise was associated with less severe hepatic fibrosis (447). Although limited in scope, meta-analyses of lifestyle intervention studies in NAFLD likewise suggest that enhanced physical activity can improve (or prevent progression of) liver histology (448). The present study was designed to clarify interactions between adipose function and inflammation, glycemic control and pathogenesis of NASH and liver fibrosis, using exercise as an intervention to ameliorate onset of insulin resistance, obesity and diabetes.

6.2 Aims

In this Chapter, we hypothesized that increased physical activity should suppress adipose inflammation and dysfunction in obese female mice. We expected this to improve insulin sensitivity in different tissues, improve glycemic control and reduce liver steatosis and liver injury, thereby reduce liver inflammation and fibrosis.

Accordingly, the specific aims were to:

1. Test whether provision of an exercise wheel prevents adipose inflammation and dysfunction in appetite defective mice prone to obesity.
2. Examine whether resultant increased physical activity improves tissue-specific and whole body insulin resistance in mice with different types of obesity (obesity, dietary, both).
3. Investigate whether exercise confers beneficial effects on hepatic steatosis and NASH.

6.3 Experimental Details

In the present study, female *foz/foz* mice were used (for details, see Section 3.1) because these animals simulate the key predisposing factors to human NASH, appetite dysregulation with over-nutrition, diabetes and metabolic syndrome. They exhibit the spectrum of simple steatosis to fibrotic NASH, depending on dietary composition (449). All experimental procedures were approved by the ANU Animal Ethics Committee (see Section 2.1.1.1).

After weaning at 4 weeks of age, groups (n=8) of *foz/foz* NOD.B10, generated by cross-breeding from the original strain reported by Arsov et al., as described elsewhere (339), and *WT* littermates were fed either standard chow or an atherogenic diet ad-libitum (4.78 kcal/g digestible energy; 23% fat, 45% carbohydrate, 0.19% cholesterol; Speciality Feeds, Glen Forrest, Australia). Half the cages were fitted with an exercise wheel for voluntary exercise, and wheel rotations were recorded by a cycle computer (Fig. 6.1). The initial cohort with male mice were provided an exercise wheel for 20 weeks (harvest at 24 week old) and the main cohort with female mice were housed with an exercise wheel for 12 weeks (harvest at 16 week old). All mice were kept on 12-hour light/dark cycle in the ANU Medical School animal facility at the Canberra Hospital.

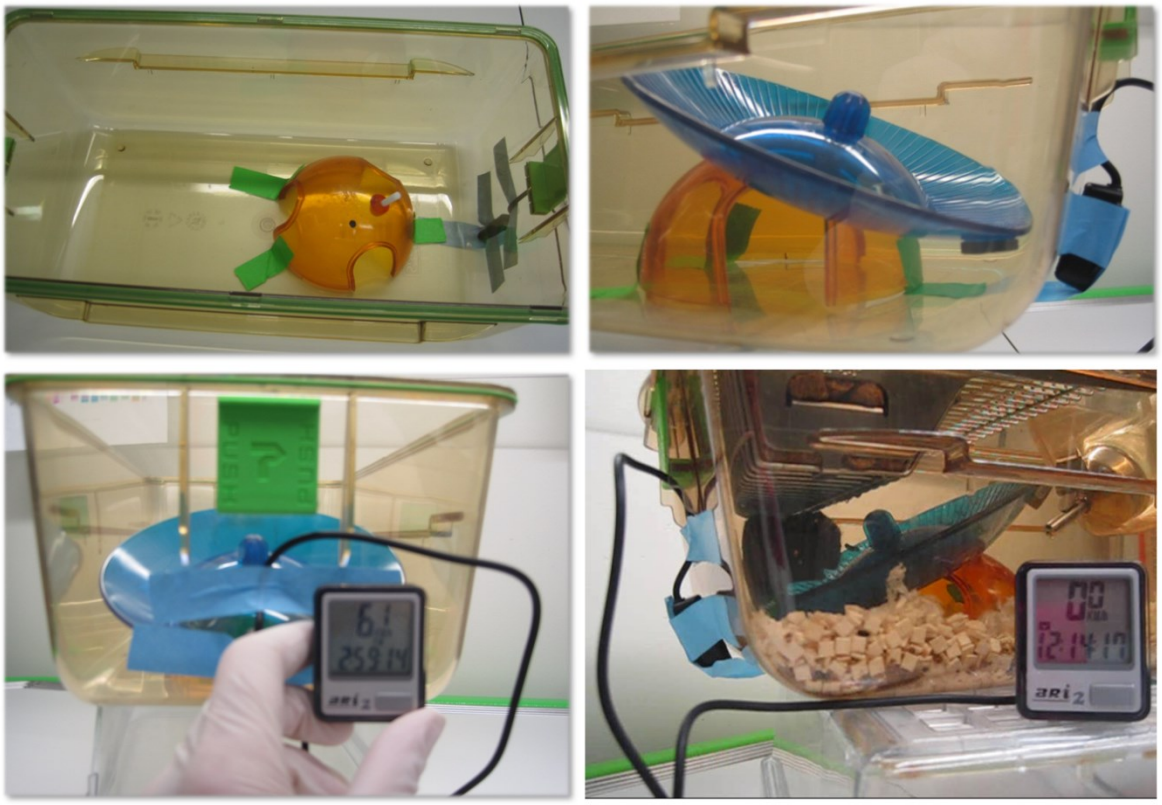

Figure 6.1: Configuration of exercise intervention in animal facility. Igloos (orange plastic structure) were fixed on the floor of the cages. Half the cages were fitted with an exercise wheel ("satellite disc" shaped structure) for regular exercise; and wheel rotations were recorded by a cycle computer (magnet fixed to underside of wheel). Exercise data were monitored and recorded regularly by Vanessa Barn (photos were provided by Vanessa Barn, who developed this apparatus).

Body weights were monitored weekly from weaning to week 14 for all mice to plot the progression of weight gain. Mice were fasted 4 hours one week before sacrifice (as explained in Section 2.2.1), and glucose tolerance was measured after intraperitoneal glucose injection (2 g/kg body weight) using a glucometer (Accu-Chek Advantage; Roche Diagnostics, Mannheim, Germany). At the time of tissue harvest (24 weeks for males, 16 weeks for females), mice were fasted 14 hours, anesthetized (100 mg/kg ketamine, 16 mg/kg xylazine) and administered insulin (1 U/kg body weight; Eli Lilly, Indianapolis, IN) by intra-aortic injection. Liver, visceral (periovarian) and subcutaneous (lumbar) WATs, and gastrocnemius muscle were collected before and 3 minutes after insulin injection for further analyses (Fig. 6.2). Later *in vivo* determination

of insulin sensitivity assay was learnt/practised at the Baker IDI Heart and Diabetes Institute, Melbourne, under the supervision of Dr Emma Estevez (see Section 2.1.5).

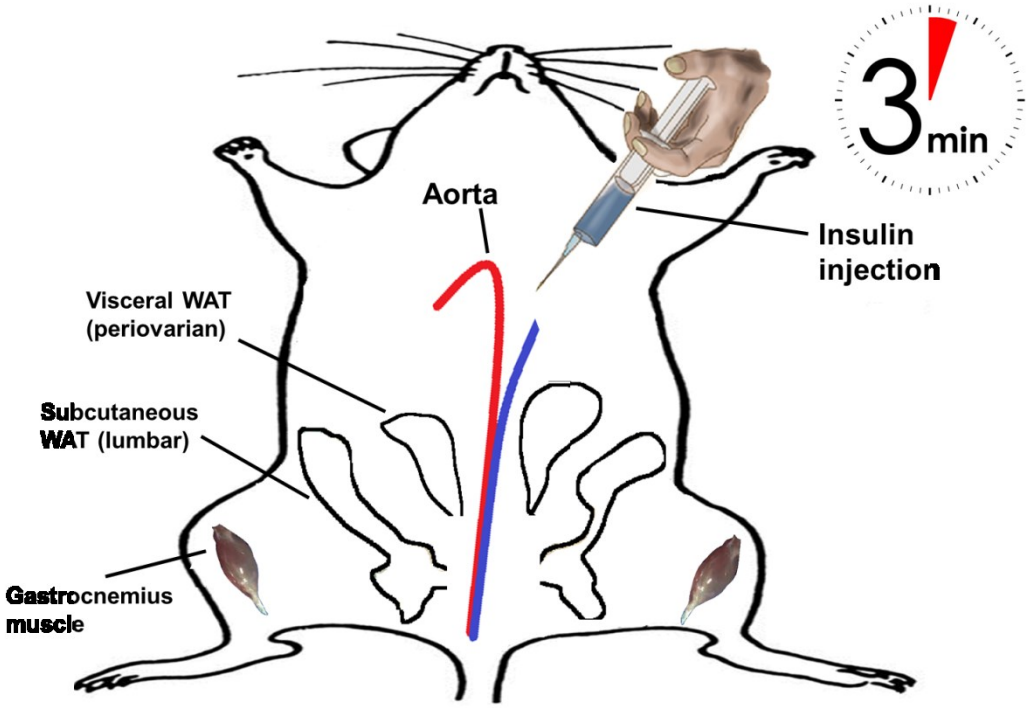

Figure 6.2: Mouse intra-aortic insulin injection and tissue collection. Insulin stimulation assay was performed during the tissue harvest. Anesthetized mice were given an intra-aortic insulin injection. Part of liver, visceral (periovarian) and subcutaneous (lumbar) WATs, and gastrocnemius muscle were excised before and 3 minutes after insulin injection. Tissue-specific insulin sensitivity was determined by measuring phospho-protein kinase B (AKT) / total-AKT ratio by western blotting (for methodology, see Section 2.3.2).

At the end of experiments, we studied adipose morphometry coupled to indicators of differentiation and inflammation to dissect the relationships between adipose compartments (see Section 2.2.3), tissue-specific insulin sensitivity and liver pathology. Data are presented as mean ± SEM. Protein/mRNA estimations were performed in duplicate. For the analysis of data significance, Prism 6 (GraphPad, La Jolla, CA) and SPSS Statistics 22 (IBM, New York, NY) software was used applying the Student's t-test for single comparison and one-way or two-way analysis of variance (ANOVA), followed by Bonferroni's *post hoc* analysis (significant when $P < 0.05$)

6.3.1 Author Contributions

Fahrettin Haczeyni designed and conducted the experiments, performed data analysis, and wrote the Chapter and a related manuscript (in process of publication in *Obesity*). Vanessa Barn supervised the animal work (breeding and maintenance) and designed details of the exercise intervention. Auvro Robin Mridha and Emma Estevez assisted the experiments. Matthew M. Yeh provided blind analysis of liver histology. Christopher J. Nolan, Kim S. Bell-Anderson, and Narcissus C.-H. Teoh contributed intellectual input, reviewed and edited the Chapter. Bruce Shadbolt provided invaluable advice on statistical analyses. Geoffrey C. Farrell directed the study, reviewed and edited the Chapter. The authors thank The Canberra Hospital research office and animal house technicians for their highly skilled technical assistance.

6.4 Results

In this Chapter, we propose exercise as an important factor that could reduce immune responses in adipose tissue that lead to inflammatory recruitment in the face of over-eating and physical inactivity. For a better understanding of exercise effects on adipose tissue, we studied both visceral and subcutaneous WATs, thereby providing more detailed insights into functional and morphological differences between different adipose sites.

6.4.1 A Pilot Study: Provision of Exercise Wheel to Male Mice

In this preliminary study, mice on the chow diet generally applied themselves to regular use of the exercise wheel, but atherogenic diet-fed male *foz/foz* mice declined using the exercise wheel after 12 weeks (16 weeks of age). Thereafter, a rapid increase of weight gain followed, and at the end of 24 weeks, both exercising and non-exercising *foz/foz* mice had similar body weight, irrespective of diet.

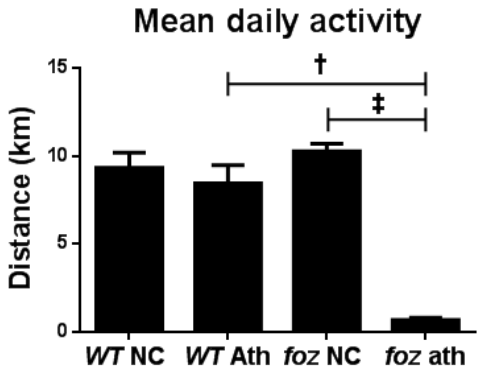

Figure 6.3: Mean daily activity in chow and atherogenic diet-fed *WT* and *foz/foz* male mice. Male *WT* mice travelled an average of 8 - 9 km in 24 hours. Chow-fed *foz/foz* mice were as active as *WT* counterparts, but atherogenic diet-fed *foz/foz* mice were sedentary. Exercise (as mean daily activity in km travelled) was measured from 6 weeks of age to 15 weeks.
Data are mean ± SEM (n=8/gp).
† $P<0.05$ vs. diet-matched WT (genotype effect); e.g., chow-fed *foz/foz* vs. *WT*
‡ $P<0.05$ vs. genotype-matched control (diet effect) e.g., atherogenic diet-fed vs. chow-fed *WT*

The running circumference of the exercise wheel was 377 mm. Accordingly, we calculated that 106 revolutions of the wheel was equal to 39.96 meters of running distance. This sample of exercise activity was measured between 6 and 15 weeks of age. A 24 week old chow-fed *WT* male mouse provided with an exercise wheel often travelled ~9 km in 24 hours (Fig. 6.3). Atherogenic diet-fed male *foz/foz* mice were notably sedentary (< 15% active as *WT* counterparts); these diabetic obese mice exercised around 1 km a day.

In *foz/foz* male mice fed either diet, exercise reduced (but did not normalize) weight gain for 16 weeks, after which this effect diminished strikingly (Fig. 6.4). Thus, in atherogenic diet-fed male *foz/foz* mice, increased physical activity slowed but failed to prevent development of obesity. The trend in reduction of weight gain declined after 16 weeks, and at the end of the experiment (24 weeks), exercise had made no difference to the total body weight in these male mice with appetite defect.

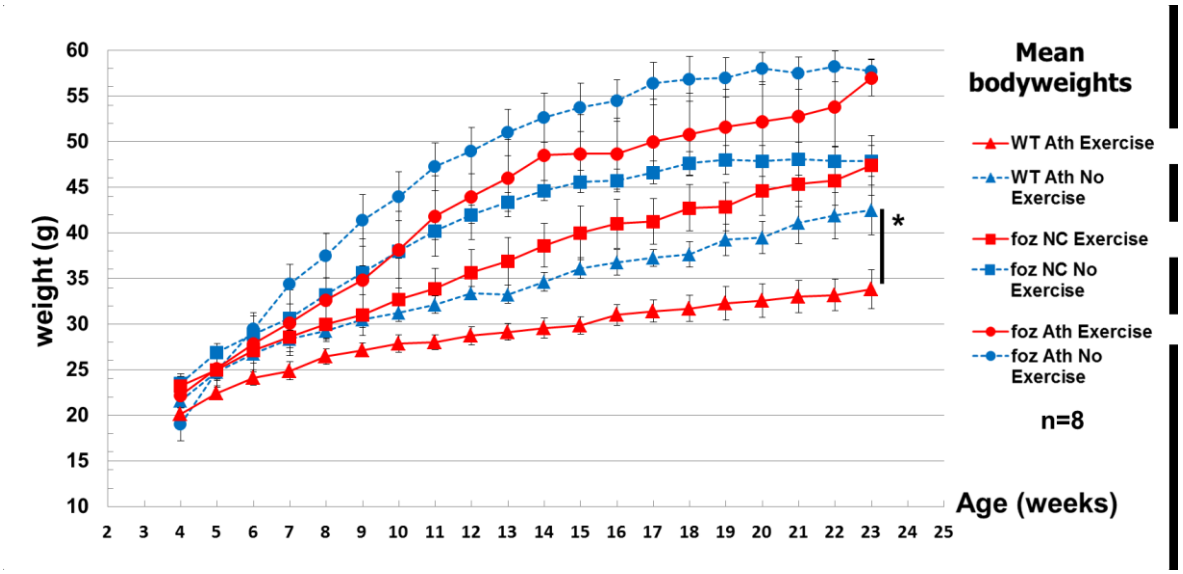

Figure 6.4: Weight gain in exercising vs. non-exercising male mice during 20 weeks of voluntary exercise. In atherogenic diet-fed *WT* mice, increased physical activity strikingly prevented excessive weight gain. Exercise conferred similar but less pronounced effects on chow-fed *WT* mice (chow-fed *WT* groups are omitted from the graphic for clarity). In *foz/foz* mice, exercise slowed development of obesity in the earlier stages, but ultimately failed to prevent obesity, irrespective of diet.
Data are mean ± SEM.
* $P<0.05$ vs. sedentary control

Increased physical activity corrected diet-induced weight gain in male *WT* mice (Fig. 6.5A). In male *foz/foz* mice, exercise did not cause any reduction in body weight at 24 weeks. Exercise improved FBG in *WT* mice on either diet (Fig. 6.5B). A similar but milder (not significant) trend was found in FBG levels for *foz/foz* mice. As a proportion of body weight, both visceral and subcutaneous WATs decreased in exercising *WT* mice on either diet (not significant for chow-fed *WT* subcutaneous WAT; Fig. 6.5C,D). In contrast, exercise appeared to increase visceral WAT in *foz/foz* mice compared to their diet-matched counterparts (Fig. 6.5C), and failed to reduce subcutaneous WAT in *foz/foz* mice, irrespective of diet (Fig. 6.5D). Finally, whereas exercise produced an impressive reduction in subcutaneous WAT of atherogenic diet or chow-fed *WT* mice, it did not reduce subcutaneous adiposity in *foz/foz* mice (Fig. 6.5D).

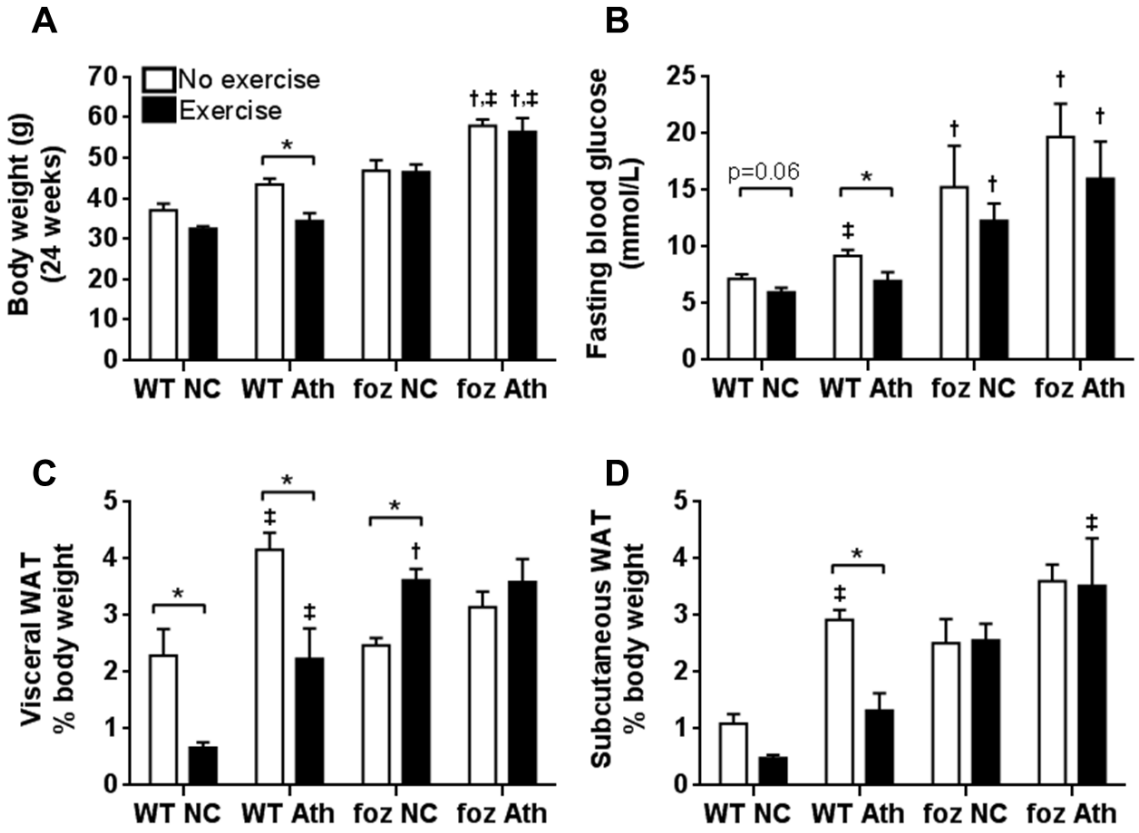

Figure 6.5: Effects of exercise on body weight, FBG, and relative visceral and subcutaneous WAT weights in male *foz/foz* and *WT* mice. (A) Atherogenic dietary feeding and *foz/foz* mutation promoted weight gain; exercise reversed this effect in atherogenic diet-fed *WT* mice, but failed to prevent excessive weight gain in *foz/foz* mice (growth curves are shown in Fig. 6.4). (B) A similar pattern was observed for FBG. (C) Exercise significantly reduced visceral (epididymal) WAT in *WT* mice, irrespective of diet. Interestingly, exercising *foz/foz* mice showed an increase of relative visceral WAT (significant for chow-fed *foz/foz* mice). (D) Exercise also decreased subcutaneous WAT in *WT* mice, but failed to influence subcutaneous WAT in *foz/foz* mice.
Data are mean ± SEM (n=8/gp).
* $P<0.05$ vs. sedentary control
† $P<0.05$ vs. diet-matched WT (genotype effect); e.g., chow-fed *foz/foz* vs. *WT*
‡ $P<0.05$ vs. genotype-matched control (diet effect) e.g., atherogenic diet-fed vs. chow-fed *WT*

Atherogenic dietary feeding significantly increased serum cholesterol levels in male *foz/foz* and *WT* mice (vs. chow-fed counterparts; Fig. 6.6A). *foz/foz* mice developed hypercholesterolemia after 20 weeks of atherogenic dietary feeding (Fig. 6.6A). Exercise failed to lower circulating serum cholesterol levels in any group. Serum insulin appeared to increase in *foz/foz* mice on both diets compared to *WT* counterparts; however, possibly because of the high variability of data, none of the groups displayed a

significant improvement with exercise (Fig. 6.6B). There was a slight decreasing trend in serum adiponectin levels of atherogenic diet-fed *foz/foz* mice vs. *WT* counterparts, and exercise failed to alter serum adiponectin levels in any group (Fig. 6.6C). Serum MCP1 levels were increased in atherogenic diet-fed *foz/foz* mice compared to *WT*, but exercise did not reverse this increase (Fig. 6.6D).

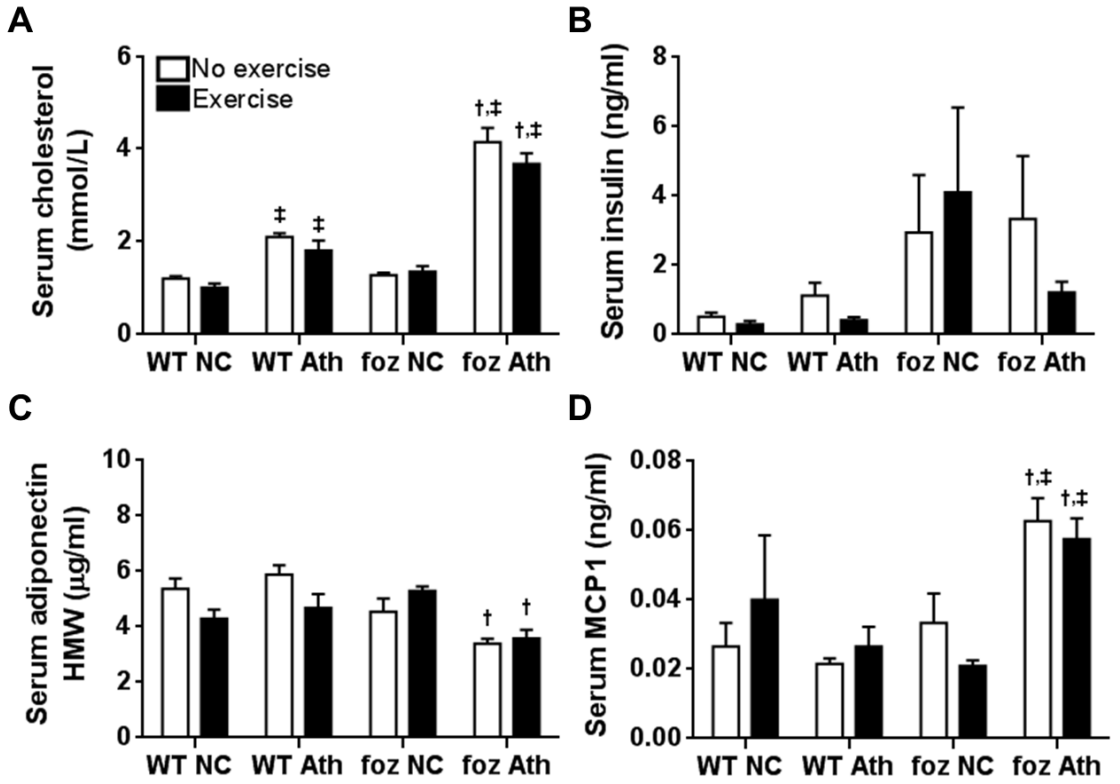

Figure 6.6: Effects of exercise on circulating serum cholesterol, insulin, adiponectin, and MCP1 in male *foz/foz* and *WT* mice. (A) Atherogenic diet-fed *foz/foz* mice developed hypercholesterolemia (vs. *WT* or diet-matched control); exercise did not protect these mice from increased serum cholesterol levels. (B) Serum insulin appeared to increase with *foz/foz* mutation irrespective of diet, although the apparent change was not significant. Exercise did not significantly affect serum insulin. (C) Atherogenic diet-fed *foz/foz* mice showed a slight but significant reduction in serum adiponectin levels, which was not altered by exercise. (D) Serum MCP1 levels were increased in atherogenic diet-fed *foz/foz* mice compared to diet-matched or genotype-matched counterparts, but exercise did not reverse either of these effects.
Data are mean ± SEM (n=8/gp).
* $P<0.05$ vs. sedentary control
† $P<0.05$ vs. diet-matched WT (genotype effect); e.g., chow-fed *foz/foz* vs. *WT*
‡ $P<0.05$ vs. genotype-matched control (diet effect) e.g., atherogenic diet-fed vs. chow-fed *WT*

Exercise had no effect on liver size in *WT* male mice, but caused a minor reduction in atherogenic diet-fed male *foz/foz* mice (9.5% relative body weight vs. 11%; $P<0.05$) (Fig. 6.7A). There may have been a subtle serum ALT reduction in atherogenic diet-fed *foz/foz* mice but this was not significant (Fig. 6.7B). A preliminary blind assessment of liver sections in the host lab indicated improvements in hepatic macro-steatosis in atherogenic diet-fed exercising *WT* mice compared to sedentary counterparts (Fig. 6.7C). On the other hand, livers of atherogenic diet-fed *foz/foz* mice displayed evidence of inflammation, indicating development of NASH; exercise failed to improve liver histology in these livers (data not shown).

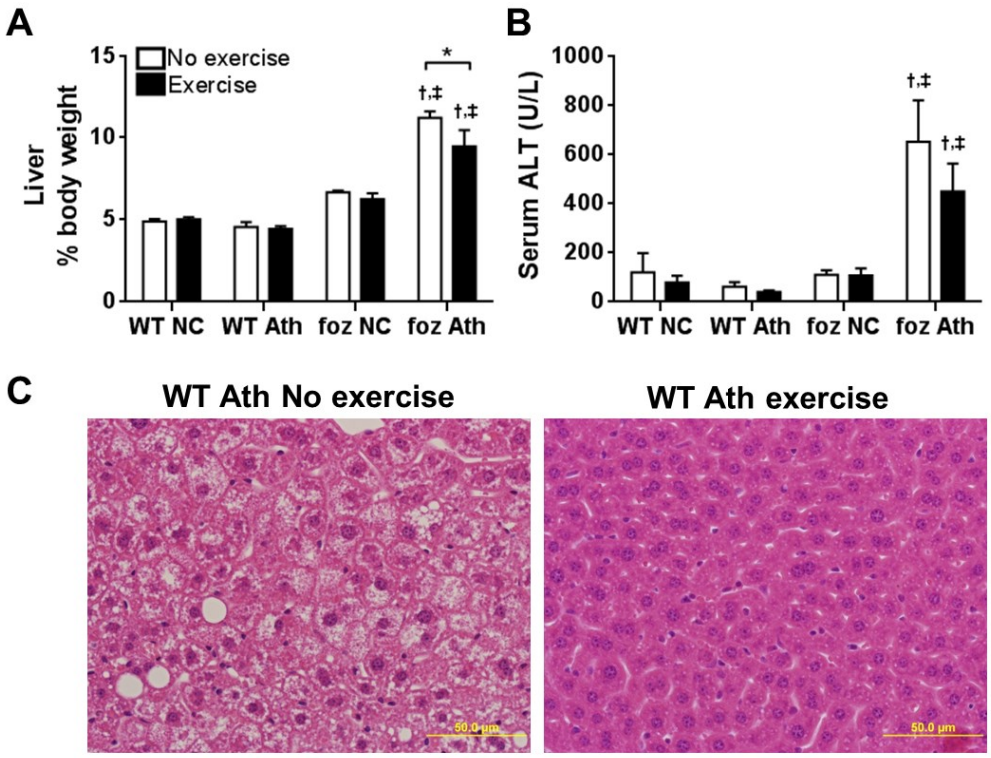

Figure 6.7: Exercise prevented steatosis in atherogenic diet-fed male *WT* mice but failed to alter liver indices in male *foz/foz* mice. (A) Atherogenic diet-fed *foz/foz* mice developed hepatomegaly (vs. *WT* mice); exercise slightly reduced but did not correct liver weights of these mice. (B) Serum ALT levels increased with atherogenic dietary feeding and *foz/foz* mutation; exercise failed to normalize high serum ALT in atherogenic diet-fed *foz/foz* mice. (C) Liver sections (50 µm scaling) of atherogenic diet-fed *WT* mice showed a complete prevention of hepatic macro-steatosis in the exercising group.
Data are mean ± SEM (n=8/gp).
* $P<0.05$ vs. sedentary control
† $P<0.05$ vs. diet-matched WT (genotype effect); e.g., chow-fed *foz/foz* vs. *WT*
‡ $P<0.05$ vs. genotype-matched control (diet effect) e.g., atherogenic diet-fed vs. chow-fed *WT*

Behavioural aberrations and rapid weight gain with declining use of the exercise wheel indicated that there would be limited value of further analyses in these mice. We therefore established another exercise cohort with female mice. Unlike the previous cohort, these mice were housed with the exercise wheel for 12 weeks, so as to identify any changes in pathophysiology (e.g., insulin signalling) and adipose function (e.g., morphology, inflammation) that could be relevant to beneficial effects of exercise on glycemic control and the liver.

6.4.2 Effects of Exercise Wheel Provision on Daily Physical Activity and Weight Gain in Female *WT* and *foz/foz* Mice

As measured by wheel rotations, dietary composition and genotype both influenced physical activity. Atherogenic diet intake tended to increase exercise in *WT* mice (9.24 vs 6.47 km/day; $P = 0.08$). In contrast, atherogenic dietary feeding reduced, but did not minimize, daily activity in *foz*/*foz* mice (4.67 km/day; $P < 0.05$) (Table 6.1).

TABLE 6.1
Daily activity in *foz/foz* and *wild-type* mice fed chow or atherogenic diet

Genotype	Diet	*n*	Running time (h/day)	Average speed (km/h)	Distance (km/day)
wild-type	chow	8	3.75 ± 0.16	1.70 ± 0.18	6.47 ± 0.94
foz/foz	chow	8	3.16 ± 0.20	1.83 ± 0.06	5.82 ± 0.48
wild-type	atherogenic	8	4.29 ± 0.24	2.13 ± 0.14	9.24 ± 0.94
foz/foz	atherogenic	8	2.77 ± 0.37†	1.66 ± 0.15	4.67 ± 0.85†

Data are mean ± SEM. †$P<0.05$ (vs. diet-matched comparison [genotype effect])

While it can be difficult to accurately measure food intake in rodent experiments (other than using metabolic cages), highly skilled animal technicians assisted this measurement based on food consumption in individual cages (see Section 2.1.2). As expected, exercise increased food consumption (particularly chow) in *WT* mice (Fig. 6.8A,B). Interestingly, there was a non-significant trend for a reduction rather than increase in food intake in *foz/foz* mice with exercise, regardless of the type of diet (Fig. 6.8A,B). The reason for this different food intake adaptation to exercise between the *WT* and *foz/foz* mice is not clear, but the possibility that exercise may (at least partly) reset appetite control in *foz/foz* mice is discussed later (Section 6.5).

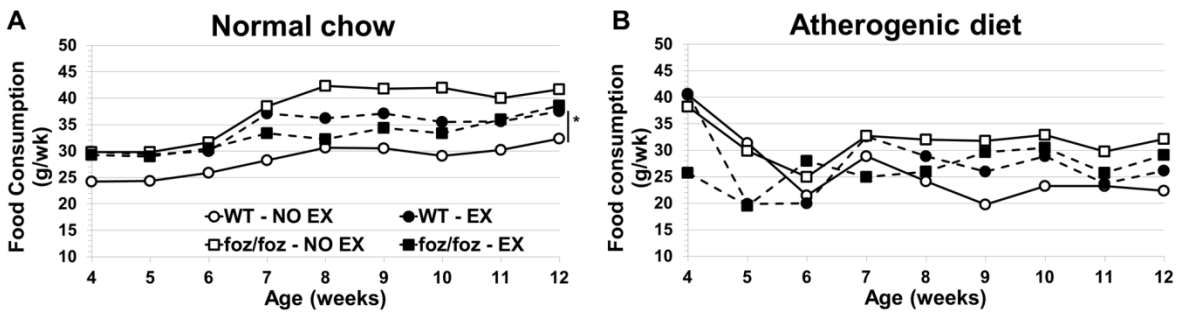

Figure 6.8: Food consumption in exercising female *foz/foz* and *WT* mice vs. non-exercising counterparts. (A,B) Compared with non-exercising mice (NO EX), food intake was higher in exercising (EX) *WT* mice on either diet, but was less in exercising *foz/foz* mice.
Data are mean ± SEM (n=8/gp; error bars are not shown for clarity).
* $P<0.05$ vs. sedentary control

Exercise had a small effect on weight gain in atherogenic diet-fed *WT* mice (Fig. 6.9B). In chow-fed *foz/foz* mice, exercise prevented excess weight gain compared to non-exercising counterparts, so that exercising mice remained similar in weight to *WT* until ~12 weeks of age (Fig. 6.9A). Atherogenic feeding for 16 weeks strikingly increased body weight in *foz*/*foz* mice (Fig. 6.9B,C). Exercise countered the sole effect of genotype (in chow-fed mice) on body weight, and exerted a significant but incomplete effect on reducing weight gain in atherogenic diet-fed *foz*/*foz* mice (Fig. 6.9C). To establish whether energy consumption was increased by exercise, we performed overnight fasting weight measurement (wheel removed). Such overnight fasting weight loss was significantly higher in all exercising groups, except for the not significant trend in chow-fed *foz*/*foz* mice (Fig. 6.9D).

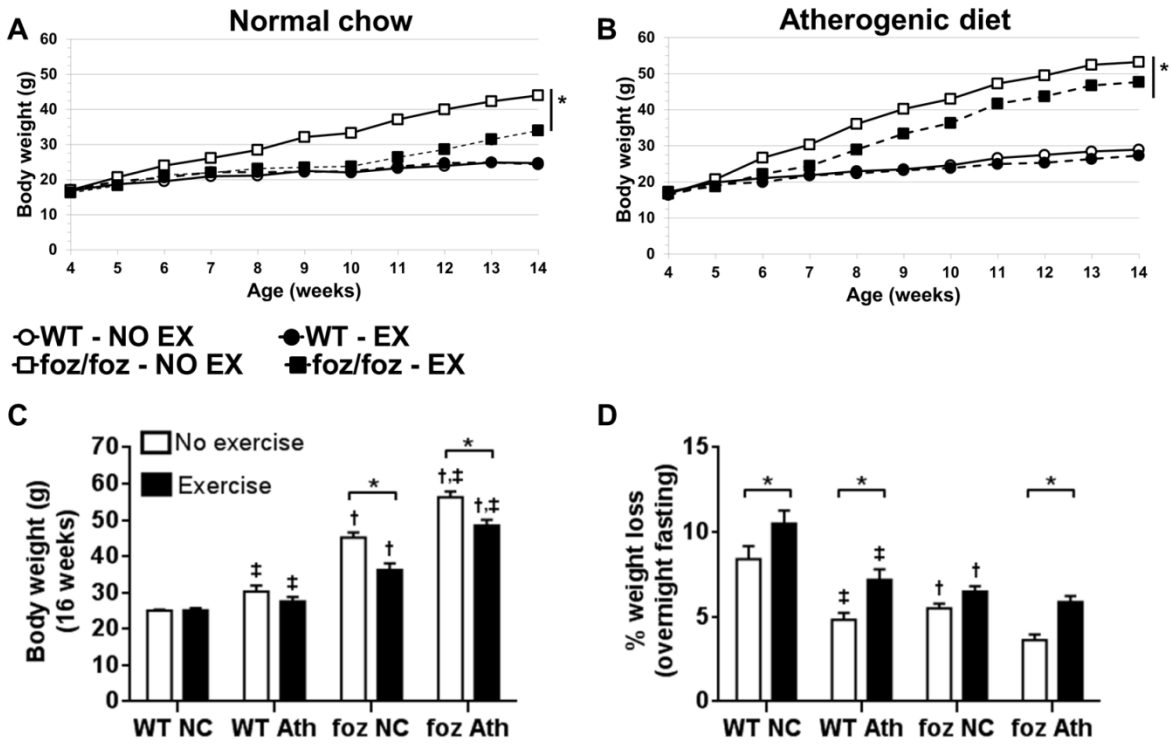

Figure 6.9: Body weight gain is curbed in exercising female *foz/foz* and *WT* mice vs. non-exercising counterparts. (A,B) Exercise prevented diet-induced weight gain in female *WT* mice, irrespective of diet, and also prevented obesity development in chow-fed *foz/foz* mice, but slowed rather than normalized weight gain in atherogenic diet-fed *foz/foz* mice. (C) At 16 weeks, exercise had caused a significant reduction in body weight in *foz/foz* mice. (D) After overnight fasting, weight loss was greater in all exercising groups.
Data are mean ± SEM (n=8/gp).
* $P<0.05$ vs. sedentary control
† $P<0.05$ vs. diet-matched WT (genotype effect); e.g., chow-fed *foz/foz* vs. *WT*
‡ $P<0.05$ vs. genotype-matched control (diet effect) e.g., atherogenic diet-fed vs. chow-fed *WT*

6.4.3 Effects of Exercise on Tissue Weights, Insulin Signal Transduction, and Markers of Adipose Differentiation

Tissue-specific insulin sensitivity was determined by the designated harvest protocol described in Section 2.1.5. Physical activity consistently increased relative gastrocnemius muscle mass, although the increase was significant only in *foz*/*foz* mice (Fig. 6.10A). Likewise, exercise significantly improved muscle AKT phosphorylation in all groups except chow-fed WT; thus post-insulin AKT-phosphorylation as a ratio of basal AKT increased with exercise (Fig. 6.10B).

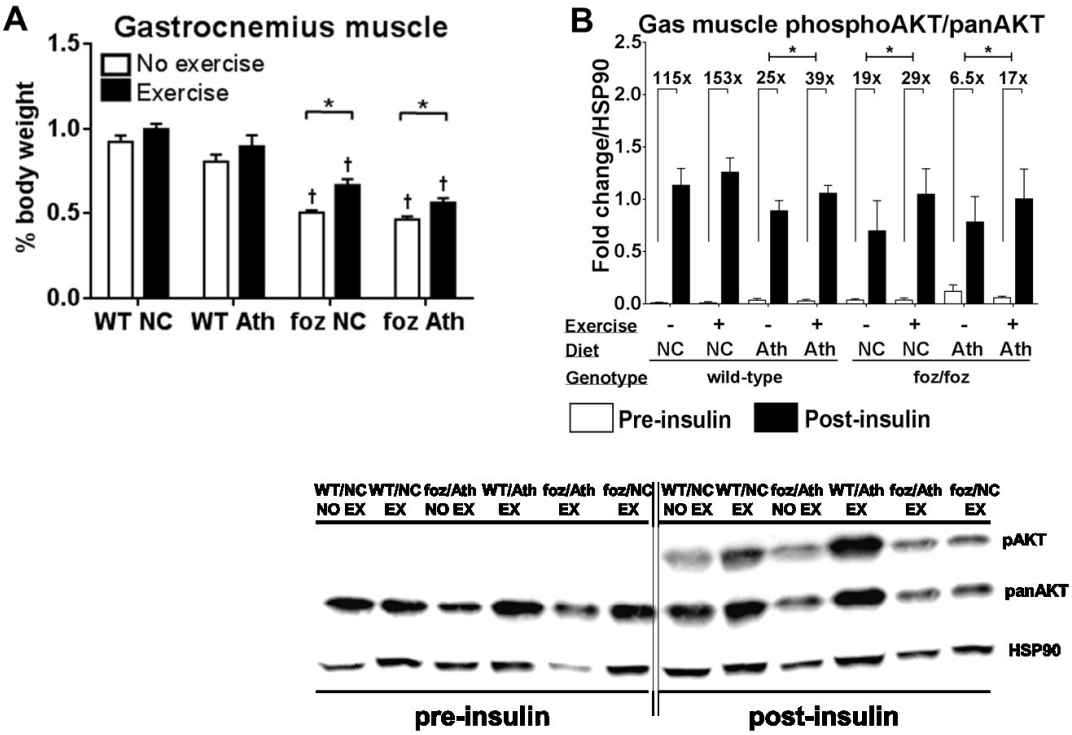

Figure 6.10: Exercise increased insulin-induced AKT phosphorylation in gastrocnemius muscle in all groups of mice. (A) Muscle samples were collected before and (collateral side) 3 minutes after intra-aortic insulin injection. Exercise increased relative muscle mass in *foz/foz* mice on both diets. (B) Insulin-stimulated AKT-phosphorylation (ratio of phospho-AKT / total-AKT) was increased by exercise in muscle of all experimental groups, and this increase was significant in *foz/foz* and atherogenic diet-fed *WT* mice (**P*<0.05 vs. pre-insulin control).
Data are mean ± SEM (n=8/gp).
* *P*<0.05 vs. sedentary control
† *P*<0.05 vs. diet-matched WT (genotype effect); e.g., chow-fed *foz/foz* vs. *WT*
‡ *P*<0.05 vs. genotype-matched control (diet effect) e.g., atherogenic diet-fed vs. chow-fed *WT*

Atherogenic diet and *foz*/*foz* genotype were each associated with increases in visceral (periovarian) and subcutaneous (lumbar) WAT mass (Fig. 6.11). The effects of exercise were most pronounced when absolute adipose weights were considered. Thus exercise markedly reduced visceral adiposity in chow-fed *foz/foz* mice (Fig. 6.11A), and this trend was observed in other groups but was not significant. Subcutaneous adiposity was significantly reduced in atherogenic diet-fed *foz/foz* mice provided with an exercise wheel (Fig. 6.11B). When adipose mass was expressed as a proportion of body weight, exercise did not significantly reduce relative visceral WAT (Fig. 6.11C), but relative

subcutaneous WAT was less in exercising atherogenic diet-fed *foz*/*foz* mice (Fig. 6.11D).

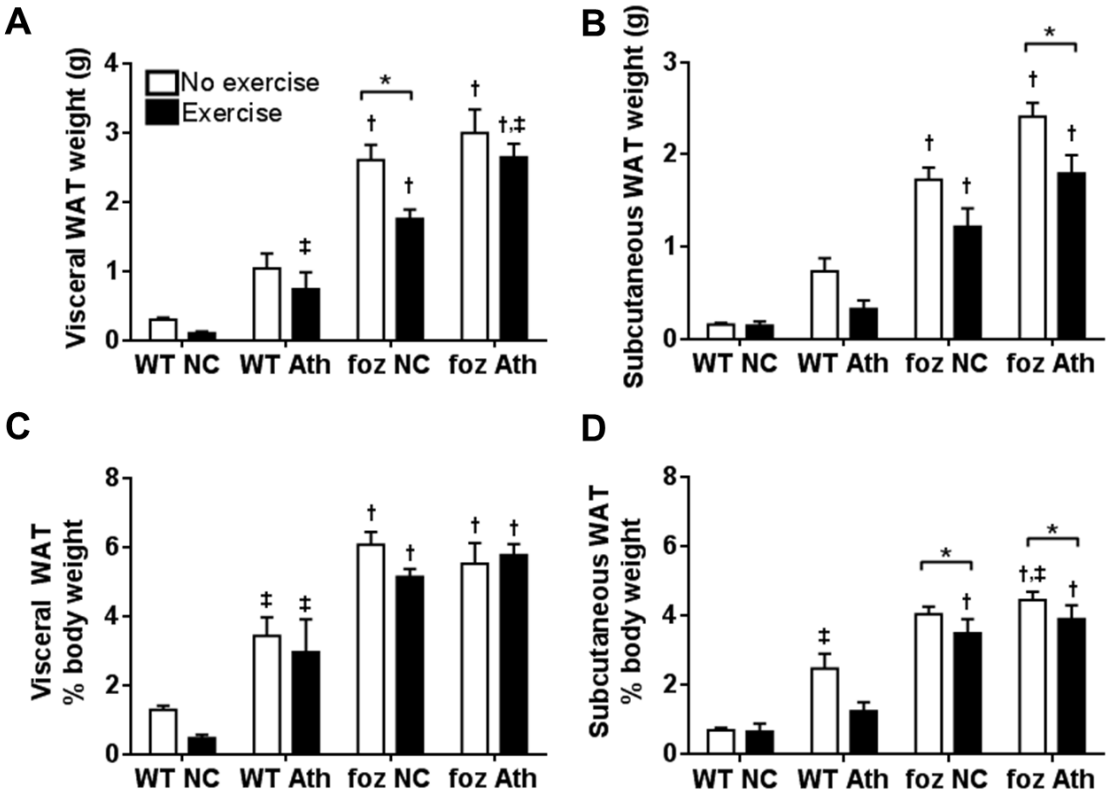

Figure 6.11: Relative and absolute adipose weights in exercising female *foz/foz* and *WT* mice vs. non-exercising counterparts. (A,C) Atherogenic diet and *foz/foz* mutation were associated with increased visceral adipose weight, and the effects of exercise were minimal (if any). The only significant exercise-related reduction in visceral WAT weight gain was in chow-fed *foz/foz* mice. (B,D) Conversely, exercise limited subcutaneous adipose expansion in *foz/foz* mice.
Data are mean ± SEM (n=8/gp).
* $P<0.05$ vs. sedentary control
† $P<0.05$ vs. diet-matched WT (genotype effect); e.g., chow-fed *foz/foz* vs. *WT*
‡ $P<0.05$ vs. genotype-matched control (diet effect) e.g., atherogenic diet-fed vs. chow-fed *WT*

A western-blotting protocol similar to that used in gastrocnemius muscle (Fig. 6.10) was also applied to adipose tissues (see Section 2.3.2) to determine tissue-specific insulin sensitivity in exercising vs. non-exercising mice. Unlike in muscle, exercise failed to enhance AKT-phosphorylation in either visceral or subcutaneous WATs (Fig. 6.12A,B).

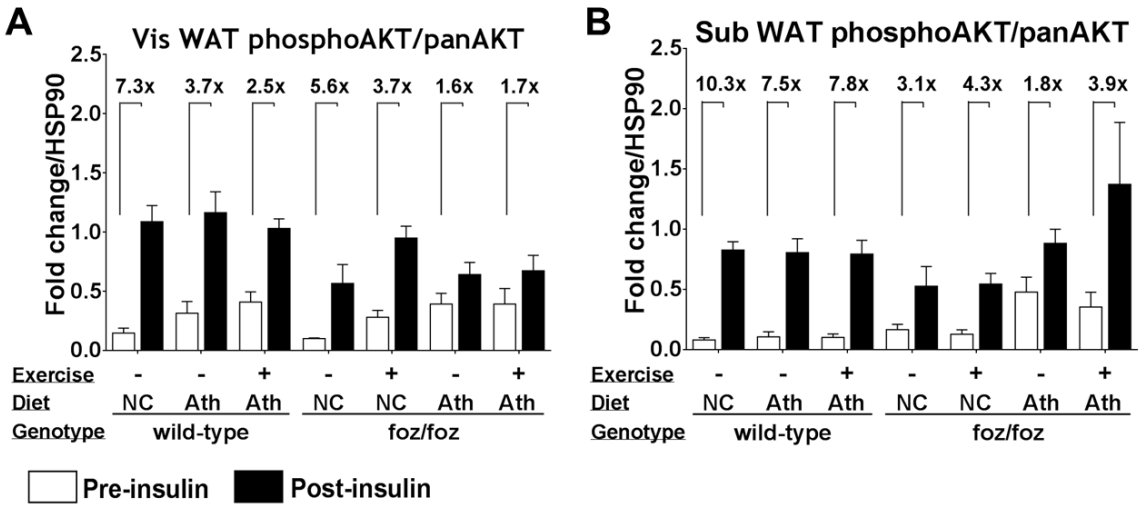

Figure 6.12: Exercise failed to enhance post-insulin AKT phosphorylation in adipose tissue of female *foz/foz* or *WT* mice. Insulin-stimulated AKT-phosphorylation (as the ratio of phospho-AKT / total-AKT) was not altered by exercise in (A) visceral (Vis) or (B) subcutaneous (Sub) WATs.
Data are mean ± SEM (n=8).

In *WT* mice, mRNA levels of *Pparγ* were similar in visceral and subcutaneous WATs and were not altered by exercise. However, in *foz*/*foz* mice, regular exercise consistently increased *Pparγ* mRNA levels in WAT, a change that was highly significant in visceral WAT (Fig. 6.13A). mRNA Levels of *Glut4*, the main insulin-regulated glucose uptake transporter in adipose (see Section 1.3.3), increased in a similar exercise-dependent pattern (Fig. 6.13B). *Prdm16* mRNA expression (see Section 1.2.6) was also higher in subcutaneous than visceral WAT in all groups, and was particularly low in atherogenic diet-fed *foz/foz* mice. Exercise countered this very low expression level of *Prdm16* mRNA in visceral adipose of *foz*/*foz* mice (Fig. 6.13C).

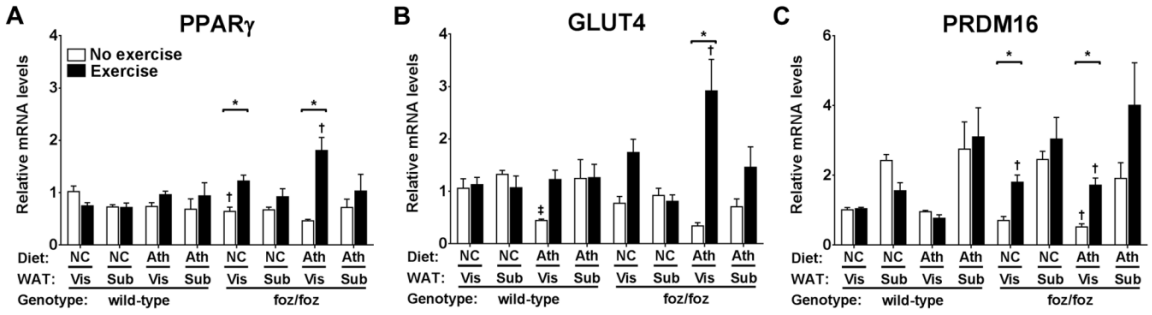

Figure 6.13: Effects of exercise on adipogenic markers in adipose sites of *foz/foz* and *WT* mice. In atherogenic diet-fed *foz/foz* mice, 12 weeks of voluntary exercise increased mRNA expression of (A) *Pparγ*, (B) *Glut4*, and (C) *Prdm16* in WATs.
Data are mean ± SEM (n=8/gp).
* $P<0.05$ vs. sedentary control
† $P<0.05$ vs. diet-matched WT (genotype effect); e.g., chow-fed *foz/foz* vs. *WT*
‡ $P<0.05$ vs. genotype-matched control (diet effect) e.g., atherogenic diet-fed vs. chow-fed *WT*

6.4.4 Effects of Exercise on Glycemic Responses

As explained in Section 6.3, mice were fasted (4 hours) one week before harvesting to measure FBG and glucose tolerance after intraperitoneal glucose injection (2 g/kg body weight). FBG increased with atherogenic dietary feeding and *foz*/*foz* mutation, being highest in atherogenic diet-fed *foz/foz* mice (Fig. 6.14A). Exercise failed to alter fasting hyperglycemia in any group (Fig 5.14A). However, the data for atherogenic diet-fed *foz/foz* mice appeared unduly influenced by 2 animals that developed severe diabetes (Fig. 6.14B).

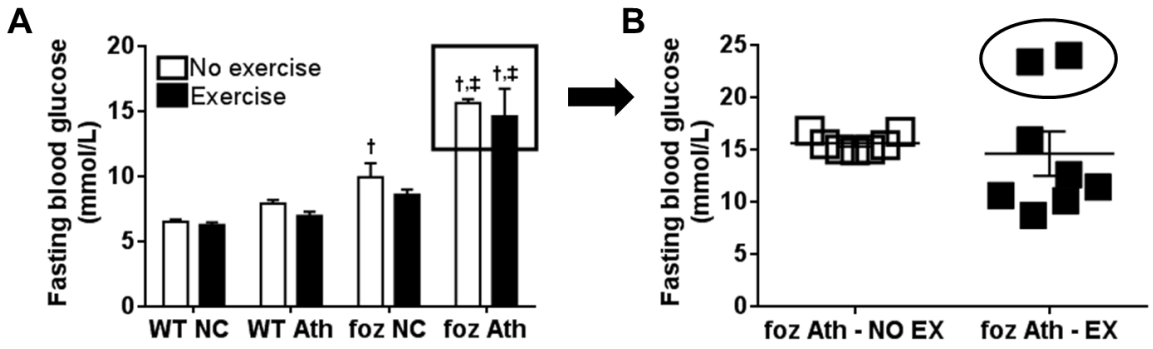

Figure 6.14: Exercise prevented development of diabetes in most, but not all, atherogenic diet-fed female *foz/foz* mice. (A) FBG increased with atherogenic dietary feeding and *foz/foz* mutation; any effects of exercise were not significant. (B) Exercise failed to improve FBG levels in atherogenic diet-fed *foz/foz* mice, largely because of 2 severely diabetic mice (circled). Data are mean ± SEM (n=8/gp).
* $P<0.05$ vs. sedentary control
† $P<0.05$ vs. diet-matched WT (genotype effect); e.g., chow-fed *foz/foz* vs. *WT*
‡ $P<0.05$ vs. genotype-matched control (diet effect) e.g., atherogenic diet-fed vs. chow-fed *WT*

The methodology for IpGTT is given in Section 2.2.1. In chow-fed *WT*, exercise did not alter intraperitoneal glucose tolerance (Fig. 6.15A-C). In chow-fed *foz/foz* mice, the substantial impairment in glucose tolerance was reversed by exercise (Fig. 6.15A,C). A similar (but lesser) response was noted in atherogenic diet-fed *WT* mice (Fig. 6.15B,C). On the other hand, exercise wheel provision had little if any effect on impaired glucose tolerance in atherogenic diet-fed *foz/foz* mice (Fig. 6.15B,C). Closer analysis revealed that this negative result was largely attributable to one cage in which animals were slow to start exercising (no rotations recorded in week 1) and overall use of the wheel was 2.5 weeks less. These are the same 2 mice that developed diabetes (see circled in Fig. 6.14B) and NASH (see later).

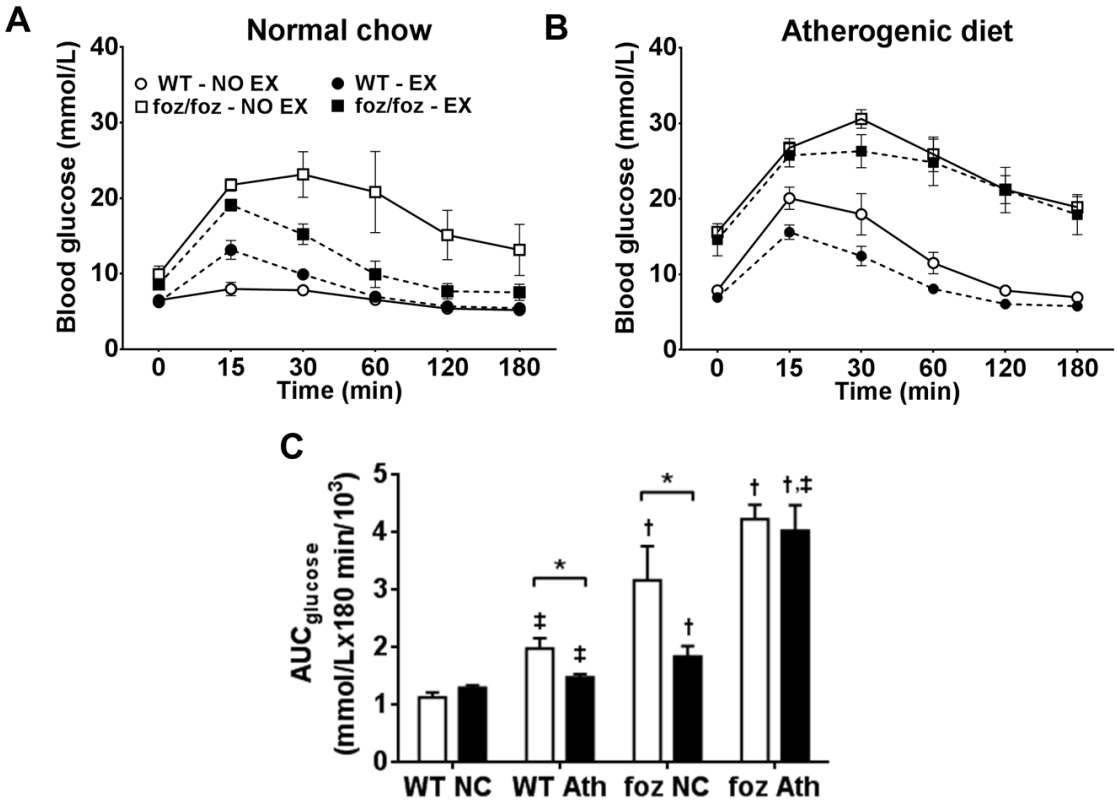

Figure 6.15: Exercise improved intraperitoneal glucose tolerance in chow-fed *foz/foz* and atherogenic diet-fed *WT* mice, but not in atherogenic diet-fed *foz/foz* mice. (A,C) Exercise was associated with a striking improvement in intraperitoneal glucose tolerance in chow-fed *foz/foz* mice, and (B,C) moderate improvement in *WT* mice. (B,C) Glucose tolerance was severely impaired and did not improve with exercise in atherogenic diet-fed *foz/foz* mice, being partially influenced by the 2 diabetic mice (depicted in Fig. 6.14B).
Data are mean ± SEM (n=8/gp).
* $P<0.05$ vs. sedentary control
† $P<0.05$ vs. diet-matched WT (genotype effect); e.g., chow-fed *foz/foz* vs. *WT*
‡ $P<0.05$ vs. genotype-matched control (diet effect) e.g., atherogenic diet-fed vs. chow-fed *WT*

In light of these ambiguous data, we established a small, separate cohort of atherogenic diet-fed *foz/foz* mice (n = 6/gp) and monitored glycemic responses over time (Fig. 6.16).

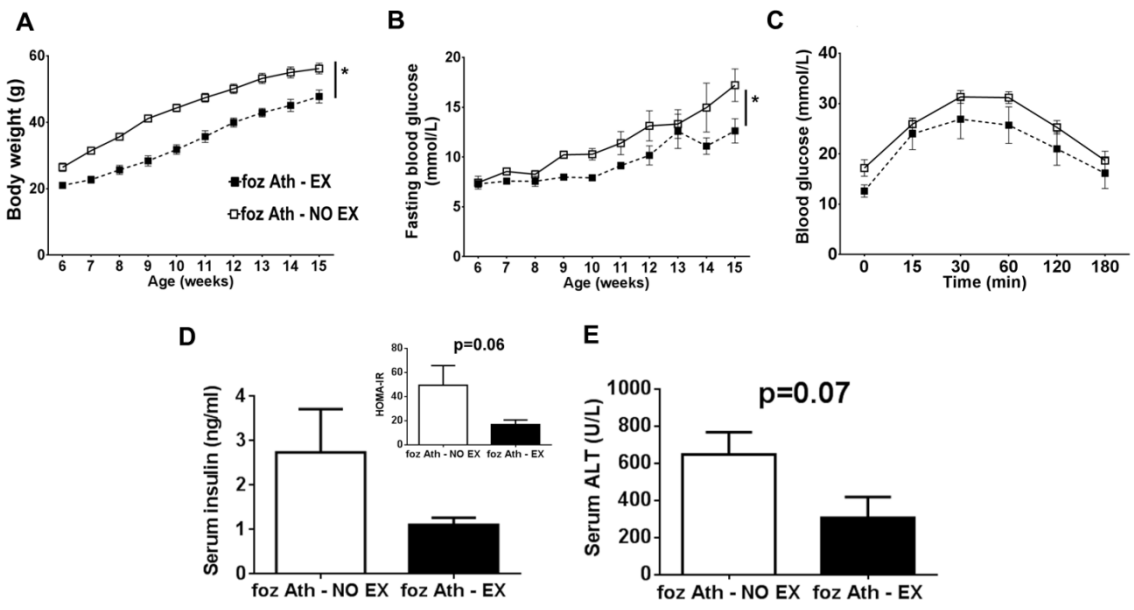

Figure 6.16: A separate cohort of atherogenic diet-fed female *foz/foz* mice with or without an exercise wheel. (A) Similar to the main cohort, exercise significantly delayed weight gain. (B) There was a break-point at ~8 weeks when the non-exercising mice developed significant hyperglycemia. (C) Exercise improved intraperitoneal glucose tolerance and (D) it appeared to delay the increase in fasting blood glucose together with a strong trend in reduction of blood insulin levels (*P*=0.1). (E) Hepatocellular injury marker serum ALT levels tended to be lower in exercising atherogenic diet-fed *foz/foz* mice than in sedentary counterparts.
Data are mean ± SEM (n=8/gp).
* *P*<0.05 vs. sedentary control

The results indicate that substantial increase in FBG following a significant weight gain (Fig. 6.16A) occurs abruptly during the 8th week of atherogenic dietary feeding in non-exercising mice. All animals became prediabetic, and this effect appeared to be delayed in exercising atherogenic diet-fed *foz/foz* mice (Fig. 6.16B). Glucose clearance after intraperitoneal administration in exercising mice was faster than sedentary counterparts (Fig. 6.16C). Serum insulin (Fig. 6.16D) and serum ALT (Fig. 6.16E) levels were less in exercising than in sedentary atherogenic diet-fed *foz/foz* mice.

6.4.5 Effects of Atherogenic Diet, *Alms1* Mutation, and Exercise on Adipose Morphometry and Inflammation

As reviewed in Section 1.4, assessment of adipocyte size is informative about the function or dysfunction of adipose tissue. Although different techniques have been used

for adipose morphometric analyses in the last 20 years, the outcome measures for these analyses have been usually the same: mean adipocyte size and number. There is a lack of strong literature comparing morphometric aspects of different adipose pads. Accordingly, two different adipose tissues, visceral and subcutaneous WATs, were analyzed for detailed adipose morphometry in the current study.

In the present study, atherogenic dietary feeding increased mean adipocyte volume in the visceral compartment of *WT* mice (1.60 vs 0.55 $\mu m^3 \times 10^5$), with similar changes in *foz/foz* mice on both diets (Fig. 6.17A). Exercise significantly increased 1000 μm^2 adipocytes in WT visceral WAT on both diet (Fig. 6.17C). In non-exercising chow-fed *foz/foz* mice, adipocytes >9000 μm^2 comprised the major population; exercise altered this accumulation towards 3000 to 6000 μm^2, although this trend was not significant. In atherogenic diet-fed *foz/foz* mice, exercise failed to alter the size of enlarged visceral adipocytes (Fig. 6.17C). The average volume of subcutaneous adipocytes also increased progressively according to diet and phenotype, the largest median volume being in non-exercising atherogenic diet-fed *foz/foz* mice. Exercise consistently reduced the mean volume of subcutaneous adipocytes in all groups (Fig. 6.17B). Thus, cell size distribution analysis revealed an increase in the subpopulation of small adipocytes in subcutaneous WAT of chow-fed *WT* mice (Fig. 6.17D). A similar trend was found in atherogenic diet-fed *WT* and chow-fed *foz/foz* mice but it was not significant. Exercise strikingly reduced the proportion of hypertrophic large adipocytes in subcutaneous WAT of atherogenic diet-fed *foz/foz* mice (Fig. 6.17D).

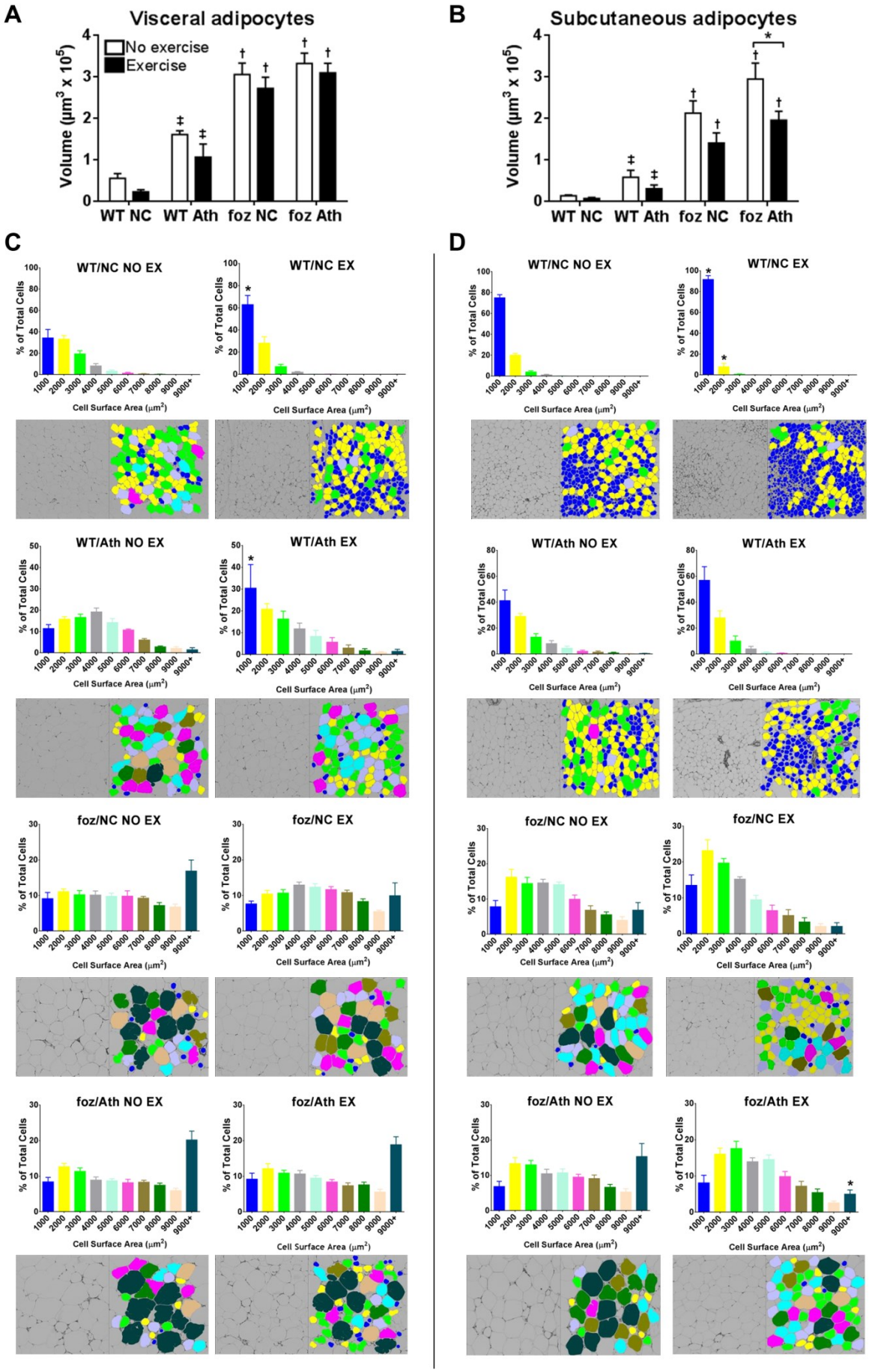
A
Visceral adipocytes
No exercise
Exercise
Volume (µm³ x 10⁵)
WT NC
WT Ath
foz NC
foz Ath
B
Subcutaneous adipocytes
C
D
WT/NC NO EX
WT/NC EX
WT/Ath NO EX
WT/Ath EX
foz/NC NO EX
foz/NC EX
foz/Ath NO EX
foz/Ath EX
% of Total Cells
Cell Surface Area (µm²)

Figure 6.17: Effects of exercise on morphometry of visceral and subcutaneous adipose of *foz/foz* and *WT* mice on chow or atherogenic diet. (A,B) Morphometry performed on H&E-stained adipose sections (160x magnification) showed that average adipocyte volume in both visceral and subcutaneous compartments increased with atherogenic diet and *foz/foz* mutation. (A) In visceral adipose, any effect of exercise was minor and not significant on adipocyte volume despite a consistent trend of reduction was found in exercising (EX) mice. (B) The effect of exercise on subcutaneous adipocytes was more pronounced, and average adipocyte volume diminished in all groups, being significant in atherogenic diet-fed *foz/foz* mice. (A,D) Adipocyte size distribution was assessed for visceral and subcutaneous WATs. (C) Exercise caused a significant increase in very small adipocytes (1000 μm^2 [elsewhere small is $\leq$ 4000 μm^2]) in *WT* mice visceral WAT, irrespective of diet. In chow-fed *foz*/*foz* mice, adipocytes between 3000 to 6000 μm^2 sizes were a major cell population in visceral WAT. Adipocytes > 9000 μm^2 appeared predominant in mice without an exercise wheel, although this analysis did not reach significance. Exercise did not alter adipocyte size distribution in visceral WAT of atherogenic diet-fed *foz/foz* mice. (D) A similar but more pronounced pattern was noted for adipocyte size distribution in subcutaneous WAT, but in exercising chow-fed *WT* mice, majority of adipocytes were between 1000 and 2000 μm^2 ($P < 0.05$). There was a strong trend for moderate-sized adipocyte accumulation in chow-fed *foz/foz* subcutaneous WAT, and this alteration was significant in atherogenic diet-fed *foz/foz* mice.
Data are mean ± SEM (n=8/gp).
* $P<0.05$ vs. sedentary control
† $P<0.05$ vs. diet-matched WT (genotype effect); e.g., chow-fed *foz/foz* vs. *WT*
‡ $P<0.05$ vs. genotype-matched control (diet effect) e.g., atherogenic diet-fed vs. chow-fed *WT*

In *WT* mice on either diet, there was no change in mRNA expression of the macrophage marker, *Cd68*. Conversely, *Cd68* mRNA was abundant in visceral (and to a lesser extent subcutaneous) adipose of *foz*/*foz* mice, irrespective of diet. Exercise at least partially reversed these effects (Fig. 6.18A). Thus, levels of *Cd11b* mRNA, a marker of pro-inflammatory immune cells (Section 1.5.6.1), were higher in non-exercising *foz*/*foz* mice adipose depots, except in chow-fed subcutaneous WAT (Fig. 6.18B); exercise decreased *Cd11b* transcript levels in both adipose sites. Levels of *Mcp1* mRNA expression were likewise increased in *foz*/*foz* adipose, particularly in the visceral depot; this increase in *Mcp1* mRNA expression was limited by exercise (Fig. 6.18C).

A detailed review about adipose crown-like structures (CLSs) is given in Section 1.5. In Chapter 4, insights with the mechanisms of formation of this multicellular unit are provided in the Results Section (see Section 4.4.4). The contiguous clumps of macrophages abutting a small adipocyte that comprise CLSs (400x magnification; Fig. 6.18E) are regarded as a marker of WAT inflammation (230). As established by number

of CLSs (normalized to 100 adipocytes), visceral WAT was highly inflamed in non-exercising atherogenic diet-fed *foz/foz* mice (Fig. 6.18D,F); exercise decreased formation of CLSs at this site. Moderate inflammation was also observed in the subcutaneous adipose of atherogenic diet-fed *foz/foz* mice (Fig. 6.18D,F), and at this site exercise also significantly diminished macrophage infiltration.

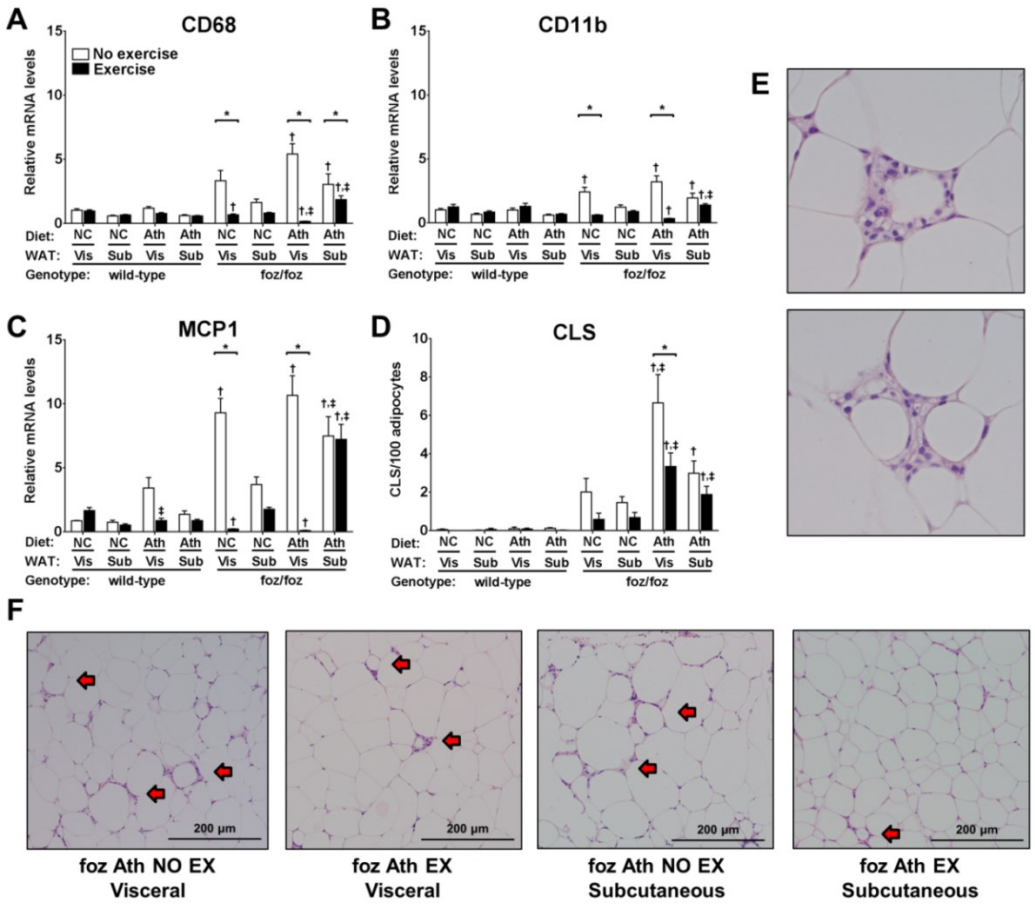

Figure 6.18: Effects of exercise on adipose inflammatory recruitment and formation of CLS in *foz/foz* and *WT* mice. (A) Exercise ameliorated the effects of atherogenic feeding on macrophage infiltration. In *foz/foz* mice, particularly in those fed atherogenic diet, *Cd68* mRNA levels were high. This increase was more pronounced in visceral (Vis) than subcutaneous (Sub) WAT. A similar profile was found for (B) *Cd11b* and (C) *Mcp1* mRNA expression. (D) The numbers of CLSs (normalized to 100 adipocytes), (E) inflammatory (F4/80 positive) macrophages surrounding an adipocyte (400x magnification), were consistent with the other inflammatory markers, (F) being highly abundant in inflamed visceral and subcutaneous WATs of *foz/foz* mice (160x magnification). (D,F) Exercise reversed the effect of atherogenic dietary feeding and *foz/foz* genotype on CLSs in both WATs.
Data are mean ± SEM (n=8/gp).
* $P<0.05$ vs. sedentary control
† $P<0.05$ vs. diet-matched WT (genotype effect); e.g., chow-fed *foz/foz* vs. *WT*
‡ $P<0.05$ vs. genotype-matched control (diet effect) e.g., atherogenic diet-fed vs. chow-fed *WT*

6.4.6 Exercise Delays or Prevents Development of NASH and Liver Fibrosis

As previously reported, liver histology was affected both by atherogenic dietary feeding and appetite defect (*foz/foz* genotype) (232). Thus, chow-fed *WT* mice had normal liver histology (Table 6.2; 160x magnification, Fig. 6.19A), whereas atherogenic dietary feeding produced minor steatosis in 2 of 8 *WT* mice. None of 8 exercising atherogenic diet-fed *WT* mice developed steatosis. In chow-fed *foz*/*foz* mice, numerous small fat droplets were evident in hepatocytes with minor liver inflammation; exercise wheel provision prevented both steatosis and inflammatory recruitment in this group (Table 6.2; Fig. 6.19A). As expected from previous studies (339), atherogenic diet-fed *foz*/*foz* mice showed hepatomegaly with extensive steatosis, substantial inflammation and ballooned hepatocytes. The resultant median NAS of 5 (range 4-6) was comprised of 4 instances of definite NASH (score 5,6), and 3 of borderline NASH (score 4) (Table 6.2). Exercise failed to prevent development of hepatomegaly in atherogenic diet-fed *foz*/*foz* mice (Fig. 6.19B), and 3 of 8 mice provided with exercise wheel still developed unequivocal NASH, but this included the 2 diabetic mice depicted in Fig. 6.14B. Of the remainder, 2 developed borderline NASH and 3 showed only simple steatosis (Table 6.2, Fig. 6.19A).

TABLE 6.2
Effects of exercise on liver histology in *foz/foz* and *WT* mice fed chow or atherogenic diet

			n	Steatosis	Inflammation	Ballooning	NAS[#]	Designation[♯]
Chow Diet	*WT*	NO EX	8	0 (-)	0 (-)	0 (-)	0 (-)	Normal (8)
		EX	8	0 (-)	0 (-)	0 (-)	0 (-)	Normal (8)
	foz/foz	NO EX	6	0.3 (0-1)	0.17 (0-1)	0 (-)	0.4 (0-1)	Normal (4) SS (1) Borderline NASH (1)
		EX	8	0 (-)	0 (-)	0 (-)	0 (-)	Normal (8)
Ath Diet	*WT*	NO EX	8	0.25 (0-1)	0 (-)	0 (-)	0.25 (0-1)	Normal (6) SS (2)
		EX	8	0 (-)	0 (-)	0 (-)	0 (-)	Normal (8)
	foz/foz	NO EX	7	2.42 (2-3)[†,‡]	1.42 (1-2)[†,‡]	1.14 (1-2)[†,‡]	5 (4-6)[†,‡]	Borderline NASH (3) Definite NASH (4)
		EX	8	2 (1-3)[†,‡]	1.12 (1-2)[†,‡]	0.75 (0-2)[†,‡,*]	3.87 (2-6)[†,‡,*]	SS (3) Borderline NASH (2) Definite NASH (3)[¶]

[♯]Expert pathologist scoring (MMY) of global liver pathology as normal, simple steatosis (SS), borderline NASH or definite NASH (338). [¶]Includes the 2 mice that developed diabetes (See Fig. 6.14B, circled) as discussed in Results. Data are median (range). [†]P<0.05 (vs. diet-matched control), [‡]P<0.05 (vs. genotype-matched control), [*]P<0.05 (vs. sedentary control) [#]NAS - NAFLD activity score (steatosis + inflammation + ballooning). SS for simple steatosis.

Development of substantial liver fibrosis in atherogenic diet-fed *foz/foz* mice after 24 weeks has been reported by the host lab several times (339, 450). Fibrosis is already evident at 16 weeks, as shown here by areas stained blue for collagen with Masson's trichrome (Fig. 6.19D). By image analysis (explained in Section 2.2.3), fibrosis was significantly less in atherogenic diet-fed *foz/foz* mice provided with an exercise wheel than in non-exercising counterparts (Fig. 6.19E,F). The effects of exercise in ameliorating liver fibrosis were confirmed by decreased collagen 1A mRNA (not shown) and protein (Fig. 6.19G), and lower expression of alpha smooth muscle actin (α-SMA) (Fig. 6.19H).

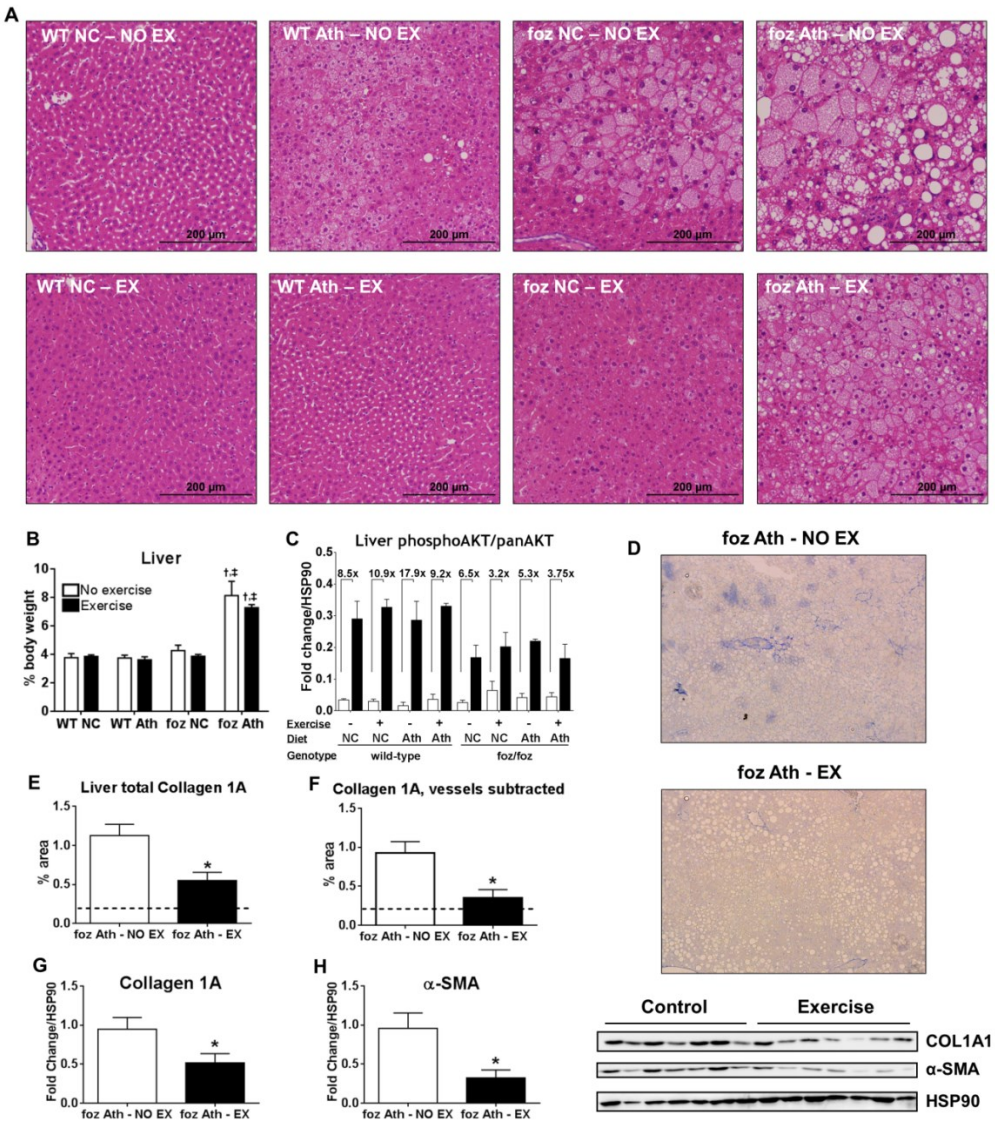

Figure 6.19: Effects of exercise on liver histology, insulin signalling and liver fibrosis in *foz/foz* and *WT* mice fed chow or atherogenic diet. (A) H&E-stained sections (160x magnification). Atherogenic dietary feeding caused steatosis in non-exercising (NO EX) *WT* mice, which was fully reversed by exercise. In *foz/foz* mice, steatosis is evident with chow diet and reversed by exercise, but NASH is present with atherogenic diet. In this example, exercise (EX) prevented NASH but simple steatosis is still present (see Table 6.2 for group effects). (B) Exercise failed to prevent hepatomegaly (expressed here as relative to body weight) in atherogenic diet-fed *foz/foz* mice, (C) or to influence insulin-stimulated AKT-phosphorylation in liver. (D-F) Exercise reduced abundance of collagen 1 positive tissue in atherogenic diet-fed *foz/foz* mice in comparison to sedentary counterparts. Correspondingly, liver fibrosis markers (G) collagen 1A and (H) α-SMA protein expression were lower in exercising atherogenic diet-fed *foz/foz* mice liver compared to non-exercising mice.
Data are mean ± SEM (n=8/gp).
* $P<0.05$ vs. sedentary control
† $P<0.05$ vs. diet-matched WT (genotype effect); e.g., chow-fed *foz/foz* vs. *WT*
‡ $P<0.05$ vs. genotype-matched control (diet effect) e.g., atherogenic diet-fed vs. chow-fed *WT*

6.5 Discussion

Metabolic obesity results from interactions between lifestyle (environmental) factors that favour energy excess and a genetically predisposed host. Tissue inflammation occurs in diabetes complications and in the fatty liver with NASH, two clinically important outcomes of metabolic obesity. Adipose inflammation invariably accompanies these disorders. In the present work, we tested whether exercise has beneficial effects on the complications of metabolic obesity in a mouse model that resembles the human condition by genetic predisposition to obesity and diabetes, and an environmental challenge (atherogenic diet).

In addition to metabolic outcomes, the results of the present experiments provide systematic data on changes in physical activity levels of mice according to gender and age. By monitoring weekly weight gain, food intake, and exercise levels, the present data contribute to understanding of the complicated relationships between body weight and physical activity levels. The first new finding was that exercise increased energy turnover sufficient to prevent both diet-induced and genetically-driven weight gain, but was less effective when these factors interacted. Thus, in atherogenic diet-fed male *foz/foz* mice, exercise slowed the rate of weight gain, but at an apparent "set point", use of the wheel declined and weight gain then accelerated. In the female cohort, two

individual animals that were slow to adopt regular exercise discontinued such use at an earlier time than their 6 littermates. It is therefore of interest to observe that these 2 mice were the only ones to develop established diabetes by age 16 weeks. Despite this limitation of the voluntary exercise approach, the combined use of intraperitoneal glucose tolerance and tissue-specific AKT-phosphorylation after insulin administration, together with static measurements of serum insulin in the sub-study, provide a clear picture of exercise-induced improvements in energy homeostasis and metabolic control.

Food intake in the exercising *foz/foz* mice was lower than for their non-exercising counterparts, but remained higher than for exercising *WT* mice (which consumed more than their non-exercising counterparts). Although *foz/foz* mice displayed reduced food consumption with exercise, weight gain in these animals still exceeded non-exercising counterparts. Considering these findings, it is not possible to clarify whether the slowing of weight gain was a direct result of exercise, or secondary to the effect of reduced food intake. A tentative conclusion is that exercise can partly reset appetite control in *foz/foz* mice, but to clarify this ambiguity, a more detailed study of neurohormonal appetite regulation would be required and this was beyond the scope of the present research. On the other hand, the changes in metabolic indices and reduction of liver fat in exercising *WT* mice are clearly not due to changes in food intake as, this increased. By analogy, we think the improvements in metabolic regulation in exercising *foz/foz* mice are mostly attributable to increased physical activity. Nonetheless, the additional benefit of calorie restriction (to mitigate overnutrition) would assist exercise effects in amelioration of metabolic indices.

Energy surplus requires WAT remodelling (see Section 1.4.5-1.4.6) (451, 452). Facing positive energy imbalance, adipocytes become lipid-engorged, and exhibit reduced glucose uptake and increased chemokine/cytokine secretion (289, 336). Conversely, healthy adipose contains a higher proportion of smaller adipocytes and

shows no inflammation (453, 454). In the present study, both atherogenic diet and *foz/foz* background were associated with increased adipocyte volume, and this was apparent in both the visceral and subcutaneous compartments. However, more detailed morphometric investigation showed that the size distribution of adipocytes differed: the percentage of cells between 2000 and 6000 μm^2 (small to medium) was higher in exercising *foz/foz* mice, even though the average adipocyte volume (assuming a spherical shape) did not change. Lipid-laden large adipocytes produce more pro-inflammatory chemokines and cytokines which regulate cellular trafficking (289). It was therefore not surprising that atherogenic diet-fed *foz/foz* mice showed abundant immune cell infiltration, particularly into visceral WAT; exercise reversed this effect, in association with lowered MCP1 production. As discussed in the previous Chapter, most of the macrophages that infiltrate adipose, assemble around very small degenerating (dying/injured) adipocytes in CLSs (230). In parallel with the morphometric and molecular findings, exercise substantially reduced CLS numbers in both visceral and subcutaneous WATs of atherogenic diet-fed *foz/foz* mice. An apparently similar effect in chow-fed *foz/foz* was not significant.

Improved muscle insulin sensitivity in exercising mice clearly contributed to greater energy consumption, as evident by higher overnight fasting weight loss; this reflects basal energy utilisation to some extent. Active muscle cells oxidize more energy and thereby diminish the systemic lipid burden in exercising mice. This energy is mostly provided by adipocytes because, for example, the increase of circulating adrenalin levels before and during exercise activates HSL in adipose tissues. This increases lipolysis and energy release (in the form of FFAs as nutrients) from adipocytes. Activation of the sympathetic nervous system may improve adipose metabolism as well as muscle. Nevertheless, as discussed next, direct effects of exercise on adipose tissue are possible and merit further investigation.

It is most likely that exercise confers beneficial effects on adipose through two different ways. Firstly, muscle inefficacy (or under-use) associated with inactivity together with over-eating creates a considerable burden on adipose sites for energy storage. Conversely, increased muscle activity reduces the lipid burden on adipocytes by clearing energy molecules (e.g., glucose) from the circulation and increasing metabolism (discussed later). This is an indirect effect of exercise on adipose metabolism. In addition to this, another secondary effect of exercise improves adipose function, "muscle-derived cytokines". Active/healthier myocytes express anti-inflammatory and insulin sensitizing myokines (such as Irisin) that improve adipocyte metabolism (455). Investigation of these muscle-derived factors is a relatively new subject in medical and sports sciences suggesting a more important role for exercise than simply balancing energy expenditure. There is also increasing evidence that muscle can release other important "myokines" into the circulation, such as IL10 and IL6 (456). Protein isolates of the muscle tissues obtained here will be useful in the future investigations to study myokine expression of exercising vs. sedentary skeletal muscle tissue.

Whether the effects of exercise on adipose were all indirect or not, this study provides clear evidence that exercise improves adipose structure and differentiation. Here this was indicated by changes in adipocyte size, and expression of PPARγ, the transcription factor which regulates glucose uptake and stimulates triglyceride storage. There was also a corresponding increase of *Glut4* mRNA, and *Prdm16*, a transcription co-regulator that controls the myocyte/brown-beige adipocyte differentiation switch that induces brown fat-like gene program (reviewed in Section 1.2.6). Bruce Spiegelman and his colleagues has reviewed that exercise increases recruitment of beige adipocytes in WAT (455), and *Prdm16*$^{-/-}$ mice develop profound visceral obesity (86). This reflects the important role that PRDM16-driven beige adipocytes plays in whole body energy

expenditure, since these cells are "mitochondria-rich" cells. In our project, we showed that suppression of this master regulator of adipocyte browning increased in concert with the adipogenic factor PPARγ and glucose transporter GLUT4.

Exercise-mediated improvement of adipocyte function has important consequences for the development of other metabolic disorders, such as NAFLD. This is because WAT sites become more responsive to circulating glucose and lipids, thereby reducing ectopic lipid deposition into liver and other cell types (457). Exercise has been shown to resolve steatosis in overweight humans with NAFLD (446, 458), and this effect was reproduced in exercising atherogenic diet-fed *WT* and chow-fed *foz/foz* mice. The exercise-mediated suppression of adipose inflammation in *foz/foz* mice was also associated with other striking improvements in liver histology, including less inflammation and injury. The exceptions were two mice that failed to take up exercise early, discontinued it prematurely and developed diabetes (resembling the conundrum of lifestyle management of metabolic disorders in clinical practice). However, exercise consistently lowered liver fibrosis in atherogenic diet-fed *foz/foz* mice. In a transectional study, moderately vigorous exercise (but not lesser forms) was associated with improved liver indices and less severe liver fibrosis, although the mechanism was not explored (447). The present study in a metabolic syndrome model of NASH with genetic predisposition to diabetes should prove suitable to clarify this protective mechanism. The possibilities include a direct relationship to reduced hepatocyte injury (by lipotoxicity) and liver inflammation, stabilisation of hepatic stellate cells (shown by decreased α-SMA expression) and decreased levels of pro-fibrogenic growth factors and other humoral mediators as explained by the host lab (339).

In conclusion, these data show that moderately vigorous exercise suppresses adipose inflammation in mice with disordered appetite control. Exercise prevented excessive weight gain and improved adipose differentiation in atherogenic diet-fed *WT* as well as

chow-fed *foz/foz* mice, and slowed weight gain in atherogenic diet-fed *foz/foz* mice in association with an increased proportion of small-medium sized adipocytes. Exercise enhanced insulin signalling in muscle, but not in liver or adipose. Even in atherogenic diet-fed *foz/foz* mice, exercise suppressed the otherwise abundant CLSs of macrophages and inflammatory transcripts, particularly in visceral but also in subcutaneous WAT. In association with prevention of diabetes, exercise reduced steatosis, improved hepatocyte ballooning, liver inflammation (less NASH) and fibrosis in atherogenic diet-fed *foz/foz* mice. Thus, in appetite-dysregulated mice fed an energy-dense diet, exercise improved muscle insulin sensitivity to delay onset of diabetes, maintain adipose function, reduce adipose inflammation and ameliorate NASH and hepatic fibrosis, the important liver complications of obesity and diabetes. In addition to the benefits of lifestyle modification for prevention and treatment of pre-diabetes and significant liver disease, these findings have implications for drug targets that could lead to similar benefits in non-exercising overweight humans. One of these, an FXR agonist, was explored in the previous Chapter.

CHAPTER 7

CHAPTER 7: Final Discussion

7.1 Persistent adipose inflammation is associated with the development of fatty liver disease

The overall aim of the research compiled into this thesis was to characterize the developmental pattern of persistent adipose inflammation and explore its relationship with metabolic disorders such as insulin resistance, T2D, hypoadiponectemia, and more specifically, fatty liver disease. Each Chapter has focused on this subject from a different point of view and discussed the results pertinent to that aspect. The major findings will be recapitulated and summarized in the present Chapter, with a perspective on how they influence thinking in the field and address future research directions.

Chapter 3 focused on the age-dependent development of obesity in mice with an appetite defect (*foz/foz*) compared to *WT* mice. The results show that the impact of such factors as *foz/foz* genotype (dysregulated appetite) and atherogenic dietary intake differ quantitatively on body weight gain. Further, the interaction between these two factors clearly worsens the obesity phenotype. Another important outcome from Chapter 3 was that adipose tissues from different parts of the body are not identical in their response to "obesification". Chapter 5 and 6 contributed further to this subject by showing that not only the pattern of weight gain, but also adipocyte functions and inflammatory phenotypes differ between different adipose compartments. In addition, Chapter 6 provided important new data about connections between increased physical activity (exercise), improved adipose function (which is linked to muscle function), and subsequent amelioration of metabolic indices and fatty liver disease.

Chapter 4 provided a more detailed insight into adipose morphometry and inflammatory recruitment. The key finding was the strong footprint of adipose

morphology in relation to inflammatory response; the latter includes TLR9 signalling (addressed in Chapter 4), and macrophage infiltration in adipose tissue. Chapter 5 brought this concept one step further by determining the phenotype of macrophages in dysfunctional vs. healthy adipose tissue. Obeticholic acid (6-ECDCA), which is a synthetic FXR agonist as well as an anti-obesogenic agent, was studied in this Chapter in an attempt to determine whether cholesterol-loading is relevant for adipose inflammatory recruitment.

7.1.1 Regional Differences Exist in White Adipose Tissues

As detailed in Chapter 1, adipose tissues from different parts of the body can differ in ontogenetic, structural and functional characteristics. This diversity affects the obesity phenotype (unhealthy vs. metabolically healthy). The sections in Chapter 1 that point to these differences are listed in Table 7.1.

Table 7
Sections outlining differences of adipose tissues.

Title		Section
The Origins of Adipose Tissue		1.2.2
Terminal Differentiation of Preadipocytes		1.2.4.3
Adipose Structural Characteristics and Functional Differences		1.2.5
Brown vs. Beige Adipocytes		1.2.6.1
Subcutaneous vs. Visceral Adiposity: An Ergonomic Issue		1.2.7
Relationship of Adipocyte Size to Function		1.4.7
Vascularization in Expanding Adipose Tissues		1.5.1
Dépôt-Specific Differences in Adipose Vascularization		1.5.1.1

In 2006, André Tchernof and his colleagues published their work investigating subcutaneous and visceral WATs in a large cohort of women (459). They found that adipocytes in subcutaneous WAT were larger compared to visceral cells. Moreover, subcutaneous WAT showed higher lipoprotein lipase activity and lipolysis rates than the visceral compartment. Interestingly, visceral WAT was significantly more sensitive to

lipolytic stimuli (e.g., forskolin, dibutyryl cAMP) than subcutaneous WAT. In another study, Tamara Tchkonia and her colleagues investigated preadipocytes from subcutaneous and visceral WATs of men and women (39). Preadipocytes from the latter compartment displayed less expression of adipogenic factors, less lipid accumulation, and higher TNFα-induced apoptosis. Although the reason is not clear, several other studies have also described how visceral adipose tissue is predisposed to develop inflammatory recruitment compared to subcutaneous dépôts. As stated in Section 1.4, visceral adiposity (visceral obesity) is central to the development of the unhealthy obesity phenotype. In fact, central obesity (the anthropometric manifestation of expanded visceral WAT) is a definitional component of metabolic syndrome as defined by the International Diabetes Federation (460).

The variation in function and size of fat dépôts in mice is analogous to that of in humans; in fact, studies of adipose tissue differences have usually been reported first in mouse models of obesity. Epidemiological studies have shown that accumulation of visceral fat in mice associates with the development of dyslipidemia, T2D, hypoadiponectemia, and even obesity-related cancers. Conversely, accumulation of subcutaneous WAT associates with more optimal (whole body) insulin sensitivity and lower risk of developing metabolic comorbidities (76). One factor that determines the differential deposition of fat is simply body ergonomy (see Section 1.2.7). Some adipose compartments are encaged around or within internal organs and inflexible tissues; an example is mesenteric fat. On the other hand, over-expansion of some adipose tissues can impair body posture and make it harder to move. When this is the case, feeding and survival in nature would be a problem for a mouse; dorsal (interscapular) fat is an example. The most flexible "organ" for storage is under the skin, as in subcutaneous lumbar WAT. In this context, it was not surprising to find lumbar WAT adiposity exceeded that of mesenteric and dorsal WATs during

development of obesity in atherogenic diet-fed *foz/foz* mice (female NOD.B10; see Chapter 3 for details) (Fig. 7.1). Surprisingly, however, we found similar levels of adiposity in Pov compared to lumbar WAT, especially by 12 weeks of age. As discussed in Section 1.2.2, Pov WAT is a visceral compartment that shows developmental and structural characteristics that are similar to other visceral depots. Despite this, in the present study, Pov WAT mass increased as much as lumbar WAT by 12 weeks of age (Fig. 7.1). This may be because ergonomic limitation is less for Pov WAT expansion than for its mesenteric visceral compartment.

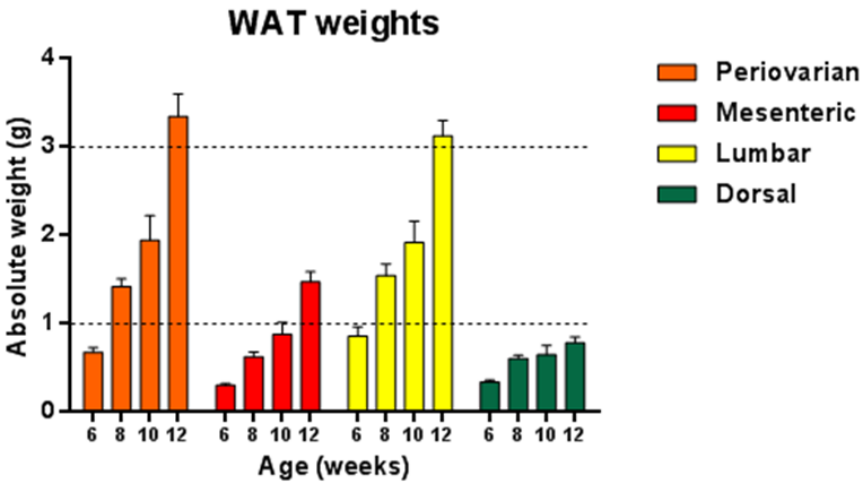

Figure 7.1: Varying rates of WAT expansion during development of obesity in atherogenic diet-fed female *foz/foz* NOD.B10 mice.

In the exercise intervention study (Chapter 6), we used mice with similar properties to those in Chapter 3 (female, NOD.B10, *foz/foz* vs. *WT* mice). The main difference was that these mice had developed to young adulthood (16 week old), and half the cohort was introduced to an exercise wheel early in life (at weaning). At 16 weeks of age, all *foz/foz* and *WT* mice, whether fed atherogenic diet or chow, showed greater Pov than lumbar WAT mass (Fig. 6.11). When considered with previous findings, we conclude

that Pov WAT shows a higher adiposity rate than lumbar until the end of early development (16 weeks of age).

As discussed later in this Section, inflammation at 16 weeks of age was already significant and substantially higher in Pov WAT than in lumbar WAT in atherogenic diet-fed *foz/foz* mice. By 28 weeks of age, though, atherogenic diet-fed *foz/foz* mice showed less Pov than lumbar WAT mass (Chapter 5; Fig. 5.9). We anticipate that in atherogenic diet-fed *foz/foz* mice, Pov WAT mass reached its peak weight between 16 and 20 weeks of age, and then started to decline at the time inflammation became persistent. The reason for that may be persistently (long-lasting) inflammation in adipose tissue reduced its capability to store ingested lipids. Interestingly, mesenteric WAT mass did not change much from 12 to 28 weeks of age, whereas lumbar adiposity showed a limited but increasing trend of expansion (Fig. 7.1, Fig. 5.9).

The evolutionary program as well as the molecular mechanisms that determine differential fat deposition remains unclear. We believe that clarifying this issue would be helpful to understand, and perhaps prevent, ectopic lipid partitioning into other organs, such as liver which was a focus of the present studies. Although some studies have attempted to identify the origins of lipids in hepatic steatosis, there is still a dearth of data to clarify whether hepatic lipid partitioning occurs from "older" fats escaped from inflamed and dysfunctional adipose tissues or from new fat synthesized in the liver (lipogenesis) from ingested carbohydrate and FAs. In the present study, liver weight was ~3.9 g in atherogenic diet-fed *foz/foz* mice (female NOD.B10) at 12 weeks of age (Fig. 7.2A). It increased to ~4.4 g at 16 weeks of age, and ~7.2 g at 28 weeks of age. Simple calculations reveal that liver weight increased ~0.5 g from 12 to 16 weeks of age, which equates to a gain of 0.125 g per week. From 16 to 28 weeks, liver weight increase was ~2.8 g, an average increase of 0.24 g weight gain per week. As seen in Figure 7.2A, liver weight gain accelerated in atherogenic diet-fed *foz/foz* mice when the

Pov WAT weight gain declined. Meanwhile, Pov WAT adiposity exhibited an increasing trend in atherogenic diet-fed *WT* mice, and consequently, liver was protected from developing hepatomegaly (a surrogate marker of steatosis) (Fig. 7.2A). This provides compelling evidence that hepatic steatosis increases when the capacity of adipose tissues, especially visceral WAT, is less well equipped to store excess energy as fat (Fig. 7.2B). The reason for these weight changes are explored further in the next section, with a particular focus on adipose morphological changes and inflammatory recruitment.

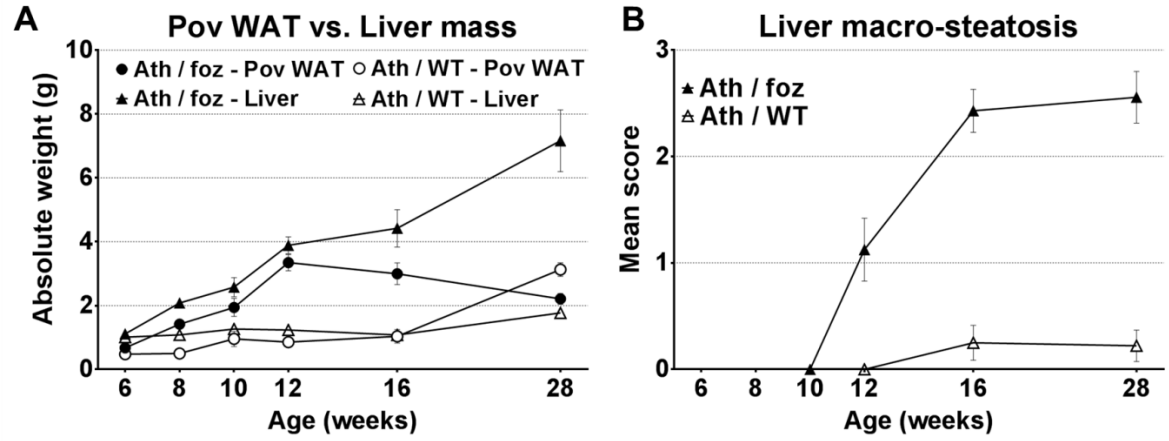

Figure 7.2: Pov WAT vs. liver mass and hepatic lipid partitioning during development of obesity in atherogenic diet-fed female *foz/foz* and *WT* NOD.B10 mice.

7.1.2 Inflammatory Recruitment is a Response to Over-Expansion of Adipose Tissue, but at What Cost?

As discussed throughout this thesis, inflammation is an immediate immune response to noxious stimuli such as pathogens, chemicals or tissue/cellular injury. Short-term (acute) inflammation is usually necessary to "fix" damaged tissues; however, when inflammatory recruitment becomes prolonged (chronic), it actually results in "tissue destruction or dysfunction" rather than healing. In this context, "undesirable persistent adipose inflammation" is the factor that makes obesity phenotype unhealthy, and the

present Section focuses on the mechanism for persistent adipose tissue inflammation as well as how it deteriorates the obesity phenotype. In the literature, mechanisms for an acute inflammatory response are well-defined, but little is known about perpetuation of persistent inflammation.

As stated in Section 1.5.6.1, single or fused macrophages coalesce around injured or dead cells. The aggregation of these macrophages is called CLSs. As discussed in Section 5.1.2, CLSs are formed by C-AMs that are activated by TLR ligands. They express pro-inflammatory factors, most importantly TNFα. The existence of CLSs occurs in the liver and possibly other tissues, but seems to be most abundant in adipose tissue (461).

The number of CLS defines the severity of adipose inflammation. In 2008, Caroline Apovian and her colleagues investigated inflammatory recruitment in adipose biopsies by quantifying the number of CLSs from 77 obese human subjects (BMI ≥ 30) (462). 50 (65%) of these individuals exhibited abundant CLS formation in adipose tissue, and this abundancy was associated with hyperinsulinemia, insulin resistance, and distorted vascular endothelial function. Moreover, those individuals with higher number of CLS also exhibited increased adipose expression of CD68 and TNFα. There are several other studies both in human and mouse adipose tissues that measure inflammation recruitment by the number of CLSs.

In the present work, the formation of CLS in visceral WAT was already evident as early as 12 weeks of age in atherogenic diet-fed *foz/foz* female NOD.B10 mice (Fig. 3.10). The number of CLS was ~5.4 per 100 adipocytes. At this stage, these animals were obese (body weight ~48 g) and pre-diabetic (FBG ~12 mmol/L). At 16 weeks of age, the number of CLSs increased to ~6.6 per 100 adipocytes (Fig. 6.18D). In addition, the obesity phenotype was worsened (body weight ~56 g), and all mice were diabetic (FBG ~15.6 mmol/L). At 28 weeks of age, body weight was 62 g (Fig. 5.2B).

Unfortunately, by the time of the submission of this thesis, quantification of CLS has not been completed in 28-week-old mice, but considering the compelling evidence of adipose restriction (Fig. 7.2A) and higher *Cd68* mRNA expression levels (Fig. 5.10), we believe the number of CLS showed a strong continuing trend of increase. In all, these data show a positive correlation between development of obesity, the number of CLS in adipose tissue, and worsening glucose tolerance.

An interesting finding was that the number of CLSs was only ~3 per 100 adipocytes in subcutaneous WAT of atherogenic diet-fed *foz/foz* mice at 16 weeks of age; this number is less than the half of what observed in visceral WAT (Fig. 6.18D). Quantification of CLS in subcutaneous WAT of 12 and 28 week old mice is underway, but the current data support the concept that visceral WAT is more prone to inflammation than subcutaneous WAT. This proposal receives strong support from the other inflammatory readouts shown in Chapter 6 (Fig. 6.18).

In atherogenic diet-fed female *foz/foz* NOD.B10 mice, exercise dramatically reduced the number of CLSs in adipose compartments. This number was only ~3.3 in visceral WAT (vs. ~6.6 in sedentary mice) and ~1.9 in subcutaneous WAT (vs. ~3 in sedentary mice) (Fig. 6.18D). This striking decrease was confirmed with other pro-inflammatory readouts. Moderately vigorous exercise clearly suppressed adipose inflammation in atherogenic diet-fed *foz/foz* mice. In addition, weight gain was less in exercising *foz/foz* mice, on either chow or atherogenic diet. Moreover, exercise completely prevented development of obesity in atherogenic diet-fed *WT* mice (< 30 g). This reduction in weight gain was associated with increased proportion of healthy small and medium-sized adipocytes, and we believe this reduction is the factor that minimized the number of CLSs in adipose compartments. In all, exercise reduced adipose inflammatory recruitment and improved adipose function, and this was associated with amelioration of NASH and hepatic fibrosis in atherogenic diet-fed *foz/foz* mice (Fig. 6.19, Table 6.2).

As opposed to this, OCA treatment failed to improve adipose inflammation and other related metabolic indices (e.g., glucose tolerance, liver histology) in atherogenic diet-fed female *foz/foz* NOD.B10 mice (see Chapter 5). Conversely, OCA ameliorated glucose intolerance and liver steatosis in atherogenic diet-fed *WT* mice compared to non-treated, possibly thorough a significant reduction in adipose inflammatory recruitment. Surprisingly, serum cholesterol levels did not change by OCA treatment in either genotype (Fig. 5.4B).

In 28 week old atherogenic diet-fed female *foz/foz* C57 mice, the number of CLS was "~15" per 100 adipocytes in visceral WAT (Fig. 4.15B). At this time, these mice weighed ~63 g, and only ~4% of their body weight was comprised of visceral WAT, whereas the liver comprised ~13% of body weight (see Chapter 4). Similar to the NOD.B10 mice, C57 mice also displayed adipose restriction at 28 weeks of age (Fig. 4.3). As discussed in the previous section, the hepatomegaly that occurred in atherogenic diet-fed *foz/foz* C57 mice was most likely the result of hepatic partitioning of lipids which were not stored (or could no longer be) in adipose tissue (Fig. 4.22).

In addition to the above discussion, all atherogenic diet-fed *foz/foz* mice (C57 and NOD.B10) developed hypoadiponectemia. It is proposed that this too was a direct result of the increased number of CLSs in adipose tissue, as well as the restriction in tissue growth (Fig. 4.5). As explained in Section 1.5.4.2, adiponectin is an insulin-sensitizer, anti-inflammatory, adipogenic factor that shows reciprocal activity with other pro-inflammatory factors, most importantly TNFα; TNFα suppresses adiponectin synthesis. The observation that tissue as well as serum adiponectin levels were considerably lower in atherogenic diet-fed *foz/foz* than in *WT* mice, in association with the severer obesity phenotype, could be attributable to the loss of beneficial effects of adiponectin on the liver.

Another striking finding from the thesis is that the average adipocyte volume was ~240,000 μm^3 in visceral WAT of atherogenic diet-fed *foz/foz* C57 mice, whereas *WT* adipocytes averaged 350,000 μm^3 (Fig. 4.6A). As discussed in Section 1.4.1, an important characteristic of obesity is the existence of lipid-engorged hypertrophic adipocytes. Conversely, atherogenic diet-fed *WT* mice displayed more hypertrophic adipocytes than *foz/foz*, yet they had less severe obesity (~41 g). The answer to this paradox lies in the number and phenotype of small adipocyte subpopulations. The data presented in Fig. 4.9 shows that chronic oxidative stress exists in visceral WAT of atherogenic diet-fed *foz/foz*, but not in *WT* mice. In addition, increased *Rip3* mRNA expression reflects to an increase of programmed "necrotic" cell death in WAT (Fig. 4.10). These findings need further confirmation by cell type-specific immunostaining assays. In the meantime, there is clear evidence that cellular damage and necrotic cell death (necroptosis vs. pyroptosis) were greater in visceral WAT of atherogenic diet-fed *foz/foz* than *WT* mice.

As elaborated in Section 1.5.7, there is increasing evidence to show that CLSs occur only around stressed dying or dead adipocytes. Several factors such as over-expansion with oxidative stress and hypoxia, lipotoxicity, and pro-inflammatory drive (increasing TNFα, lower adiponectin) result in degeneration of adipocytes. Considering the fact that there were ~15 CLSs per 100 adipocytes in visceral WAT of atherogenic diet-fed *foz/foz* C57 mice, this also means 15 of every 100 adipocytes were small and degenerating. This relatively high proportion of cells ultimately affects adipocyte size distribution in WAT. Accordingly, atherogenic diet-fed *foz/foz* mice exhibited a higher proportion of small adipocytes compared to *WT*, but it seems likely that these cells (surrounded by CLSs) were unhealthy and dysfunctional (Fig. 4.8). This opposes the general belief that adipose tissues with higher number of small adipocytes are healthier. This is an entirely novel finding in the literature, established by detailed adipose morphometry techniques.

Further analysis is now required to show whether how these small adipocytes degenerate by pyroptosis, necroptosis or perhaps a combination of each pro-inflammatory pathways.

A final very novel finding of the thesis is that macrophages recognize these degenerating adipocytes by TLR9 activation. As explained in Section 1.5.3.1, injured adipocytes exhibit ultrastructural abnormalities and their degeneration creates necrotic debris that presumably include oligonucleotide particles (CpG DNA) which activate TLR9 signaling. TLR9 signalling may be relevant to neighbouring adipocytes (some of which were shown to exhibit TLR9 expression) and macrophages. Although somewhat preliminary, the data presented here that TLR9 expression was evident in a small proportion of adipocytes. On the other hand, a large proportion of macrophages displayed TLR9 expression. The use of BM chimeric mice demonstrated that activation of TLR9 on BM-derived cells combined with greater level of chemokines (e.g., RANTES, MCP1) and cytokine (e.g., IP10, IFNγ) expression is associated with infiltration of macrophages (perhaps monocytes) into adipose tissue (Fig. 4.18A). In Chapter 4, the strong connection between TLR9 signalling and macrophage infiltration was shown in inflamed adipose tissues by several techniques (mRNA analysis, flow cytometry, etc.). Nevertheless, future studies demand direct demonstration of TLR9 expression specifically in CLS macrophages, for example by using immunohistochemistry, and this is an immediate future direction in this research.

7.1.3 Concluding Summary

The most important and novel findings for this PhD thesis are:

- *foz/foz* mice, especially those fed an atherogenic diet, display properties of unhealthy obesity and metabolic disorders that are homologous to human, such as insulin resistance and fatty liver disease. It therefore provides a useful and

relevant model to study development of obesity in relation to adipose expansion, adipose inflammation, and adipose dysfunction.

- Over-expansion (hyperplasticity) in adipose tissue is characterized by greater numbers of lipid-engorged hypertrophic adipocytes.
- Long term continuity of energy surplus (after 16 weeks of age in atherogenic diet-fed *foz/foz* mice) results in degeneration of adipocytes. This considerably increases the proportion of small ("sick") adipocytes in inflamed and dysfunctional adipose tissues.
- Small degenerating adipocytes appear to die via a programme of pro-inflammatory necrotic cell death (pyroptosis vs. necroptosis).
- Small degenerating adipocytes presumably release damage/danger-associated molecular patterns to the tissue micro-environment; macrophages recognize these DAMPs via TLR9 signaling.
- Classically-activated pro-inflammatory macrophages are enriched for TLR9 signalling. They coalesce around small dying adipocytes most likely in order to minimize any harmful effects to other cells and the whole tissue.
- Pro-inflammatory macrophages migrate into the adipose tissue from bone marrow precursors.
- The activation of inflammatory response in adipose tissue may confer beneficial effects at early stages of development, but persistent adipose inflammation confers harmful effects on body.
- Hypoadiponectemia results from adipose tissue inflammation and dysfunction, is associated with impaired insulin sensitivity and glucose clearance.
- Loss of function in adipose tissue, as well as its restriction, is connected to hepatic lipid partitioning and transition of simple steatosis to NASH.

CHAPTER 7: Final Discussion

- Obeticholic acid treatment improved adipose morphology and reduced adipose inflammation in atherogenic diet-fed *WT* mice, but not in *foz/foz*.
- Increased physical activity by provision of an exercise wheel prevents adipose inflammation and dysfunction in appetite-defective mice prone to obesity.
- Exercise improves whole body glucose tolerance and confers beneficial effects of hepatic steatosis and NASH.

CHAPTER 7: Final Discussion

REFERENCES

REFERENCES

1. Moodie AR. Australia: the healthiest country by 2020. *Med J Aust* 2008;**189:** 588-590.

2. Obesity: A National Epidemic and its Impact on Australia. Obesity Australia, 2014.

3. Australian Bureau of Statistics: Australian Demographic Statistics

Available from: www.abs.gov.au.

4. Overweight and obesity rates across Australia, 2011-12. The National Health Performance Agency, 2013.

5. World Health Organization: Global database on body mass index. Available from: apps.who.int/bmi/index.jsp.

6. Pi-Sunyer FX. The obesity epidemic: pathophysiology and consequences of obesity. *Obes Res* 2002;**10 Suppl 2:** 97S-104S.

7. Obesity and workplace absenteeism among older Australians. Australian Institute of Health and Welfare, 2005.

8. Obesity and mental health. National Obesity Observatory, 2011.

9. Spiegelman BM, Enerback S. "The adipocyte: a multifunctional cell". *Cell Metab* 2006;**4:** 425-427.

10. Ottaviani E, Malagoli D, Franceschi C. The evolution of the adipose tissue: a neglected enigma. *Gen Comp Endocrinol* 2011;**174:** 1-4.

11. Development of ob/ob mice 1949. Available from: http://jaxmice.jax.org/strain/000632.html.

12. Hummel KP, Dickie MM, Coleman DL. Diabetes, a new mutation in the mouse. *Science* 1966;**153:** 1127-1128.

13. Jequier E. Leptin signaling, adiposity, and energy balance. *Ann N Y Acad Sci* 2002;**967:** 379-388.

14. Zhang Y, Proenca R, Maffei M, Barone M, Leopold L, Friedman JM. Positional cloning of the mouse obese gene and its human homologue. *Nature* 1994;**372:** 425-432.

15. Adipose as a Connective Tissue. Available from: http://www.anatomyatlases.org/MicroscopicAnatomy/Section03/Section03.shtml.

16. Galic S, Oakhill JS, Steinberg GR. Adipose tissue as an endocrine organ. *Mol Cell Endocrinol* 2010;**316:** 129-139.

17. Jo J, Gavrilova O, Pack S, Jou W, Mullen S, Sumner AE*, et al.* Hypertrophy and/or Hyperplasia: Dynamics of Adipose Tissue Growth. *PLoS Comput Biol* 2009;**5:** e1000324.

18. Liu M, Guo L, Liu Y, Pei Y, Li N, Jin M*, et al.* Adipose stromal-vascular fraction-derived paracrine factors regulate adipogenesis. *Mol Cell Biochem* 2014;**385:** 115-123.

19. Mariman EC, Wang P. Adipocyte extracellular matrix composition, dynamics and role in obesity. *Cell Mol Life Sci* 2010;**67:** 1277-1292.

20. Esteve Rafols M. Adipose tissue: cell heterogeneity and functional diversity. *Endocrinol Nutr* 2014;**61:** 100-112.

21. Lee MJ, Wu Y, Fried SK. Adipose tissue heterogeneity: implication of depot differences in adipose tissue for obesity complications. *Mol Aspects Med* 2013;**34:** 1-11.

22. Wan DC, Longaker MT. Fat or fiction: origins matter. *Cell Metab* 2014;**19:** 900-901.

23. Seale P, Kajimura S, Spiegelman BM. Transcriptional control of brown adipocyte development and physiological function--of mice and men. *Genes Dev* 2009;**23:** 788-797.

24. Scholz H, Kirschner KM. A role for the Wilms' tumor protein WT1 in organ development. *Physiology (Bethesda)* 2005;**20:** 54-59.

25. Chau YY, Bandiera R, Serrels A, Martinez-Estrada OM, Qing W, Lee M*, et al.* Visceral and subcutaneous fat have different origins and evidence supports a mesothelial source. *Nat Cell Biol* 2014;**16:** 367-375.

26. Symonds ME. Brown adipose tissue growth and development. *Scientifica (Cairo)* 2013;**2013:** 305763.

27. Nombela-Arrieta C, Ritz J, Silberstein LE. The elusive nature and function of mesenchymal stem cells. *Nat Rev Mol Cell Biol* 2011;**12:** 126-131.

28. Bradley TR, Metcalf D. The growth of mouse bone marrow cells in vitro. *Aust J Exp Biol Med Sci* 1966;**44:** 287-299.

29. Han J, Koh YJ, Moon HR, Ryoo HG, Cho CH, Kim I*, et al.* Adipose tissue is an extramedullary reservoir for functional hematopoietic stem and progenitor cells. *Blood* 2010;**115:** 957-964.

30. Lane MD, Tang QQ. From multipotent stem cell to adipocyte. *Birth Defects Res A Clin Mol Teratol* 2005;**73:** 476-477.

31. Gurevitch O, Slavin S, Resnick I, Khitrin S, Feldman A. Mesenchymal progenitor cells in red and yellow bone marrow. *Folia Biol (Praha)* 2009;**55:** 27-34.

32. Fraser JK, Wulur I, Alfonso Z, Hedrick MH. Fat tissue: an underappreciated source of stem cells for biotechnology. *Trends Biotechnol* 2006;**24:** 150-154.

33. Zuk PA, Zhu M, Ashjian P, De Ugarte DA, Huang JI, Mizuno H*, et al.* Human adipose tissue is a source of multipotent stem cells. *Mol Biol Cell* 2002;**13:** 4279-4295.

34. Kern S, Eichler H, Stoeve J, Kluter H, Bieback K. Comparative analysis of mesenchymal stem cells from bone marrow, umbilical cord blood, or adipose tissue. *Stem Cells* 2006;**24:** 1294-1301.

35. Rosen ED, MacDougald OA. Adipocyte differentiation from the inside out. *Nat Rev Mol Cell Biol* 2006;**7:** 885-896.

36. Feve B. Adipogenesis: cellular and molecular aspects. *Best Pract Res Clin Endocrinol Metab* 2005;**19:** 483-499.

37. Rigamonti A, Brennand K, Lau F, Cowan CA. Rapid cellular turnover in adipose tissue. *PLoS One* 2011;**6:** e17637.

38. Arner E, Westermark PO, Spalding KL, Britton T, Ryden M, Frisen J*, et al.* Adipocyte turnover: relevance to human adipose tissue morphology. *Diabetes* 2010;**59:** 105-109.

39. Tchkonia T, Lenburg M, Thomou T, Giorgadze N, Frampton G, Pirtskhalava T*, et al.* Identification of depot-specific human fat cell progenitors through distinct expression profiles and developmental gene patterns. *Am J Physiol Endocrinol Metab* 2007;**292:** E298-307.

40. Peirce V, Carobbio S, Vidal-Puig A. The different shades of fat. *Nature* 2014;**510:** 76-83.

41. Gesta S, Tseng YH, Kahn CR. Developmental origin of fat: tracking obesity to its source. *Cell* 2007;**131:** 242-256.

42. Ali AT, Hochfeld WE, Myburgh R, Pepper MS. Adipocyte and adipogenesis. *Eur J Cell Biol* 2013;**92:** 229-236.

43. Guilak F, Lott KE, Awad HA, Cao Q, Hicok KC, Fermor B*, et al.* Clonal analysis of the differentiation potential of human adipose-derived adult stem cells. *J Cell Physiol* 2006;**206:** 229-237.

44. Izadpanah R, Trygg C, Patel B, Kriedt C, Dufour J, Gimble JM*, et al.* Biologic properties of mesenchymal stem cells derived from bone marrow and adipose tissue. *J Cell Biochem* 2006;**99:** 1285-1297.

45. Chazenbalk G, Bertolotto C, Heneidi S, Jumabay M, Trivax B, Aronowitz J*, et al.* Novel pathway of adipogenesis through cross-talk between adipose tissue macrophages, adipose stem cells and adipocytes: evidence of cell plasticity. *PLoS One* 2011;**6:** e17834.

46. Fischbach C, Spruss T, Weiser B, Neubauer M, Becker C, Hacker M*, et al.* Generation of mature fat pads in vitro and in vivo utilizing 3-D long-term culture of 3T3-L1 preadipocytes. *Exp Cell Res* 2004;**300:** 54-64.

47. Steward AJ, Kelly DJ. Mechanical regulation of mesenchymal stem cell differentiation. *J Anat* 2014.

48. Liu LF, Shen WJ, Zhang ZH, Wang LJ, Kraemer FB. Adipocytes decrease Runx2 expression in osteoblastic cells: roles of PPARgamma and adiponectin. *J Cell Physiol* 2010;**225:** 837-845.

49. Dani C, Smith AG, Dessolin S, Leroy P, Staccini L, Villageois P*, et al.* Differentiation of embryonic stem cells into adipocytes in vitro. *J Cell Sci* 1997;**110 (Pt 11):** 1279-1285.

50. Cawthorn WP, Scheller EL, MacDougald OA. Adipose tissue stem cells meet preadipocyte commitment: going back to the future. *J Lipid Res* 2012;**53:** 227-246.

51. Murray A. Cell cycle checkpoints. *Curr Opin Cell Biol* 1994;**6:** 872-876.

52. Bertoli C, Skotheim JM, de Bruin RA. Control of cell cycle transcription during G1 and S phases. *Nat Rev Mol Cell Biol* 2013;**14:** 518-528.

53. Hardwick LJ, Ali FR, Azzarelli R, Philpott A. Cell cycle regulation of proliferation versus differentiation in the central nervous system. *Cell Tissue Res* 2015;**359:** 187-200.

54. Tang QQ, Otto TC, Lane MD. Mitotic clonal expansion: a synchronous process required for adipogenesis. *Proc Natl Acad Sci U S A* 2003;**100:** 44-49.

55. Barak Y, Nelson MC, Ong ES, Jones YZ, Ruiz-Lozano P, Chien KR*, et al.* PPAR gamma is required for placental, cardiac, and adipose tissue development. *Mol Cell* 1999;**4:** 585-595.

56. Jones JR, Barrick C, Kim KA, Lindner J, Blondeau B, Fujimoto Y*, et al.* Deletion of PPARgamma in adipose tissues of mice protects against high fat diet-induced obesity and insulin resistance. *Proc Natl Acad Sci U S A* 2005;**102:** 6207-6212.

57. Svensson PA, Jernas M, Sjoholm K, Hoffmann JM, Nilsson BE, Hansson M*, et al.* Gene expression in human brown adipose tissue. *Int J Mol Med* 2011;**27:** 227-232.

58. Hansen JB, Kristiansen K. Regulatory circuits controlling white versus brown adipocyte differentiation. *Biochem J* 2006;**398:** 153-168.

59. Gerin I, Dolinsky VW, Shackman JG, Kennedy RT, Chiang SH, Burant CF*, et al.* LXRbeta is required for adipocyte growth, glucose homeostasis, and beta cell function. *J Biol Chem* 2005;**280:** 23024-23031.

60. Ye J, DeBose-Boyd RA. Regulation of cholesterol and fatty acid synthesis. *Cold Spring Harb Perspect Biol* 2011;**3**.

61. Saely CH, Geiger K, Drexel H. Brown versus white adipose tissue: a mini-review. *Gerontology* 2012;**58:** 15-23.

62. Park A, Kim WK, Bae KH. Distinction of white, beige and brown adipocytes derived from mesenchymal stem cells. *World J Stem Cells* 2014;**6:** 33-42.

63. Cifuentes M, Albala C, Rojas CV. Differences in lipogenesis and lipolysis in obese and non-obese adult human adipocytes. *Biol Res* 2008;**41:** 197-204.

64. Kershaw EE, Flier JS. Adipose tissue as an endocrine organ. *J Clin Endocrinol Metab* 2004;**89:** 2548-2556.

65. Cousin B, Cinti S, Morroni M, Raimbault S, Ricquier D, Penicaud L*, et al.* Occurrence of brown adipocytes in rat white adipose tissue: molecular and morphological characterization. *J Cell Sci* 1992;**103 (Pt 4):** 931-942.

66. Milner RE, Wang LC, Trayhurn P. Brown fat thermogenesis during hibernation and arousal in Richardson's ground squirrel. *Am J Physiol* 1989;**256:** R42-48.

67. Fedorenko A, Lishko PV, Kirichok Y. Mechanism of fatty-acid-dependent UCP1 uncoupling in brown fat mitochondria. *Cell* 2012;**151:** 400-413.

68. Oelkrug R, Kutschke M, Meyer CW, Heldmaier G, Jastroch M. Uncoupling protein 1 decreases superoxide production in brown adipose tissue mitochondria. *J Biol Chem* 2010;**285:** 21961-21968.

69. Rosenbaum M, Leibel RL. Adaptive thermogenesis in humans. *Int J Obes (Lond)* 2010;**34 Suppl 1:** S47-55.

70. Wu J, Cohen P, Spiegelman BM. Adaptive thermogenesis in adipocytes: is beige the new brown? *Genes Dev* 2013;**27:** 234-250.

71. Modre-Osprian R, Osprian I, Tilg B, Schreier G, Weinberger KM, Graber A. Dynamic simulations on the mitochondrial fatty acid beta-oxidation network. *BMC Syst Biol* 2009;**3:** 2.

72. Divakaruni AS, Brand MD. The regulation and physiology of mitochondrial proton leak. *Physiology (Bethesda)* 2011;**26:** 192-205.

73. Kadenbach B. Introduction to mitochondrial oxidative phosphorylation. *Adv Exp Med Biol* 2012;**748:** 1-11.

74. Murphy MP. How mitochondria produce reactive oxygen species. *Biochem J* 2009;**417:** 1-13.

75. Thorpe GW, Fong CS, Alic N, Higgins VJ, Dawes IW. Cells have distinct mechanisms to maintain protection against different reactive oxygen species: oxidative-stress-response genes. *Proc Natl Acad Sci U S A* 2004;**101:** 6564-6569.

76. Foster MT, Softic S, Caldwell J, Kohli R, de Kloet AD, Seeley RJ. Subcutaneous Adipose Tissue Transplantation in Diet-Induced Obese Mice Attenuates Metabolic Dysregulation While Removal Exacerbates It. *Physiol Rep* 2013;**1**.

77. Lidell ME, Betz MJ, Dahlqvist Leinhard O, Heglind M, Elander L, Slawik M*, et al.* Evidence for two types of brown adipose tissue in humans. *Nat Med* 2013;**19:** 631-634.

78. Long JZ, Svensson KJ, Tsai L, Zeng X, Roh HC, Kong X*, et al.* A smooth muscle-like origin for beige adipocytes. *Cell Metab* 2014;**19:** 810-820.

79. Harms M, Seale P. Brown and beige fat: development, function and therapeutic potential. *Nat Med* 2013;**19:** 1252-1263.

80. Bartesaghi S, Hallen S, Huang L, Svensson PA, Momo RA, Wallin S*, et al.* Thermogenic activity of UCP1 in human white fat-derived beige adipocytes. *Mol Endocrinol* 2015;**29:** 130-139.

81. Tanuma Y, Tamamoto M, Ito T, Yokochi C. The occurrence of brown adipose tissue in perirenal fat in Japanese. *Arch Histol Jpn* 1975;**38:** 43-70.

82. Cannon B, Nedergaard J. Brown adipose tissue: function and physiological significance. *Physiol Rev* 2004;**84:** 277-359.

83. Collins S, Surwit RS. The beta-adrenergic receptors and the control of adipose tissue metabolism and thermogenesis. *Recent Prog Horm Res* 2001;**56:** 309-328.

84. Seale P, Bjork B, Yang W, Kajimura S, Chin S, Kuang S*, et al.* PRDM16 controls a brown fat/skeletal muscle switch. *Nature* 2008;**454:** 961-967.

85. Farmer SR. Brown fat and skeletal muscle: unlikely cousins? *Cell* 2008;**134:** 726-727.

86. Cohen P, Levy JD, Zhang Y, Frontini A, Kolodin DP, Svensson KJ*, et al.* Ablation of PRDM16 and beige adipose causes metabolic dysfunction and a subcutaneous to visceral fat switch. *Cell* 2014;**156:** 304-316.

87. Frishman WH. Cardiology patient page. Beta-adrenergic blockers. *Circulation* 2003;**107:** e117-119.

88. Reichrath J. The skin is a fascinating endocrine organ. *Dermatoendocrinol* 2009;**1:** 195-196.

89. Albers KM, Davis BM. The skin as a neurotrophic organ. *Neuroscientist* 2007;**13:** 371-382.

90. Cartlidge P. The epidermal barrier. *Semin Neonatol* 2000;**5:** 273-280.

91. Uitto J, Olsen DR, Fazio MJ. Extracellular matrix of the skin: 50 years of progress. *J Invest Dermatol* 1989;**92:** 61S-77S.

92. Li L, Fukunaga-Kalabis M, Herlyn M. Isolation and cultivation of dermal stem cells that differentiate into functional epidermal melanocytes. *Methods Mol Biol* 2012;**806:** 15-29.

93. Hausman GJ, Campion DR, Richardson RL, Martin RJ. Adipocyte development in the rat hypodermis. *Am J Anat* 1981;**161:** 85-100.

94. Wildman RP, Sowers MR. Adiposity and the menopausal transition. *Obstet Gynecol Clin North Am* 2011;**38:** 441-454.

95. Samocha-Bonet D, Chisholm DJ, Tonks K, Campbell LV, Greenfield JR. Insulin-sensitive obesity in humans - a 'favorable fat' phenotype? *Trends Endocrinol Metab* 2012;**23:** 116-124.

96. Rosen ED, Spiegelman BM. Adipocytes as regulators of energy balance and glucose homeostasis. *Nature* 2006;**444:** 847-853.

97. Zhang W, Cline MA, Gilbert ER. Hypothalamus-adipose tissue crosstalk: neuropeptide Y and the regulation of energy metabolism. *Nutr Metab (Lond)* 2014;**11:** 27.

98. Chaudhri O, Small C, Bloom S. Gastrointestinal hormones regulating appetite. *Philos Trans R Soc Lond B Biol Sci* 2006;**361:** 1187-1209.

99. Kalra SP, Dube MG, Pu S, Xu B, Horvath TL, Kalra PS. Interacting appetite-regulating pathways in the hypothalamic regulation of body weight. *Endocr Rev* 1999;**20:** 68-100.

100. Schwartz GJ. Integrative capacity of the caudal brainstem in the control of food intake. *Philos Trans R Soc Lond B Biol Sci* 2006;**361:** 1275-1280.

101. Adan RA, Tiesjema B, Hillebrand JJ, la Fleur SE, Kas MJ, de Krom M. The MC4 receptor and control of appetite. *Br J Pharmacol* 2006;**149:** 815-827.

102. Parker JA, Bloom SR. Hypothalamic neuropeptides and the regulation of appetite. *Neuropharmacology* 2012;**63:** 18-30.

103. Scheer FA, Morris CJ, Shea SA. The internal circadian clock increases hunger and appetite in the evening independent of food intake and other behaviors. *Obesity (Silver Spring)* 2013;**21:** 421-423.

104. Newsholme P, Cruzat V, Arfuso F, Keane K. Nutrient regulation of insulin secretion and action. *J Endocrinol* 2014;**221:** R105-120.

105. Breen DM, Giacca A. Effects of insulin on the vasculature. *Curr Vasc Pharmacol* 2011;**9:** 321-332.

106. Hyun E, Ramachandran R, Hollenberg MD, Vergnolle N. Mechanisms behind the anti-inflammatory actions of insulin. *Crit Rev Immunol* 2011;**31:** 307-340.

REFERENCES

107. Michael MD, Kulkarni RN, Postic C, Previs SF, Shulman GI, Magnuson MA*, et al.* Loss of insulin signaling in hepatocytes leads to severe insulin resistance and progressive hepatic dysfunction. *Mol Cell* 2000;**6:** 87-97.

108. Fu Z, Gilbert ER, Liu D. Regulation of insulin synthesis and secretion and pancreatic Beta-cell dysfunction in diabetes. *Curr Diabetes Rev* 2013;**9:** 25-53.

109. Safarik RH, Joy RM, Curry DL. Episodic release of insulin by rat pancreas: effects of CNS and state of satiety. *Am J Physiol* 1988;**254:** E384-388.

110. Schenk S, Saberi M, Olefsky JM. Insulin sensitivity: modulation by nutrients and inflammation. *J Clin Invest* 2008;**118:** 2992-3002.

111. Mitrou P, Raptis SA, Dimitriadis G. Insulin action in morbid obesity: a focus on muscle and adipose tissue. *Hormones (Athens, Greece)* 2013;**12:** 201-213.

112. Cobb J, Gall W, Adam KP, Nakhle P, Button E, Hathorn J*, et al.* A novel fasting blood test for insulin resistance and prediabetes. *J Diabetes Sci Technol* 2013;**7:** 100-110.

113. Klueh U, Liu Z, Cho B, Ouyang T, Feldman B, Henning TP*, et al.* Continuous glucose monitoring in normal mice and mice with prediabetes and diabetes. *Diabetes Technol Ther* 2006;**8:** 402-412.

114. Cavaghan MK, Ehrmann DA, Polonsky KS. Interactions between insulin resistance and insulin secretion in the development of glucose intolerance. *J Clin Invest* 2000;**106:** 329-333.

115. Tohyama Y, Takano T, Yamamura H. B cell responses to oxidative stress. *Curr Pharm Des* 2004;**10:** 835-839.

116. Defrance T, Casamayor-Palleja M, Krammer PH. The life and death of a B cell. *Adv Cancer Res* 2002;**86:** 195-225.

117. Leahy JL. Pathogenesis of type 2 diabetes mellitus. *Arch Med Res* 2005;**36:** 197-209.

118. Cnop M, Welsh N, Jonas JC, Jorns A, Lenzen S, Eizirik DL. Mechanisms of pancreatic beta-cell death in type 1 and type 2 diabetes: many differences, few similarities. *Diabetes* 2005;**54 Suppl 2:** S97-107.

119. Svacina S. Treatment of obese diabetics. *Adv Exp Med Biol* 2012;**771:** 459-464.

120. Murakami U, Uchida K. Contents of myofibrillar proteins in cardiac, skeletal, and smooth muscles. *J Biochem* 1985;**98:** 187-197.

121. Jensen J, Rustad PI, Kolnes AJ, Lai YC. The role of skeletal muscle glycogen breakdown for regulation of insulin sensitivity by exercise. *Front Physiol* 2011;**2:** 112.

122. Radda GK. Control of energy metabolism during muscle contraction. *Diabetes* 1996;**45 Suppl 1:** S88-92.

123. Sugi H. Molecular mechanism of ATP-dependent actin-myosin interaction in muscle contraction. *Jpn J Physiol* 1993;**43:** 435-454.

124. Gestrelius S, Borgstrom P. A dynamic model of smooth muscle contraction. *Biophys J* 1986;**50:** 157-169.

125. Kraegen EW, Bruce C, Hegarty BD, Ye JM, Turner N, Cooney G. AMP-activated protein kinase and muscle insulin resistance. *Front Biosci (Landmark Ed)* 2009;**14:** 4658-4672.

126. Holmes BF, Sparling DP, Olson AL, Winder WW, Dohm GL. Regulation of muscle GLUT4 enhancer factor and myocyte enhancer factor 2 by AMP-activated protein kinase. *Am J Physiol Endocrinol Metab* 2005;**289:** E1071-1076.

127. Sakamoto K, Holman GD. Emerging role for AS160/TBC1D4 and TBC1D1 in the regulation of GLUT4 traffic. *Am J Physiol Endocrinol Metab* 2008;**295:** E29-37.

128. Wolfe RR. Effects of insulin on muscle tissue. *Curr Opin Clin Nutr Metab Care* 2000;**3:** 67-71.

129. Dimitriadis G, Mitrou P, Lambadiari V, Maratou E, Raptis SA. Insulin effects in muscle and adipose tissue. *Diabetes Res Clin Pract* 2011;**93 Suppl 1:** S52-59.

130. Bolster DR, Jefferson LS, Kimball SR. Regulation of protein synthesis associated with skeletal muscle hypertrophy by insulin-, amino acid- and exercise-induced signalling. *Proc Nutr Soc* 2004;**63:** 351-356.

131. Conejo R, Valverde AM, Benito M, Lorenzo M. Insulin produces myogenesis in C2C12 myoblasts by induction of NF-kappaB and downregulation of AP-1 activities. *J Cell Physiol* 2001;**186:** 82-94.

132. Chang L, Chiang SH, Saltiel AR. Insulin signaling and the regulation of glucose transport. *Mol Med* 2004;**10:** 65-71.

133. Lizcano JM, Alessi DR. The insulin signalling pathway. *Curr Biol* 2002;**12:** R236-238.

134. Richter EA, Hargreaves M. Exercise, GLUT4, and skeletal muscle glucose uptake. *Physiol Rev* 2013;**93:** 993-1017.

135. Kirwan JP, del Aguila LF. Insulin signalling, exercise and cellular integrity. *Biochem Soc Trans* 2003;**31:** 1281-1285.

136. Jones RG, Elford AR, Parsons MJ, Wu L, Krawczyk CM, Yeh WC*, et al.* CD28-dependent activation of protein kinase B/Akt blocks Fas-mediated apoptosis by preventing death-inducing signaling complex assembly. *J Exp Med* 2002;**196:** 335-348.

137. Trumper K, Trumper A, Trusheim H, Arnold R, Goke B, Horsch D. Integrative mitogenic role of protein kinase B/Akt in beta-cells. *Ann N Y Acad Sci* 2000;**921:** 242-250.

138. Zierath JR. Invited review: Exercise training-induced changes in insulin signaling in skeletal muscle. *J Appl Physiol (1985)* 2002;**93:** 773-781.

139. de Souza EO, Tricoli V, Bueno Junior C, Pereira MG, Brum PC, Oliveira EM*, et al.* The acute effects of strength, endurance and concurrent exercises on the Akt/mTOR/p70(S6K1) and AMPK signaling pathway responses in rat skeletal muscle. *Braz J Med Biol Res* 2013;**46:** 343-347.

140. Long YC, Cheng Z, Copps KD, White MF. Insulin receptor substrates Irs1 and Irs2 coordinate skeletal muscle growth and metabolism via the Akt and AMPK pathways. *Mol Cell Biol* 2011;**31:** 430-441.

141. Hong J, Kim BW, Choo HJ, Park JJ, Yi JS, Yu DM*, et al.* Mitochondrial complex I deficiency enhances skeletal myogenesis but impairs insulin signaling through SIRT1 inactivation. *J Biol Chem* 2014;**289:** 20012-20025.

142. Krook A, Bjornholm M, Galuska D, Jiang XJ, Fahlman R, Myers MG, Jr.*, et al.* Characterization of signal transduction and glucose transport in skeletal muscle from type 2 diabetic patients. *Diabetes* 2000;**49:** 284-292.

143. Hey-Mogensen M, Hojlund K, Vind BF, Wang L, Dela F, Beck-Nielsen H*, et al.* Effect of physical training on mitochondrial respiration and reactive oxygen species release in skeletal muscle in patients with obesity and type 2 diabetes. *Diabetologia* 2010;**53:** 1976-1985.

144. Bylund-Fellenius AC, Idstrom JP, Holm S. Muscle respiration during exercise. *Am Rev Respir Dis* 1984;**129:** S10-12.

145. Oberbach A, Bossenz Y, Lehmann S, Niebauer J, Adams V, Paschke R*, et al.* Altered fiber distribution and fiber-specific glycolytic and oxidative enzyme activity in skeletal muscle of patients with type 2 diabetes. *Diabetes care* 2006;**29:** 895-900.

146. Kubasiak LA, Hernandez OM, Bishopric NH, Webster KA. Hypoxia and acidosis activate cardiac myocyte death through the Bcl-2 family protein BNIP3. *Proc Natl Acad Sci U S A* 2002;**99:** 12825-12830.

147. Keung EC, Li Q. Lactate activates ATP-sensitive potassium channels in guinea pig ventricular myocytes. *J Clin Invest* 1991;**88:** 1772-1777.

148. Hegarty BD, Furler SM, Ye J, Cooney GJ, Kraegen EW. The role of intramuscular lipid in insulin resistance. *Acta Physiol Scand* 2003;**178:** 373-383.

149. Consitt LA, Bell JA, Houmard JA. Intramuscular lipid metabolism, insulin action, and obesity. *IUBMB Life* 2009;**61:** 47-55.

150. Yang J, Cron P, Thompson V, Good VM, Hess D, Hemmings BA*, et al.* Molecular mechanism for the regulation of protein kinase B/Akt by hydrophobic motif phosphorylation. *Mol Cell* 2002;**9:** 1227-1240.

151. Kandel ES, Hay N. The regulation and activities of the multifunctional serine/threonine kinase Akt/PKB. *Exp Cell Res* 1999;**253:** 210-229.

152. Vadlakonda L, Dash A, Pasupuleti M, Anil Kumar K, Reddanna P. The Paradox of Akt-mTOR Interactions. *Front Oncol* 2013;**3:** 165.

153. Wan X, Helman LJ. Levels of PTEN protein modulate Akt phosphorylation on serine 473, but not on threonine 308, in IGF-II-overexpressing rhabdomyosarcomas cells. *Oncogene* 2003;**22:** 8205-8211.

154. Lin K, Lin J, Wu WI, Ballard J, Lee BB, Gloor SL*, et al.* An ATP-site on-off switch that restricts phosphatase accessibility of Akt. *Sci Signal* 2012;**5:** ra37.

155. Chan TO, Zhang J, Rodeck U, Pascal JM, Armen RS, Spring M*, et al.* Resistance of Akt kinases to dephosphorylation through ATP-dependent conformational plasticity. *Proc Natl Acad Sci U S A* 2011;**108:** E1120-1127.

156. Leclerc GM, Leclerc GJ, Fu G, Barredo JC. AMPK-induced activation of Akt by AICAR is mediated by IGF-1R dependent and independent mechanisms in acute lymphoblastic leukemia. *J Mol Signal* 2010;**5:** 15.

157. Tzivion G, Dobson M, Ramakrishnan G. FoxO transcription factors; Regulation by AKT and 14-3-3 proteins. *Biochim Biophys Acta* 2011;**1813:** 1938-1945.

158. McCabe MP, Busija L, Fuller-Tyszkiewicz M, Ricciardelli L, Mellor D, Mussap A. Sociocultural influences on strategies to lose weight, gain weight, and increase muscles among ten cultural groups. *Body Image* 2015;**12:** 108-114.

159. Tamori Y, Deng WM. Compensatory cellular hypertrophy: the other strategy for tissue homeostasis. *Trends Cell Biol* 2014;**24:** 230-237.

160. Gilbert RG, Wu AC, Sullivan MA, Sumarriva GE, Ersch N, Hasjim J. Improving human health through understanding the complex structure of glucose polymers. *Anal Bioanal Chem* 2013;**405:** 8969-8980.

161. Berg JM TJ, Stryer L. Triacylglycerols Are Highly Concentrated Energy Stores. In: Freeman; WH (ed). *Biochemistry. 5th edition.*, 2002.

162. Nakamura MT, Yudell BE, Loor JJ. Regulation of energy metabolism by long-chain fatty acids. *Prog Lipid Res* 2014;**53:** 124-144.

163. Kadegowda AK, Bionaz M, Piperova LS, Erdman RA, Loor JJ. Peroxisome proliferator-activated receptor-gamma activation and long-chain fatty acids alter lipogenic gene networks in bovine mammary epithelial cells to various extents. *J Dairy Sci* 2009;**92:** 4276-4289.

164. Pappenheimer JR, Michel CC. Role of villus microcirculation in intestinal absorption of glucose: coupling of epithelial with endothelial transport. *J Physiol* 2003;**553:** 561-574.

165. Diamond JM, Karasov WH, Cary C, Enders D, Yung R. Effect of dietary carbohydrate on monosaccharide uptake by mouse small intestine in vitro. *J Physiol* 1984;**349:** 419-440.

166. Hussain MM. Intestinal lipid absorption and lipoprotein formation. *Curr Opin Lipidol* 2014;**25:** 200-206.

167. Maldonado-Valderrama J, Wilde P, Macierzanka A, Mackie A. The role of bile salts in digestion. *Adv Colloid Interface Sci* 2011;**165:** 36-46.

168. Berg JM TJ, Stryer L. Important Derivatives of Cholesterol Include Bile Salts and Steroid Hormones. In: Freeman WH (ed). *Biochemistry. 5th edition*, 2002.

169. Barth CA. Regulation and interaction of cholesterol, bile salt and lipoprotein synthesis in liver. *Klin Wochenschr* 1983;**61:** 1163-1170.

170. Kullak-Ublick GA, Stieger B, Hagenbuch B, Meier PJ. Hepatic transport of bile salts. *Semin Liver Dis* 2000;**20:** 273-292.

171. Kuipers F, Stroeve JH, Caron S, Staels B. Bile acids, farnesoid X receptor, atherosclerosis and metabolic control. *Curr Opin Lipidol* 2007;**18:** 289-297.

172. Mencarelli A, Renga B, Migliorati M, Cipriani S, Distrutti E, Santucci L*, et al.* The bile acid sensor farnesoid X receptor is a modulator of liver immunity in a rodent model of acute hepatitis. *J Immunol* 2009;**183:** 6657-6666.

173. Fiorucci S, Rizzo G, Donini A, Distrutti E, Santucci L. Targeting farnesoid X receptor for liver and metabolic disorders. *Trends Mol Med* 2007;**13:** 298-309.

174. Ory DS. Nuclear receptor signaling in the control of cholesterol homeostasis: have the orphans found a home? *Circ Res* 2004;**95:** 660-670.

175. Teodoro JS, Rolo AP, Palmeira CM. Hepatic FXR: key regulator of whole-body energy metabolism. *Trends Endocrinol Metab* 2011;**22:** 458-466.

176. Cipriani S, Mencarelli A, Palladino G, Fiorucci S. FXR activation reverses insulin resistance and lipid abnormalities and protects against liver steatosis in Zucker (fa/fa) obese rats. *J Lipid Res* 2010;**51:** 771-784.

177. Tso P, Balint JA. Formation and transport of chylomicrons by enterocytes to the lymphatics. *Am J Physiol* 1986;**250:** G715-726.

178. Blanchette-Mackie EJ, Scow RO. Effects of lipoprotein lipase on the structure of chylomicrons. *J Cell Biol* 1973;**58:** 689-708.

179. Mahley RW, Hui DY, Innerarity TL, Beisiegel U. Chylomicron remnant metabolism. Role of hepatic lipoprotein receptors in mediating uptake. *Arteriosclerosis* 1989;**9:** I14-18.

180. Shimizu Y, Nikami H, Tsukazaki K, Machado UF, Yano H, Seino Y*, et al.* Increased expression of glucose transporter GLUT-4 in brown adipose tissue of fasted rats after cold exposure. *Am J Physiol* 1993;**264:** E890-895.

181. Fabres-Machado U, Saito M. The effect of adipose cell size on the measurement of GLUT 4 in white adipose tissue of obese mice. *Braz J Med Biol Res* 1995;**28:** 369-376.

182. Grillo CA, Piroli GG, Hendry RM, Reagan LP. Insulin-stimulated translocation of GLUT4 to the plasma membrane in rat hippocampus is PI3-kinase dependent. *Brain Res* 2009;**1296:** 35-45.

183. Ren H, Yan S, Zhang B, Lu TY, Arancio O, Accili D. Glut4 expression defines an insulin-sensitive hypothalamic neuronal population. *Mol Metab* 2014;**3:** 452-459.

184. Blot V, McGraw TE. Molecular mechanisms controlling GLUT4 intracellular retention. *Mol Biol Cell* 2008;**19:** 3477-3487.

185. Vroegrijk IO, van Klinken JB, van Diepen JA, van den Berg SA, Febbraio M, Steinbusch LK*, et al.* CD36 is important for adipocyte recruitment and affects lipolysis. *Obesity (Silver Spring)* 2013;**21:** 2037-2045.

186. van Oort MM, van Doorn JM, Bonen A, Glatz JF, van der Horst DJ, Rodenburg KW*, et al.* Insulin-induced translocation of CD36 to the plasma membrane is reversible and shows similarity to that of GLUT4. *Biochim Biophys Acta* 2008;**1781:** 61-71.

187. Bonen A, Dyck DJ, Ibrahimi A, Abumrad NA. Muscle contractile activity increases fatty acid metabolism and transport and FAT/CD36. *Am J Physiol* 1999;**276:** E642-649.

188. Sonnino S, Prinetti A. Membrane domains and the "lipid raft" concept. *Curr Med Chem* 2013;**20:** 4-21.

189. Cohen AW, Hnasko R, Schubert W, Lisanti MP. Role of caveolae and caveolins in health and disease. *Physiol Rev* 2004;**84:** 1341-1379.

190. Cohen AW, Combs TP, Scherer PE, Lisanti MP. Role of caveolin and caveolae in insulin signaling and diabetes. *Am J Physiol Endocrinol Metab* 2003;**285:** E1151-1160.

191. Parton RG, del Pozo MA. Caveolae as plasma membrane sensors, protectors and organizers. *Nat Rev Mol Cell Biol* 2013;**14:** 98-112.

192. Kandror KV, Pilch PF. The sugar is sIRVed: sorting Glut4 and its fellow travelers. *Traffic* 2011;**12:** 665-671.

193. Shigematsu S, Watson RT, Khan AH, Pessin JE. The adipocyte plasma membrane caveolin functional/structural organization is necessary for the efficient endocytosis of GLUT4. *J Biol Chem* 2003;**278:** 10683-10690.

194. Chiang SH, Baumann CA, Kanzaki M, Thurmond DC, Watson RT, Neudauer CL*, et al.* Insulin-stimulated GLUT4 translocation requires the CAP-dependent activation of TC10. *Nature* 2001;**410:** 944-948.

195. Zhang HH, Huang J, Duvel K, Boback B, Wu S, Squillace RM*, et al.* Insulin stimulates adipogenesis through the Akt-TSC2-mTORC1 pathway. *PLoS One* 2009;**4:** e6189.

196. Matsuzaki H, Daitoku H, Hatta M, Tanaka K, Fukamizu A. Insulin-induced phosphorylation of FKHR (Foxo1) targets to proteasomal degradation. *Proc Natl Acad Sci U S A* 2003;**100:** 11285-11290.

197. Munekata K, Sakamoto K. Forkhead transcription factor Foxo1 is essential for adipocyte differentiation. *In Vitro Cell Dev Biol Anim* 2009;**45:** 642-651.

198. Viollet B, Andreelli F. AMP-activated protein kinase and metabolic control. *Handb Exp Pharmacol* 2011**:** 303-330.

199. Shen WJ, Patel S, Miyoshi H, Greenberg AS, Kraemer FB. Functional interaction of hormone-sensitive lipase and perilipin in lipolysis. *J Lipid Res* 2009;**50:** 2306-2313.

200. Brady MJ, Bourbonais FJ, Saltiel AR. The activation of glycogen synthase by insulin switches from kinase inhibition to phosphatase activation during adipogenesis in 3T3-L1 cells. *J Biol Chem* 1998;**273:** 14063-14066.

201. Berwick DC, Hers I, Heesom KJ, Moule SK, Tavare JM. The identification of ATP-citrate lyase as a protein kinase B (Akt) substrate in primary adipocytes. *J Biol Chem* 2002;**277:** 33895-33900.

202. Stumpel F, Burcelin R, Jungermann K, Thorens B. Normal kinetics of intestinal glucose absorption in the absence of GLUT2: evidence for a transport pathway requiring glucose phosphorylation and transfer into the endoplasmic reticulum. *Proc Natl Acad Sci U S A* 2001;**98:** 11330-11335.

203. McArthur MJ, Atshaves BP, Frolov A, Foxworth WD, Kier AB, Schroeder F. Cellular uptake and intracellular trafficking of long chain fatty acids. *J Lipid Res* 1999;**40:** 1371-1383.

204. Strawford A, Antelo F, Christiansen M, Hellerstein MK. Adipose tissue triglyceride turnover, de novo lipogenesis, and cell proliferation in humans measured with 2H2O. *Am J Physiol Endocrinol Metab* 2004;**286:** E577-588.

205. Reshef L, Olswang Y, Cassuto H, Blum B, Croniger CM, Kalhan SC*, et al.* Glyceroneogenesis and the triglyceride/fatty acid cycle. *J Biol Chem* 2003;**278:** 30413-30416.

206. Thiam AR, Farese RV, Jr., Walther TC. The biophysics and cell biology of lipid droplets. *Nat Rev Mol Cell Biol* 2013;**14:** 775-786.

207. Brasaemle DL. Thematic review series: adipocyte biology. The perilipin family of structural lipid droplet proteins: stabilization of lipid droplets and control of lipolysis. *J Lipid Res* 2007;**48:** 2547-2559.

208. Dalen KT, Schoonjans K, Ulven SM, Weedon-Fekjaer MS, Bentzen TG, Koutnikova H*, et al.* Adipose tissue expression of the lipid droplet-associating proteins S3-12 and

perilipin is controlled by peroxisome proliferator-activated receptor-gamma. *Diabetes* 2004;**53:** 1243-1252.

209. Arimura N, Horiba T, Imagawa M, Shimizu M, Sato R. The peroxisome proliferator-activated receptor gamma regulates expression of the perilipin gene in adipocytes. *J Biol Chem* 2004;**279:** 10070-10076.

210. Sahu-Osen A, Montero-Moran G, Schittmayer M, Fritz K, Dinh A, Chang YF*, et al.* CGI-58/ABHD5 is phosphorylated on Ser239 by protein kinase A: control of subcellular localization. *J Lipid Res* 2015;**56:** 109-121.

211. Fujimoto T, Parton RG. Not just fat: the structure and function of the lipid droplet. *Cold Spring Harb Perspect Biol* 2011;**3**.

212. Hickenbottom SJ, Kimmel AR, Londos C, Hurley JH. Structure of a lipid droplet protein; the PAT family member TIP47. *Structure* 2004;**12:** 1199-1207.

213. Bulankina AV, Deggerich A, Wenzel D, Mutenda K, Wittmann JG, Rudolph MG*, et al.* TIP47 functions in the biogenesis of lipid droplets. *J Cell Biol* 2009;**185:** 641-655.

214. Hodges BD, Wu CC. Proteomic insights into an expanded cellular role for cytoplasmic lipid droplets. *J Lipid Res* 2010;**51:** 262-273.

215. Soccio RE, Breslow JL. Intracellular cholesterol transport. *Arterioscler Thromb Vasc Biol* 2004;**24:** 1150-1160.

216. Robenek H, Severs NJ. Lipid droplet growth by fusion: insights from freeze-fracture imaging. *J Cell Mol Med* 2009;**13:** 4657-4661.

217. Gan LT, Van Rooyen DM, Koina ME, McCuskey RS, Teoh NC, Farrell GC. Hepatocyte free cholesterol lipotoxicity results from JNK1-mediated mitochondrial injury and is HMGB1 and TLR4-dependent. *J Hepatol* 2014;**61:** 1376-1384.

218. Robenek H, Buers I, Robenek MJ, Hofnagel O, Ruebel A, Troyer D*, et al.* Topography of lipid droplet-associated proteins: insights from freeze-fracture replica immunogold labeling. *J Lipids* 2011;**2011:** 409371.

219. Cohen AW, Razani B, Schubert W, Williams TM, Wang XB, Iyengar P*, et al.* Role of caveolin-1 in the modulation of lipolysis and lipid droplet formation. *Diabetes* 2004;**53:** 1261-1270.

220. Forest C, Tordjman J, Glorian M, Duplus E, Chauvet G, Quette J*, et al.* Fatty acid recycling in adipocytes: a role for glyceroneogenesis and phosphoenolpyruvate carboxykinase. *Biochem Soc Trans* 2003;**31:** 1125-1129.

221. Le Lay S, Krief S, Farnier C, Lefrere I, Le Liepvre X, Bazin R*, et al.* Cholesterol, a cell size-dependent signal that regulates glucose metabolism and gene expression in adipocytes. *J Biol Chem* 2001;**276:** 16904-16910.

222. Yang ZX, Shen W, Sun H. Effects of nuclear receptor FXR on the regulation of liver lipid metabolism in patients with non-alcoholic fatty liver disease. *Hepatol Int* 2010;**4:** 741-748.

223. Abdelkarim M, Caron S, Duhem C, Prawitt J, Dumont J, Lucas A*, et al.* The farnesoid X receptor regulates adipocyte differentiation and function by promoting peroxisome proliferator-activated receptor-gamma and interfering with the Wnt/beta-catenin pathways. *J Biol Chem* 2010;**285:** 36759-36767.

224. Lundgren M, Svensson M, Lindmark S, Renstrom F, Ruge T, Eriksson JW. Fat cell enlargement is an independent marker of insulin resistance and 'hyperleptinaemia'. *Diabetologia* 2007;**50:** 625-633.

225. Meyer LK, Ciaraldi TP, Henry RR, Wittgrove AC, Phillips SA. Adipose tissue depot and cell size dependency of adiponectin synthesis and secretion in human obesity. *Adipocyte* 2013;**2:** 217-226.

226. Mohamed-Ali V, Pinkney JH, Coppack SW. Adipose tissue as an endocrine and paracrine organ. *Int J Obes Relat Metab Disord* 1998;**22:** 1145-1158.

227. Marques BG, Hausman DB, Martin RJ. Association of fat cell size and paracrine growth factors in development of hyperplastic obesity. *Am J Physiol* 1998;**275:** R1898-1908.

228. Chaves VE, Junior FM, Bertolini GL. The metabolic effects of growth hormone in adipose tissue. *Endocrine* 2013;**44:** 293-302.

229. Roberts R, Hodson L, Dennis AL, Neville MJ, Humphreys SM, Harnden KE*, et al.* Markers of de novo lipogenesis in adipose tissue: associations with small adipocytes and insulin sensitivity in humans. *Diabetologia* 2009;**52:** 882-890.

230. Murano I, Barbatelli G, Parisani V, Latini C, Muzzonigro G, Castellucci M*, et al.* Dead adipocytes, detected as crown-like structures, are prevalent in visceral fat depots of genetically obese mice. *J Lipid Res* 2008;**49:** 1562-1568.

231. Tchoukalova YD, Koutsari C, Karpyak MV, Votruba SB, Wendland E, Jensen MD. Subcutaneous adipocyte size and body fat distribution. *Am J Clin Nutr* 2008;**87:** 56-63.

232. Larter CZ, Yeh MM, Van Rooyen DM, Teoh NC, Brooling J, Hou JY*, et al.* Roles of adipose restriction and metabolic factors in progression of steatosis to steatohepatitis in obese, diabetic mice. *Journal of gastroenterology and hepatology* 2009;**24:** 1658-1668.

233. Meena VP, Seenu V, Sharma MC, Mallick SR, Bhalla AS, Gupta N*, et al.* Relationship of adipocyte size with adiposity and metabolic risk factors in Asian Indians. *PLoS One* 2014;**9:** e108421.

234. Gathercole LL, Morgan SA, Bujalska IJ, Hauton D, Stewart PM, Tomlinson JW. Regulation of lipogenesis by glucocorticoids and insulin in human adipose tissue. *PLoS One* 2011;**6:** e26223.

235. Rutkowski JM, Stern JH, Scherer PE. The cell biology of fat expansion. *J Cell Biol* 2015;**208:** 501-512.

236. Trayhurn P. Hypoxia and adipose tissue function and dysfunction in obesity. *Physiol Rev* 2013;**93:** 1-21.

237. Hausman GJ, Richardson RL. Adipose tissue angiogenesis. *J Anim Sci* 2004;**82:** 925-934.

238. Wood IS, Stezhka T, Trayhurn P. Modulation of adipokine production, glucose uptake and lactate release in human adipocytes by small changes in oxygen tension. *Pflugers Arch* 2011;**462:** 469-477.

239. Bekhite MM, Finkensieper A, Rebhan J, Huse S, Schultze-Mosgau S, Figulla HR*, et al.* Hypoxia, leptin, and vascular endothelial growth factor stimulate vascular endothelial cell differentiation of human adipose tissue-derived stem cells. *Stem Cells Dev* 2014;**23:** 333-351.

240. Zheng C, Liu Z. Vascular function, insulin action, and exercise: an intricate interplay. *Trends Endocrinol Metab* 2015.

241. Villaret A, Galitzky J, Decaunes P, Esteve D, Marques MA, Sengenes C*, et al.* Adipose tissue endothelial cells from obese human subjects: differences among depots in angiogenic, metabolic, and inflammatory gene expression and cellular senescence. *Diabetes* 2010;**59:** 2755-2763.

242. Tran KV, Gealekman O, Frontini A, Zingaretti MC, Morroni M, Giordano A*, et al.* The vascular endothelium of the adipose tissue gives rise to both white and brown fat cells. *Cell Metab* 2012;**15:** 222-229.

243. Halper J, Kjaer M. Basic components of connective tissues and extracellular matrix: elastin, fibrillin, fibulins, fibrinogen, fibronectin, laminin, tenascins and thrombospondins. *Adv Exp Med Biol* 2014;**802:** 31-47.

244. Sharma NS, Nagrath D, Yarmush ML. Adipocyte-derived basement membrane extract with biological activity: applications in hepatocyte functional augmentation in vitro. *FASEB J* 2010;**24:** 2364-2374.

245. Semenza GL. Oxygen sensing, hypoxia-inducible factors, and disease pathophysiology. *Annu Rev Pathol* 2014;**9:** 47-71.

246. He Q, Gao Z, Yin J, Zhang J, Yun Z, Ye J. Regulation of HIF-1{alpha} activity in adipose tissue by obesity-associated factors: adipogenesis, insulin, and hypoxia. *Am J Physiol Endocrinol Metab* 2011;**300:** E877-885.

247. Takeda N, O'Dea EL, Doedens A, Kim JW, Weidemann A, Stockmann C*, et al.* Differential activation and antagonistic function of HIF-{alpha} isoforms in macrophages are essential for NO homeostasis. *Genes Dev* 2010;**24:** 491-501.

248. Aouadi M. HIF-2alpha blows out the flames of adipose tissue macrophages to keep obesity in a safe zone. *Diabetes* 2014;**63:** 3169-3171.

249. Nakayama K. cAMP-response element-binding protein (CREB) and NF-kappaB transcription factors are activated during prolonged hypoxia and cooperatively regulate the induction of matrix metalloproteinase MMP1. *J Biol Chem* 2013;**288:** 22584-22595.

250. Bruick RK. Oxygen sensing in the hypoxic response pathway: regulation of the hypoxia-inducible transcription factor. *Genes Dev* 2003;**17:** 2614-2623.

251. Schiffrin EL. Oxidative stress, nitric oxide synthase, and superoxide dismutase: a matter of imbalance underlies endothelial dysfunction in the human coronary circulation. *Hypertension* 2008;**51:** 31-32.

252. Karbownik-Lewinska M, Szosland J, Kokoszko-Bilska A, Stepniak J, Zasada K, Gesing A*, et al.* Direct contribution of obesity to oxidative damage to macromolecules. *Neuro Endocrinol Lett* 2012;**33:** 453-461.

253. Mylonas C, Kouretas D. Lipid peroxidation and tissue damage. *In vivo (Athens, Greece)* 1999;**13:** 295-309.

254. Niki E. Lipid peroxidation products as oxidative stress biomarkers. *Biofactors* 2008;**34:** 171-180.

255. Mayr M, Sidibe A, Zampetaki A. The paradox of hypoxic and oxidative stress in atherosclerosis. *J Am Coll Cardiol* 2008;**51:** 1266-1267.

256. Ding H, Aljofan M, Triggle CR. Oxidative stress and increased eNOS and NADPH oxidase expression in mouse microvessel endothelial cells. *J Cell Physiol* 2007;**212:** 682-689.

257. Elahi MM, Kong YX, Matata BM. Oxidative stress as a mediator of cardiovascular disease. *Oxid Med Cell Longev* 2009;**2:** 259-269.

258. Mates JM. Effects of antioxidant enzymes in the molecular control of reactive oxygen species toxicology. *Toxicology* 2000;**153:** 83-104.

259. Rizak J, Tan H, Zhu H, Wang JF. Chronic treatment with the mood-stabilizing drug lithium up-regulates nuclear factor E2-related factor 2 in rat pheochromocytoma PC12 cells in vitro. *Neuroscience* 2014;**256:** 223-229.

260. Hayes JD, Chanas SA, Henderson CJ, McMahon M, Sun C, Moffat GJ*, et al.* The Nrf2 transcription factor contributes both to the basal expression of glutathione S-transferases in mouse liver and to their induction by the chemopreventive synthetic antioxidants, butylated hydroxyanisole and ethoxyquin. *Biochem Soc Trans* 2000;**28:** 33-41.

261. Zelko IN, Mariani TJ, Folz RJ. Superoxide dismutase multigene family: a comparison of the CuZn-SOD (SOD1), Mn-SOD (SOD2), and EC-SOD (SOD3) gene structures, evolution, and expression. *Free Radic Biol Med* 2002;**33:** 337-349.

262. Sabater D, Arriaran S, Romero Mdel M, Agnelli S, Remesar X, Fernandez-Lopez JA*, et al.* Cultured 3T3L1 adipocytes dispose of excess medium glucose as lactate under abundant oxygen availability. *Sci Rep* 2014;**4:** 3663.

263. Hosogai N, Fukuhara A, Oshima K, Miyata Y, Tanaka S, Segawa K*, et al.* Adipose tissue hypoxia in obesity and its impact on adipocytokine dysregulation. *Diabetes* 2007;**56:** 901-911.

264. Echigoya Y, Morita S, Itou T, Sakai T. Effects of extracellular lactate on production of reactive oxygen species by equine polymorphonuclear leukocytes in vitro. *Am J Vet Res* 2012;**73:** 1290-1298.

265. Spector JA, Mehrara BJ, Greenwald JA, Saadeh PB, Steinbrech DS, Bouletreau PJ*, et al.* Osteoblast expression of vascular endothelial growth factor is modulated by the extracellular microenvironment. *Am J Physiol Cell Physiol* 2001;**280:** C72-80.

266. Giordano A, Murano I, Mondini E, Perugini J, Smorlesi A, Severi I*, et al.* Obese adipocytes show ultrastructural features of stressed cells and die of pyroptosis. *J Lipid Res* 2013;**54:** 2423-2436.

267. Sun K, Tordjman J, Clement K, Scherer PE. Fibrosis and adipose tissue dysfunction. *Cell Metab* 2013;**18:** 470-477.

268. Hotamisligil GS. Endoplasmic reticulum stress and the inflammatory basis of metabolic disease. *Cell* 2010;**140:** 900-917.

269. Fulda S, Gorman AM, Hori O, Samali A. Cellular stress responses: cell survival and cell death. *Int J Cell Biol* 2010;**2010:** 214074.

270. Yin X, Lanza IR, Swain JM, Sarr MG, Nair KS, Jensen MD. Adipocyte mitochondrial function is reduced in human obesity independent of fat cell size. *J Clin Endocrinol Metab* 2014;**99:** E209-216.

271. De Pauw A, Tejerina S, Raes M, Keijer J, Arnould T. Mitochondrial (dys)function in adipocyte (de)differentiation and systemic metabolic alterations. *Am J Pathol* 2009;**175:** 927-939.

272. Ioannou GN, Haigh WG, Thorning D, Savard C. Hepatic cholesterol crystals and crown-like structures distinguish NASH from simple steatosis. *J Lipid Res* 2013;**54:** 1326-1334.

273. Boya P, Kroemer G. Lysosomal membrane permeabilization in cell death. *Oncogene* 2008;**27:** 6434-6451.

274. Li MD. Leptin and beyond: an odyssey to the central control of body weight. *Yale J Biol Med* 2011;**84:** 1-7.

275. Sweeney G. Leptin signalling. *Cell Signal* 2002;**14:** 655-663.

276. Myers MG, Jr., Leibel RL, Seeley RJ, Schwartz MW. Obesity and leptin resistance: distinguishing cause from effect. *Trends Endocrinol Metab* 2010;**21:** 643-651.

277. Ren J. Leptin and hyperleptinemia - from friend to foe for cardiovascular function. *J Endocrinol* 2004;**181:** 1-10.

278. Ambati S, Kim HK, Yang JY, Lin J, Della-Fera MA, Baile CA. Effects of leptin on apoptosis and adipogenesis in 3T3-L1 adipocytes. *Biochem Pharmacol* 2007;**73:** 378-384.

279. Gruver AL, Ventevogel MS, Sempowski GD. Leptin receptor is expressed in thymus medulla and leptin protects against thymic remodeling during endotoxemia-induced thymus involution. *J Endocrinol* 2009;**203:** 75-85.

280. Velloso LA, Savino W, Mansour E. Leptin action in the thymus. *Ann N Y Acad Sci* 2009;**1153:** 29-34.

281. Cani PD, Bibiloni R, Knauf C, Waget A, Neyrinck AM, Delzenne NM*, et al.* Changes in gut microbiota control metabolic endotoxemia-induced inflammation in high-fat diet-induced obesity and diabetes in mice. *Diabetes* 2008;**57:** 1470-1481.

282. Hara K, Horikoshi M, Yamauchi T, Yago H, Miyazaki O, Ebinuma H*, et al.* Measurement of the high-molecular weight form of adiponectin in plasma is useful for the prediction of insulin resistance and metabolic syndrome. *Diabetes care* 2006;**29:** 1357-1362.

283. Awazawa M, Ueki K, Inabe K, Yamauchi T, Kubota N, Kaneko K*, et al.* Adiponectin enhances insulin sensitivity by increasing hepatic IRS-2 expression via a macrophage-derived IL-6-dependent pathway. *Cell Metab* 2011;**13:** 401-412.

284. Doumatey AP, Bentley AR, Zhou J, Huang H, Adeyemo A, Rotimi CN. Paradoxical Hyperadiponectinemia is Associated With the Metabolically Healthy Obese (MHO) Phenotype in African Americans. *J Endocrinol Metab* 2012;**2:** 51-65.

285. Bouskila M, Pajvani UB, Scherer PE. Adiponectin: a relevant player in PPARgamma-agonist-mediated improvements in hepatic insulin sensitivity? *Int J Obes (Lond)* 2005;**29 Suppl 1:** S17-23.

286. Maeda N, Takahashi M, Funahashi T, Kihara S, Nishizawa H, Kishida K*, et al.* PPARgamma ligands increase expression and plasma concentrations of adiponectin, an adipose-derived protein. *Diabetes* 2001;**50:** 2094-2099.

287. Matsuda M, Shimomura I. Roles of adiponectin and oxidative stress in obesity-associated metabolic and cardiovascular diseases. *Rev Endocr Metab Disord* 2014;**15:** 1-10.

288. Chen SJ, Yen CH, Huang YC, Lee BJ, Hsia S, Lin PT. Relationships between inflammation, adiponectin, and oxidative stress in metabolic syndrome. *PLoS One* 2012;**7:** e45693.

289. Skurk T, Alberti-Huber C, Herder C, Hauner H. Relationship between adipocyte size and adipokine expression and secretion. *J Clin Endocrinol Metab* 2007;**92:** 1023-1033.

290. Kadowaki T, Yamauchi T. Adiponectin and adiponectin receptors. *Endocr Rev* 2005;**26:** 439-451.

291. Fantuzzi G. Adipose tissue, adipokines, and inflammation. *J Allergy Clin Immunol* 2005;**115:** 911-919; quiz 920.

292. Folco EJ, Rocha VZ, Lopez-Ilasaca M, Libby P. Adiponectin inhibits pro-inflammatory signaling in human macrophages independent of interleukin-10. *J Biol Chem* 2009;**284:** 25569-25575.

293. Lafontan M. Adipose tissue and adipocyte dysregulation. *Diabetes Metab* 2014;**40:** 16-28.

294. Lo JC, Ljubicic S, Leibiger B, Kern M, Leibiger IB, Moede T*, et al.* Adipsin is an adipokine that improves beta cell function in diabetes. *Cell* 2014;**158:** 41-53.

295. Flier JS, Cook KS, Usher P, Spiegelman BM. Severely impaired adipsin expression in genetic and acquired obesity. *Science* 1987;**237:** 405-408.

296. Balistreri CR, Caruso C, Candore G. The role of adipose tissue and adipokines in obesity-related inflammatory diseases. *Mediators Inflamm* 2010;**2010:** 802078.

297. Espat NJ, Copeland EM, Moldawer LL. Tumor necrosis factor and cachexia: a current perspective. *Surg Oncol* 1994;**3:** 255-262.

298. Fain JN, Bahouth SW, Madan AK. TNFalpha release by the nonfat cells of human adipose tissue. *Int J Obes Relat Metab Disord* 2004;**28:** 616-622.

299. Lee BC, Lee J. Cellular and molecular players in adipose tissue inflammation in the development of obesity-induced insulin resistance. *Biochim Biophys Acta* 2014;**1842:** 446-462.

300. Hotamisligil GS, Peraldi P, Budavari A, Ellis R, White MF, Spiegelman BM. IRS-1-mediated inhibition of insulin receptor tyrosine kinase activity in TNF-alpha- and obesity-induced insulin resistance. *Science* 1996;**271:** 665-668.

301. Makki K, Froguel P, Wolowczuk I. Adipose tissue in obesity-related inflammation and insulin resistance: cells, cytokines, and chemokines. *ISRN Inflamm* 2013;**2013:** 139239.

302. Lawrence T. The nuclear factor NF-kappaB pathway in inflammation. *Cold Spring Harb Perspect Biol* 2009;**1:** a001651.

303. Zhang HH, Halbleib M, Ahmad F, Manganiello VC, Greenberg AS. Tumor necrosis factor-alpha stimulates lipolysis in differentiated human adipocytes through activation

of extracellular signal-related kinase and elevation of intracellular cAMP. *Diabetes* 2002;**51:** 2929-2935.

304. Pereira SS, Alvarez-Leite JI. Adipokines: biological functions and metabolically healthy obese profile. *Journal of Receptor, Ligand and Channel Research* 2014.

305. Kanda H, Tateya S, Tamori Y, Kotani K, Hiasa K, Kitazawa R*, et al.* MCP-1 contributes to macrophage infiltration into adipose tissue, insulin resistance, and hepatic steatosis in obesity. *J Clin Invest* 2006;**116:** 1494-1505.

306. Fasshauer M, Klein J, Kralisch S, Klier M, Lossner U, Bluher M*, et al.* Monocyte chemoattractant protein 1 expression is stimulated by growth hormone and interleukin-6 in 3T3-L1 adipocytes. *Biochem Biophys Res Commun* 2004;**317:** 598-604.

307. Deshmane SL, Kremlev S, Amini S, Sawaya BE. Monocyte chemoattractant protein-1 (MCP-1): an overview. *J Interferon Cytokine Res* 2009;**29:** 313-326.

308. Curat CA, Miranville A, Sengenes C, Diehl M, Tonus C, Busse R*, et al.* From blood monocytes to adipose tissue-resident macrophages: induction of diapedesis by human mature adipocytes. *Diabetes* 2004;**53:** 1285-1292.

309. Mandrekar P, Ambade A, Lim A, Szabo G, Catalano D. An essential role for monocyte chemoattractant protein-1 in alcoholic liver injury: regulation of proinflammatory cytokines and hepatic steatosis in mice. *Hepatology* 2011;**54:** 2185-2197.

310. Christiansen T, Richelsen B, Bruun JM. Monocyte chemoattractant protein-1 is produced in isolated adipocytes, associated with adiposity and reduced after weight loss in morbid obese subjects. *Int J Obes (Lond)* 2005;**29:** 146-150.

311. Weisberg SP, Hunter D, Huber R, Lemieux J, Slaymaker S, Vaddi K*, et al.* CCR2 modulates inflammatory and metabolic effects of high-fat feeding. *J Clin Invest* 2006;**116:** 115-124.

312. Jialal I, Devaraj S, Kaur H, Adams-Huet B, Bremer AA. Increased chemerin and decreased omentin-1 in both adipose tissue and plasma in nascent metabolic syndrome. *J Clin Endocrinol Metab* 2013;**98:** E514-517.

313. Odegaard JI, Ganeshan K, Chawla A. Adipose tissue macrophages: Amicus adipem? *Cell Metab* 2013;**18:** 767-768.

314. Charriere G, Cousin B, Arnaud E, Andre M, Bacou F, Penicaud L*, et al.* Preadipocyte conversion to macrophage. Evidence of plasticity. *J Biol Chem* 2003;**278:** 9850-9855.

315. Weisberg SP, McCann D, Desai M, Rosenbaum M, Leibel RL, Ferrante AW, Jr. Obesity is associated with macrophage accumulation in adipose tissue. *J Clin Invest* 2003;**112:** 1796-1808.

316. Davies LC, Jenkins SJ, Allen JE, Taylor PR. Tissue-resident macrophages. *Nat Immunol* 2013;**14:** 986-995.

317. Prieur X, Mok CY, Velagapudi VR, Nunez V, Fuentes L, Montaner D*, et al.* Differential lipid partitioning between adipocytes and tissue macrophages modulates macrophage lipotoxicity and M2/M1 polarization in obese mice. *Diabetes* 2011;**60:** 797-809.

318. Wermuth PJ, Jimenez SA. The significance of macrophage polarization subtypes for animal models of tissue fibrosis and human fibrotic diseases. *Clin Transl Med* 2015;**4:** 2.

319. Fujisaka S, Usui I, Bukhari A, Ikutani M, Oya T, Kanatani Y*, et al.* Regulatory mechanisms for adipose tissue M1 and M2 macrophages in diet-induced obese mice. *Diabetes* 2009;**58:** 2574-2582.

320. Brake DK, Smith EO, Mersmann H, Smith CW, Robker RL. ICAM-1 expression in adipose tissue: effects of diet-induced obesity in mice. *Am J Physiol Cell Physiol* 2006;**291:** C1232-1239.

321. Cinti S, Mitchell G, Barbatelli G, Murano I, Ceresi E, Faloia E*, et al.* Adipocyte death defines macrophage localization and function in adipose tissue of obese mice and humans. *J Lipid Res* 2005;**46:** 2347-2355.

322. Kearney CJ, Cullen SP, Tynan GA, Henry CM, Clancy D, Lavelle EC*, et al.* Necroptosis suppresses inflammation via termination of TNF- or LPS-induced cytokine and chemokine production. *Cell Death Differ* 2015.

323. Herold C, Rennekampff HO, Engeli S. Apoptotic pathways in adipose tissue. *Apoptosis* 2013;**18:** 911-916.

324. Irrinki KM, Mallilankaraman K, Thapa RJ, Chandramoorthy HC, Smith FJ, Jog NR*, et al.* Requirement of FADD, NEMO, and BAX/BAK for aberrant mitochondrial function in tumor necrosis factor alpha-induced necrosis. *Mol Cell Biol* 2011;**31:** 3745-3758.

325. Christofferson DE, Yuan J. Necroptosis as an alternative form of programmed cell death. *Curr Opin Cell Biol* 2010;**22:** 263-268.

326. Fink SL, Cookson BT. Apoptosis, pyroptosis, and necrosis: mechanistic description of dead and dying eukaryotic cells. *Infect Immun* 2005;**73:** 1907-1916.

327. Miao EA, Rajan JV, Aderem A. Caspase-1-induced pyroptotic cell death. *Immunol Rev* 2011;**243:** 206-214.

328. Stienstra R, Tack CJ, Kanneganti TD, Joosten LA, Netea MG. The inflammasome puts obesity in the danger zone. *Cell Metab* 2012;**15:** 10-18.

329. Franchi L, Eigenbrod T, Munoz-Planillo R, Nunez G. The inflammasome: a caspase-1-activation platform that regulates immune responses and disease pathogenesis. *Nat Immunol* 2009;**10:** 241-247.

330. Bergsbaken T, Fink SL, Cookson BT. Pyroptosis: host cell death and inflammation. *Nat Rev Microbiol* 2009;**7:** 99-109.

331. Gornicka A, Fettig J, Eguchi A, Berk MP, Thapaliya S, Dixon LJ*, et al.* Adipocyte hypertrophy is associated with lysosomal permeability both in vivo and in vitro: role in adipose tissue inflammation. *Am J Physiol Endocrinol Metab* 2012;**303:** E597-606.

332. Eguchi A, Feldstein AE. Lysosomal Cathepsin D contributes to cell death during adipocyte hypertrophy. *Adipocyte* 2013;**2:** 170-175.

333. Guicciardi ME, Leist M, Gores GJ. Lysosomes in cell death. *Oncogene* 2004;**23:** 2881-2890.

334. Shi Y, Liu CH, Roberts AI, Das J, Xu G, Ren G*, et al.* Granulocyte-macrophage colony-stimulating factor (GM-CSF) and T-cell responses: what we do and don't know. *Cell Res* 2006;**16:** 126-133.

335. Feng D, Tang Y, Kwon H, Zong H, Hawkins M, Kitsis RN*, et al.* High-fat diet-induced adipocyte cell death occurs through a cyclophilin D intrinsic signaling pathway independent of adipose tissue inflammation. *Diabetes* 2011;**60:** 2134-2143.

336. Lionetti L, Mollica MP, Lombardi A, Cavaliere G, Gifuni G, Barletta A. From chronic overnutrition to insulin resistance: the role of fat-storing capacity and inflammation. *Nutr Metab Cardiovasc Dis* 2009;**19:** 146-152.

337. Strissel KJ, Stancheva Z, Miyoshi H, Perfield JW, 2nd, DeFuria J, Jick Z*, et al.* Adipocyte death, adipose tissue remodeling, and obesity complications. *Diabetes* 2007;**56:** 2910-2918.

338. Arsov T, Silva DG, O'Bryan MK, Sainsbury A, Lee NJ, Kennedy C*, et al.* Fat aussie--a new Alstrom syndrome mouse showing a critical role for ALMS1 in obesity, diabetes, and spermatogenesis. *Mol Endocrinol* 2006;**20:** 1610-1622.

339. Farrell GC, Mridha AR, Yeh MM, Arsov T, Van Rooyen DM, Brooling J*, et al.* Strain dependence of diet-induced NASH and liver fibrosis in obese mice is linked to diabetes and inflammatory phenotype. *Liver Int* 2014;**34:** 1084-1093.

340. Silversand C, Haux C. Improved high-performance liquid chromatographic method for the separation and quantification of lipid classes: application to fish lipids. *J Chromatogr B Biomed Sci Appl* 1997;**703:** 7-14.

341. Kleiner DE, Brunt EM, Van Natta M, Behling C, Contos MJ, Cummings OW*, et al.* Design and validation of a histological scoring system for nonalcoholic fatty liver disease. *Hepatology* 2005;**41:** 1313-1321.

342. Gorzelniak K, Janke J, Engeli S, Sharma AM. Validation of endogenous controls for gene expression studies in human adipocytes and preadipocytes. *Horm Metab Res* 2001;**33:** 625-627.

343. Sajic T, Hopfgartner G, Szanto I, Varesio E. Comparison of three detergent-free protein extraction protocols for white adipose tissue. *Anal Biochem* 2011;**415:** 215-217.

344. Bradford MM. A rapid and sensitive method for the quantitation of microgram quantities of protein utilizing the principle of protein-dye binding. *Anal Biochem* 1976;**72:** 248-254.

345. Loomba R, Abraham M, Unalp A, Wilson L, Lavine J, Doo E*, et al.* Association between diabetes, family history of diabetes, and risk of nonalcoholic steatohepatitis and fibrosis. *Hepatology* 2012;**56:** 943-951.

346. Farrell GC, Wong VW, Chitturi S. NAFLD in Asia--as common and important as in the West. *Nat Rev Gastroenterol Hepatol* 2013;**10:** 307-318.

347. Kloting N, Bluher M. Adipocyte dysfunction, inflammation and metabolic syndrome. *Rev Endocr Metab Disord* 2014;**15:** 277-287.

348. Garg A. Adipose tissue dysfunction in obesity and lipodystrophy. *Clin Cornerstone* 2006;**8 Suppl 4:** S7-S13.

349. Farrell GC, Larter CZ. Nonalcoholic fatty liver disease: from steatosis to cirrhosis. *Hepatology* 2006;**43:** S99-S112.

350. De Minicis S, Day C, Svegliati-Baroni G. From NAFLD to NASH and HCC: pathogenetic mechanisms and therapeutic insights. *Curr Pharm Des* 2013;**19:** 5239-5249.

351. Neuschwander-Tetri BA. Hepatic lipotoxicity and the pathogenesis of nonalcoholic steatohepatitis: the central role of nontriglyceride fatty acid metabolites. *Hepatology* 2010;**52:** 774-788.

352. Farrell GC, van Rooyen D, Gan L, Chitturi S. NASH is an Inflammatory Disorder: Pathogenic, Prognostic and Therapeutic Implications. *Gut and liver* 2012;**6:** 149-171.

353. Cusi K. Role of obesity and lipotoxicity in the development of nonalcoholic steatohepatitis: pathophysiology and clinical implications. *Gastroenterology* 2012;**142:** 711-725 e716.

354. Chitturi S, Abeygunasekera S, Farrell GC, Holmes-Walker J, Hui JM, Fung C*, et al.* NASH and insulin resistance: Insulin hypersecretion and specific association with the insulin resistance syndrome. *Hepatology* 2002;**35:** 373-379.

355. Manchanayake J, Chitturi S, Nolan C, Farrell GC. Postprandial hyperinsulinemia is universal in non-diabetic patients with nonalcoholic fatty liver disease. *Journal of gastroenterology and hepatology* 2011;**26:** 510-516.

356. Gastaldelli A, Harrison SA, Belfort-Aguilar R, Hardies LJ, Balas B, Schenker S*, et al.* Importance of changes in adipose tissue insulin resistance to histological response during thiazolidinedione treatment of patients with nonalcoholic steatohepatitis. *Hepatology* 2009;**50:** 1087-1093.

357. Yu J, Shen J, Sun TT, Zhang X, Wong N. Obesity, insulin resistance, NASH and hepatocellular carcinoma. *Semin Cancer Biol* 2013;**23:** 483-491.

358. Matsuzaka T, Shimano H. Molecular mechanisms involved in hepatic steatosis and insulin resistance. *J Diabetes Investig* 2011;**2:** 170-175.

359. Lanthier N, Molendi-Coste O, Cani PD, van Rooijen N, Horsmans Y, Leclercq IA. Kupffer cell depletion prevents but has no therapeutic effect on metabolic and inflammatory changes induced by a high-fat diet. *FASEB J* 2011;**25:** 4301-4311.

360. Mraz M, Haluzik M. The role of adipose tissue immune cells in obesity and low-grade inflammation. *J Endocrinol* 2014;**222:** R113-127.

361. Altintas MM, Azad A, Nayer B, Contreras G, Zaias J, Faul C*, et al.* Mast cells, macrophages, and crown-like structures distinguish subcutaneous from visceral fat in mice. *J Lipid Res* 2011;**52:** 480-488.

362. Marshall JD, Maffei P, Collin GB, Naggert JK. Alstrom syndrome: genetics and clinical overview. *Curr Genomics* 2011;**12:** 225-235.

363. Collin GB, Marshall JD, Ikeda A, So WV, Russell-Eggitt I, Maffei P*, et al.* Mutations in ALMS1 cause obesity, type 2 diabetes and neurosensory degeneration in Alstrom syndrome. *Nat Genet* 2002;**31:** 74-78.

364. Heydet D, Chen LX, Larter CZ, Inglis C, Silverman MA, Farrell GC*, et al.* A truncating mutation of Alms1 reduces the number of hypothalamic neuronal cilia in obese mice. *Dev Neurobiol* 2013;**73:** 1-13.

365. Tandra S, Yeh MM, Brunt EM, Vuppalanchi R, Cummings OW, Unalp-Arida A*, et al.* Presence and significance of microvesicular steatosis in nonalcoholic fatty liver disease. *J Hepatol* 2011;**55:** 654-659.

366. Pasquali R, Patton L, Gambineri A. Obesity and infertility. *Curr Opin Endocrinol Diabetes Obes* 2007;**14:** 482-487.

367. Pasquali R, Gambineri A. Metabolic effects of obesity on reproduction. *Reprod Biomed Online* 2006;**12:** 542-551.

368. Steyn NP, McHiza ZJ. Obesity and the nutrition transition in Sub-Saharan Africa. *Ann N Y Acad Sci* 2014;**1311:** 88-101.

369. O'Neill LA, Golenbock D, Bowie AG. The history of Toll-like receptors - redefining innate immunity. *Nat Rev Immunol* 2013;**13:** 453-460.

370. Medzhitov R. Pattern recognition theory and the launch of modern innate immunity. *J Immunol* 2013;**191:** 4473-4474.

371. Kumar H, Kawai T, Akira S. Pathogen recognition by the innate immune system. *Int Rev Immunol* 2011;**30:** 16-34.

372. Medzhitov R, Preston-Hurlburt P, Janeway CA, Jr. A human homologue of the Drosophila Toll protein signals activation of adaptive immunity. *Nature* 1997;**388:** 394-397.

373. Rock FL, Hardiman G, Timans JC, Kastelein RA, Bazan JF. A family of human receptors structurally related to Drosophila Toll. *Proc Natl Acad Sci U S A* 1998;**95:** 588-593.

374. Wesche H, Henzel WJ, Shillinglaw W, Li S, Cao Z. MyD88: an adapter that recruits IRAK to the IL-1 receptor complex. *Immunity* 1997;**7:** 837-847.

375. Muzio M, Ni J, Feng P, Dixit VM. IRAK (Pelle) family member IRAK-2 and MyD88 as proximal mediators of IL-1 signaling. *Science* 1997;**278:** 1612-1615.

376. Yamamoto M, Sato S, Hemmi H, Hoshino K, Kaisho T, Sanjo H*, et al.* Role of adaptor TRIF in the MyD88-independent toll-like receptor signaling pathway. *Science* 2003;**301:** 640-643.

377. Volchenkov R, Sprater F, Vogelsang P, Appel S. The 2011 Nobel Prize in physiology or medicine. *Scand J Immunol* 2012;**75:** 1-4.

378. Lim KH, Staudt LM. Toll-like receptor signaling. *Cold Spring Harb Perspect Biol* 2013;**5:** a011247.

379. Takeuchi O, Hoshino K, Kawai T, Sanjo H, Takada H, Ogawa T*, et al.* Differential roles of TLR2 and TLR4 in recognition of gram-negative and gram-positive bacterial cell wall components. *Immunity* 1999;**11:** 443-451.

380. Lai Y, Yi G, Chen A, Bhardwaj K, Tragesser BJ, Rodrigo AV*, et al.* Viral double-strand RNA-binding proteins can enhance innate immune signaling by toll-like Receptor 3. *PLoS One* 2011;**6:** e25837.

381. Jurk M, Heil F, Vollmer J, Schetter C, Krieg AM, Wagner H*, et al.* Human TLR7 or TLR8 independently confer responsiveness to the antiviral compound R-848. *Nat Immunol* 2002;**3:** 499.

382. Hemmi H, Takeuchi O, Kawai T, Kaisho T, Sato S, Sanjo H*, et al.* A Toll-like receptor recognizes bacterial DNA. *Nature* 2000;**408:** 740-745.

383. Guggemoos S, Hangel D, Hamm S, Heit A, Bauer S, Adler H. TLR9 contributes to antiviral immunity during gammaherpesvirus infection. *J Immunol* 2008;**180:** 438-443.

384. Kumagai Y, Takeuchi O, Akira S. TLR9 as a key receptor for the recognition of DNA. *Adv Drug Deliv Rev* 2008;**60:** 795-804.

385. Papatriantafyllou M. Innate immunity: TLR9 mutations reveal a new level of self tolerance. *Nat Rev Immunol* 2012;**12:** 7.

386. Khazen W, M'Bika JP, Collinet M, Tramoni M, Chany C, Achour A*, et al.* Differentiation-dependent expression of interferon gamma and toll-like receptor 9 in 3T3-F442A adipocytes. *Biochimie* 2007;**89:** 669-675.

387. Schaffler A, Scholmerich J. Innate immunity and adipose tissue biology. *Trends Immunol* 2010;**31:** 228-235.

388. Zhang X, Mosser DM. Macrophage activation by endogenous danger signals. *J Pathol* 2008;**214:** 161-178.

389. Schroder K, Hertzog PJ, Ravasi T, Hume DA. Interferon-gamma: an overview of signals, mechanisms and functions. *J Leukoc Biol* 2004;**75:** 163-189.

390. Wu H, Ghosh S, Perrard XD, Feng L, Garcia GE, Perrard JL*, et al.* T-cell accumulation and regulated on activation, normal T cell expressed and secreted upregulation in adipose tissue in obesity. *Circulation* 2007;**115:** 1029-1038.

391. Madani R, Karastergiou K, Ogston NC, Miheisi N, Bhome R, Haloob N*, et al.* RANTES release by human adipose tissue in vivo and evidence for depot-specific differences. *Am J Physiol Endocrinol Metab* 2009;**296:** E1262-1268.

392. Krinninger P, Brunner C, Ruiz PA, Schneider E, Marx N, Foryst-Ludwig A*, et al.* Role of the adipocyte-specific NF-kappaB activity in the regulation of IP-10 and T cell migration. *Am J Physiol Endocrinol Metab* 2011;**300:** E304-311.

393. Geissmann F, Manz MG, Jung S, Sieweke MH, Merad M, Ley K. Development of monocytes, macrophages, and dendritic cells. *Science* 2010;**327:** 656-661.

394. Auffray C, Sieweke MH, Geissmann F. Blood monocytes: development, heterogeneity, and relationship with dendritic cells. *Annu Rev Immunol* 2009;**27:** 669-692.

395. Gordon S, Taylor PR. Monocyte and macrophage heterogeneity. *Nat Rev Immunol* 2005;**5:** 953-964.

396. Packard AE, Leung PY, Vartanian KB, Stevens SL, Bahjat FR, Stenzel-Poore MP. TLR9 bone marrow chimeric mice define a role for cerebral TNF in neuroprotection induced by CpG preconditioning. *J Cereb Blood Flow Metab* 2012;**32:** 2193-2200.

397. Kienesberger PC, Oberer M, Lass A, Zechner R. Mammalian patatin domain containing proteins: a family with diverse lipolytic activities involved in multiple biological functions. *J Lipid Res* 2009;**50 Suppl:** S63-68.

398. Mairal A, Langin D, Arner P, Hoffstedt J. Human adipose triglyceride lipase (PNPLA2) is not regulated by obesity and exhibits low in vitro triglyceride hydrolase activity. *Diabetologia* 2006;**49:** 1629-1636.

399. Rezamand P, Watts JS, Yavah KM, Mosley EE, Ma L, Corl BA*, et al.* Relationship between stearoyl-CoA desaturase 1 gene expression, relative protein abundance, and its fatty acid products in bovine tissues. *J Dairy Res* 2014;**81:** 333-339.

REFERENCES

400. Montoudis A, Seidman E, Boudreau F, Beaulieu JF, Menard D, Elchebly M*, et al.* Intestinal fatty acid binding protein regulates mitochondrion beta-oxidation and cholesterol uptake. *J Lipid Res* 2008;**49:** 961-972.

401. Poirier Y, Antonenkov VD, Glumoff T, Hiltunen JK. Peroxisomal beta-oxidation--a metabolic pathway with multiple functions. *Biochim Biophys Acta* 2006;**1763:** 1413-1426.

402. Immunological Genome Project. immune cell database]. Available from: https://www.immgen.org/.

403. Shi H, Kokoeva MV, Inouye K, Tzameli I, Yin H, Flier JS. TLR4 links innate immunity and fatty acid-induced insulin resistance. *J Clin Invest* 2006;**116:** 3015-3025.

404. Ahmad R, Al-Mass A, Atizado V, Al-Hubail A, Al-Ghimlas F, Al-Arouj M*, et al.* Elevated expression of the toll like receptors 2 and 4 in obese individuals: its significance for obesity-induced inflammation. *J Inflamm (Lond)* 2012;**9:** 48.

405. Vila IK, Badin PM, Marques MA, Monbrun L, Lefort C, Mir L*, et al.* Immune cell Toll-like receptor 4 mediates the development of obesity- and endotoxemia-associated adipose tissue fibrosis. *Cell Rep* 2014;**7:** 1116-1129.

406. Kaufmann SH. Immunology's foundation: the 100-year anniversary of the Nobel Prize to Paul Ehrlich and Elie Metchnikoff. *Nat Immunol* 2008;**9:** 705-712.

407. Sica A, Mantovani A. Macrophage plasticity and polarization: in vivo veritas. *J Clin Invest* 2012;**122:** 787-795.

408. Mosser DM, Edwards JP. Exploring the full spectrum of macrophage activation. *Nat Rev Immunol* 2008;**8:** 958-969.

409. Martinez FO, Gordon S. The M1 and M2 paradigm of macrophage activation: time for reassessment. *F1000Prime Rep* 2014;**6:** 13.

410. Gosselin D, Link VM, Romanoski CE, Fonseca GJ, Eichenfield DZ, Spann NJ*, et al.* Environment drives selection and function of enhancers controlling tissue-specific macrophage identities. *Cell* 2014;**159:** 1327-1340.

411. Murray PJ, Wynn TA. Protective and pathogenic functions of macrophage subsets. *Nat Rev Immunol* 2011;**11:** 723-737.

412. Baer M, Dillner A, Schwartz RC, Sedon C, Nedospasov S, Johnson PF. Tumor necrosis factor alpha transcription in macrophages is attenuated by an autocrine factor that preferentially induces NF-kappaB p50. *Mol Cell Biol* 1998;**18:** 5678-5689.

413. Witsell AL, Schook LB. Tumor necrosis factor alpha is an autocrine growth regulator during macrophage differentiation. *Proc Natl Acad Sci U S A* 1992;**89:** 4754-4758.

414. Fernandez-Riejos P, Najib S, Santos-Alvarez J, Martin-Romero C, Perez-Perez A, Gonzalez-Yanes C*, et al.* Role of leptin in the activation of immune cells. *Mediators Inflamm* 2010;**2010:** 568343.

415. Bourlier V, Zakaroff-Girard A, Miranville A, De Barros S, Maumus M, Sengenes C*, et al.* Remodeling phenotype of human subcutaneous adipose tissue macrophages. *Circulation* 2008;**117:** 806-815.

416. Fujisaka S, Usui I, Kanatani Y, Ikutani M, Takasaki I, Tsuneyama K*, et al.* Telmisartan improves insulin resistance and modulates adipose tissue macrophage polarization in high-fat-fed mice. *Endocrinology* 2011;**152:** 1789-1799.

417. Brancato SK, Albina JE. Wound macrophages as key regulators of repair: origin, phenotype, and function. *Am J Pathol* 2011;**178:** 19-25.

418. Raes G, De Baetselier P, Noel W, Beschin A, Brombacher F, Hassanzadeh Gh G. Differential expression of FIZZ1 and Ym1 in alternatively versus classically activated macrophages. *J Leukoc Biol* 2002;**71:** 597-602.

419. Vogel DY, Glim JE, Stavenuiter AW, Breur M, Heijnen P, Amor S*, et al.* Human macrophage polarization in vitro: maturation and activation methods compared. *Immunobiology* 2014;**219:** 695-703.

420. Odegaard JI, Ricardo-Gonzalez RR, Goforth MH, Morel CR, Subramanian V, Mukundan L*, et al.* Macrophage-specific PPARgamma controls alternative activation and improves insulin resistance. *Nature* 2007;**447:** 1116-1120.

421. Chawla A. Control of macrophage activation and function by PPARs. *Circ Res* 2010;**106:** 1559-1569.

422. Berg JM TJ, Stryer L. Important Derivatives of Cholesterol Include Bile Salts and Steroid Hormones. In: Freeman WH (ed). *Biochemistry. 5th edition.*

423. Ali AH, Carey EJ, Lindor KD. Recent advances in the development of farnesoid X receptor agonists. *Ann Transl Med* 2015;**3:** 5.

424. Modica S, Gadaleta RM, Moschetta A. Deciphering the nuclear bile acid receptor FXR paradigm. *Nucl Recept Signal* 2010;**8:** e005.

425. Rizzo G, Disante M, Mencarelli A, Renga B, Gioiello A, Pellicciari R*, et al.* The farnesoid X receptor promotes adipocyte differentiation and regulates adipose cell function in vivo. *Mol Pharmacol* 2006;**70:** 1164-1173.

426. Maneschi E, Vignozzi L, Morelli A, Mello T, Filippi S, Cellai I*, et al.* FXR activation normalizes insulin sensitivity in visceral preadipocytes of a rabbit model of MetS. *J Endocrinol* 2013;**218:** 215-231.

427. Zhang Y, Ge X, Heemstra LA, Chen WD, Xu J, Smith JL*, et al.* Loss of FXR protects against diet-induced obesity and accelerates liver carcinogenesis in ob/ob mice. *Mol Endocrinol* 2012;**26:** 272-280.

428. Cariou B, van Harmelen K, Duran-Sandoval D, van Dijk TH, Grefhorst A, Abdelkarim M*, et al.* The farnesoid X receptor modulates adiposity and peripheral insulin sensitivity in mice. *J Biol Chem* 2006;**281:** 11039-11049.

429. Neuschwander-Tetri BA, Loomba R, Sanyal AJ, Lavine JE, Van Natta ML, Abdelmalek MF*, et al.* Farnesoid X nuclear receptor ligand obeticholic acid for non-cirrhotic, non-alcoholic steatohepatitis (FLINT): a multicentre, randomised, placebo-controlled trial. *Lancet* 2015;**385:** 956-965.

430. Chang CK, Tso TK, Snook JT, Huang YS, Lozano RA, Zipf WB. Cholesteryl ester transfer and cholesterol esterification in type 1 diabetes: relationships with plasma glucose. *Acta Diabetol* 2001;**38:** 37-42.

431. Huang Y, von Eckardstein A, Wu S, Assmann G. Cholesterol efflux, cholesterol esterification, and cholesteryl ester transfer by LpA-I and LpA-I/A-II in native plasma. *Arterioscler Thromb Vasc Biol* 1995;**15:** 1412-1418.

432. Ma Y, Huang Y, Yan L, Gao M, Liu D. Synthetic FXR agonist GW4064 prevents diet-induced hepatic steatosis and insulin resistance. *Pharm Res* 2013;**30:** 1447-1457.

433. Tou JC, Wade CE. Determinants affecting physical activity levels in animal models. *Exp Biol Med (Maywood)* 2002;**227:** 587-600.

434. Westerterp KR. Assessment of physical activity level in relation to obesity: current evidence and research issues. *Med Sci Sports Exerc* 1999;**31:** S522-525.

435. Seefeldt V, Malina RM, Clark MA. Factors affecting levels of physical activity in adults. *Sports Med* 2002;**32:** 143-168.

436. Speakman JR, Selman C. Physical activity and resting metabolic rate. *Proc Nutr Soc* 2003;**62:** 621-634.

437. Black BL, Croom J, Eisen EJ, Petro AE, Edwards CL, Surwit RS. Differential effects of fat and sucrose on body composition in A/J and C57BL/6 mice. *Metabolism* 1998;**47:** 1354-1359.

438. Bachmanov AA, Reed DR, Beauchamp GK, Tordoff MG. Food intake, water intake, and drinking spout side preference of 28 mouse strains. *Behav Genet* 2002;**32:** 435-443.

439. Kinabo JL, Durnin JV. Thermic effect of food in man: effect of meal composition, and energy content. *Br J Nutr* 1990;**64:** 37-44.

440. Manzel A, Muller DN, Hafler DA, Erdman SE, Linker RA, Kleinewietfeld M. Role of "Western diet" in inflammatory autoimmune diseases. *Curr Allergy Asthma Rep* 2014;**14:** 404.

441. Cordain L, Eaton SB, Sebastian A, Mann N, Lindeberg S, Watkins BA*, et al.* Origins and evolution of the Western diet: health implications for the 21st century. *Am J Clin Nutr* 2005;**81:** 341-354.

442. Sandnabba NK, Lagerspetz KM, Jensen E. Effects of testosterone exposure and fighting experience on the aggressive behavior of female and male mice selectively bred for intermale aggression. *Horm Behav* 1994;**28:** 219-231.

443. Nyberg J, Sandnabba K, Schalkwyk L, Sluyter F. Genetic and environmental (inter)actions in male mouse lines selected for aggressive and nonaggressive behavior. *Genes Brain Behav* 2004;**3:** 101-109.

444. Dalleck LC, Van Guilder GP, Richardson TB, Bredle DL, Janot JM. A community-based exercise intervention transitions metabolically abnormal obese adults to a metabolically healthy obese phenotype. *Diabetes Metab Syndr Obes* 2014;**7:** 369-380.

445. Colberg SR, Sigal RJ, Fernhall B, Regensteiner JG, Blissmer BJ, Rubin RR*, et al.* Exercise and type 2 diabetes: the American College of Sports Medicine and the American Diabetes Association: joint position statement. *Diabetes care* 2010;**33:** e147-167.

446. Larson-Meyer DE, Heilbronn LK, Redman LM, Newcomer BR, Frisard MI, Anton S*, et al.* Effect of calorie restriction with or without exercise on insulin sensitivity, beta-cell function, fat cell size, and ectopic lipid in overweight subjects. *Diabetes care* 2006;**29:** 1337-1344.

447. Kistler KD, Brunt EM, Clark JM, Diehl AM, Sallis JF, Schwimmer JB. Physical activity recommendations, exercise intensity, and histological severity of nonalcoholic fatty liver disease. *Am J Gastroenterol* 2011;**106:** 460-468; quiz 469.

448. Musso G, Cassader M, Rosina F, Gambino R. Impact of current treatments on liver disease, glucose metabolism and cardiovascular risk in non-alcoholic fatty liver disease (NAFLD): a systematic review and meta-analysis of randomised trials. *Diabetologia* 2012;**55:** 885-904.

449. Larter CZ, Yeh MM, Haigh WG, Van Rooyen DM, Brooling J, Heydet D*, et al.* Dietary modification dampens liver inflammation and fibrosis in obesity-related fatty liver disease. *Obesity (Silver Spring)* 2013;**21:** 1189-1199.

450. Van Rooyen DM, Gan LT, Yeh MM, Haigh WG, Larter CZ, Ioannou G*, et al.* Pharmacological cholesterol lowering reverses fibrotic NASH in obese, diabetic mice with metabolic syndrome. *J Hepatol* 2013;**59:** 144-152.

451. Palou A, Pico C, Bonet ML. Nutritional potential of metabolic remodelling of white adipose tissue. *Curr Opin Clin Nutr Metab Care* 2013;**16:** 650-656.

452. Sun K, Kusminski CM, Scherer PE. Adipose tissue remodeling and obesity. *J Clin Invest* 2011;**121:** 2094-2101.

453. Feng B, Zhang T, Xu H. Human adipose dynamics and metabolic health. *Ann N Y Acad Sci* 2013;**1281:** 160-177.

454. Henninger AM, Eliasson B, Jenndahl LE, Hammarstedt A. Adipocyte hypertrophy, inflammation and fibrosis characterize subcutaneous adipose tissue of healthy, non-obese subjects predisposed to type 2 diabetes. *PLoS One* 2014;**9:** e105262.

455. Pedersen BK. Muscles and their myokines. *J Exp Biol* 2011;**214:** 337-346.

456. Gleeson M. Immune function in sport and exercise. *J Appl Physiol (1985)* 2007;**103:** 693-699.

457. Suganami T, Tanaka M, Ogawa Y. Adipose tissue inflammation and ectopic lipid accumulation. *Endocr J* 2012;**59:** 849-857.

458. Oh S, Tanaka K, Tsujimoto T, So R, Shida T, Shoda J. Regular exercise coupled to diet regimen accelerates reduction of hepatic steatosis and associated pathological conditions in nonalcoholic fatty liver disease. *Metab Syndr Relat Disord* 2014;**12:** 290-298.

459. Tchernof A, Belanger C, Morisset AS, Richard C, Mailloux J, Laberge P*, et al.* Regional differences in adipose tissue metabolism in women: minor effect of obesity and body fat distribution. *Diabetes* 2006;**55:** 1353-1360.

460. Alberti KG, Zimmet P, Shaw J. Metabolic syndrome--a new world-wide definition. A Consensus Statement from the International Diabetes Federation. *Diabet Med* 2006;**23:** 469-480.

461. Itoh M, Kato H, Suganami T, Konuma K, Marumoto Y, Terai S*, et al.* Hepatic crown-like structure: a unique histological feature in non-alcoholic steatohepatitis in mice and humans. *PLoS One* 2013;**8:** e82163.

462. Apovian CM, Bigornia S, Mott M, Meyers MR, Ulloor J, Gagua M*, et al.* Adipose macrophage infiltration is associated with insulin resistance and vascular endothelial dysfunction in obese subjects. *Arterioscler Thromb Vasc Biol* 2008;**28:** 1654-1659.

REFERENCES

APPENDICES

APPENDICES

Appendix A

Major kits and compounds (alphabetical order):

- Adipose morphometry: Leica Application Suite software (LAS), Leica Microsystems, Wetzlar, Germany
- Atherogenic diet: Speciality Feeds, Glen Forrest, Australia
- cDNA synthesis: High-Capacity cDNA Reverse Transcription Kit, Life Sciences, Carlsbad, CA, USA
- Chemical compounds: Sigma Chemicals, St Louis, MO, USA
- Chemiluminescence detection: Western Lightining Plus, Perkin-Elmer, Boston, MA, USA
- Chow diet: Gordon's Speciality Stockfeed, Sydney, Australia
- Collagenase: Whittington, CA, USA
- Cycle Computer: Bri2, Echowell, Taiwan
- Densitometric analysis: MultiGauge Software, FujiFilm, Tokyo, Japan
- ELISA kits: R&D Systems, Minneapolis, MN, USA
- Exercise Wheel: ASIFTB-PC, Able Scientific, Canning Vale, Australia
- Formalin: HD, Scientific Supplies, Wetherill Park, NSW, Australia
- Gill's hematoxylin: ProSciTech, Kirwan, QLD, Australia
- Glucometer: Accu-Check Advantage, Roche Diagnostics, Mannheim, Germany
- Image analysis: ImageJ, NIH, Bethesda, MD, USA
- Insulin ELISA kit: EZRMI-13K Mouse Insulin ELISA, EMD Millipore, Darmstadt, Germany
- Insulin: Humalog 100U/ml, Eli Lilly, Indianapolis, IN, USA
- Ketamine & xylazine: Troy Laboratories, Smithfield, NSW, Australia
- Liver fibrosis: Masson's trichrome, POCD Healthcare, Sydney, NSW, Australia
- qPCR reaction mix: iQ SYBR Green Supermix, Bio-Rad Laboratories, Hercules, CA, USA
- qPCR reaction: iQ5 Real-Time Thermal Cycler, Bio-Rad Laboratories, Hercules, CA, USA

APPENDICES

- Quantification of RNA: Nanodrop 1000, ThermoScientific, Waltham, MA, USA
- RNA isolation kit: Promega SV Total RNA Isolation System, Madison, WI, USA
- Statistics: Prism6 (Graphpad Software, La jolla, CA, USA)
  and SPSS Statistics 22 (IBM, New York, NY, USA)
- Total RNA isolation: TRI Reagent, Sigma Chemicals, St Louis, MO, USA

Other suppliers: Amresco (Solon, OH, USA), SAFC Biosciences (Brooklyn, VIC, Australia), GE Healthcare (Sydney, NSW, Australia), Applied Biosystems (Carlsbad, CA, USA), Pierce (Rockford, IL, USA), QIAGEN (Concaster, VIC, Australia), Chem-Supply (Adelaide, SA, Australia), BD Biosciences (Melbourne, VIC, Australia).

Note:

Primers: All qPCR primers were obtained from Sigma-Aldrich St Louis, MO, USA, specifically KiCqStart SYBR Green Primers by RefSeq Accession.

Antibodies: Antibody information for Western Blotting, Immunohistochemistry and Flow Cytometry are stated under relevant protocol in Appendix B.

Appendix B

Oil red-O (ORO) Staining Protocol

Process maximum 16 samples at any time.

- Prepare 0.25% **ORO stock solution** in 100% isopropanol. Vortex well and filter via a 70 µm cell strainer into a 50 ml falcon tube.
- Prepare fresh 10% dextran solution before the experiment
- Prepare **ORO working solution** of 6:4 (ORO:dextran) and filter it before use
- Weigh 50 mg of frozen samples in a 1.5 ml Eppendorf tube
- Homogenize with a disposable plastic homogeniser in 500 µl ORO working solution
- Keep the samples on ice until incubation
- Incubate the samples in an orbital shaker at low speed for 1 h at cold room
- Centrifuge @ 10000 g for 5 minutes, and discard supernatant
- Add 1 ml 60% isopropanol, disturb the pellet with a 25 G needle and vortex
- Centrifuge @ 10000 g for 5 minutes, and discard supernatant
- Add 1 ml 60% isopropanol and vortex
- Centrifuge @ 10000 g for 5 minutes, and discard supernatant
- Add 1 ml 60% isopropanol
- Centrifuge @ 10000 g for 5 minutes, and discard supernatant and let dry for 2 minutes
- Add 1 ml 100% isopropanol, disturb the pellet with a 25 G needle and vortex
- Centrifuge @ 12000 g for 5 minutes
- Keep the supernatant, use 96-well plate. Measure the absorbance @ 450 nm
- Use 100% isopropanol as negative control; deduct the value from absorbance.

* ORO stock solution – 0.25 g in 100 ml absolute isopropanol; molecular weight of ORO 408.49, accordingly stock solution 6.12 mM

* ORO working solution – 3.67 mM (3.67 x ½ - 5 times)

APPENDICES

Immunohistochemistry

Process maximum 12 slides at any time, to prevent sections drying out (approximately 5h)

- Heat slides in oven, 10 minutes @ 60°C and immerse them in xylene, 30 minutes
- Prepare 300 ml ARB*
- Rehydrate through ethanol gradient (high to low) and place in deionized water (dH_2O)
- Immerse slides in ARB, and place in decloaking chamber, 3 minutes @ 123°C. Cool down to room temperature.
- Wash slides in dH_2O x 3
- Wash slides through series of 1X TBS-T* (1.5L)
- Drain off excess TBS-T and outline sections with DAKO wax pen
- Cover sections with Chemicon blocking solution (blue cap), 5 minutes @ room temperature, moisture tray
- Dilute antibody with antibody diluent (300 µl/slide)
    - Incubation – 90 minutes @ room temperature, or overnight @ 4^0C, moisture tray

- Drain off blocking solution and dip slides into TBS-T
- Cover sections with primary antibody and incubate
- Prepare hydrogen peroxide solution* (HPS) (300 µl/slide)
- Change the first cup of TBS-T and wash slides in after primary antibody
- Cover sections with HPS and incubate for 10 minutes @ room temperature, moisture tray
- Wash slides in TBS-T. Prepare secondary antibody in Antibody Diluent
    - Incubation – 30 minutes @ room temperature, moisture tray

- Cover sections with secondary antibody and incubate
- Wash slides in TBS-T
- Cover sections with Chemicon Streptavidin (pink) and incubate for 10 minutes
- Prepare Chromagen/DAB reagent*
- Wash slides in TBS-T. Filter DAB with 0.22 µm Millex
- Cover sections with DAB reagent and incubate for 15 minutes in dark
- Discard DAB on slide and excess DAB in specific waste bottle
- Wash slides in running hot water, 3-5 minutes
- Counterstain with Gill's hematoxylin, 30 seconds!
- Wash under running water
- Cover sections with ammonium alcohol, 10 seconds, then immerse in water
- Dehydrate through ethanol gradient (low to high)
- Immerse in xylene and mount slides
- Put wax (Pertex) on the cover slips, make sure no air bubble is trapped

*ARB - 0.882g sodium citrate tribasic dehydrate, 250 ml dH_2O, 0.6 ml 25% Tween-20, Adjust pH to 6.0 using HCl, Add dH_2O to 300 ml final volume

*TBS-T – 150 ml 10X TBS buffer, 1350 ml dH_2O, Add 6 ml 25% Tween-20, Divide into 4-5 cups

*HPS – 120 µl 50% H_2O_2, 1880 µl dH_2O, 2 ml final volume of 3% H_2O_2

*DAB – 12 µl solution A and 300 µl solution B, for each slide

1^o Ab – F4-80 (AbD Serotec Cl:A3-1), 2^o Ab – Anti-Rat Biotin Ab (F4-80)

APPENDICES

RNA Isolation using TRI reagent and Promega SV Total RNA Kit

General comments:

- *A dedicated work area for RNA only is designated in the host laboratory*
- *DEPC-treated H_2O was used for all solutions*
- *Adjust centrifuge to 4^0C before starting*
- *Label 2 x 2 ml tube + 2 x 1.5 ml tube + 1 x 1.5 ml tube + 1 x 0.6 ml tube per sample to use during the protocol*

- Prepare 2 tubes of (same) adipose tissue sample (between 30 and 40 mg) in 2 ml Eppendorf tube
- Homogenize the samples in 1 ml **TRIzol** and stand for 5 minutes @ room temperature. Centrifuge for 10 minutes @ 13000 g @ 4^0C
- Isolate supernatant (approximately 800 µl solution) to a new tube (discard lipid layer)
- Add 200 µl **chloroform**, vortex 15 seconds, stand for 15 minutes @ room temperature. Centrifuge for 15 minutes @ 13000 g @ 4^0C
- Transfer clear upper phase to a new tube and combine the same samples
- Add 400 µl 95% **ethanol** and mix by pipetting
- Transfer half of it in into spin coloumn from Promega SV kit. Centrifuge for 1 minute @ 13000 g
- Discard eluate with 1 ml pipette, and add the rest of the solution into the tube and repeat centrifugation
- Add 50 µl **DNase I** solution per tube. Incubate for 15 minutes at room temperature
- Add 200 µl **DSA** per tube. Centrifuge for 1 minute @ 13000 g
- Add 600 µl **RWA** per tube. Centrifuge for 1 minute @ 13000 g
- Add 300 µl **RWA** per tube. Centrifuge for 2 minutes @ maximum g
- Add 20 µl dH_2O. Centrifuge for 1 minute @ 13000 g
- Depending on the amount of the sample, add 10-15 µl dH_2O. Centrifuge for 1 minute @ 13000 g

Solutions:

- DNase I: (40 µl Yellow core + 5 µl 0.09 M $MnCl_2$ + 5 µl DNase I) x tube number
- RNA lysis buffer: 1 ml BME + 50 ml RLA
- RNA wash solution: 100 ml 95% ethanol + 58.8 ml RWA
- DNase stop solution: 40 ml 95% ethanol + 26.5 ml DSA

Quick calculation for 12 samples:

DNase I: 520 µl Yellow + 65 µl $MnCl_2$ + 65 µl DNase I (1.5 ml Eppendorf tube)
DSA: 1.5 ml 95% ethanol + 1 ml DSA (15 ml falcon) store @ 4^0C
RWA: 7.37 ml 95% ethanol + 4.33 ml RWA (50 ml falcon) store @ 4^0C
95% ethanol: 14.25 ab ethanol + 0.75 dH_2O (50 ml falcon) store @ 4^0C

APPENDICES

cDNA Synthesis

(Applied Biosystems' High-Capacity cDNA Reverse Transcription kit, plus RNase inhibitor)

- Thaw one aliquot of extracted RNA samples and kit components on ice
- Prepare diluted RNA samples using spreadsheet below

Sample ID	RNA ng/µl	RNA µg/µl	Vol RNA to give 5µg	Vol H_2O required
	x	= x / 1000	= 5 / RNA µg/µl	= 10 – vol RNA µg/µl

- Add to new PCR plate or individual microtubes required volume RNA and DEPC water (total volume = 10 µl), return undiluted samples to freezer
- For each sample, make up Master Mix as shown below:

Reagent	*Volume required (µl)*
RT buffer	2
100 mM dNTPs	0.8
RT random primers	2
MultiScribe reverse transcriptase	1
RNase OUT	1
DEPC water	3.2
Total reagent volume	10 µl per sample

- Pipette 10 µl of Master Mix into each well of plate or microtubes
- Seal plate or tubes, mix and spin down
- Start the reaction

(Involving 3 incubation steps: 10 minutes at 25°C, 2 hours at 37°C, and 5 minutes at 85°C to inactivate enzyme)

- Chill on ice
- Add 30 µl PCR-grade dH_2O, to give cDNA concentration of 0.1µg/µl
- Store at -20°C until needed

APPENDICES

Primer Design for SYBR Green-Based qPCR

- Decide on the target gene
- NCBI -> Gene (write the name) -> Genomic sequence (FASTA) [copy the whole thing on word]
- On the right side, find Nucleotide of the gene -> Origin (mRNA seq) (FASTA) [copy entire sequence on Words document]
- NCBI - Primer Blast copy the symbol (>gi…) and paste the mRNA seq
- "Refseq" mRNA organism
- PCR product size
- Exon junction span (primer must span exon-exon junction)
- PerlPrimer v1.1.2.1 or Primer3
- After design: bienzyme.enzim.hu primer search ePCR cDNA 1000 DNA 100000
- Copy the product sequence and paste to www.dna.utah.edu/umelt/um.php (Run uMelt HETS)
- Thermodynamic set, most recent

Most primers are obtained from Sigma-Aldrich St Louis, MO, USA, specifically KiCqStart SYBR Green Primers by RefSeq Accession.

APPENDICES

SYBR Green-Based qPCR

- Prepare sample dilutions depending on the target genes
- Abundant expression 1:30 dilution (ie. 5 µl stock cDNA + 145 µl PCR-grade dH_2O)
- For each sample, make up Q-PCR Mix as shown below

Reagent	*Volume required (µl)*
2X SYBR- Mix	10
F primer (10 µM)	0.5
R primer (10 µM)	0.5
dH_2O	5
Total reagent volume	16 µl

- Add 16 µl of Q-PCR Mix into Q-PCR plate (duplicate samples)
- Add 4 µl of cDNA samples, standards and dH_2O (in duplicate)
- Seal plate, mix and spin
- Load plate, select required run protocol and plate set-up
- Common reaction 45 x 60^0C [95-60-72]

For qPCR standard, pool cDNA samples (at least 3 samples from each treatment group) to make standards

3-5 µl from each sample was used to make pooled cDNA (use cDNA undiluted)

Make 5 standards as below

Standard 1	1:5 dilution
Standards 2-5 seri	1:5 dilutions

APPENDICES

Protein Isolation from Liver:

- Weigh 60-80 mg tissue
- Add 9x volume ERK buffer (to make 10% homogenate), homogenize, and centrifuge at 10000 rpm @ 4 ^{0}C for 5 minutes
- Transfer to new 1.5 ml tube (leaving fatty upper layer behind)
- Centrifuge at 10000 rpm @ 4 C for 5 minutes
- Aliquot into 3 tubes and snap freeze
- Keep the rest for protein estimation
- Dilute 1:30 for whole liver

ERK buffer:

	Conc (buffer)	Conc (stock)	Vol (ml) to make 50 ml	Inhibitors for 10 ml
HEPES	50 mM	1M	2.5	For 10 ml add:
NaCl	150 mM	2M	3.75	
$MgCl_2$	1.5 mM	1M	0.075	100 µl protease inhibitor cocktail
EGTA	1 mM	200 mM	0.25	*And*
Glycerol	10%	80%	6.25	100 µl phosphatase inhibitor cocktail
Triton X-100	0.1%	1%	5.0	
dH_2O	-	-	32.175	

Stock Solutions:

1M Hepes: mw 238.3

23.83 g / 100 ml dH_2O

2M NaCl: mw 58.44

11.688 g / 100 ml dH_2O

1M $MgCl_2$: mw 95.21

4.76 g / 50 ml dH_2O

200 mM EGTA: mw 380.3

3.803 g / 50 ml dH_2O

APPENDICES

Detergent-free protein extraction protocol for Adipose Tissue

General comments
Designate an area to conduct the procedures
Adjust centrifuge to 4^0C and heat block to 55^0C

- Homogenize adipose tissue (harvest tubes >2 ml) in 0.5 ml **Isolation medium*** and 1875 µl **chloroform/methanol (1:2)***
- Keep homogenized tissue on ice and mix sporadically for 15 minutes
- Diluate homogenate with 625 µl of **chloroform** and 625 µl of dH_2O
- Split the homogenate into 2 2 ml tubes and label carefully
- Centrifuge for 7 minutes @ 800 g @ 4^0C
- Isolate the protein disks into new 2 ml tubes (keep the same samples together)

Protein precipitation:

- Add 3 volumes of **10 % TCA*** and keep @ -20^0C overnight
- Centrifuge for 30 minutes @ 7500 g @ 4^0C
- Discard supernatant
- Add 1 ml of acetone (ice cold!) and gently wash pellet (keep an eye on the pellet) to avoid its dispersion
- Repeat the previous stage and carefully dry the pellet
- Resuspend the pellet in **resuspension buffer*** (approximately 200 or 300 µl)
- Keep the protein at -20 ^{0}C or -80^0C

***Isolation medium** – 50 mM Tris, 150 mM NaCl, 0.2 mM EDTA and protease inhibitors

100 ml solution: 5 ml 1 M Tris, 15 ml 1 M NaCl, 200 µl 100 mM EDTA, p. inhibitors and dH_2O

100 ml 1 M Tris: 12.1 g Tris and dH_2O

100 ml 1 M NaCl: 5.84 g NaCl and dH_2O

***10% TCA** – add 10 g TCA into 80 ml acetone and after stirring complete the solution to 100 ml

***Resuspension buffer** – 0.1% SDS in 40 mM Tris solution

100 ml solution: 4 ml 1 M Tris, 95 ml dH_2O and 1 ml 10% SDS

APPENDICES

Protein Isolation from muscle:

Prepare lysis buffer as below (make 5 ml aliquots and store at -20^{0}C):

HEPES	0.48 g
EGTA	0.08 g
Beta-glycerophosphate	1.08 g
DTT	0.015 g
Na3VO4	0.018 g
Glycerol	10 ml
Triton X	1 ml

Make up to 100 ml with dH_2O

Prior to use of 5 ml solution and add:

25 µl protease inhibitor

25 µl phosphatase inhibitor

50 µl 100 mM NaF (100 mM NaF – 0.02 g to 5 ml dH_2O)

50 µl 100 mM PMSF (100 mM PMSF – 0.09 g to 5 ml DMSO)

- Homogenise 50 mg muscle in 300 µl lysis buffer (work on ice)
- Centrifuge samples for 20 minutes @ 13,000 rpm @ 4^{0}C
- Change the tubes and centrifuge supernatant for 10 minutes @ 13,000 rpm @ 4^{0}C
- Freeze samples or keep on ice until use

- For protein assay dilute samples 1:50 with dH_2O
- Perform protein assay

APPENDICES

Protein Estimation:

Standards

prepare a serial dilution standard curve:

60 µl protein + 30 µl dH_2O

Starting protein = 1.45 mg/ml BSA [5x 1/5 dilutions]

Do each standard and sample in duplicate

Reagent A' = 20 µl of reagent S + 1 ml of reagent A

- Add 5 µl standard / sample / blank per well
- Add 25 µl Reagent A' to each sample (using repeat pipettor)
- Add 200 µl Reagent B
- Stand for 15 minutes @ room temperature
- Read at 750 nm in plate reader
- Calculate standard curve and corresponding protein concentration of samples

- Calculate 300 µg (protein solution + dH_2O = 50 µl)
- 2.5X loading dye + 1 tube DTT
- Add 50 µl loading dye to samples
- Boil mixture at 95^0C for 5 minutes
- Ready to use, or can be stored at -20^0C

APPENDICES

Western Blot protocol for Adipose Tissue

Adjust heat block to 55^0C

Keep primary antibody dilutions at 4^0C

- Prepare resolving gel and stacking gel without adding TEMED
- Decide on the appropriate concentration for acrylamide gel (7.5x to 12x)
- Wipe glass apparatus with ethanol and put sponge on stands
- Put the glass into the cuff and locate into the stand
- Add TEMED into resolving gel; using a 1 ml micropipette, add it into the glass until the green level; add butanol onto the gel
- After polymerisation suck out the butanol and wipe with a layer of paper towel
- Add TEMED to the stacking gel and put it into the glass until top
- Put the comb into the gel, and add a little more stacking gel onto the comb to prevent the gel drying out
- When the gels are ready take the comb out
- Put gels into the tank and add 1 X running buffer; label the tank for gels
- Load the samples (15-30 µg sample, 5 µl ladder)
- Start the machine with 100 V 10 minutes, then leave it 125 V for 2 hours
- Cut PVDF membranes to 9 x 6 cm
- Fix membranes in methanol for 30 seconds then leave them in the transfer buffer
- When gels are ready, put them in transfer buffer with glass
- Wet 4 blotting papers per gel with transfer buffer
- Wet the drawer with transfer buffer
- Put 2 blotting papers into drawer and open the glass, locate the gel onto papers and put 2 more blotting papers on top
- Finish blotting in 30 minutes using automated transfer system
- Incubate the membranes in Ponceau for 5 minutes at room temperature
- After bands are visualized, wash them twice with TBST
- Incubate the membranes in TBST adding couple of drops absolute NaOH
- Cut the membranes into strips from the relevant marker sizes (bands of interest)
- Write the sample ID and the size on every strip using a pencil
- Incubate the strips in 5 % skim milk for 1 hour
- Prepare primary antibody solutions
- Wash the strips in TBST for 3 times, especially if primary antibody is diluted in BSA
- Incubate the strips in primary antibody solution overnight in the cold room (4^0C)
- Wash the strips in TBST for 3 times
- Incubate them in secondary antibody solution for 2 hours at room temperature
- Wash the strips in TBST for 3 times
- Finish densitometric analysis with chemiluminescence substrate (mentioned in Appendix A

Adiponectin Ab: 1/100 dilution in 5% skim milk (Santa Cruz)
Total AKT Ab: 1/1000 dilution in 5% BSA (Cell Signaling)
Phospho AKT Ab: 1/1000 dilution in 5% BSA (Cell Signaling)
HSP90 Ab: 1/10000 dilution in 0.5% skim milk (R&D systems)
Secondary antibody use according to data sheet of related product.

APPENDICES

Adipocyte and SVF isolation from Adipose

Prepare 15 ml falcon tubes with 10 ml sterile PBS added for each sample.

Put the shaker in the incubator and adjust it to 37^0C

Put your FBS at 4^0C

Prepare sterile PBS, filters and tubes before starting the protocol

- Wash adipose tissue samples with sterile PBS and mince it very finely with blades or small scissors
- Put the minced tissues into 9 ml **digestion buffer** (falcon tube) and leave on ice
- After finishing the harvest add **10 X collagenase buffer** to your samples
- Incubate the tissue for 30 minutes @ 37^0C with constant shaking
- After 30 minutes, examine cells by microscope (large cells are adipocytes, small ones are SVF)
- If needed, an additional 10 minutes of digestion can be used
- After incubation, add EDTA to a final concentration of 10 mM; and incubate 5 minutes
- Pre-wet 180 μm filters with PBS; filter the sample solutions
- Centrifuge at 150 g for 8 minutes at 4^0C (floating layer is adipocytes)
- Collect floating adipocytes in a 15 ml tube and add 3 volumes of **FACS buffer;** keep on ice
- Pre-wet 100 μm filters with PBS, shake the remained of sample solutions, then filter them to a new clean Falcon tube
- Wash filters with 10 ml **FACS buffer** twice to collect remaining samples on filters
- Centrifuge at 500 g for 10 minutes at 4^0C
- Discard the supernatant, resuspend the pellet in 0.5 ml **RBC lysis buffer** and incubate for 5 minutes at room temperature
- Centrifuge at 500 g for 10 minutes at 4^0C
- Resuspend the pellet in 4 ml **FACS buffer**
- Centrifuge adipocytes at 150 g for 8 minutes at 4^0C and keep the floating layer
- Count the cells by hemocytometer (50 μm trypan blue + 50 μm sample)
- Calculate the cell number for each sample.

Digestion buffer: HBSS + 0.5% BSA

FACS buffer: PBS + 1% FBS + 25 mM HEPES + 1 mM EDTA

Collagenase solution: 10 mg/ml in digestion buffer

RBC lysis buffer: 155 mM NH_4Cl, 10 mM $KHCO_3$, 0.1 M EDTA

And 0.2% Tween 20

APPENDICES

Flow Cytometry (Cell surface and Intracellular Antigens)

- Prepare the plate lay-out for the assay (standards, controls, and samples)
- Prepare tubes (number depending on the antibodies) of 50 µl **FACS buffer** for single cell controls
- Put 10^6 cells in wells for each sample
- In a separate tube, mix the samples for a final number of 9 x 10^6 cells
- Divide 9 of 10^6 cells evenly in wells (antibody number + 2 single cell control)
- Add 0.5 mg of Fc-block (anti-Cd16/32) and incubate for 10 minutes in 4^0C refrigerator
- Prepare your master mix in **FACS buffer** up to your sample number (for 1 sample, 50 µl master mix needed; accordingly volume for samples + antibody standards + 2 single cell controls)

  1/100 – 1/200 or 1/400 µl antibody dilutions

- Prepare single cell controls
- Spin the plate 1340 rpm 8^0C 4 minutes
- Wash the cells with 200 µl **FACS buffer** and spin the plate 1340 rpm, 8^0C, 4 minutes
- Add your M-Mix and single cell control dilutions to the wells
- Cover the plate with aluminium foil and incubate at 4^0C for 30 minutes
- Add 150 µl **FACS buffer** per well, centrifuge at 1340 rpm, 8^0C, 4 minutes
- Flick off the supernatant and wash one more time with 200 µl **FACS buffer,** and centrifuge at 1340 rpm, 8^0C, 4 minutes
- Decant of the supernatant and resuspend the sample pellets and single cell control in 1 ml of **0.2% Tween 20;** incubate for 15 minutes at room temperature
- Centrifuge, discard supernatant and add intracellular antibody
- Cover the plate with aluminium foil and incubate at 4^0C for 30 minutes
- Add 150 µl **FACS buffer** per well and centrifuge at 1340 rpm, 8^0C, 4 minutes
- Flick off the supernatant and wash one more time with 200 µl **FACS buffer** and centrifuge at 1340 rpm, 8^0C, 4 minutes
- Optional: Fix cells by adding 200 µl of 10% NBF for 10 minutes on ice, in the dark
- Spin the plate 1340 rpm, 8^0C, 4 minutes
- Resuspend samples and controls in 120 µl FACS buffer and transfer to FACS tube

TLR9 Antibody: FITC-TLR9 (Cat number – 11 9093 80; e-Biosciences)

F4/80 Antibody: APC-F4/80 (Cat number – 123115; Biolegend)

Liver Research Group, 2014 (We were young ☺)